

THESIS/
REPORTS

Hunt,
W.A.

HYDRAULIC INVESTIGATIONS OF
PIPELINE TRANSPORT OF MIXTURES
OF WOOD CHIPS AND WATER IN
STEEL PIPES

Prepared by

Dr. William A. Hunt, Principal
Investigator

James E. Borg, Graduate Research
Assistant

October 15, 1977

CEE

CEM

UNITED STATES DEPARTMENT OF AGRICULTURE
FOREST SERVICE

INT Missoula FSL

RECEIVED

January 26, 1978

REPLY TO: 4040 Cooperation

SUBJECT: Final report, hydraulic chip pipeline
research (Grant No. 1, MSU)


TO: Director, INT

JAN 30 1978
Intermountain Forest &
Range Experiment Station



Attached, per my conversation with Ernie Piz, is a copy of the final report of research conducted by MSU under Grant No. 1.

Copies of the report have been provided to industrial firms and consultants that have shown recent interest in the technology. Rulon Gardner will continue to act in a consulting role with these firms.


ROLAND L. BARGER
Program Manager

Attachment

Report on file in Station Library

HYDRAULIC INVESTIGATIONS OF
PIPELINE TRANSPORT OF MIXTURES
OF WOOD CHIPS AND WATER IN
STEEL PIPES

Prepared by

Dr. William A. Hunt, Principal
Investigator

James E. Borg, Graduate Research
Assistant

October 15, 1977

HYDRAULIC INVESTIGATIONS OF PIPELINE TRANSPORT OF MIXTURES
OF WOOD CHIPS AND WATER IN STEEL PIPES

Final Report

Submitted to

Mr. Rulon B. Gardner, Project Leader
Intermountain Forest and Range Experiment Station
USDA Forest Service
Bozeman, Montana

Prepared by

Dr. William A. Hunt, Principal Investigator
James E. Borg, Graduate Research Assistant
Department of Civil Engineering and Engineering Mechanics
Montana State University
Bozeman, Montana

October 15, 1977

ABSTRACT

The description of the facilities, an outline of the test procedures and a summary of the results of hydraulic investigations of the energy losses of mixtures of wood chips and water flowing in steel pipelines are presented. Energy loss correlations by previous investigators are reviewed. Pump performance and unstable flow conditions are summarized graphically. Studies conducted for predicting corrosion rates of interior pipe walls are reported.

An equation for calculating the friction factor for mixtures and water is developed from analysis of data collected from tests run in 3-, 4-, 6-, 8- and 12-in.- (75-, 100-, 150-, 200-, and 300-mm) diameter pipes. Observed data is presented graphically with the friction factor correlation equation.

A critical flow factor giving the minimum safe operating conditions based on velocity, concentration and pipe diameter is used in a design application.

TABLE OF CONTENTS

	<u>Page</u>
ABSTRACT	ii
TABLE OF CONTENTS	iii
LIST OF FIGURES	v
LIST OF TABLES	vi
LIST OF NOTATIONS	vii
1. INTRODUCTION	1
1.1 Scope of Problem	1
1.2 Scope of Report	3
2. HISTORICAL REVIEW OF SOLIDS PIPELINES	4
2.1 Slurry Pipelines	4
2.2 Wood-chip Pipelines	5
2.2.1 Pulp and Paper Research Institute of Canada	6
2.2.2 Queen's University	7
2.2.3 Shell Pipeline	7
2.2.4 Laval University	8
2.2.5 U.S. Forest Service - Montana State University	8
3. PILOT LINE TEST PROGRAM	16
3.1 Outline of Studies	16
3.2 Test Facilities	17
4. ENERGY LOSS AND FLOW CONTROL STUDIES	25
4.1 Hydraulic Transport Parameters	25
4.2 Energy Loss Correlations	30
4.2.1 Flow regimes	30
4.2.2 Review of head loss equations	31
4.2.3 Proposed energy loss correlation model	33
4.2.4 Evaluation of correlation model	35
4.3 Pump Performance	45
4.3.1 Mainline pump	45
4.3.2 Off-line booster pump	52
4.4 Monitoring and Controlling Flow Conditions	59
4.4.1 Pipeline supervisory systems	60
4.4.2 Pilot line supervisory systems	61
4.5 Wood Chip Injection System	87

	<u>Page</u>
5. CORROSION STUDIES	95
5.1 Scope of Problem	95
5.1.1 Purpose	95
5.1.2 Specific objectives	96
5.2 Review of Methods	96
5.2.1 Spool test	96
5.2.2 Coupon test	97
5.2.3 Galvanic method	97
5.2.4 Electrical resistance method	99
5.2.5 Ultrasonic devices	99
5.2.6 Polarization resistance method	100
5.3 Theory of Polarization Method	100
5.3.1 Definitions	100
5.3.2 Exchange current density	101
5.3.3 Polarization types	103
5.3.4 Mixed potential theory	108
5.4 Effects of Changes of System Parameters	112
5.4.1 Velocity	112
5.4.2 Oxidizing agent	114
5.4.3 Temperature	115
5.4.4 pH	118
5.5 Application of Polarization Method	118
5.5.1 Tafel extrapolation	118
5.5.2 Weight loss calculation	119
5.6 Development of Mixed Potential Corrosometer	120
5.6.1 Principles of corrosometer design	121
5.6.2 Bench-scale tests	122
5.6.3 Carrier water tests	133
5.7 Pilot Line Corrosion Tests	147
5.7.1 Apparatus modification	147
5.7.2 Test procedure	153
5.7.3 Test results	154
5.8 Evaluation of Corrosometer Studies	154
5.8.1 Wood-chip pipeline results	169
5.8.2 General conclusions	169
5.8.3 Recommendations	170
6. APPLICATION OF FRICTION LOSS CORRELATIONS	172
ACKNOWLEDGMENTS	182
LITERATURE REVIEW	183

LIST OF FIGURES

<u>Figure</u>	<u>Page</u>
1A. Wood-chip pipeline test loop layout	18
1B. Head loss measurement circuit	19
2A. Main pump station - plan view	20
2B. Main pump station - elevation (section A-A)	21
2C. Main pump station - elevation view (section B-B)	22
3. Typical sample of wood chips	27
4-9. Friction factor ratio, f_m/f , vs flow/concentration parameter, ψ	40
10-11. Pilot line system headcurves	47
12. Dimensionless pump characteristics	51
13. Off-line remote booster pump	54
14. Characteristic curve of booster pump	58
15. Energy gradient-velocity curves for slurry flows	63
16. Energy gradient-velocity curves for wood-chip pipelines	65
17-26. Effects of planned, unplanned changes of flow rate	70
27. Injection system for 4-in. laboratory test line	90
28. Injection system for pilot line studies	92
29. Galvanic method of corrosion measurement	98
30. Electrical resistance method of corrosion measurement	98
31. Hydrogen electrode on platinum	102
32. Activation-polarization curve of a hydrogen electrode	104
33. Concentration gradients during hydrogen evolution	104
34. Concentration polarization curve	107
35. Reversible zinc electrode	107
36. Zinc mixed electrode	110
37. Electrode kinetic behavior of pure zinc	111
38. Behavior of metal M in acid	111
39. Effect of velocity on electrochemical behavior of normal metal	113
40. Effect of velocity on electrochemical behavior of active- passive metal	113
41. Effect of oxidizing agent concentration on current density	116
42. Effect of oxidizer concentration on electrochemical behavior of an active-passive metal	116
43. Effect of temperature on anodic dissolution behavior	117
44. Applied current cathodic polarization curve	117
45. Corrosometer circuit for cathodic polarization	123
46-49. Anodic polarization of active-passive electrode	129
50. Pipe-ring corrosometer test apparatus	135
51-53. Cathodic polarization curves with carrier water electrolyte	139
54. Effects of concentration on Tafel region	142
55-58. Cathodic polarization curves for bench tests	143
59-60. Differential pressure control system	149
61-62. Pipeline corrosometer electrode assembly	151
63-75. Cathodic polarization curves for pilot line tests	155
76. Head loss and power dissipation for 700,000 tons/year	179

LIST OF TABLES

<u>Table</u>	<u>Page</u>
1. Energy requirements for transportation	1
2. Size gradation of wood chips for pilot line investigations	28
3. Properties of pipes and solids for evaluating friction factor model	36
4. Summary of range of experimental data and accuracy of friction factor model	38
5. Percent standard deviation between observed and calculated friction factors by concentration and pipe diameters	39
6. Operation of off-line remote booster pump	56
7. Flow characteristics for non-steady conditions	69
8. Electrochemical equivalents for various elements	119
9. Analysis of test electrode materials	124
10. Anodic polarization characteristics for bench tests of pipeline corrosometer in 10% H_2SO_4	128
11. Anodic polarization curve parameters of active-passive metal in sulfuric acid solutions	128
12. Cathodic polarization of pipe-ring corrosometer	137
13. Corrosion rates for wood-chip pipeline determined from bench tests	137
14. Corrosion rates for wood-chip pipeline determined from pilot line tests	168
15a. Head loss and power for 700,000 tons/year throughput	175
15b. Head loss and power for 634,780 metric tons/year throughput	176
16. Design alternatives for 700,000 tons/year throughput	181

NOTATION

A, A_1	- empirical coefficient, dimensionless; surface area, m^2 (ft^2 , cm^2)
a_i	- empirical coefficients ($i = 1, 2, \dots$), dimensionless;
B_v	- valence of atoms;
C_B	- concentration of reacting ions in bulk solution of electrolyte
C_d	- drag coefficient of single particle in quiescent volume of carrier water, dimensionless;
C, C_v	- volumetric concentration of solids in mixture (decimal fraction), dimensionless;
d	- representative chip dimension, defined using method of Alger and Simon, m, (ft);
d_c	- characteristic dimension of wood chip, sum of squares of dimensions of mean chip size, m, (ft);
d_n	- weighted mean nominal particle diameter, m, (ft); this is the diameter of a sphere having the same volume as the particle;
D	- internal diameter of pipe, m, (ft); diffusion coefficient of reacting ions in electrochemical reaction;
e	- pipe wall roughness based on equivalent sand grain roughness, m, (ft);
f, f_D	- Darcy-Weisbach friction factor, dimensionless;
f_F	- the Fanning friction factor ($f_D = 4f_F$), dimensionless;
f_m	- the Darcy-Weisbach friction factor for mixtures of wood chips and water, dimensionless;
F	- Faraday's constant;
g	- gravitational acceleration, 9.81 m/sec^2 , (32.2 ft/sec^2);
G, G_1	- functional notation symbol;
h, h_L	- energy loss of clear water per unit weight of water, m-kN/kN, (ft-lbf/lbf);
h_m	- energy loss of mixture per unit weight of water, m-kN/kN, (ft-lbf/lbf);

- i - hydraulic gradient of clear water, expressed as m of water/m of pipe length, $\frac{2}{2}$ (ft of water/ft of pipe length), current density, amp/cm²;
- i_L - limiting diffusion current density, amp/cm³;
- i_m - hydraulic gradient of mixture, m of water/m of pipe length, (ft of water/ft of pipe length);
- i_o - exchange current density, amp/cm²;
- I - corrosion current density, amp/cm²;
- k - ratio of characteristic chip dimension to pipe diameter, d_c/D , dimensionless;
- k_1 - empirical coefficient, 180, dimensionless;
- K - fluid consistency index, units consistent with those in generalized Reynolds Number, electrochemical equivalent, grams/coulomb;
- L - length of pipe, m, (ft);
- m - empirical exponent, -1.5, dimensionless;
- M - mass of metal lost in electrochemical process, grams;
- n - fluid behavior index, dimensionless, number of electrons transferred in electrochemical reactions;
- N - number of observed data points used in computing standard deviation;
- Δp - pressure drop, kN/m², (lbf/ft²);
- P - power required for friction loss, hp/mi (kw/km);
- Q_c - volumetric flow rate of wood chip particles, m³/sec, (ft³/sec);
- Q_m - volumetric flow rate of mixture, m³/sec, (ft³/sec);
- Q_w - volumetric flow rate of clear water, m³/sec, (ft³/sec);
- R - gas constant, N-m/(°R-mole);
- Re, Re_w - Reynolds Number of water or mixture, VD/ν , using kinematic viscosity of carrier water, dimensionless;
- Re_g - generalized Reynolds Number, $V^{2-n} D^n / 8^{n-1} K$, dimensionless;

- $r_{\text{oxidation}}$ - rate of oxidation in electrochemical reactions;
- $r_{\text{reduction}}$ - rate of reduction in electrochemical reactions;
- S_{odc}, s - specific gravity of solid particles;
- T - absolute temperature, °R or °K;
- V, V_m - mean velocity of mixture flow, m/sec, (ft/sec);
- V_s - settling velocity of particle, m/sec, (ft/sec);
- \dot{W} - throughput of wood chips, dry weight basis, tons/day, (metric tons/day);
- W_{aw} - gram atomic weight;
- x, x_i - empirical exponents, ($i = 1, 2, \dots$), dimensionless;
- X - thickness of diffusion layer adjacent to electrode in electrolyte;
- y - empirical exponent, dimensionless;
- z_1 - thickness of uniform layer of metal loss, cm;
- β - Tafel constant in polarization process;
- γ - unit weight of water, kN/m^3 , (lbf/ft^3);
- ϵ - percent difference, expressed as a decimal, between calculated and observed value of data point;
- μ - dynamic viscosity of carrier water, kg/m-sec , kN-sec/m^2 , (lbf-sec/ft^2);
- ν - kinematic viscosity of carrier water, m^2/sec , (ft^2/sec);
- η_a - activation overvoltage in polarization reactions;
- η_c - concentration overvoltage in polarization process;
- ρ - density of carrier water, kg/m^3 , ($\text{lbf-sec}^2/\text{ft}^4$, slug/ft^3);
density of electrode material, gm/cm^3 ;
- ρ_s - density of solid particles, kg/m^3 , ($\text{lbf-sec}^3/\text{ft}^4$, slug/ft^3);
- σ - percent standard deviation, expressed as a decimal;
- ϕ_1 - empirical coefficient, dimensionless;
- ϕ_i - percent increase in friction factor caused by wood chips, expressed as decimal, dimensionless;
- ψ - friction factor correlation parameter developed from Reynolds Number, pipe Froude Number and concentration of solids, dimensionless;

1. INTRODUCTION^{1/}

1.1 Scope of Problem

The use of hydraulic pipelines offers a method for transporting low-valued forest products, such as wood chips, over long distances economically competitive with railway and truck transport. Pipeline transportation of wood chips produces the same general cost advantages realized by moving other solids, such as coal, gilsonite and mineral ores, in pipelines. The principal economic advantages over other modes of transportation are derived from one or more of the following characteristics: (1) lower maintenance costs, (2) lower labor costs, and (3) greater immunity to inflation of operating costs. In areas where no alternate mode of transportation exists, a preliminary study by Hunt and Schmidt (1965) has indicated pipelines show a saving as high as 50 to 60 percent over road construction costs.

Pipelines require the least amount of energy per ton-mile of material moved of the different transportation modes compared in the CAST Report (Agricultural Engineering, 1974) of the Task Force on Energy in Agriculture. The different energy requirements per ton-mile (W-hr/kN-km) given are shown in Table 1.

Table 1. Energy requirements for transportation

<u>Mode of Transportation</u>	<u>Btu/ton-mile</u>	<u>W-hr/kN-km</u>
Pipeline	450	9.2
Barge	680	13.9
Railway	670	13.7
Truck	3,800	77.8
Air	42,000	860.0

^{1/} Chapters 1-4, 6 authored and edited by Dr. William A. Hunt, Professor, Department of Civil Engineering and Engineering Mechanics, Montana State University, Bozeman, Montana.

The 1.5 to 1 and the 9:1 ratios of energy consumption for rail and truck, respectively, to pipeline transport indicates that pipelines should be given consideration from the standpoint of energy conservation alone.

The low relative energy requirements for operating pipelines coupled with the current levels (1976) and projected future increases in the costs of energy and labor have caused renewed interest in wood-chip pipelines among the nation's larger producers of pulp, paper and other fiber products when contemplating moving from 500 to 3,000 tons (4480 to 26,880 kN) of wood chips per day to processing centers. A serious consideration of wood-chip pipelines has been hampered in the past by a lack of technological data on which decisions involving large capital investment are based. A limited amount of the data necessary for assessing the feasibility of a wood-chip pipeline in a given location is available from fragmented proprietary sources and in the occasional individual reports appearing in the literature.

The investigations reported herein were conducted to supplement the existing technology relevant to the feasibility, design and operation of wood-chip pipelines with data and information in the following specific areas: (1) friction loss correlations necessary to predict power requirements for prototype-scale pipelines, (2) a system capable of continuously injecting large quantities of wood chips into a pipeline, (3) the corrosive effects of water and wood-chip mixtures on steel pipes, (4) the operation of a remote pump station in a wood-chip pipeline, and (5) procedures for monitoring flow and initiating action to reduce the probability of plugging the line. The results of these and previous investigations will be presented as a reference for the existing technology of wood-chip pipelines.

1.2 Scope of Report

The purpose of this report is to present to engineers and other planning personnel the fundamental hydrodynamic relationships governing the design and operation of hydraulic pipelines transportating wood chips together with an outline of the basic requirements for the components to be established for a given system. The report of the pilot line studies conducted at Montana State University augments those topics of the pipeline and plant installations found in common usage in the pipeline and forest products industries. The chipping of the wood prior to entering the pipeline and the processing of chips discharging from the pipe, except for separating the surface water from chips, are not included in this report.

The following sections cover a historical review of slurry pipelines transporting other solids and wood-chip pipeline research, a discussion of the pilot line studies conducted at Montana State University, and an application to wood-chip pipeline design illustrating the results of the pilot line studies.

2. HISTORICAL REVIEW OF SOLIDS PIPELINES

2.1 Slurry Pipelines

Solids have been transported by pipelines since the advent of the centrifugal pump. The successful correlation of the flow parameters of a few liquid-solid mixtures (coal, sand, gravel, cement, limestone, and iron ore) in the 1950's established a rational procedure for the design and optimization of two-phase transport systems. These developments and further refinements through research have brought about an increasing range of materials, throughputs and line lengths considered for pipeline transport as indicated in a Colorado School of Mines study (1963) and subsequently updated by Hughes et al. (1972) and Wasp (1969).

Aside from several intraplant installations for transferring solids in chemical processing operations and disposal of waste containing solids from an industrial plant, the utilization of pipelines for the transport of solids over long distances is illustrated by the following four installations which are now operating or have operated successfully.

A 6-in.-dia, 72-mile (150-mm-dia, 116-km) pipeline has been transporting 700 to 1,000 tons (6272 to 8960 kN) of gilsonite per day since 1959 (Bond, 1957; Fulkerson and Rinne, 1959; Henderson, 1962) in southern Utah.

From 1957 to 1963 a 10-in.-dia, 108-mile (250-mm-dia, 174-km) line was used for hauling 3800 tons (34048 kN) of coal per day in Ohio (Dauber, 1957). It ceased operating when a competing railroad reduced its rates for coal shipment below those offered by the pipeline.

Coal for the Mohave Power Plant in southern California has been supplied at a rate of approximately 9,000 tons (80640 kN) per day by an

18-in.-dia, 273-mile (46-mm-dia, 440-km) pipeline across Arizona since 1970 (Love, 1969).

Mining of approximately 6100 tons (54650 kN) per day of iron ore was made economically feasible through the construction of the 9-in.-dia, 53-mile (255-mm-dia, 85-km) slurry pipeline in Tasmania (Wasp, 1969). This line has been operating successfully since 1967.

Three coal slurry lines of 780,900 and 1,000 miles (1250, 1450, and 1600-km) in length are in the planning stages or in construction within the continental United States according to a July, 1975 report (Reese, 1975).

2.2 Wood-chip Pipelines

A combination of factors including the relatively low capacity of the average pulp mill, reasonably close proximity of the wood supply to these mills, the relatively wide dispersion of the geographical centers of the harvest areas from the mill and a reasonably well-developed network of railroad and roads precluded any consideration of hydraulic pipelines as a primary mode of transportation for wood chips prior to the mid-1950's. The constantly increasing distance between the centers of the harvest areas and the mills, the increasing costs and the environmental considerations associated with developing new road systems into isolated areas, and the development of foreign harvest areas to supply mills and countries short of pulpwood created a strong interest in the potential of hydraulic pipelines for transporting wood chips in the late 1950's. A summary of the major known research and development of wood-chip pipelines of the past 20 years is summarized in the following paragraphs.

2.2.1 Pulp and Paper Research Institute of Canada (PPRIC). Elliott and de Montmorency (1963) of the Pulp and Paper Research Institute of Canada (PPRIC) were among the first to conduct research on wood-chip pipelines. In 1960 they presented data and a graph which fit the following empirical correlation for estimating the energy loss due to friction¹ in a wood-chip pipeline as a function of the concentration of solids, velocity, and diameter from studies with 8-in.-dia (200-mm-dia) pipe:

$$(i_m - i)/C_v \cdot i = 211 (\sqrt{D}/V_m)^{2.25} \quad (1)$$

where i_m = hydraulic gradient of mixture expressed as ft of water/ft of pipe length (m of water/m of pipe length);
 i = hydraulic gradient of clear water, ft/ft (m/m);
 C_v = volumetric concentration of solids (decimal fraction), dimensionless;
 D = internal diameter of pipe, ft (m); and
 V_m = mean velocity of mixture flow, ft/sec (m/sec).

Elliott also conducted studies on 6-, 8-, and 10-in.-dia (150-, 200-, and 250-mm-dia) steel pipelines at Marathon, Ontario in 1964 for the PPRIC and a consortium of ten firms subsidizing these studies. Data from the latter tests are proprietary and have not been released.

¹Different authors and investigators use the terms "pressure loss," "head loss," "hydraulic loss," and "energy loss" interchangeably at times to denote energy dissipated as heat due to friction between the pipe wall and the fluid or internally within the fluid by turbulence. These terms are related by the following equation:

$$i = h_L/L = \Delta p/\gamma L.$$

An order-of-magnitude economic feasibility study by Elliott and de Montmorency showed wood-chip pipelines to be competitive with other modes of transportation.

2.2.2 Queen's University. Faddick (1963) presented the following correlation for energy loss due to friction in wood-chip pipelines based on studies with a 4-in.-dia (100-mm-dia) aluminum pipe at Queen's University in Kingston, Ontario in 1961-63:

$$(i_m - i_v) C_v \cdot i = 2.51 (4gD/V_m^2)^{1.42} \quad (2)$$

where g is the gravitational acceleration, 32.2 ft/sec^2 ,
(9.81 m/sec^2).

Faddick's results appeared to give predicted values of pressure drop as much as 30 percent higher than those of the Elliott and de Montmorency.

2.2.3 Shell Pipeline. The research and development of the Shell Pipeline Company initiated some investigations of wood-chip pipelines on a 4,000-ft (1220-m) test loop of 8-in.-dia (200-mm-dia) pipe at Houston in 1962-63. As the investigators claimed the results to be inconclusive, this system was dismantled and further tests were conducted on a shorter line of 2-in.-dia (50-mm-dia) clear plastic pipe using scaled down wood chips. The results of the Shell test are proprietary and have not been released.

An economic analysis of the wood-chip pipeline for a proposed pulpwood harvest on Kadashan Bay in Alaska by Shell gave results similar to those obtained independently by Hunt and Schmidt (1965) indicating a savings of nearly 60 percent of the cost of developing a truck haul system.

2.2.4 Laval University. In 1967-68 Soucy (1968) conducted tests on friction losses in wood-chip pipelines of 6-in.-dia (150-mm-dia) acrylic pipes in his studies at Quebec City. The data observed in Soucy's tests were obtained for use in the studies at Montana State University.

2.2.5 U.S. Forest Service - Montana State University. With an increasing amount of National Forest woodlands being committed to pulpwood harvest in the late 1950's, the U.S. Forest Service became aware of the need to develop methods for reducing the cost of handling and transporting low-valued forest products to processing centers. In 1961 Montana State University (MSU) entered into a cooperative aid agreement with the Intermountain Forest and Range Experiment Station of the U.S. Forest Service in Ogden, Utah to initiate studies on the hydraulic transport of wood-chips in pipelines. The scope of these studies conducted by the Department of Civil Engineering and Engineering Mechanics of MSU as part of this cooperative aid agreement are outlined below.

Library search. A literature review and a state-of-the-art study conducted by Hunt (1962) indicated sufficient technology for transporting solids in pipelines had been developed to make this mode of delivering wood chips over long distances technically feasible.

Preliminary economic studies. An economic analysis for transporting wood chips in single pipelines over long distances was performed by Hunt and Schmidt (1965) using the pressure loss correlations from the Queen's University report. The study showed wood-chip pipelines to be economically feasible and justified conducting an experimental research program to provide basic engineering data required to design and operate a wood-chip pipeline.

In subsequent economic analyses completed in 1967 with data from the Queen's report, Hoffman (Hoffman, 1967; Hunt and Hoffman, 1968) developed a method for optimizing a network of pipelines transporting wood chips. An application of this work to a system of pipelines connecting widely separated harvest areas in northwestern Montana showed a pipeline network to be highly competitive with a truck transportation system.

Chip moisture content. The initial experimental research on this program was completed by Schmidt (1968, 1965) in 1964 on the effects of pressure and time on the specific gravity, moisture content and volume of wood chips in a water slurry. The results indicate that the wood chips will attain a stabilized saturated condition within 2 to 3 minutes of exposure to pressures increased 15 psig (103 kN/m^2 gage) above the ambient atmospheric conditions.

Pipe expansion losses. An investigation by Charley (1966) showed the energy loss coefficient for axisymmetric expansions in pipelines to be less for mixtures of wood chips and water than for clear water.

Valve losses. Johnson (1968), in his study of the effect of wood chips on the energy loss characteristics of valves, showed the loss coefficient for mixtures with 20 percent concentration of wood chips were from 20 to 50 percent higher than those for clear water for the same flow rate and opening in the four different types of valves tested. The mechanism of plug formations caused by partial valve openings was observed in the clear acrylic pipes used for Johnson's tests.

Pump performance. In a study of the effect of wood chips on the performance characteristics of centrifugal pumps, Page (with Hunt, 1966)

showed that for mixtures carrying up to 20 percent concentration by volume the head and efficiency curves for 3 different pumps were from 5 to 10 percent lower and the brake horsepower curves were from 5 to 10 percent higher than those respective curves for pumping clear water.

Injection system analysis. A lock-hopper system modeled after a "slug" pump patented by Riechl and Jones (U.S. Patent No. 2,672,372) in the coal slurry development for the Consolidated Coal Company was proposed as a method for injecting large volumes of wood chips continuously into a pipeline under high pressure as a means of increasing the distance between pump stations. Hendrix (with Hunt, 1968) performed an analysis of the operational procedure and outlined the type of mechanical devices required to arrest the waterhammer developed if this slug-pump system were to be used for wood-chip pipelines. The results indicated the method to be technically feasible but the cost of installing, operating and maintaining a system of this level of sophistication would be prohibitive. He concluded that closer spacing of pump stations using a number of centrifugal pumps in series was more economical.

Pipe friction losses. In 1968-69, as a Graduate Research Assistant at MSU, Faddick (1970) conducted studies of energy loss due to friction on 3- and 4-in.-dia (75- and 100-mm-dia) acrylic pipes in a 700-ft (213-m) test loop to confirm the previously reported work of other investigators. He used uniform-sized plastic chips to two different specific gravities, 0.92 and 1.05, to simulate the wood chips and eliminate the size distribution factor from the correlations. Faddick attempted to correlate his data and that of other investigators using the Durand (Durand and Condolios, 1952) equation:

$$(i_m - i)/C_v i = k_1 V_m^2 [\sqrt{g d_n / V_s^2}] / gD \quad (3)$$

The terms, not previously defined, are:

k_1 = constant, 180 from Gilbert (1960);

d_n = weighted mean nominal particle diameter, ft (m);
this is the diameter of a sphere having the same
volume as the particle;

V_s = settling velocity of particle, ft/sec (m/sec); and

m = constant, -1.5 from Gilbert.

Faddick's analysis showed this equation to be inadequate for correlating the energy loss for mixtures of wood chips and water flowing in pipes.

Using the data he collected from four sets of tests using plastic chips and the three sets of wood-chip data of other investigators previously noted, Faddick proposed calculating the energy loss due to friction in wood-chip pipelines using the Darcy-Weisbach equation:

$$h_L = f_D (L/D) V_m^2 / 2g \quad (4)$$

where h_L = energy loss due to pipe friction, ft-lb_f/lb_f of
fluid flowing (m-N/N of fluid flowing); and

f_D = the Darcy-Weisbach friction factor, dimensionless.

For evaluating the friction factor, Faddick used a curve-fitting technique to obtain the relation:

$$\log f_m = a_1 C_v (d/D)^x + a_2 \log(Re_m) + a_3 C_v (d/D)^y \log(Re_m)^2 \quad (5)$$

in which a_1 , a_2 , a_3 , x , and y are empirical coefficients determined experimentally to be $a_1 = .0254$, $a_2 = 0.327$, $a_3 = -0.0008$, $x = .002$, and $y = .001$.

Other terms in this equation not previously defined are:

d = representative chip dimension defined using method of Alger and Simon ((1968), ft (cm);

f_m = Darcy-Weisbach friction factor for mixtures of wood chips and water, dimensionless; and

Re_m = Reynolds Number of mixture, VD/ν , where ν is the kinematic viscosity of the carrier water; Re_m is dimensionless.

Eq. (5) was developed for values of the Reynolds Number ranging from 100,000 to 600,000 with the discrepancy between the predicted value of the fraction factor f_m and that observed in the tests ranging from 29 percent at the lower values of the Reynolds Number down to less than 2 percent in the upper ranges.

Gow (with Hunt, 1971) continued the friction loss studies using wood chips in 4-in.-dia (100-mm-dia) acrylic and 6-in.-dia (150-mm-dia) aluminum pipes. He developed energy loss correlations for mixtures of wood chips and water using the Fanning equation:

$$h_L = 4f_F (L/D) V_m^2 / 2g \quad (6)$$

where f_F is the Fanning friction factor, dimensionless

(note: $f_D = 4f_F$).

Gow's evaluation of the friction factor, f_F , is dependent on the flow regime occurring in the pipeline. He classed the flow as either being "pseudo"-laminar or "pseudo"-turbulent (analogous to the laminar and turbulent regimes found in the flow of clear liquids).

Gow used the sliding bed regime of the hydraulic transport of solids for the "pseudo"-laminar regime in which all the solids settle into a layer on the invert of the pipe and slide along the pipe with virtually no relative motion between the individual particles of solids. He found the critical velocity at which the sliding bed forms for mixtures containing wood chips to be in the range of 5.5 to 7.5 fps (1.68 to 2.29 m/s) for the two pipe diameters used in his investigations. "Pseudo"-laminar flow occurs when the flow velocity is less than the critical velocity and "pseudo"-turbulent flow occurs when the average flow velocity is above the critical velocity. In the latter regime the level of turbulence in the fluid is sufficient to maintain some or all of the particles in suspension.

In the "pseudo"-laminar regime the friction factor is that proposed by Metzner and Reed (1955):

$$f_F = 16/Re_g \quad (7)$$

where Re_g is the generalized Reynolds Number:

$$Re_g = (V_m^{2-n} D^n / 8^{n-1} K) \quad (8)$$

in which

n = fluid behavior index, dimensionless; and

K = fluid consistency index, units consistent with those in the generalized Reynolds Number.

Gow calculated the values of n and K from the experimental energy-loss data of the "pseudo"-laminar regime which occurred for values of Re_g less than 3,000. Values of n decreased from unity for clear water to approximately 0.3 for 20 percent concentrations. Values of K increase from the viscosity

of clear water to approximately 0.05 for 20 percent concentration. The maximum percent deviation between the friction factors calculated by Eq. (6) and the measured values was approximately 4 percent; the average deviation of all values was less than 1 percent.

Gow evaluated the Fanning friction factor, f_F , for the "pseudo"-turbulent flow regime for wood-chip mixtures in smooth pipes using an equation developed from that given by Dodge and Metzner (1959) for turbulent non-Newtonian flows. Gow's equation is:

$$1/\sqrt{f_F} = A \log (Re_W \sqrt{f_F}) - 0.4 - A \log \phi_1. \quad (9)$$

where A and $\log \phi_1$ are empirical coefficients determined experimentally, and Re_W is the Reynolds Number based on the average mixture velocity and viscosity of the carrier water. Gow found the values of the quantity $\log \phi_1$ to range from approximately 1.35 at 5 percent concentration up to 3.18 at concentrations of 20 percent. The values of A varied from 5.9 at 5 percent up to values of approximately 15.3 at 20 percent concentrations. The maximum percent deviation between the friction factors calculated by Eq. (8) and the values observed in the "pseudo"-turbulent flow regime (Re_g greater than 3,000) was less than 4 percent; the average deviation was less than one percent.

Effluent characteristics. The pollutional characteristics of the carrier water of a wood-chip pipeline, a major factor in the economic feasibility of such a system, were investigated by Asano et al. (1974) of the Environmental Engineering Section of the Department of Civil Engineering and Engineering Mechanics at MSU. These studies showed that the carrier water of a mixture of wood chips and water containing 25 percent by

volume lodgepole pine chips has the following pollutants after 8 hours of agitation simulating pipeline transport: 1200-1600 mg/l of chemical oxygen demand (COD), 400-500 mg/l of biochemical oxygen demand (BOD), 500-700 mg/l of total organic carbon (TOC), 800-1200 mg/l of total solids (94 percent in the volatile fraction), a pH in the 5.0-5.2 range, and 3,000 color units (CU).

In a subsequent study Shane et al. (1975) showed that the wood-chip carrier water can be reclaimed to a desirable quality by the combined operations of chemical coagulation with a massive lime dosage and a single stage carbon adsorption. This study also showed the biological treatability of the wood-chip carrier water to be generally poor and that chemical coagulation and flocculation is not an effective method for the removal of the color.

Pilot line investigations. In 1972 a 2345-ft (715-m) pilot line of 8 5/8-in.-dia (220-mm-dia) steel pipeline was constructed at Montana State University to obtain energy loss data to augment that taken on 3-, 4-, and 6-in.-dia (75-, 100-, and 150-mm-dia) pipes and to test the validity of extrapolating the correlations proposed by Gow (with Hunt, 1971) and Faddick (1970) to pipes of larger diameters using data obtained in the same overall experimental program. The pilot line operations were also designed to collect data concerning (1) injection system design, (2) remote pump station installation, (3) monitoring, interpreting, and controlling flow conditions in the pipelines, and (4) the corrosive effects of mixtures of wood chips and water on steel pipes. The data collection for these studies was completed in November, 1974; the analysis and subsequent findings are discussed in the following sections.

3. PILOT LINE TEST PROGRAM

3.1 Outline of Studies

The pilot line studies on wood-chip pipelines conducted at Montana State University and presented in this report included the three areas categorized as hydraulic transport, electrochemical reaction, and mechanical design. These investigations were conducted to augment existing data on energy losses due to pipe friction and to obtain data on (1) corrosion effects, (2) flow control procedures, (3) injection methods, and (4) remote pump operations for developing guidelines for design and operation of wood-chip pipelines.

The energy loss correlations, pump performance, remote pump operation, flow control and monitoring, and injection system studies are directly related to the flow behavior in the hydraulic transport of a mixture of wood chips and water; this category will be discussed in Part 4.

The corrosion studies deal with the chemical interaction occurring between the mixture and the interior wall of the pipe; this phase of the studies will appear in Part 5.

The specifics of each of these phases and a discussion of their results are presented following a brief description of the physical layout and general operation of the test loop facilities used in the studies. More detailed descriptions of the facilities, instrumentation, test procedures and all test data are on file with the Department of Civil Engineering, Montana State University.

3.2 Test Facilities

The pipe test loop shown in the schematic diagram in Fig. 1 was constructed of 2345 feet (715-m) of API steel line pipe with an ID of 8.212 in. (208-mm). Piezometer rings were tapped into both the outgoing and incoming lines at both ends and at the center of the two 600-ft (183-m) test sections. An 800-ft (244-m) section of 12.375-in.-dia (314-mm-dia) API line pipe was placed at the location of the test section in the incoming line for a series of runs on large diameter pipe in the latter stages of the program.

The mechanical equipment housed in the control center included the main line centrifugal pump, the live storage reservoir and injection system, a chip storage bin, a rotating screened drum and a weir tank.

An elevation view of a section through the control center indicating the arrangement of the chip injection and separation systems is given in Fig. 2. During the test runs the wood chips dropped into the injection system by gravity flow then were mixed with water from the live storage tank in which the injection system was located. The mixture was then drawn into the suction of the pump and forced through the test loop. The incoming line from the test loop discharged into a rotating screened drum where the surface water was mechanically separated from the chips. The effluent water drained into the head box located behind a calibrated weir. The wood chips tumbled through the rotating screened drum and back into the injection system for recycling through the test loop as the effluent passed over the weir and returned to the live storage tank.

The remote pump station included a centrifugal pump connected in a bypass line (similar to the petroleum line operations) and the suction and

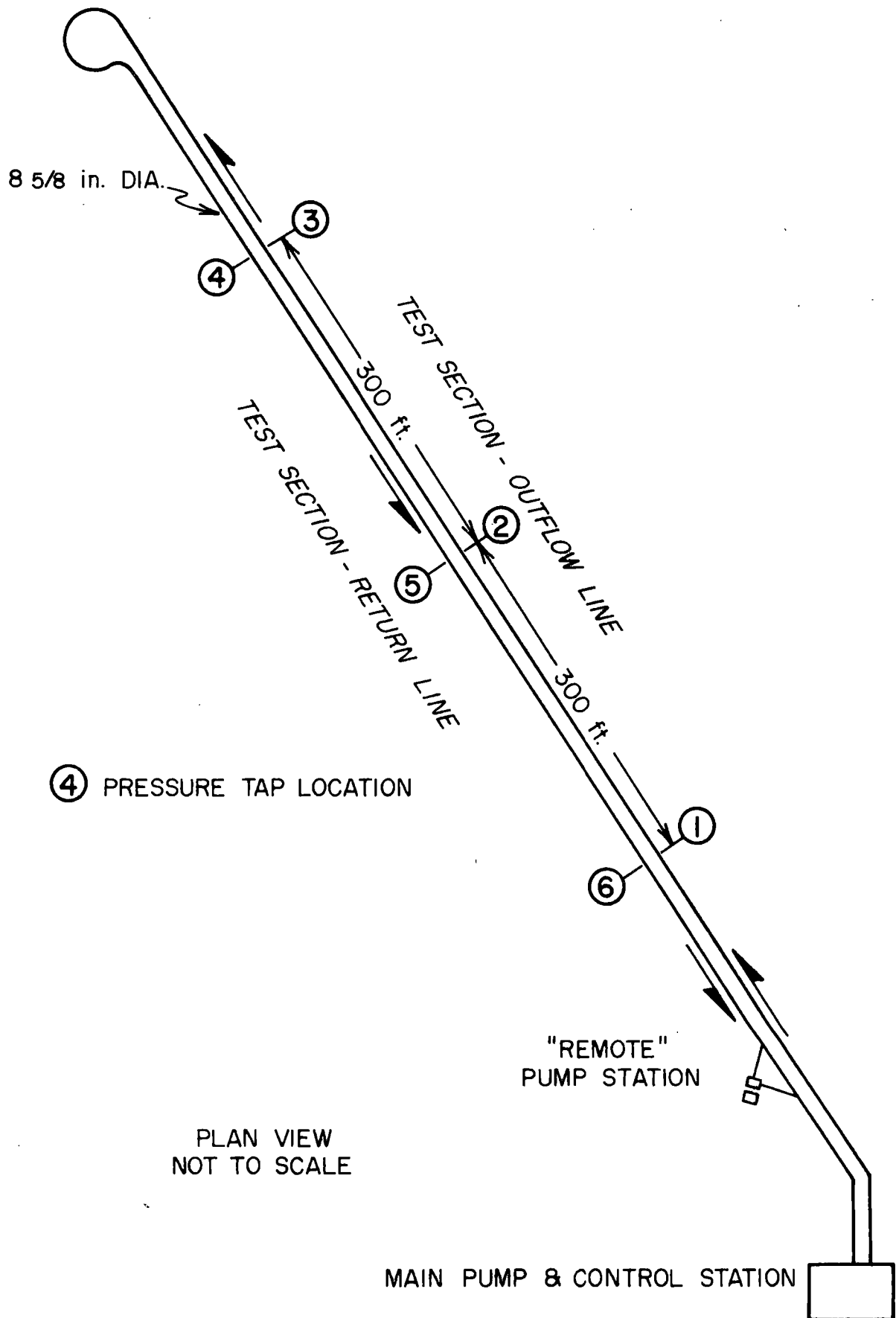


FIG. 1A. WOOD CHIP PIPELINE TEST LOOP LAYOUT

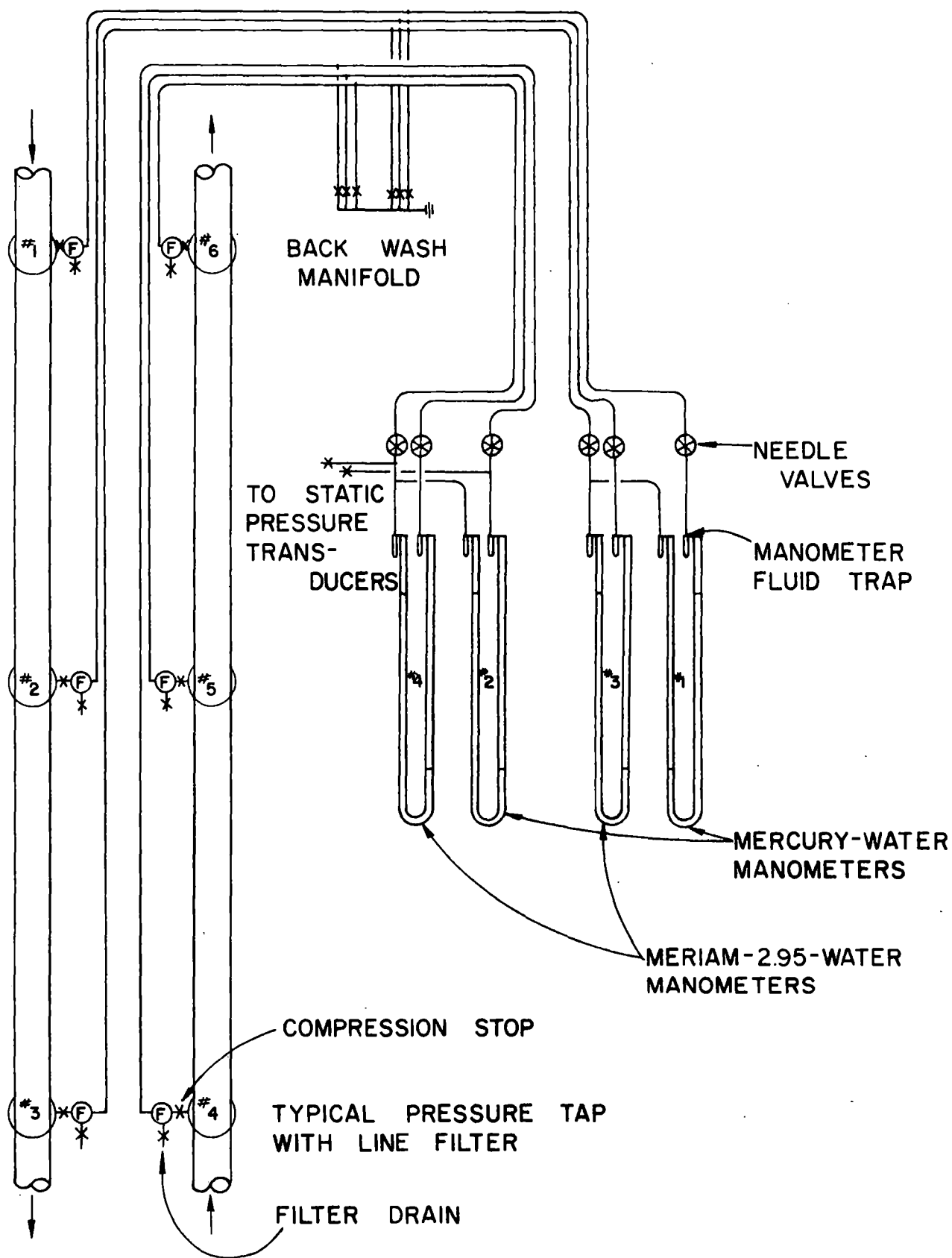
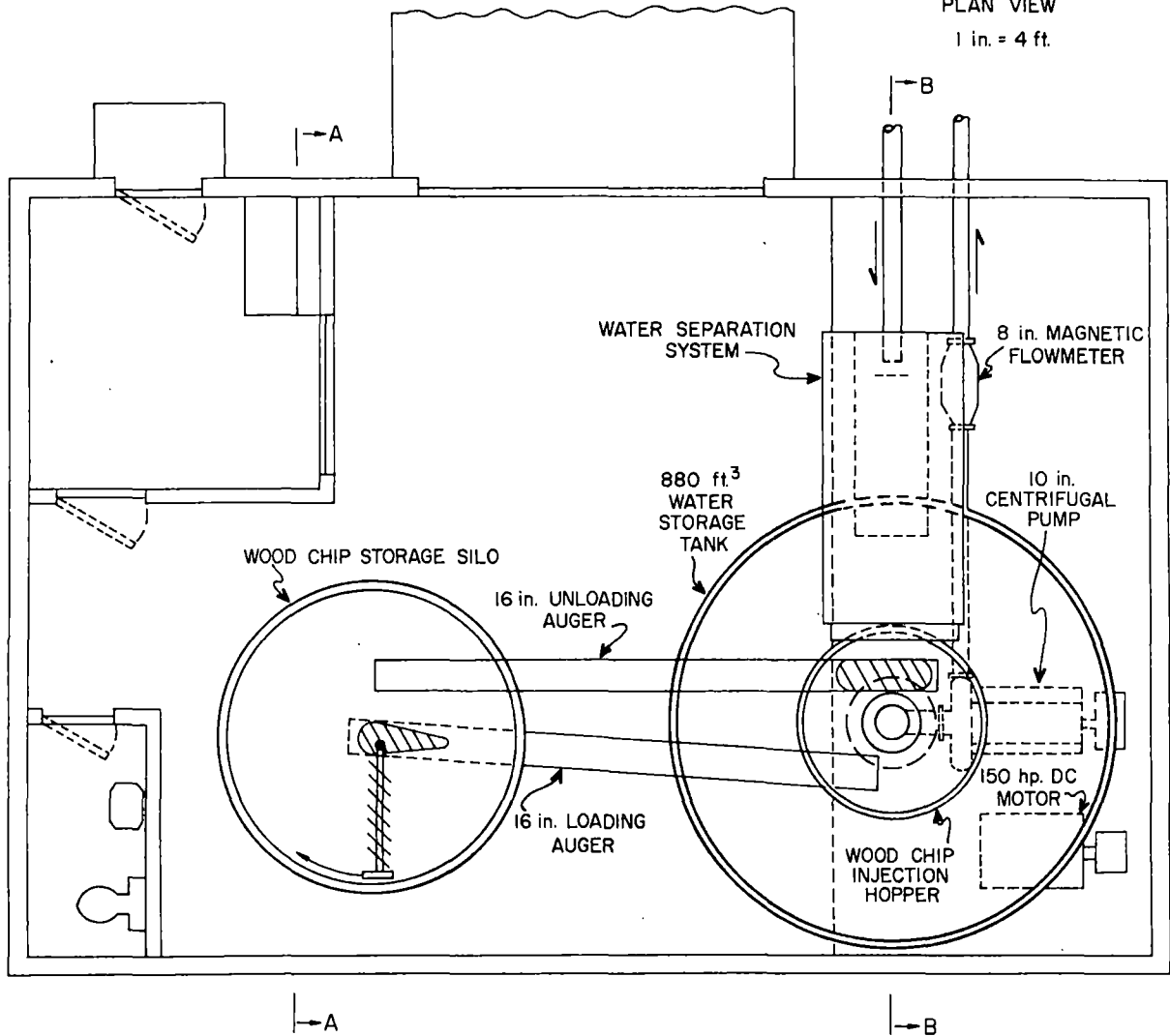


FIG. 1B. HEADLOSS MEASUREMENT CIRCUIT

FIG. 2A. MAIN PUMP STATION
PLAN VIEW
1 in. = 4 ft.



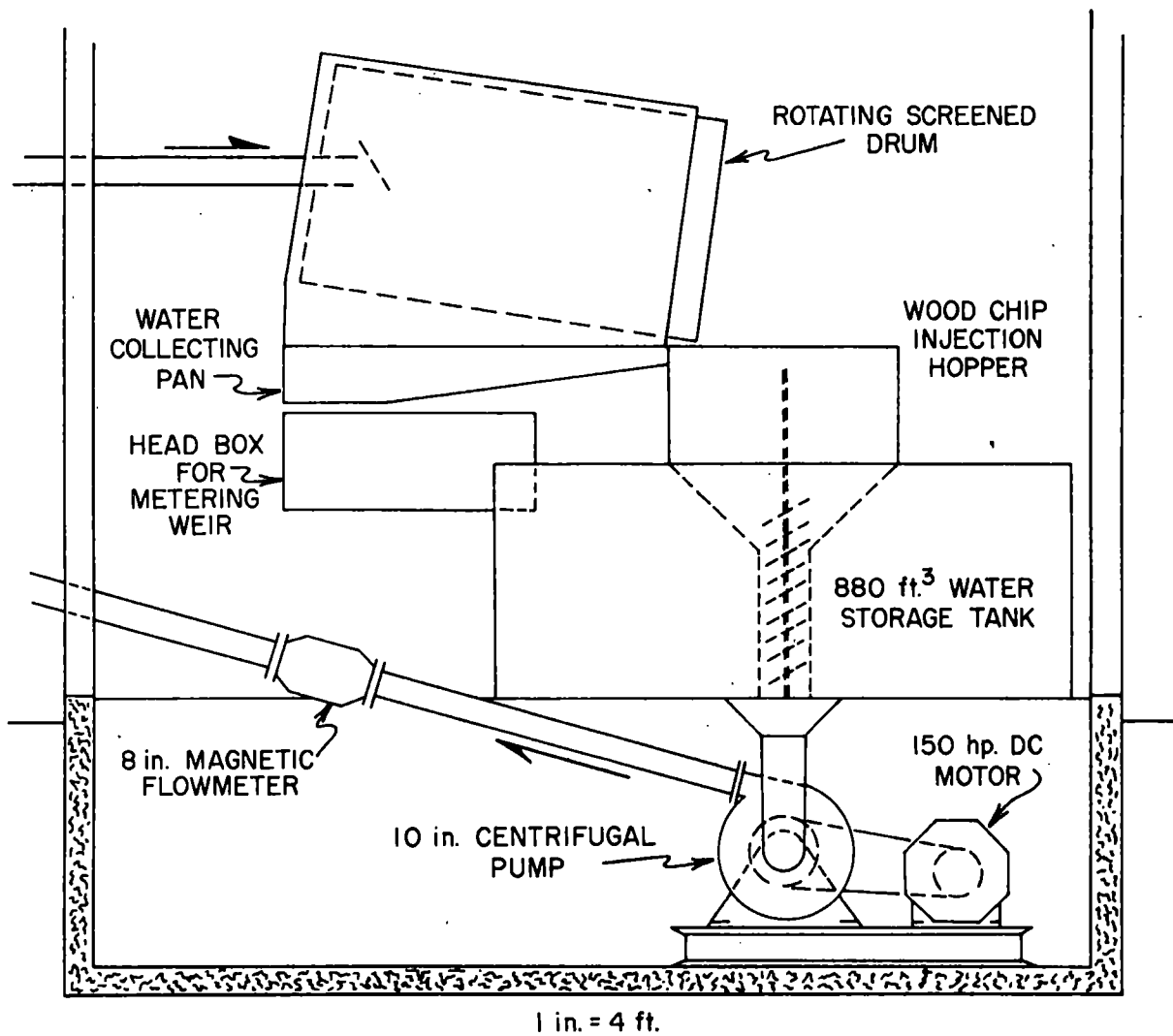


FIG. 2C. MAIN PUMP STATION ELEVATION - SECTION B-B

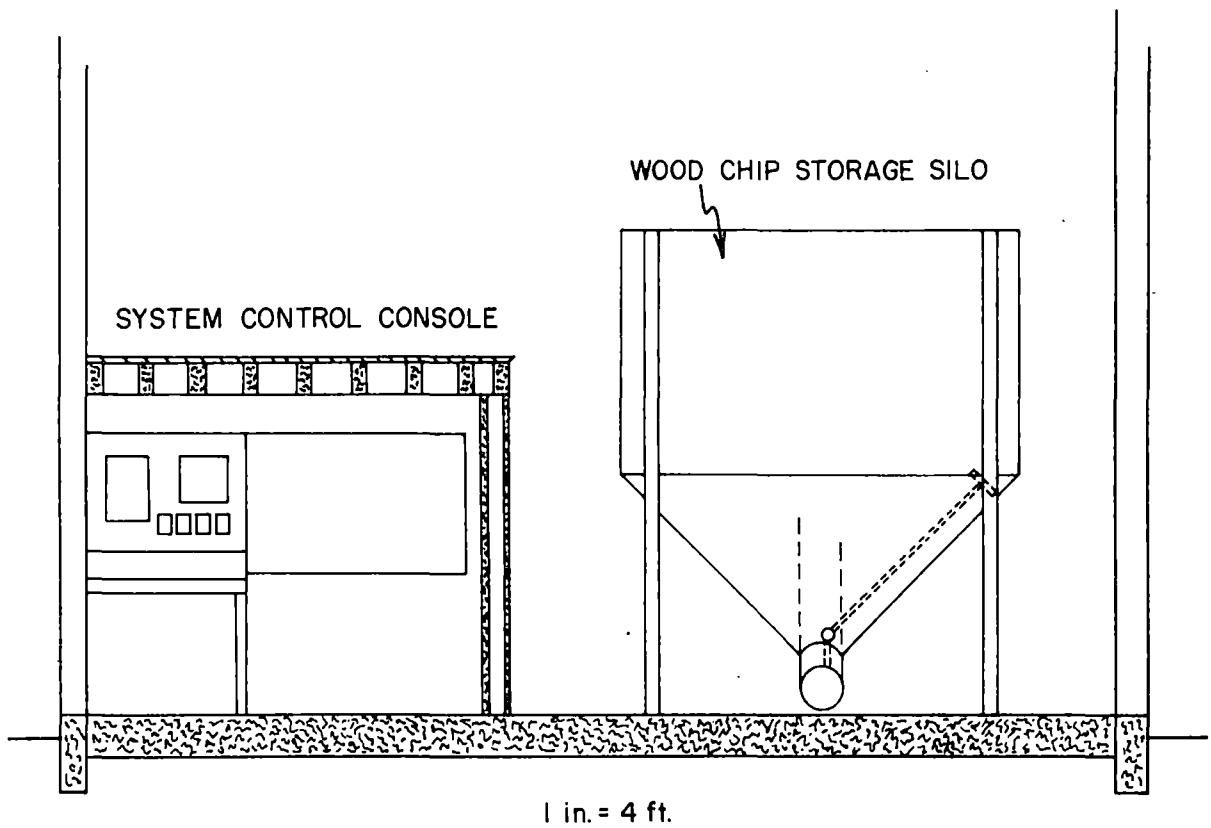


FIG. 2B. MAIN PUMP STATION ELEVATION-SECTION A-A

discharge control valves. The remote pump and valves were electronically operated from the main control center. A swing check valve was installed in the main line for the remote pump operation tests. The by-pass junctions and checkvalves were placed in operation only during the remote pump tests in the final phases of the pilot line program.

A specially-developed device for estimating the rate of corrosion on the internal pipe walls was installed and tested at the corrosion monitoring station on the return line. The device and operational technique were completed during the final phases of the program.

The description of the instrumentation in the following sections serves only to indicate how the data were gathered.

Differential manometers connected between stations 1 and 2, 1 and 3, 4 and 6, and 5 and 6 (refer to Fig. 1), respectively, were used to measure the energy losses due to friction in both test sections. A 4-channel strip chart recorder continuously monitored the fluctuations in line pressures from transducers connected to the piezometer rings at stations 4 and 6 and on the discharge flange of the pump.

The volumetric flow rate of the mixture was measured by an 8-in. (20-mm) magnetic flowmeter; fluctuations in the flow rate were monitored on the strip chart recorder.

The flow rate of the make-up water was monitored by an electronically-operated probe, specially constructed to track continuously the water surface level in the headbox behind the weir, giving a continuous record of the flow rate of make-up water entering the injection system.

A description of the functions of the equipment and instrumentation used in the remote pump tests, corrosion studies, and injection system design will be discussed in subsequent subsections dealing with those specific topics.

4. ENERGY LOSS AND FLOW CONTROL

4.1 Hydraulic Transport Parameters

The hydraulic transport of wood chips in pipelines is characterized as the motion of discrete solid particles in a water carrier and is governed by the following parameters (Bain and Bonnington, 1970):

1. pipeline parameters: (a) diameter, (b) slope of pipeline, (c) roughness of interior pipe wall;
2. liquid parameters: (a) density, (b) viscosity;
3. solid particles parameters: (a) density, (b) size distribution, (c) shape; and
4. system flow parameters: (a) velocity of flow, (b) concentration of solids in flowing mixture, (c) ratio of particle size to size of pipe cross section.

The description and quantification of the hydraulic transport parameters for the pilot line investigations are summarized in the following.

Friction loss data were obtained for pipes of two internal diameters, 8.212 in. (208-mm) and 12.375 in. (314-mm), having relative roughness ratios, e/D , of .000138 and .000167, respectively. The average relative roughness ratios were calculated from the Colebrook-White equation given by Rouse (1946) as

$$1/\sqrt{f} = 1.74 - 2\log_{10}(2e/D + 18.7/Re\sqrt{f}) \quad (10)$$

and friction loss data for flows of clear water obtained from 163 points recorded on the 8-in.-dia (200-mm-dia) and 102 points recorded for the 12-in.-dia (300-mm-dia) test pipes. The friction losses were determined from

differential pressure measurements made on a 300-ft (91.4-m) and a 600-ft (183-m) length in each of the two test sections. The slope of the pipe in the test sections was a constant throughout the pilot line program.

The carrier liquid was water; its viscosity and density were calculated for the temperature recorded for each observation from a table of properties for water at standard conditions (Vennard, 1961).

The solid particles were wood chips (95 percent lodgepole pine by species) obtained from a local sawmill. The wood chips used in the test were partially graded by segregating those not passing a 1.5-in. (38-mm) screen and those passing a 0.25-in. (6-mm) screen from those pumped through the test loop. The specific gravity of lodgepole pine chips was not readily ascertained because it varies from one chip to another and with time of immersion and ambient pressure of the carrier water. The chips received from the sawmill had an initial specific gravity of approximately 0.85 based on a "green" weight equal to twice the oven dry weight of representative samples. Schmidt (1968, 1965) shows a maximum specific gravity of 1.13 was possible with 100 percent saturation of the pore space; but he stated that air pockets trapped by the intruding water make attainment of this maximum value extremely difficult. Based on a comparison of the tendency of wood chips to settle towards the invert of the clear acrylic pipe observed in Gow's work (with Hunt, 1971) with this same tendency of the plastic chips of specific gravity of 1.04-1.05 used by Faddick (1970), the specific gravity of the wood chips was assumed to be in the range from 1.00 to 1.05. The shape of the wood chips is an elongated oblong plate, as seen in Fig. 3. The size distribution of the wood chips used in the pilot line investigations is given in Table 2.



Fig. 3. Sample of Typical Wood Chips

Table 2. Size gradation of wood chips for pilot line investigations

Screen size retained mm	% total sample	Average length, mm	Dimensions width, mm	Thickness, mm	Diagonal distance, d_c , mm
25.4	0	--	--	--	--
19.0	1.4	35.6	20.3	5.1	41.3
12.7	23.0	28.4	17.8	5.3	33.9
9.5	30.3	33.0	11.3	5.1	35.3
6.4	42.6	27.6	7.3	4.0	28.8
>6.4	2.7	25.4	3.8	1.3	25.7

Weighted mean diagonal distance, $d_c = 32.0$ mm

Wood chips entering the pulp-making process may have gradations with the top size up to 2 x 1.25 x 0.4 inches (50mm x 30mm x 10mm). The gradation in Table 1 is only representative for the lodgepole pine species obtained from a local sawmill.

Maximum concentration of 30% (by volume, $C = Q_{\text{chips}}/Q_{\text{mixture}}$) have been attained in the MSU pilot line investigations. The minimum economic concentrations are in the 15-20% range.

The pH of the carrier water falls to 5.0-6.5 with substances leaching out of the chips.

The individual chip particles consist of cellulose and lignin substances having a specific gravity of 1.55 to 1.60; these materials account for only 25 percent of the volume of the chip. Approximately 75 percent of the chip volume is void space filled with water forced into the chip by the line pressure of pipeline. Nearly 100 percent saturation of the void space occurs at pressures of 15 to 20 psig.

The velocity of flow is found by dividing the volumetric flow rate of the mixture indicated on a magnetic flowmeter at the time of observation by the cross section area of the pipe in the test section.

The concentration of solids, C_v , defined on a volume basis, is given as

$$C_v = Q_c/Q_m = 1 - Q_w/Q_m \quad (11)$$

where C_v = concentration of solids, volume basis, ratio of volumetric flow rate of solids to volumetric flow rate of total mixture, dimensionless

Q_c = volumetric flow rate of wood chips, ft^3/sec , m^3/sec

Q_m = volumetric flow rate of mixture, ft^3/sec , m^3/sec

Q_w = volumetric flow rate of make-up water, ft^3/sec , m^3/sec

The flow rate of the mixture was obtained from a magnetic flowmeter and the flow rate of the make-up water was obtained from a probe tracking the water surface in the headbox behind a weir discharging the pipeline effluent into the live storage tank (refer to Fig. 2).

Both flow rates and the manometer deflections indicating the energy losses in the test sections were obtained simultaneously by photographing the digital readout of the voltmeters connected to the magnetic flowmeter and the weir probe and the manometers with a 35 mm camera. The readings were recorded when the slides were projected on a screen. Ten photographs were taken at random time intervals when a steady state was indicated for each set of flow conditions. More complete details of the methods for conducting the runs and collecting the data are on file at Montana State University.

4.2 Energy Loss Correlations

Studies of the energy loss (or more commonly referred to as "head loss") due to pipe friction were conducted (1) to augment the existing data for mixtures of wood chips and water flowing in pipes with additional data from nominal 8-in.-dia (200-mm-dia) pipes and original data on nominal 12-in.-dia (300-mm-dia) pipes, and (2) to develop a correlation to predict accurately the energy losses in pipes of larger diameters and over a wider range of flows than is now possible with existing correlations. The development of the model for the prediction of energy loss due to friction is given following a discussion of the limitations on the existing equations for head losses in wood-chip pipelines.

4.2.1 Flow regimes. The energy loss equations for transporting solids in pipelines have been presented in terms of the increase in the energy gradient for the flow of the mixtures over that of clear water for the same volumetric flow rate. The magnitude of this increase in energy gradient depends upon which of four flow regimes of liquid-solid mixtures is occurring in the pipeline. The four regimes defined by Faddick (1970) are:

1. homogeneous flow occurs when the particles are small enough to be held in a constant state of suspension and give the mixture an apparent viscosity different from that of the carrying fluid;
2. heterogeneous suspension flow occurs when the intensity of turbulence is sufficient to support all the solids in suspension although the concentration of solids or bulk density of the mixture may not be uniform throughout the cross section of the flow area;
3. heterogeneous saltation occurs when the intensity of turbulence cannot support all the particles and the gravitational force causes the heavier particles to settle out of the suspension; the settled particles then bounce or roll along the invert of the pipe by the motion of the flow; and

4. bedload flow occurs when the particles deposited on the invert of the pipe are moved along in a sliding fashion by the motion of the flow above the layer of particles on the bed.

In the heterogeneous flow regimes the fluid and solid components comprise two distinct phases: the transporting medium and the discrete particles.

Although no attempt has been made to quantitatively classify the transport processes into the flow regimes by evaluating the hydraulic transport parameters, the probable occurrence of these regimes in the investigations will be discussed in later sections of the report. The behavior of the chips (both plastic and wood) observed in the tests conducted in acrylic pipes during the studies of Faddick (1970) and Gow (1971) indicated the occurrence of the heterogeneous suspension, heterogeneous saltation and bedload regimes. Although no provision was made for observing flows in the pilot line facilities, it is assumed that all three of these regimes were present at one time or another during the study.

4.2.2 Review of head loss equations. The form of the equation for predicting the energy loss for mixtures of liquids and solids occurring in the heterogeneous and bedload regimes is given by Worster (1952) for coal-water mixtures based on the original form presented by Durand (1952) for the transporting sands and gravels in pipelines. The quotation given by Worster is:

$$(i_m - i) / i C_v = 81 [gD(s-1) / V_m^2 \sqrt{C_d}]^{1.5} \quad (12)$$

in which C_d is the drag coefficient of a single particle of the solid material settling in a quiescent tank of the carrier fluid and s is the

ratio of the specific gravity of the solid particles to the specific gravity of the carrier fluid. Eq. (12) is not suitable for predicting the energy loss in the transport of wood chips in pipelines because of the difficulty in ascertaining the specific gravity of the solids and in determining an appropriate value for the drag coefficient. Eq. (1) developed by Elliott (with de Montmorency, 1963) and Eqs. (2) and (3) by Faddick at Queen's University are formed similar to Eq. (12). Eqs. (1) and (2) do not include the effect of the particle-to-pipe size ratio. Eq. (3) contains the settling velocity of wood chips based on observations of plastic chips, all of which were of the same specific gravity in the individual batches tested. The variability of the specific gravity from particle to a particle in wood chips and the uncertainty of the precise specific gravity reduces the reliability of Eq. (3). None of the proposed equations (1, 2, 3, or 12) consider the viscosity of the carrier water, a significant factor in the intensity of turbulence which holds the heavier-than-water particles in suspension during transport. All the equations referred to above indicate the excess energy gradient to be linearly proportional to the concentration to the solids in the mixture; this was not found to be the case when all the data available for wood-chip pipelines were examined.

The energy loss correlation proposed by Faddick (1970) in Eq. (5) incorporates the particle-to-pipe size ratio and the viscosity of the carrier fluids but does not converge to the clear water friction factor equation throughout the range of velocities when the concentration is zero. The differences between the friction factors given by Eq. (5) and those observed in Faddick's test increase with decreasing velocities and increasing pipe diameters.

The correlations proposed by Gow (1971) in Eqs. (7), (8), and (9) include the particle-to-pipe size ratio and the effect of viscosity indirectly in the evaluation of the mixture behavior index, n , and the mixture consistency index, K . Gow's correlations were found to give inconsistent results when friction factors predicted for flows in 8-in.-dia (200-mm-dia) pipes were compared with values given by Elliott (1963).

4.2.3 Proposed energy loss correlation model. The excess energy loss gradient, $(i_m - i)$, for transporting mixtures of liquids and solids in pipelines is expressed by the Darcy-Weisbach equation as

$$(i_m - i) = (h_m - h)/L = (f_m - f)(V_m^2/2gD) \quad (13)$$

The fractional increase in the energy gradient, obtained by dividing Eq. (13) by $i = fV_m^2/2gD$, may then be written as the proportional increase in the friction factor caused by the presence of the solids in the flow:

$$(i_m - i)/i = (f_m - f)/f = (f_m/f) - 1 \quad (14)$$

The excess friction factor, $(f_m/f) - 1$, is a function of the concentration of solids, characteristic particle size, flow velocity of the mixture, pipe diameter, density and viscosity of the carrier fluid, the density of the solids, and the gravitational attraction and may be written as:

$$(f_m/f) - 1 = G(C_v, d_c, V_m, D, \rho, \mu, \rho_s, g) \quad (15)$$

The variability of the specific gravity of the chips and its proximity to unity allowed the ratio of the density of the solids to the density of the water to be taken as unity; eliminating the density of solids from the

functional relation of Eq. (15). It should also be noted that the effect of wall roughness is included indirectly through the evaluation of the friction factor for clear water flows. The characteristic chip size, d_c , is calculated as the square root of the sum of the squares of the weighted mean chip dimensions indicated in Table 2. The ratio of the characteristic chip dimension to the pipe diameters, k , ($k=d_c/D$), is used as the particle-to-pipe size ratio.

Including the kinematic viscosity, ν , ($\nu=\mu/\rho$) in the list of independent variables in place of the dynamic (absolute) viscosity, μ , and the fluid density, ρ , reduces the dimensions of all the independent variables to kinematic terms, length and time. This permits the excess friction factor to be expressed as a function of four dimensionless parameters which may be written as:

$$(f_m/f) - 1 = G_1[(V^3/\nu g), (D^{1.5}g^{0.5}/\nu), C_v, (d_c/D)] \quad (16)$$

In the selection of a mathematical model for fitting the data to a single equation including all four of the dimensionless groups of Eq. (16), the concentration and particle-to-pipe size ratio were modified to satisfy the following boundary conditions:

1. the friction factor for the mixture should be identical with that of clear water when the concentration is zero and should approach an infinite value when the concentration of solids approaches unity (a condition depicting a solid plug in the pipeline); and
2. the friction factor of the mixture containing a given concentration of solids should increase with an increase in the particle-to-pipe size ratio, k , approaching an infinite value as a limit when k approaches unity, and should decrease as the particle-to-pipe size ratio decreases approaching a value independent of the particle size as k approaches zero.

The model selected to meet the above-stated conditions is given as:

$$\frac{f_m}{f} - 1 = A_1 \left(\frac{V_m}{Vg}\right)^{x_1} \left(\frac{D^{1.5} g^{0.5}}{V}\right)^{x_2} \left(\frac{C}{1-C}\right)^{x_3} + x_4 \ln(1-k) \quad (17)$$

where the coefficient A_1 and the exponents x_1 , x_2 , x_3 , and x_4 are determined by a regression analysis for the curve of best fit applied to the experimental data.

4.2.4 Evaluation of correlation model. A total of 922 data points were used in evaluating the coefficient and exponents of Eq. (17); 485 were recorded in the tests performed for the pilot line investigations of energy losses in wood-chip pipelines at Montana State University, including 342 for the nominal 8-in.-dia (200-mm-dia) pipe and 121 for the nominal 12-in.-dia (300-mm-dia) pipe. The range of parameters in the pilot line studies are shown in Tables 3 and 4 along with a summary of the 437 data points from previous investigators. Other data in Table 3 will be discussed in a subsequent section.

Analysis of data. The analytical methods used in evaluating the coefficient and exponents in Eq. (17) and in determining its accuracy are outlined in the following paragraphs.

A friction factor for the mixture was calculated from the energy loss and flow velocity recorded for each data point using the Darcy-Weisbach equation

$$f_m = 2gDh_m / V_m^2 L \quad (18)$$

The friction factor for a clear water flow of the same velocity was calculated for each run using either the Colebrook-White formula, Eq. (10),

Table 3. Properties of pipes and solids for evaluation of friction factor model

Name (location)	Pipe diameter, mm (in.)	Pipe type	Solids type	Specific gravity, solids	Particle-to-pipe size ratio, k
(1)	(2)	(3)	(4)	(5)	(6)
1. Hunt (MSU)*	314.3 (12.375)	steel	wood	1.00- 1.05	.098
2. Hunt (MSU)*	208.5 (8.212)	steel	wood	1.00- 1.05	.150
3. Gow (MSU)	148.9 (5.864)	alumi- num	wood	1.00- 1.05	.206
4. Gow (MSU)	100.0 (3.938)	acrylic	wood	1.00- 1.05	.307
5. Faddick (MSU)	100.0 (3.938)	acrylic	plastic	1.04	.161
6. Johnson (MSU)	100.0 (3.938)	acrylic	plastic	1.04	.161
7. Faddick (MSU)	100.0 (3.938)	acrylic	plastic	0.92	.161
8. Faddick (MSU)	76.2 (3.000)	acrylic	plastic	1.04	.211
9. Faddick (MSU)	76.2 (3.000)	acrylic	plastic	0.92	.211
10. Elliott (PPRIC)	213.7 (8.412)	alumi-	wood	1.00- 1.05	.149
11. Soucy (Laval)	152.4 (6.000)	acrylic	wood	1.15	.209
12. Faddick (Queen's)	102.3 (4.026)	alumi-	wood	1.13	.312

*Pilot line tests

for the data points obtained from tests on the steel pipes and using the smooth pipe resistance equation of Nikuradse [12],

$$1/\sqrt{f} = 2\log_{10}(\text{Re}_w \sqrt{f}) - 0.8 \quad (19)$$

for the tests conducted in aluminum and acrylic pipes.

Using the expression for the excess friction factor, $(f_m/f) - 1$, as the dependent variable "Y" and the four dimensionless groups, $(V_m^3/\nu g)$, $(D^{1.5}g^{0.5}/\nu)$, $(C/1-C)$ and $(1-k)$ as independent variables Z_1 , Z_2 , Z_3 , and Z_4 , respectively, Eq. (17) is expressed as a linear equation:

$$\log Y = \log A_1 = x_1 \log Z_1 + x_2 \log Z_2 + x_3 \log Z_3 + x_4 (\log Z_3)(\ln Z_4) \quad (20)$$

The linearization and the evaluation of the Y and Z terms for each data point allowed the coefficient A_1 and the exponents x_1 , x_2 , x_3 , and x_4 to be calculated using a step-wise regression analysis developed for biomedical research at the University of California at Los Angeles (Dixon, 1967).

Mixture friction factor. The resulting equation for calculating the friction factor of mixtures of wood chips and water is

$$\frac{f_m}{f} - 1 = 197 \left(\frac{V_m^3}{\nu g} \right)^{-0.988} \left(\frac{D^{1.5}g^{0.5}}{\nu} \right)^{.647} \left(\frac{C}{1-C} \right)^{.838} + .930 \ln(1-k) \quad (21)$$

when the first two parameters on the right hand side are combined,

Eq. (21) becomes

$$\frac{f_m}{f} - 1 = 197 \left(\frac{D^{.970}g^{1.312}V_m^{.342}}{\nu^{2.964}} \right) \left(\frac{C}{1-C} \right)^{.838} + .930 \ln(1-k) \quad (22)$$

The accuracy of Eq. (22) is summarized in Table 4 giving the standard deviation of the curve fit for the data of each investigator and the percentage

Table 4. Summary of range of experimental data and accuracy of friction factor

Name (pipe, dia- meter, mm)	Concen- tration, %	Velocity range, m/sec (ft/sec)	No. of observed points, N_o	No. of accepted points, N_a	Standard deviation, σ %	Accuracy of model,** % of points		
						$\epsilon < 5\%$	$< 15\%$	$< 25\%$
	(7)	(8)	(9)	(10)	(11)	(12)	(13)	(14)
1. Hunt (314)	0-26	0.64-1.34 (2.1-4.4)	143	86	14.9	31	69	90
2. Hunt (208)	7-26	0.94-3.35 (3.1-11.0)	342	341	12.3	38	71	97
3. Gow (149)	9-20	0.88-1.31 (2.9-4.3)	53	16	23.9	0	19	88
4. Gow (100)	9-24	1.74-2.90 (5.7-9.5)	47	39	5.8	64	97	100
5. Faddick (100)	9-32	0.79-3.05 (2.6-10.0)	95	87	12.4	32	77	97
6. Johnson (100)	10-20	1.22-3.05 (4.0-10.0)	28	28	14.4	39	79	86
7. Faddick (100)	9-27	0.82-2.41 (2.7-7.9)	68	57	11.5	54	79	96
8. Faddick (76)	10-27	1.28-2.77 (4.2-9.1)	23	23	6.8	56	100	100
9. Faddick (76)	7-26	1.52-2.44 (5.0-8.0)	29	29	6.0	62	100	100
10. Elliott (214)	10-30	1.16-3.45 (3.8-11.3)	29	27	14.8	37	63	96
11. Soucy (152)	9-20	0.91-3.17 (3.0-10.4)	41	41	10.4	34	93	100
12. Faddick (102)	7-17	1.55-2.59 (5.1-8.5)	24	21	18.7	0	43	100
Total			922	795	12.1	38	75	96

**Based on 795 accepted data points

of data points whose calculated values are within 5, 15 and 25 percent of those observed based on the difference ϵ , in percent, calculated as

$$\epsilon = [(f_{\text{calc}}/f_{\text{obs}}) - 1] \times 100 \quad (23)$$

The percent standard deviation is

$$\sigma = \sqrt{\sum \left(\frac{f_{\text{calc}}}{f_{\text{obs}}} - 1 \right)^2 / (N-m-1)} / f_{\text{obs}} \quad (24)$$

where N = number of observations

m = number of degrees of freedom, 4.

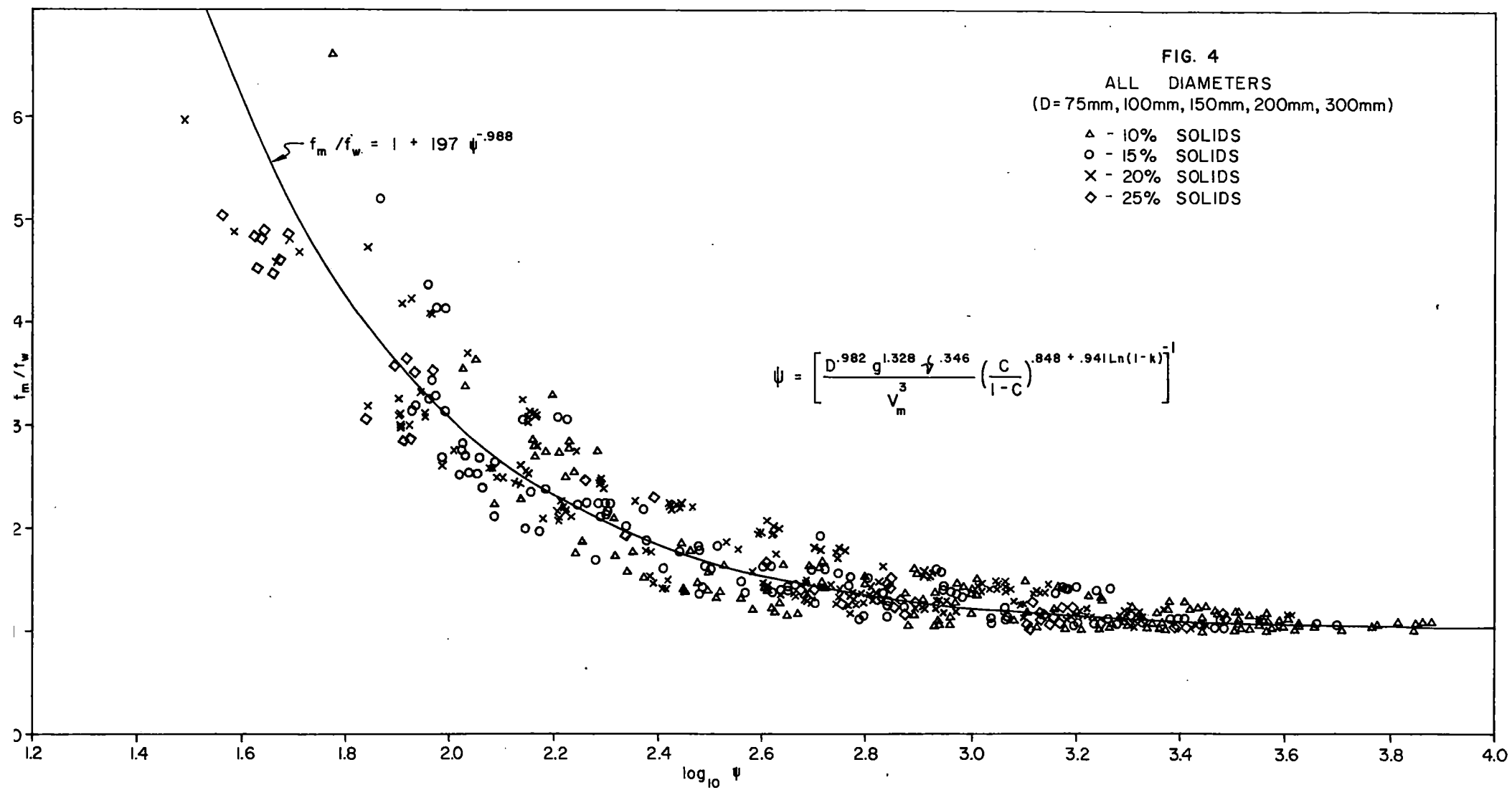
The number of accepted data points given on col. 10 of Table 4 indicates all those not rejected as outliers at the 5 percent level of significance as determined from the relation.

$$\frac{f_{\text{obs}} - f_{\text{cal}}}{\sigma f_{\text{cal}}} > 2 \quad (25)$$

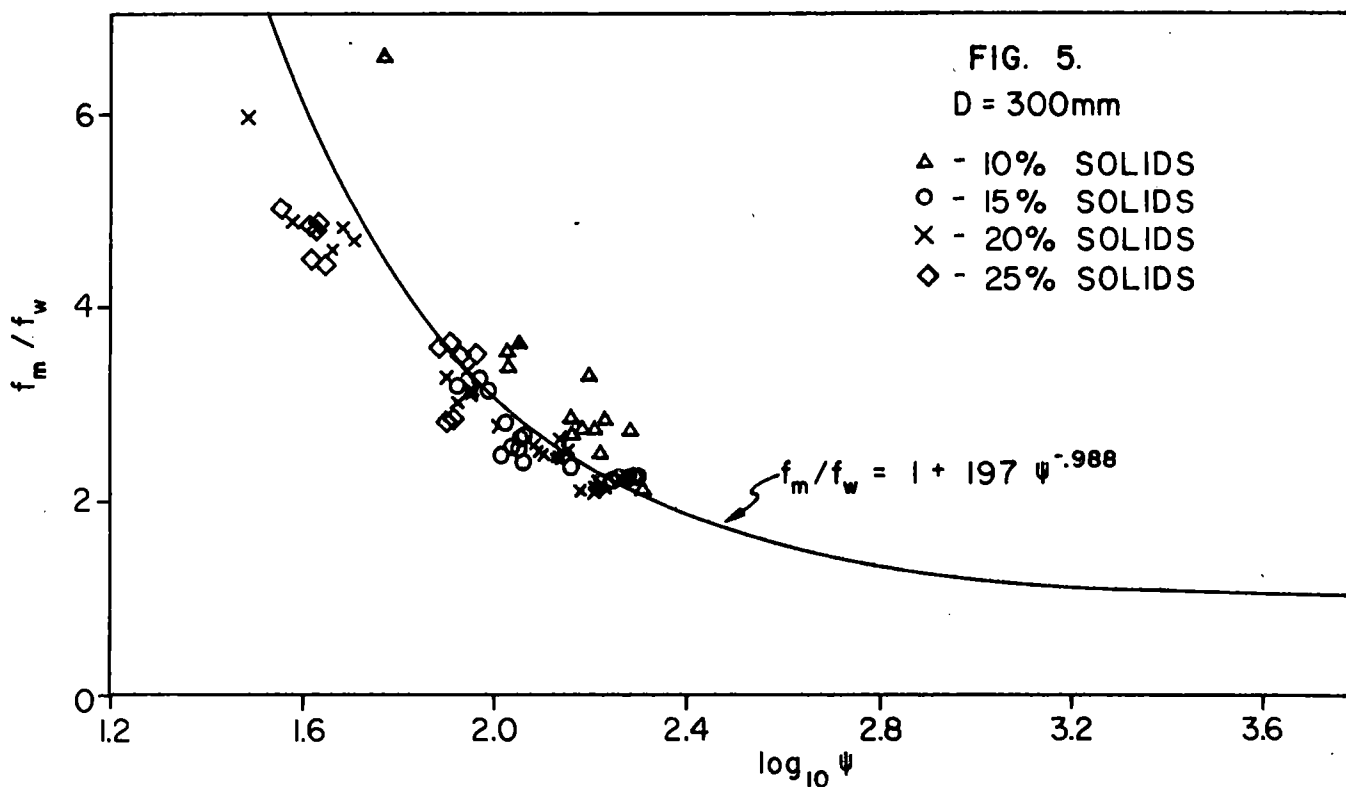
Table 5 shows the percent standard deviation of observed friction factors from those calculated using Eq. (22) according to pipe diameter and concentration of wood chips.

Table 5. Percent standard deviation between observed and calculated friction factors by concentrations and pipe diameters

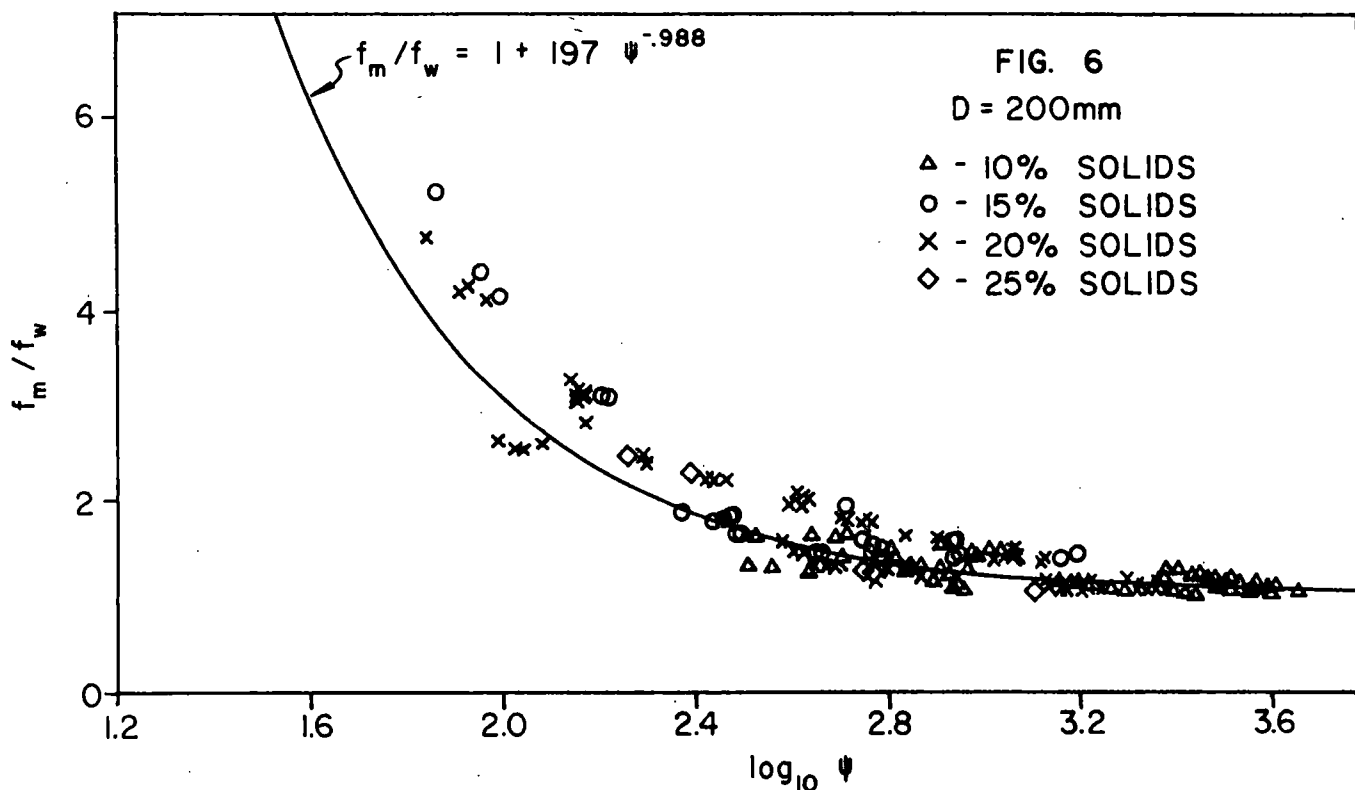
Pipe diameter class, mm	Concentration of solids					All Conc.
	10%	15%	20%	25%	30%	
300	22.7	8.3	11.1	19.7	--	14.7
200	9.8	10.0	15.1	10.4	16.6	12.3
150	14.4	14.2	13.4	--	--	13.7
100	12.1	12.6	10.7	8.1	18.0	11.6
75	4.6	5.9	4.4	10.3	--	5.8



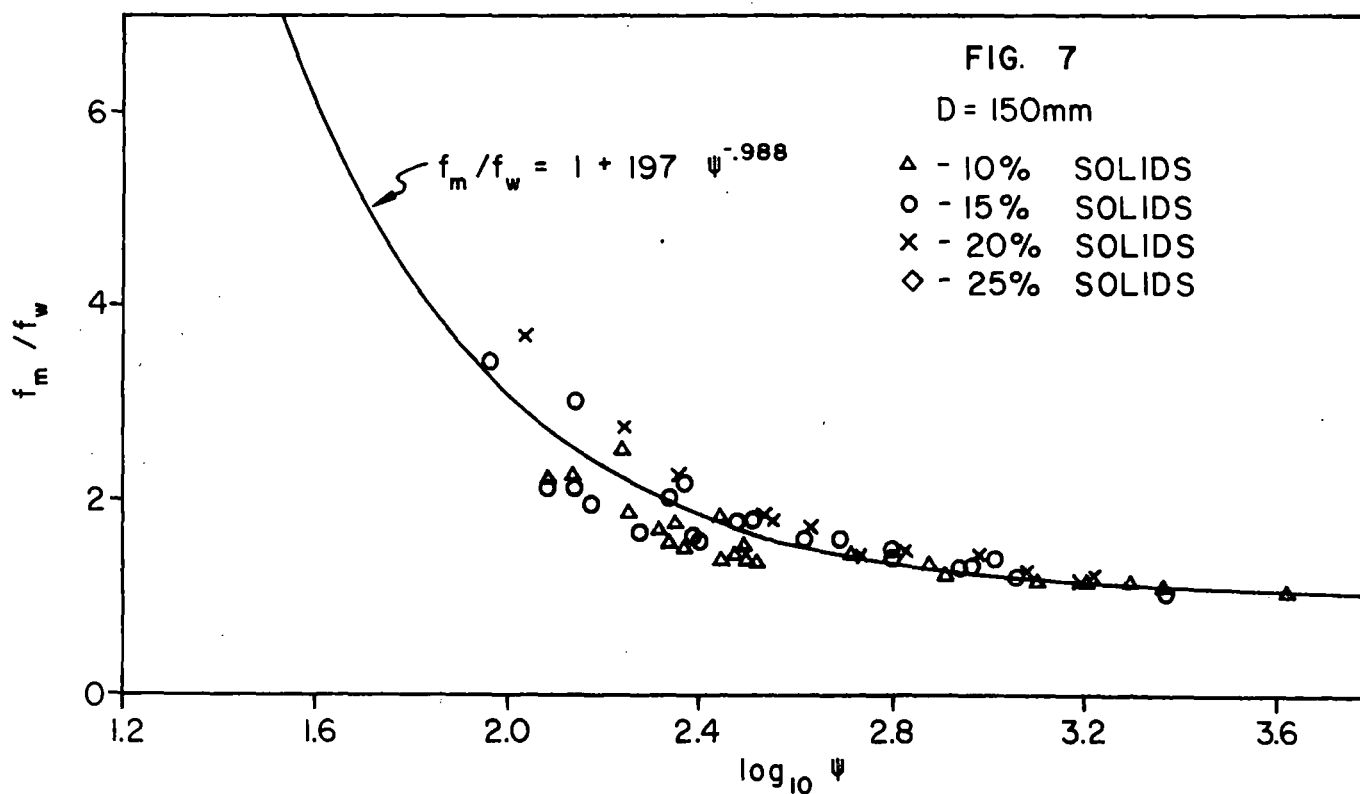
FRICITION FACTOR RATIO FOR MIXTURES OF WOOD CHIPS AND WATER.



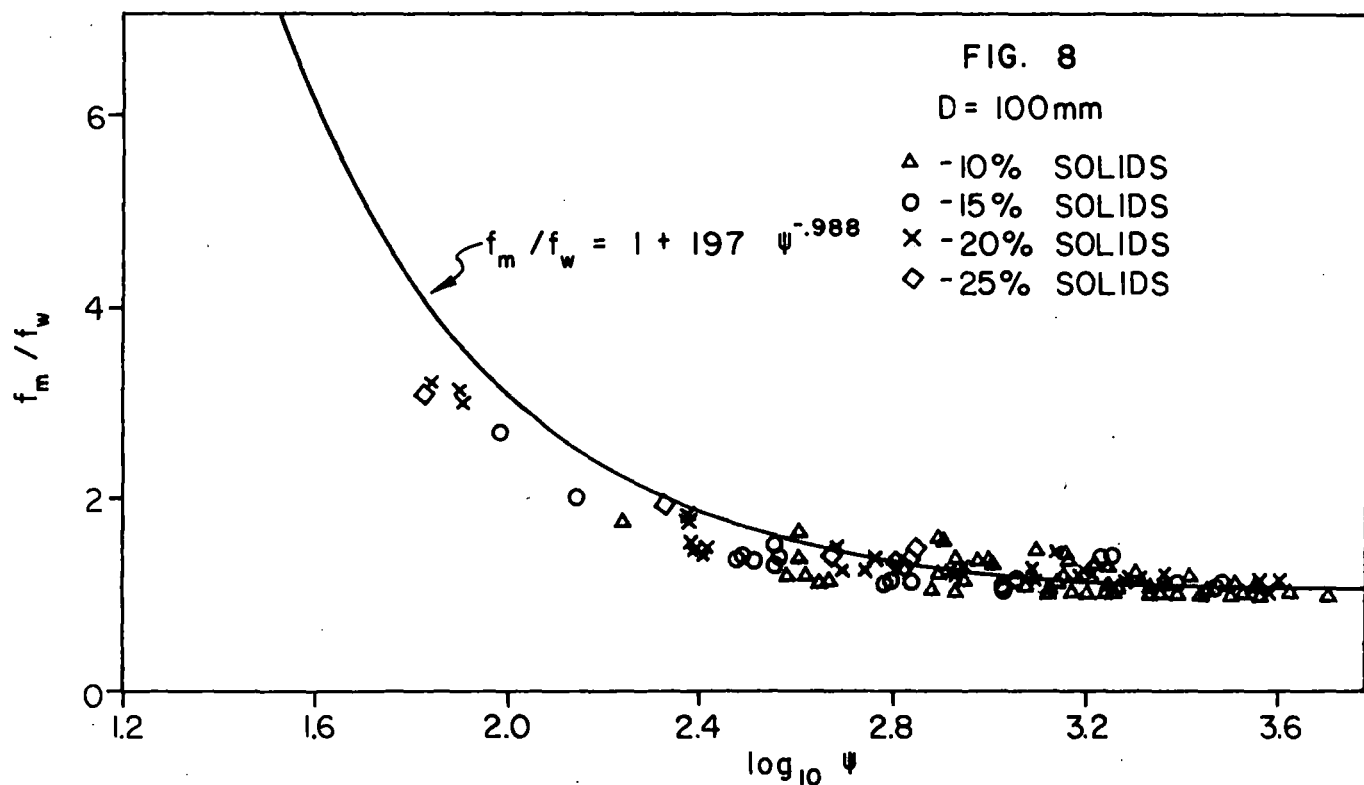
FRICITION FACTOR RATIO FOR MIXTURE OF WOOD CHIPS AND WATER.



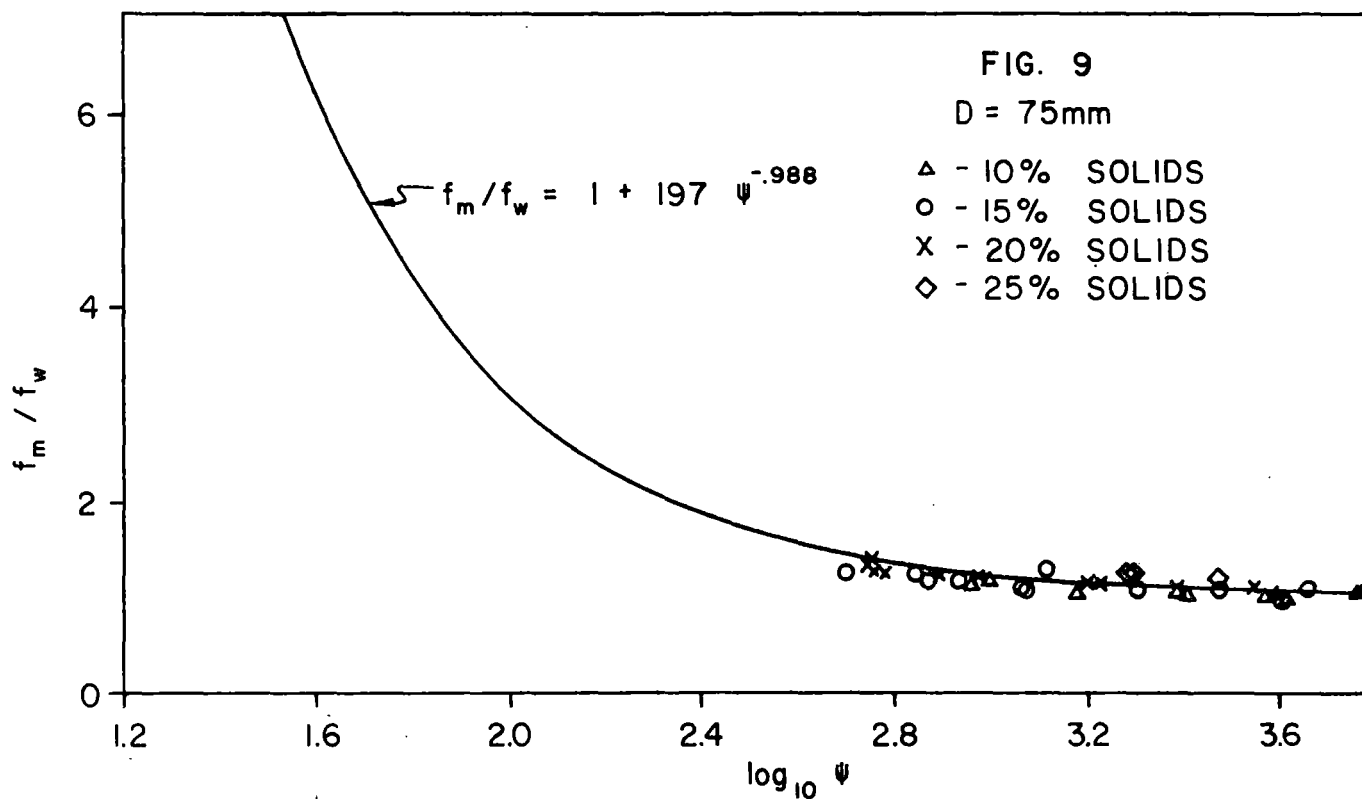
FRICITION FACTOR RATIO FOR MIXTURE OF WOOD CHIPS AND WATER.



FRICITION FACTOR RATIO FOR MIXTURES OF WOOD CHIPS
AND WATER.



FRICITION FACTOR RATIO FOR MIXTURES OF WOOD CHIPS
AND WATER.



FRICTION FACTOR RATIO FOR MIXTURES OF WOOD CHIPS
AND WATER.

Graphs in Figs. 4-9, inclusive, show the ratio of the mixture friction factor to that for clear water, f_m/f , given as a function of the dimensionless parameter

$$\psi = \left[\frac{D^{.982} g^{1.328} v^{.346}}{V_m^3} \left(\frac{C}{1-C} \right)^{.848 + .941 \ln(1-k)} \right]^{-1} \quad (26)$$

for the pipes of the different diameters and for the different concentration of wood chips. A composite of the results from all investigators is given by concentration classes in Fig. 4. The data from all studies for each diameter of pipe are shown in Figs. 5-9. Instabilities noted while observing the data for the tests conducted on the 12-in.-dia (300-mm-dia) pipes are reflected by the dispersion of points about the curve of Eq. (21) in Fig. 5. An examination of the differences between the calculated and experimental friction factors for all the data points of the individual investigators for the 6- and 8-in.-dia (200- and 150-mm-dia) pipes indicates the distribution of points with respect to the curves and Figs. 6 and 7 may be caused by the differences in the experimental methods employed. The apparent independence from the specific gravity for the friction factors of mixtures of wood chips and water is further substantiated by the graph for the 4-in.-dia (100-mm-dia) pipe (Fig. 8) which includes data from both types of plastic chips and data on wood chips from two different investigators. The graph for the 3-in.-dia (75-mm-dia) pipe (Fig. 9) includes the data from plastic chips of two specific gravities, 0.92 and 1.05, and indicates that the effects of particle density are not significant in this range of specific gravities.

The data summarized in Tables 4 and 5 and indicated on Figs. 4-9 show that the energy loss due to friction in pipelines transporting wood chips

may be determined by calculating a friction factor for the mixture from the equation

$$\frac{f_m}{f} - 1 = 197 \left(\frac{D^{.970} g^{1.312} v^{.342}}{v_m^{2.964}} \right) \left(\frac{C}{1-C} \right)^{.838 + .930 \ln(1-k)} \quad (27)$$

which (1) includes the effects of concentration of solids, the particle-to-pipe size ratio, and the viscosity of the carrier water, (2) reduces to the friction factor for clear water when the solids concentration approaches zero, (3) gives values with a standard deviation of 12 percent from data observed on pipes of 3-, 4-, 6-, 8-, and 12-in. (75-, 100-, 150-, 200-, and 300-mm) diameters. The method and correlation presented is valid only for neutrally-buoyant, chip-shaped particles and may be employed without resorting to laboratory tests for confirming mixture properties.

4.3 Pump Performance

The performance of the pumps is one of the most important factors in the successful operation of any liquid, slurry or solids-handling pipeline. In addition to the determining the effects of wood chips on the performance characteristics of the pumps, a feasible method for operating booster pump stations along long pipelines must be established. The pump performance characteristics of the mainline pump and the feasibility of an off-line booster pump were investigated and are discussed in the following paragraphs.

4.3.1 Mainline pump. Data for determining the performance characteristics of the mainline pump of the pilot line were recorded for all friction loss test points. The mainline pump was 10-in. (25-cm) type CBE centrifugal

pump manufactured by the Barrett-Haentjens Company and installed with an 18-in. (45-cm), 3-blade, model P3998-3-10142 impeller powered by a 150-hp, (115-kw) 500-v, D-C motor supplied by the A. O Smith Corporation.

The hydraulic pumping head developed by the pump was measured by a 140-inch (356-cm) mercury-water differential manometer connected to the pipeline on the suction and discharge sides of the pump. The pump speed, voltage and amperage into the pump motor, the volumetric flow rate through the pump and the concentration of wood chips were recorded for each test point. A series of ten points were observed for each flow rate. The flow rate in the pipeline was controlled by varying the rotational speed of the pump. The performance characteristics of the mainline pump are summarized in Figs. 10 and 11.

The relationship between pumping head required for different concentrations of wood chips and the discharge (volumetric flow rate) is given for the pilot line set up for 2345 ft (715 m) of 8 5/8-in.-dia (208-mm-dia) pipe in Fig. 10 and for 1545 ft (471 m) of 8 5/8-in.- and 800 ft (244 m) of 12-in.-dia. (300-mm-dia) pipe in Fig. 11. The data for the tests with clear water in the configuration with both 8 5/8-in.- and 12-in.-dia pipes is also shown in Fig. 11.

These figures indicate the following factors affecting pump selection:

1. As the concentration of wood chips in a pipeline increases, the volumetric flow rate decreases for a pump operating at a given rotational speed. For example, at 1075 rpm the discharge is 1725 gpm ($0.109 \text{ m}^3/\text{s}$) with clear water and only 1425 gpm ($0.090 \text{ m}^3/\text{s}$) with a mixture containing approximately

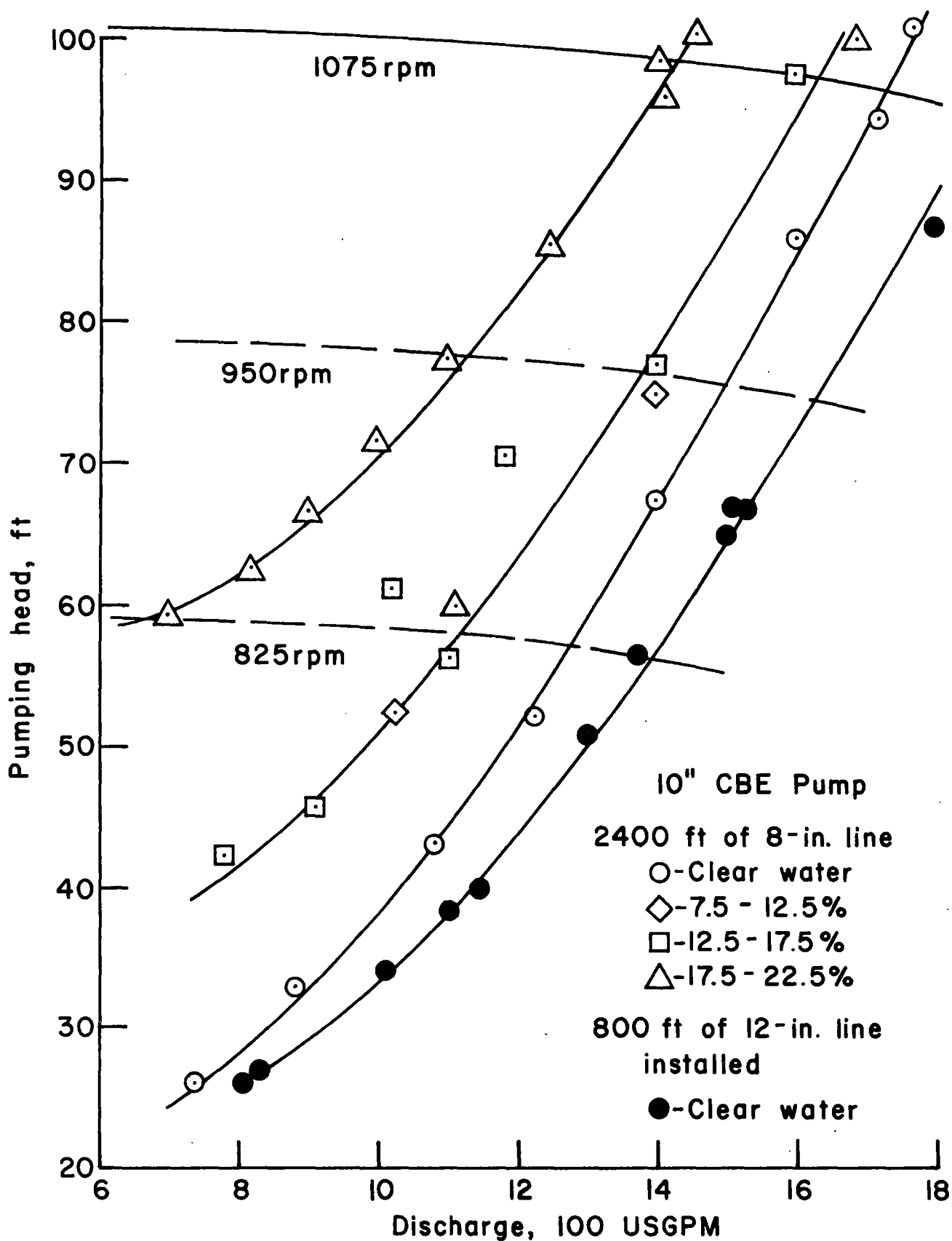


FIG. 10: PILOT LINE SYSTEM HEAD CURVES

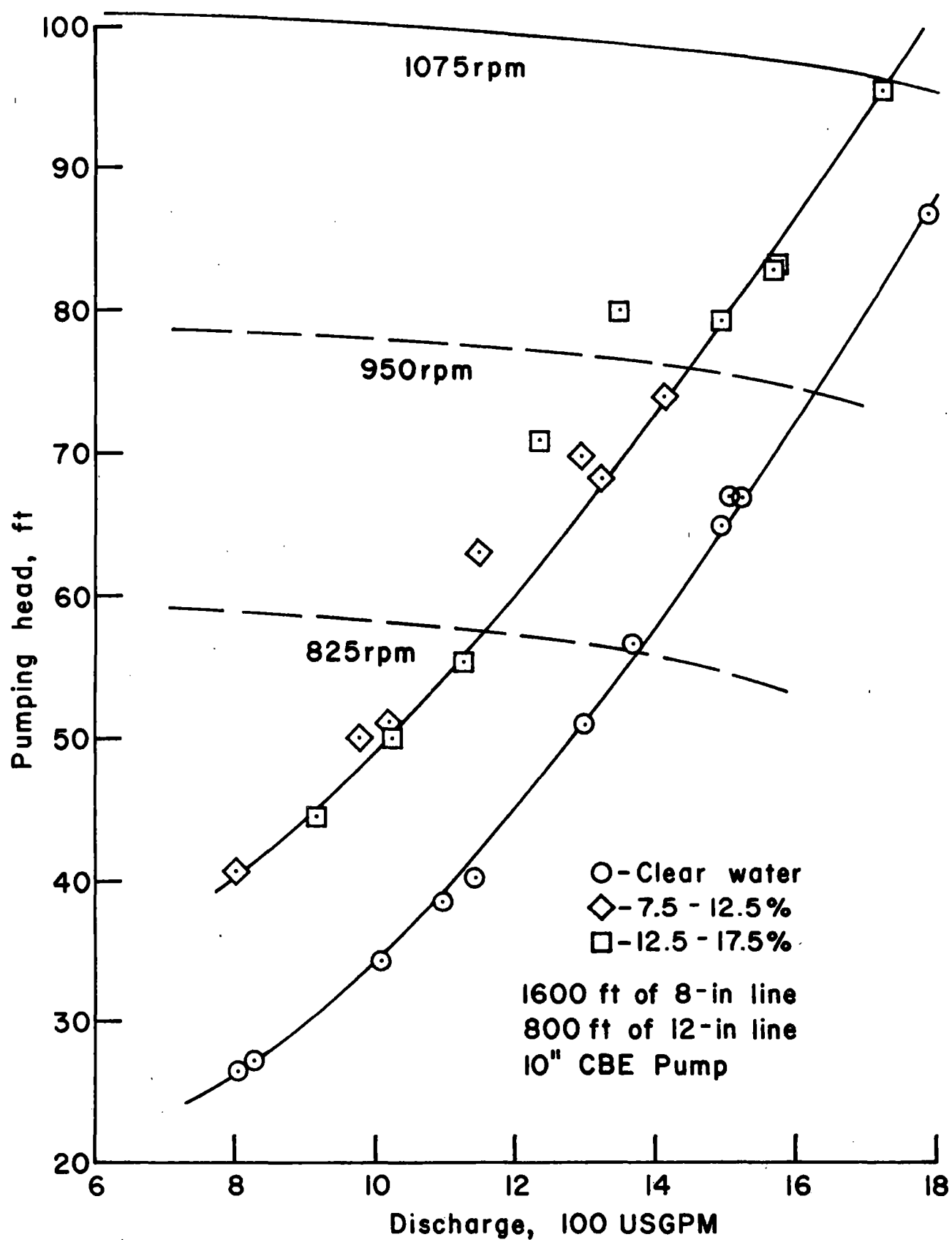


FIG. II: PILOT LINE SYSTEM HEAD CURVES

20 percent concentration of wood chips in 2345 ft (715 m) of 8 5/8-in.-dia (208-mm-dia) pipe. The difference between the flow rate of clear water and that of a mixture carrying flow rate of a given concentration of wood chips becomes greater as the pump speed is reduced.

2. For a given flow rate, the pumping head required and the rotational speed of the pump increase with the increase in the concentration of wood chips transported by the mixture. For example, the pumping head and pump rotational speed requirements for a flow rate of 1100 gpm ($0.069 \text{ m}^3/\text{s}$) are 44.5 ft (13.57 m) at 769 rpm for clear water, 57.8 ft (17.62 m) at 825 rpm for 10-15 percent wood chips, and 77 ft (23.48 m) at 950 rpm for 20 percent wood chips.

The effects may be predicted by using the energy loss correlation of Eq. (27) to calculate the pumping head requirements for different flow rates for a given concentration for any proposed installation to obtain points on a "system head curve". The operating point of any pump is determined by superimposing the system-head curve over the head-discharge characteristic curves obtained for a pump from the manufacturer.

The head-discharge characteristic curves for a given pump is obtained by operating the pump at a constant rotational speed and determining the head developed by the pump for several different flow rates. The curves for other rotational speeds are then determined analytically by the pump similarity laws:

$$Q_n = Q_0 (N_n/N_0) \quad (28)$$

$$H_n = H_0 (N_n/N_0)^2 \quad (29)$$

These relations indicate a single curve giving the reduced head, H/N^2 , as a function of the reduced discharge, Q/N , may be used to represent the characteristics of a centrifugal pump for a given liquid or a given mixture. Pump manufacturers have ascertained that the similarity laws, Eqs. (28) and (29), are only approximate for pump speed ratios greater than 1.5 to 1.0 and for impellers having velocity components in the axial direction. The change of rotational speed of a pump alters the internal flow patterns within the impeller thereby causing minor variations in the pump efficiency for different rotational speed.

The effect of wood chips ranging in concentration from 7.5 to 22.5 percent by volume on the pump performance was examined by graphing the reduced pump head and pump efficiency as functions of the reduced discharge for the test data and comparing the results with the reduced head and efficiency curves based on the data supplied for clear water tests conducted by the manufacturer.

These data presented in Fig. 12 indicate the wood chips have no appreciable effect on the head-discharge characteristics of the pump with the 3-vaned impeller provided as 80 percent of the test data were within 2 percent of the manufacturer's curve developed with clear water. This is well within the range of random experimental errors based on the minimum scale reading of the tachometer used to measure the rotational speed of the pump.

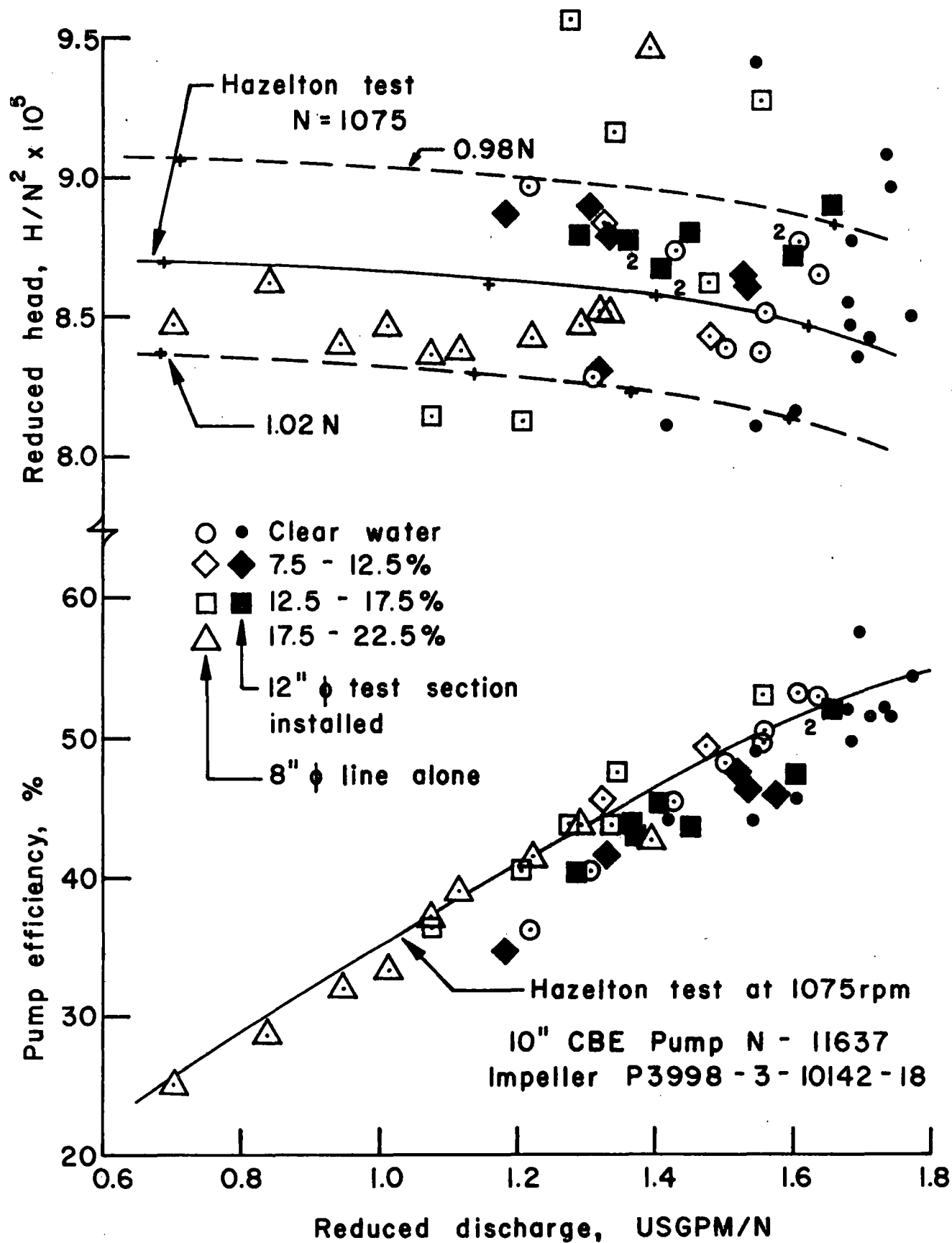


FIG. 12: PUMP CHARACTERISTICS

The pump efficiency for 70 percent of the test points was within 7 percent of that given by the manufacturer for tests conducted with clear water for the pump operating at a rotational speed of 1075 rpm. The random scatter of data for observed test points for both clear water and wood chips mixtures alike indicates the presence of wood chips in the mixture being pumped had no appreciable effect on the pump efficiency for the 3-vaned impeller used.

The negligible effects of the wood chips on the head-discharge characteristics and the efficiency of the 10-in. (250-mm) mainline pump are consistent with the findings of Page (1966) in tests conducted with simulated wood chips on 3-, 4-, and 5-in. (75-, 100-, and 125-mm) pumps supplied by three different manufacturers.

4.3.2 Off-line booster pump. Booster pumps are placed in pipelines to provide the hydraulic head to overcome loss in head caused by friction and changes in elevation. Pipelines subjected to fluctuations in the volumetric flow rate are designed with booster pump stations which may be bypassed during periods of low flow rates when the head losses caused by frictional pipe resistance are significantly less than those during high flow periods. Oil products lines, municipal water systems and sewage collection lines operating as forced mains are examples of pipelines with off-line booster pumps.

A series of tests was conducted to investigate the feasibility of operating an off-line booster pump in a wood-chip pipeline. A Barrett-Haentjens 5-in. (125-mm) type CTL centrifugal pump was installed approximately 160 ft (48.8 m) upstream from the discharge end of the pilot

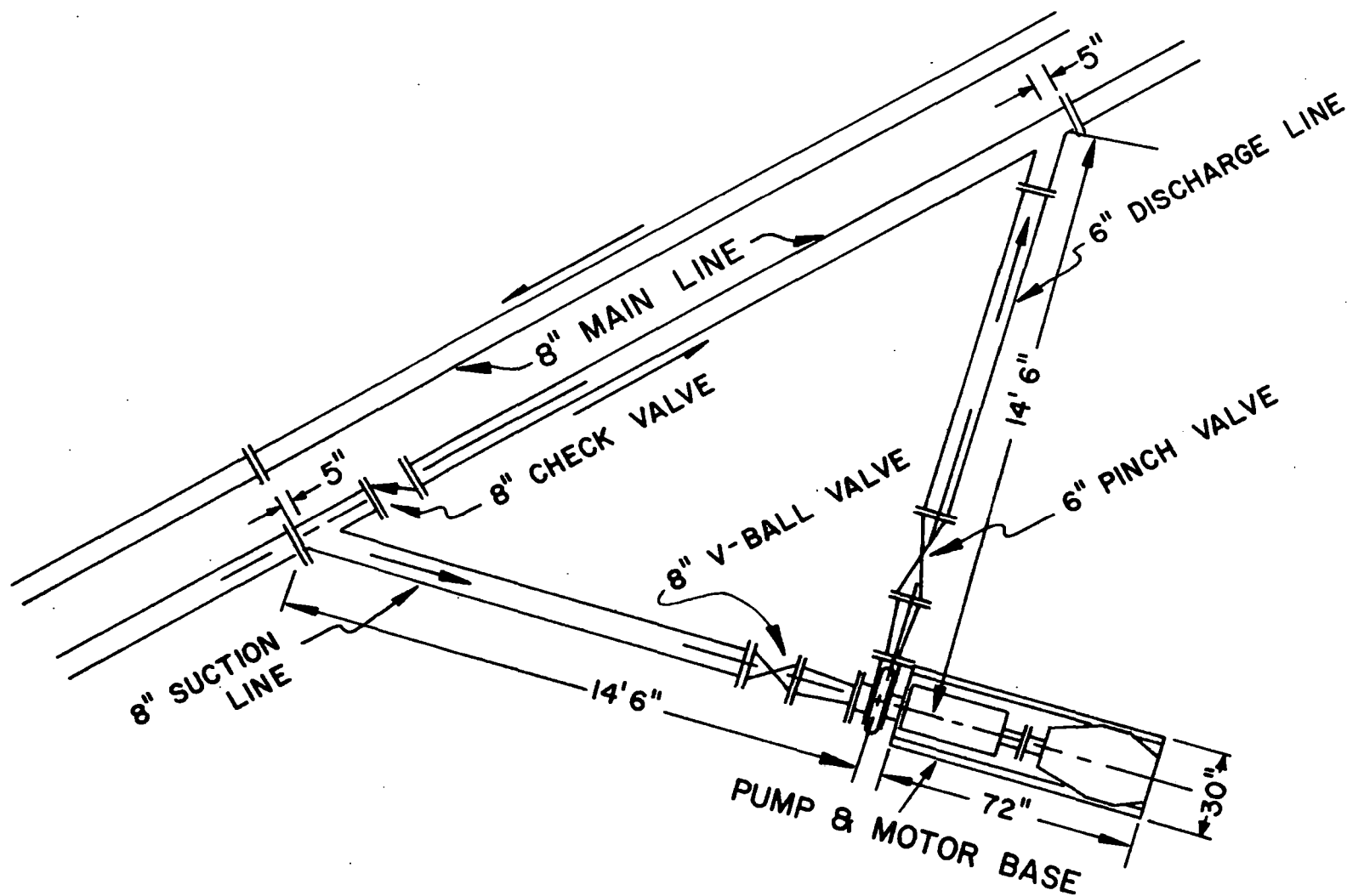
line to simulate a remote controlled off-line booster pump station. A schematic diagram of the installation is shown in Fig. 13. The pump was powered by a Westinghouse 25-hp (20-kw) type SK D-C motor obtained from U.S. Navy surplus. The motor was operated from a General Electric 50-kw silicon D-C power supply through a magnetic timestarter; motor speed was controlled by a rheostat. Both the pump and motor had been used in previous wood-chip pipeline studies (Page, 1966; Johnson, 1968; Faddick, 1970; Gow, 1971) and were available although not the appropriate choice for a prototype installation.

A 6-in. (150-mm) Massco/Grigsby low pressure pinch valve and an 8-in. (200-mm) Fisher type 478-E V-ball were installed in the discharge and suction lines, respectively, of the off-line booster pump test station. Both valves were actuated by air-operated positioners. The check valve in the main line was uncontrolled and was operated solely by the direction of the pressure gradient across the valve.

The suction and discharge valves and the rotational speed of the booster pump were all electrically controlled from the pilot line control center.

The series of tests conducted included six flow rates with clear water to establish the test procedure and establish baseline data for the response of the pilot line system and four flow rates with low concentrations (8-12 percent) of wood chips being transported.

The procedure for conducting the tests was as follows. The flow rate for clear water within the range of operation of the booster pump was established in the 8 5/8-in.-dia (208-mm) test line with the booster pump



SCALE - 1" = 4'

FIG. 13. OFF-LINE REMOTE BOOSTER PUMP STATION.

off and the suction and discharge valves in the by-pass line closed. The flow rate, head loss in the pipeline test section upstream from the by-pass, the differential head across the booster pump (pressure connections made upstream from the suction valve and downstream from the discharge valve) and the differential across the mainline pump were observed. The booster pump was turned on (if initially off), the suction valve and discharge valves were opened (in the sequence given). The above-listed data observations were noted again and compared with the data taken with the suction and discharge valves closed. The difference between the data observed when the booster pump was in an operating mode and when it was not in the operating mode with clear water indicated all the mainline flow was passing through the booster pump. The test was completed by closing the discharge and suction valves in the booster pump by-pass line and recording the data. The observations indicated that the flow conditions returned to those prevailing in the system prior to the test.

Flow conditions observed with clear water during a 3-run test series are given in columns 1-6 of Table 6. The paired data (1A and 1B, 2A and 2B, etc.) show how the system responds when the mainline pump is held at a constant rotational speed with the booster pump in operating and non-operating modes. When the booster pump is functioning correctly in the operating mode, the following conditions occur. The flow rate increases as the head on the mainline pump decreases slightly, following the characteristic curve of the pump for a constant speed. The head developed across the booster pump increases significantly over that in the off-line mode. (The negative head observed for the non-operating mode indicates the

Table 6. Operation of off-line remote booster pump

Test run	1A	1B	2A	2B	3A	3B	4A	4B	5A	5B	6A	6B	7A	7B
	(1)	(2)	(3)	(4)	(5)	(6)	(7)	(8)	(9)	(10)	(11)	(12)	(13)	(14)
Flow rate, UGGPM	702	895	807	925	902	981	994	1021	795	862	1036	1042	1199	1208
Concentration, %	0	0	0	0	0	0	8.5	8.5	10.0	10.0	11.0	10.5	10.7	13.4
<u>Mainline Pump</u>														
Head	28.2	27.1	33.1	32.6	38.0	37.6	42.1	41.6	32.1	31.8	56.4	57.2	68.4	67.7
RPM	840	840	910	910	980	980	1000	1000	870	870	1170	1170	1290	1290
<u>Remote Pump</u>														
Mode ^a	OFF	ON	OFF	ON	OFF	ON	OFF	ON	OFF	ON	ON	OFF	OFF	ON
Head ^b	-0.8	+9.5	-0.8	+6.9	-0.8	+3.2	-0.9	-0.5	-0.6	+2.8	-0.8	-1.4	-1.0	-1.4
RPM	800	760	785	740	810	770	880	820	900	840	1020	1060	880	880
<u>Head Loss in</u>														
<u>Mainline</u> ^c ft/100 ft	0.703	0.982	0.908	1.161	1.117	1.429	1.288	1.518	0.883	1.042	1.960	2.025	2.454	2.454

a - "Off" is condition with suction and discharge valves closed, "on" is with both valves open

b - Differential pressure head between a point upstream from the suction valve and one downstream from discharge valve in booster pump line

c - Measured in nominal 600-ft test section ending approximately 40 ft upstream from junction of main line with suction line to booster pump line

pressure head upstream from the suction valve is greater than that just downstream from the discharge valve; i.e., the head loss through the check valve in the main line.) The head loss due to pipe friction measured in the test length immediately upstream from the booster pump station increases with the increased flow. (These data were observed as a check on the pump performance and flow data.)

The test procedure developed for checking the operation of the "off-line" booster pump was then applied when a concentration of 7-10 percent wood chips were added to the water. The results of the two 2-run test series conducted indicated that the by-pass line on the suction side of the booster pump became packed with wood chips during the non-operating mode and rendered the booster pump ineffective after the first 2-run operational tests. The second 2-run series was conducted after an 8-day shutdown to repair an operational problem on the rotating screened drum and wood-chip injection upstream.

Flow conditions observed with wood chips in the mixture during two 2-run series are given in columns 7-10 and 11-14, respectively, of Table 6. Although the data for runs 4 and 5 tend to indicate the booster pump is functioning properly, the plotting of those points on the characteristic curve of Fig. 14 shows the head differences measured between the suction and discharge valves to be significantly less than that which the pump can develop. This behavior was diagnosed to be caused by the formation of a loosely-packed plug of wood chips located between the suction and discharge valves which created a great resistance to flow and a great amount of head loss.

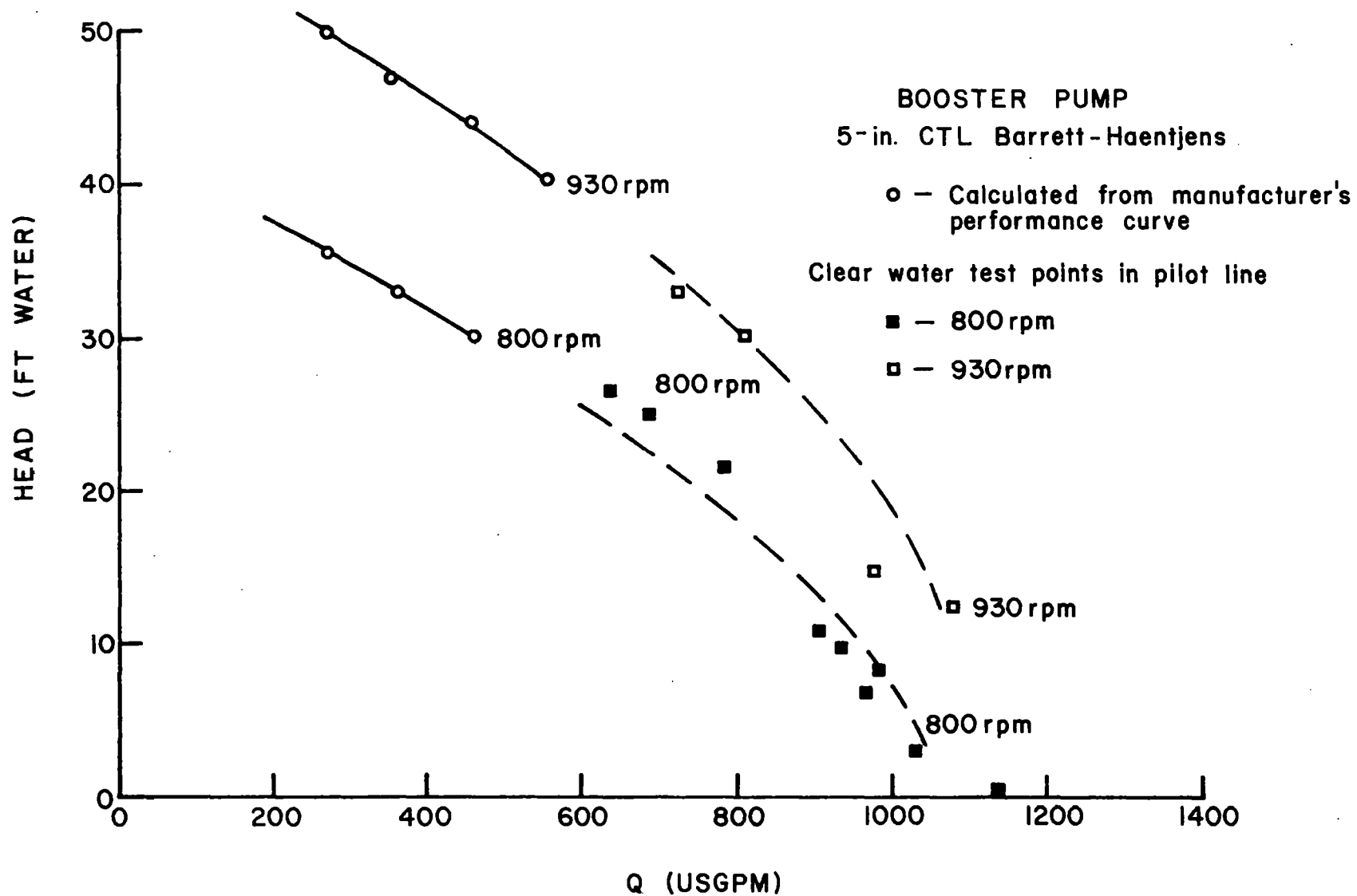


FIG. 14. BOOSTER PUMP CHARACTERISTICS.

The data of runs 6 and 7 indicate that (1) no head is effectively developed by the booster pump and (2) no flow is passing through the off-line booster pump even though the pump maintained its rotational speed. This condition was diagnosed to be caused by the formation of a tightly-packed plug of wood chips in the suction and discharge lines. This diagnosis was verified when the suction and discharge lines were disconnected.

The results of the tests conducted indicate that use of an off-line booster pump in a wood-chip pipeline system is not operationally feasible because of a tendency for blockages to form in the suction and discharge lines when the booster pump is not operating.

The alternative to an off-line booster pump for increasing the flow rate in a wood-chip pipeline system is to design the booster stations to include one or more variable speed pumps at each installation.

4.4 Monitoring and Controlling Flow Conditions

The operation of any pipeline for predetermined flow conditions over long periods of time depends on the capability of the system to (a) monitor flow parameters at different points in the line, (b) interpret the cause and effect of unplanned changes in the observed parameters at these points, and (c) alter the flow conditions to respond to the changes without adversely affecting the operation of the pipeline. The importance of designing pipelines to perform these vital functions with a high degree of reliability has long been recognized in transportation of petrochemical products and is now reaching a high level of sophistication in the water and wastewater handling industries. The necessity of monitoring, interpreting and controlling the flow conditions in pipelines transporting

solids is accentuated by the possibility of unexpected changes in flow conditions causing a blockage of the pipe to occur.

4.4.1 Pipeline supervisory systems. Oil and gas pipelines and an increasing number of water transmission and distribution systems have electronically-equipped supervisory systems installed to monitor and control the flow conditions automatically with manual interrupt capabilities. The supervisory system of any given pipeline is designed specifically for the conditions to be encountered in that given pipeline (or distribution system) during its design life. The pipeline engineer needs to recognize and understand the effects of changes, both planned and unplanned, in the flow conditions on the pipeline system to be able to work with the communication and instrumentation engineers in developing a suitable supervisory system.

The line pressure, volumetric flow rate (or the velocity of flow) and the specific gravity of the fluid are the parameters monitored in oil and gas pipelines. The specific gravity is not generally measured in water transmission and distribution systems. Monitoring the concentration of solids entering the pipeline is required in slurry systems. As these parameters are observed, they are compared with predetermined values for the flow conditions at that point in the pipeline system for that time. If the observed data are outside the acceptable limits of the normal values, a signal calling for corrective action is generated. The response to the signal occurs in the form of a change in the status of one or more control devices (usually pumps or valves). The most significant part of this process is the specification of "normal" values and "acceptable" limits of the flow parameters for given operations of the pipeline system. It is

essential that data from operating and experimental pipelines are obtained to develop these criteria. As records of previous investigations of wood-chip pipelines do not provide operation data of this sort, both steady and non-steady flow conditions were monitored in the pilot line during the study.

4.4.2 Pilot line supervisory system. The supervisory system installed in the 2345 ft (715-mm) pilot line facilities for these investigations on the hydraulic transport of wood chips was equipped with instrumentation suitable for visually monitoring the following flow conditions in the pipe system continuously:

1. pump discharge pressure;
2. volumetric flow rate of mixture of wood chips and water;
3. volumetric flow rate of make-up water;
4. differential pressure across four test lengths of pipe;
5. differential pressure head between suction and discharge sections of mainline pump;
6. rotational speed of mainline pump; and
7. input power to mainline pump.

The volumetric flow rate of the mixture, the pump discharge pressure, and the line pressures at points approximately 1500 and 2100 ft (457 and 640 m), respectively, downstream from the pump discharge were recorded continuously on a 4-channel strip chart recorder.

Flow control was effected manually by regulating the power into the D-C motor driving the mainline pump as there were no valves in the system. The required flow control was determined by the operator observing the tests.

The application of results of the data recorded and observations of changes occurring in the flow conditions in the test loop for designing supervisory equipment for wood-chip pipelines are presented in the following paragraphs.

a. Steady-state conditions. An approximation for the "normal" value of the pressure at any point in a pipeline transporting wood chip may be determined from the energy loss correlations given in Section 4.2 for various combinations of pipe diameters, wood-chip concentrations and flow rates.

The optimum design flow rate for a slurry pipeline is that which will give the minimum head loss for a given concentration of solids without causing a blockage of the pipe. An understanding of the general relationship between the energy gradient (head loss per unit length of pipe) and the mean velocity of transport for slurries, shown in Fig. 15, is the essential to the design of a slurry pipeline. The energy gradient passes through a minimum as the flow velocity decreases. The velocity at which this minimum energy loss is called the "critical" velocity and occurs when the solids in suspension begin to settle out and are transported by rolling or bouncing along the bottom (invert) of the pipe in the saltation flow regime. A further reduction in the mean flow velocity causes the quantity of solids settling out to inhibit the saltation movements and to form a bed of solids which slides along the pipe invert under the shearing action caused by the flow of the fluid relative to this "sliding bed". As the quantity of solids transported in the sliding bed increases, the probability of a blockage of the pipe increases.

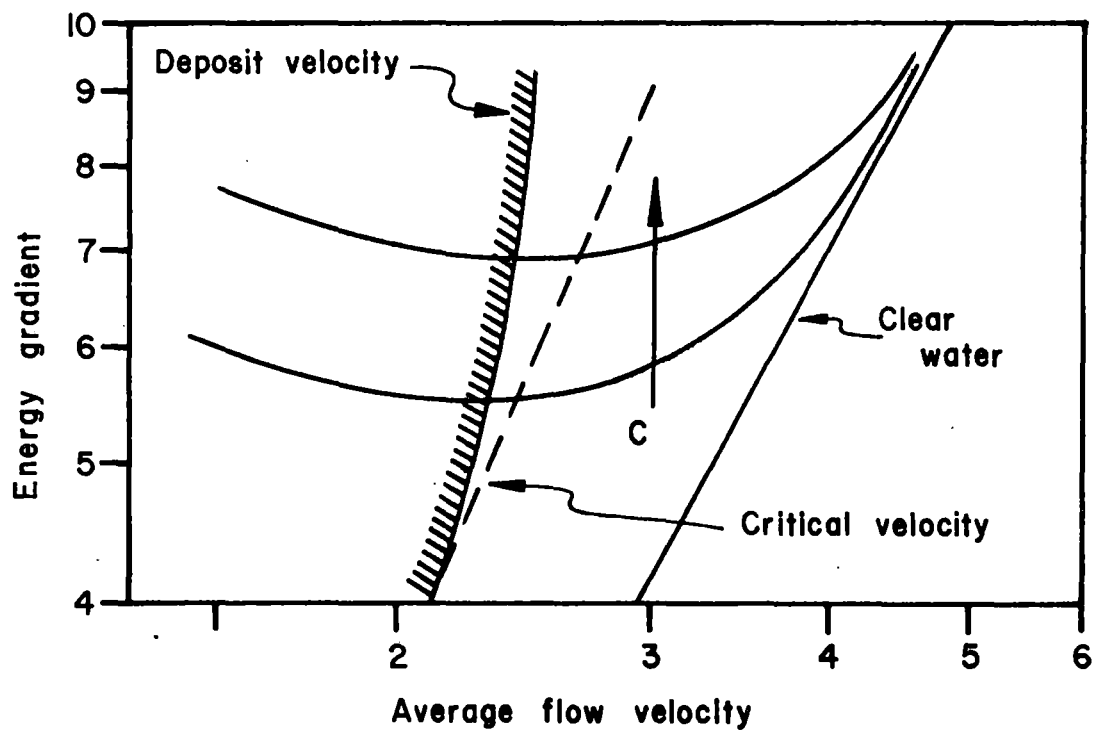


FIG. 15. ENERGY GRADIENTS IN SLURRY FLOWS.

From the foregoing discussion, it is evident that the critical velocity is the minimum safe design velocity. The critical velocity for wood-chip pipelines of a given diameter carrying a given concentration of chips are determined by a numerical differentiation procedure using Eqs. (18) and (27) as follows:

1. calculate f_m for a given velocity from Eq. (27),
2. calculate the energy loss for that velocity using a rearranged form of Eq. (18),
3. increment velocity and repeat steps 1 and 2,
4. compare energy loss for each velocity with that of preceding trial until the minimum is reached.

By using this procedure, the critical velocities for 8-, 12-, and 16-in.-dia (200-, 300-, and 400-mm-dia) pipes carrying 25 percent concentrations of wood chips were found to be 4.3, 4.8, and 5.2 fps (1.31, 1.46, and 1.59 m/s), respectively. The energy loss gradients for those pipes with clear water and with mixtures of wood chips and water containing 25 percent solids are shown in Fig. 16.

The critical values of the dimensionless slurry transport parameter, ψ , defined by Eq. (26) were found to be 127.5, 126.8, and 128.5 for the 8-, 12-, and 16-in.-dia pipes, respectively, using these critical velocities. This narrow range of values indicates that the critical velocity may be determined by setting ψ equal to 130 and solving Eq. (26) for the minimum safe design velocity.

A mean flow velocity varying from 0.5 to 1.0 fps (0.15 to 0.30 m/s) greater than the critical velocity is used as the working design velocity for a slurry pipeline transporting solids heavier than wood chips. Using

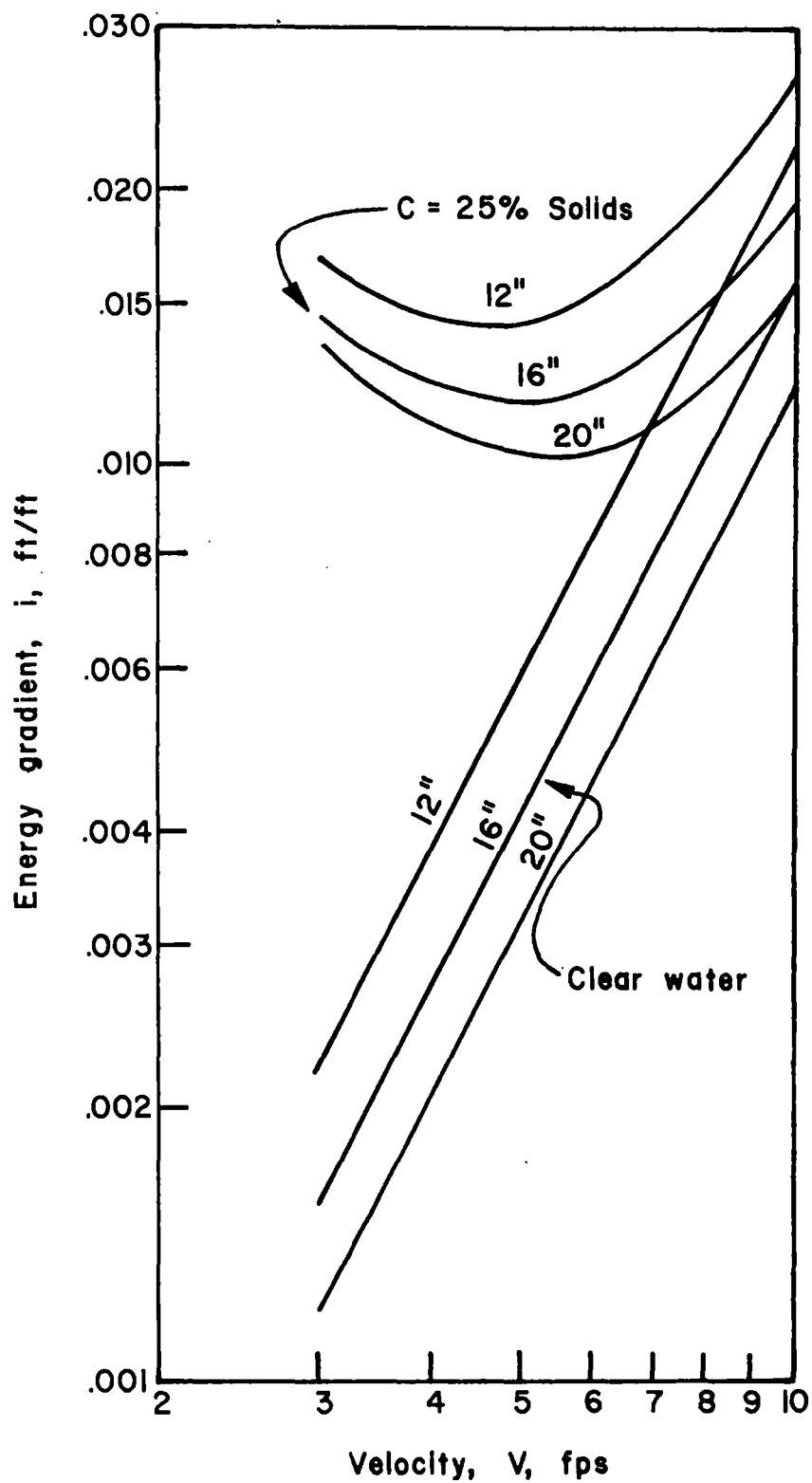


FIG. 16. ENERGY GRADIENTS FOR MIXTURES OF WOOD CHIPS AND WATER.

these values as safety factors applied to the critical velocities for 8-, 12-, and 16-in.-dia (200-, 300-, and 400-mm-dia) pipelines carrying 25 percent wood chips, the corresponding values of the dimensionless slurry transport parameter, ψ , are found to vary from 169 to 218; this suggests that using ψ equal to 200 in Eq. (26) will give an initial working design velocity.

Although the critical velocity occurs for values of ψ in the range of 125 to 130, steady-state conditions were observed for values of ψ as low as 29 in the 8-in.-dia (200-mm-dia) pipe and 39 in the 12-in.-dia (300-mm-dia) pipe when mixtures carrying 16 percent concentrations of wood chips were flowing. The flow conditions required to obtain these low values of ψ were produced by slowly reducing the flow rate and carefully controlling the concentrations of wood chips. Long period (80-90 sec) pressure undulations occurred at the point 1500 ft (457 m) downstream from the pump discharge flange while the flow was being stepped down. These undulations were noted on the strip chart records. By constantly monitoring the line pressure and flow rates and making minor adjustments, flow was stabilized during the time interval in which the observations were made. The sound of the wood chips in the pipe for low values of ψ was noticeably different from that for ψ above 200, indicating the flow to be in the bed load regime in the lower range of ψ .

b. Non-steady state conditions. The size and location of pumps and the pipe diameter for a proposed pipeline are selected for maximum and minimum steady state flow conditions anticipated in the system. Operating procedures and devices are then designed to respond to the effects estimated for non-steady state conditions caused by planned or unplanned changes of

flow in the system. The specification of the best procedures and devices for these unsteady flow periods requires that the engineer have some understanding of the effects of the unsteady flow conditions likely to occur.

Conditions producing a stoppage in the flow or a reduction of the flow rate below the critical velocity defined in the previous section are of greatest concern in the design of slurry pipelines as either could result in the occurrence of a blockage.

Although these critical flow conditions could not be predicted or programmed into the tests, periods of unsteadiness in the flow occurred with sufficient frequency to recognize their characteristics and to make the operational adjustments to attain steady flow again. Partial blockages of the pipe which were broken up and expelled by increasing the flow rate and pump discharge pressure then re-establishing the steady flow conditions occurred three times. On two other occasions steady flow was not re-established and blockages resulted. The continuous monitoring of the flow rate and pressure at three locations in the experimental pipeline recorded three types of unsteady flow conditions which will be illustrated with reproduced records of the strip charts. Although the data on the strip charts lack the accuracy required for attaining the level of precision necessary for the friction factor calculations, the charts provided excellent records of the relative changes in the flow conditions at the particular stations monitored and the interrelationships of the conditions at any station to the others. The interpretation of strip chart patterns occurring frequently and subsequent actions performed in the control of the test loop are reviewed to aid in developing design criteria and operational guidelines for wood-chip pipelines.

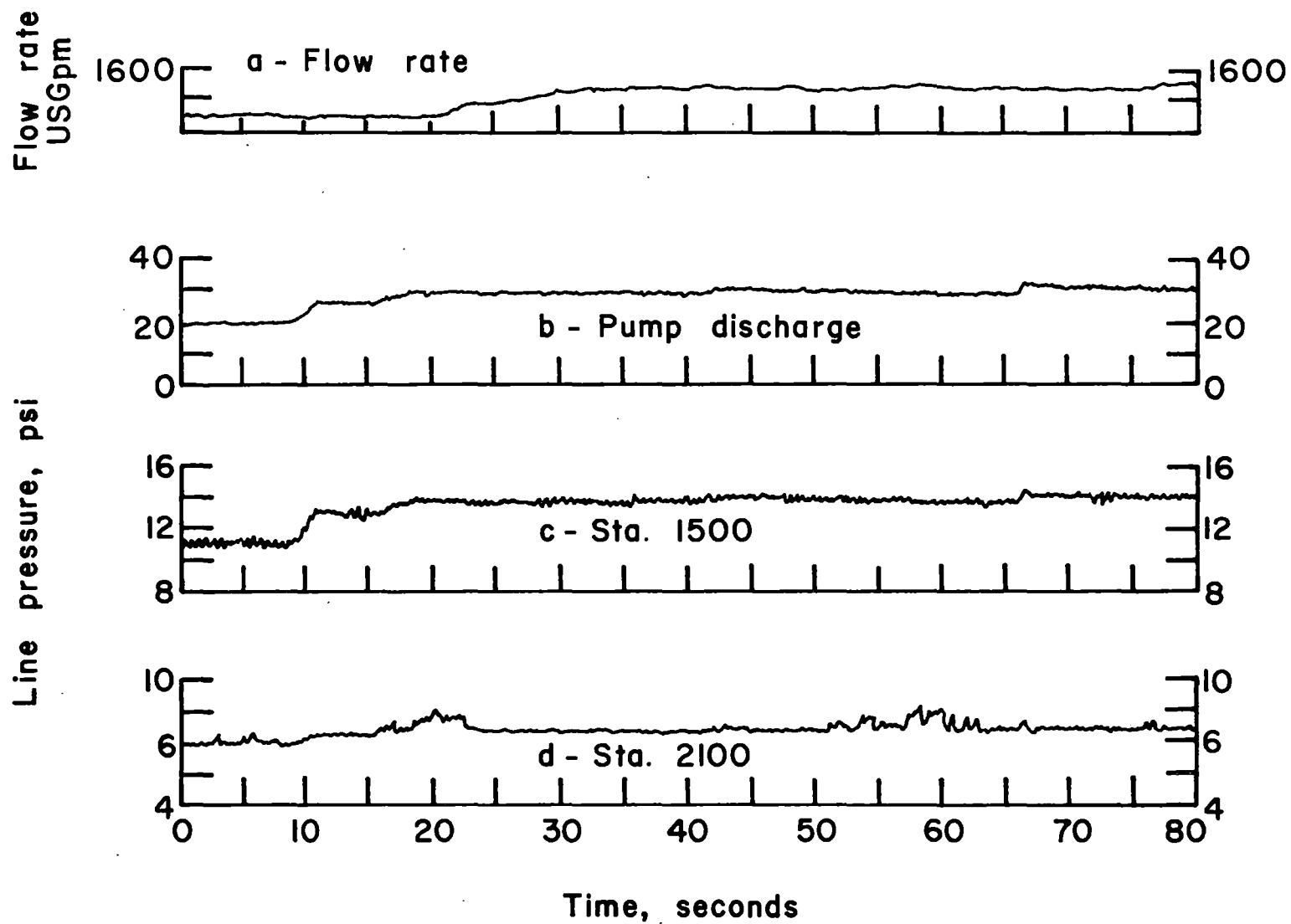
The three types of unsteady flow conditions encountered in the operation of the wood-chip test loop are (1) planned, (2) minor unplanned, and (3) major (or severe) unplanned changes in the flow rate in the system or in the line pressure at a given point. Segments of strip charts illustrating these three types are shown in Figs. 17-26; flow characteristics and the type of unsteady flow for each of the examples are summarized in Table 7. The velocity, concentration of wood chips and dimensionless slurry parameter ψ are given for initial and final conditions of flow for planned changes; values for the variables are given for flow conditions prevailing prior to the unplanned changes. Flow characteristics given in Figs. 17-25 were obtained when the test loop was made up entirely of 8 5/8-in.-dia (208-mm-dia) pipe; the 800-ft (244-m) section of 12 3/4-in.-dia (314-mm-dia) pipe was included in the test loop when the flow shown in Fig. 26.

The mixture flow rate, in USGPM, is shown in section a of each figure; the pressure at the pump discharge flange is given in section b; the line pressure approximately 1500 ft (457 m) from the discharge flange on the pump (also at the upstream end of the 600-ft (183-m) test length in the return line) in section c; the line pressure approximately 2100 ft (640 m) downstream from the pump (at the downstream end of the test length in the return line) is shown in section d. The initial point for each sequence is in the steady state flow preceding the change shown.

Planned changes in flow conditions are those occurring as part of a predetermined program established for the operation of the pipeline and illustrated by the changes of flow conditions effected between steady state data runs shown in Figs. 17-20.

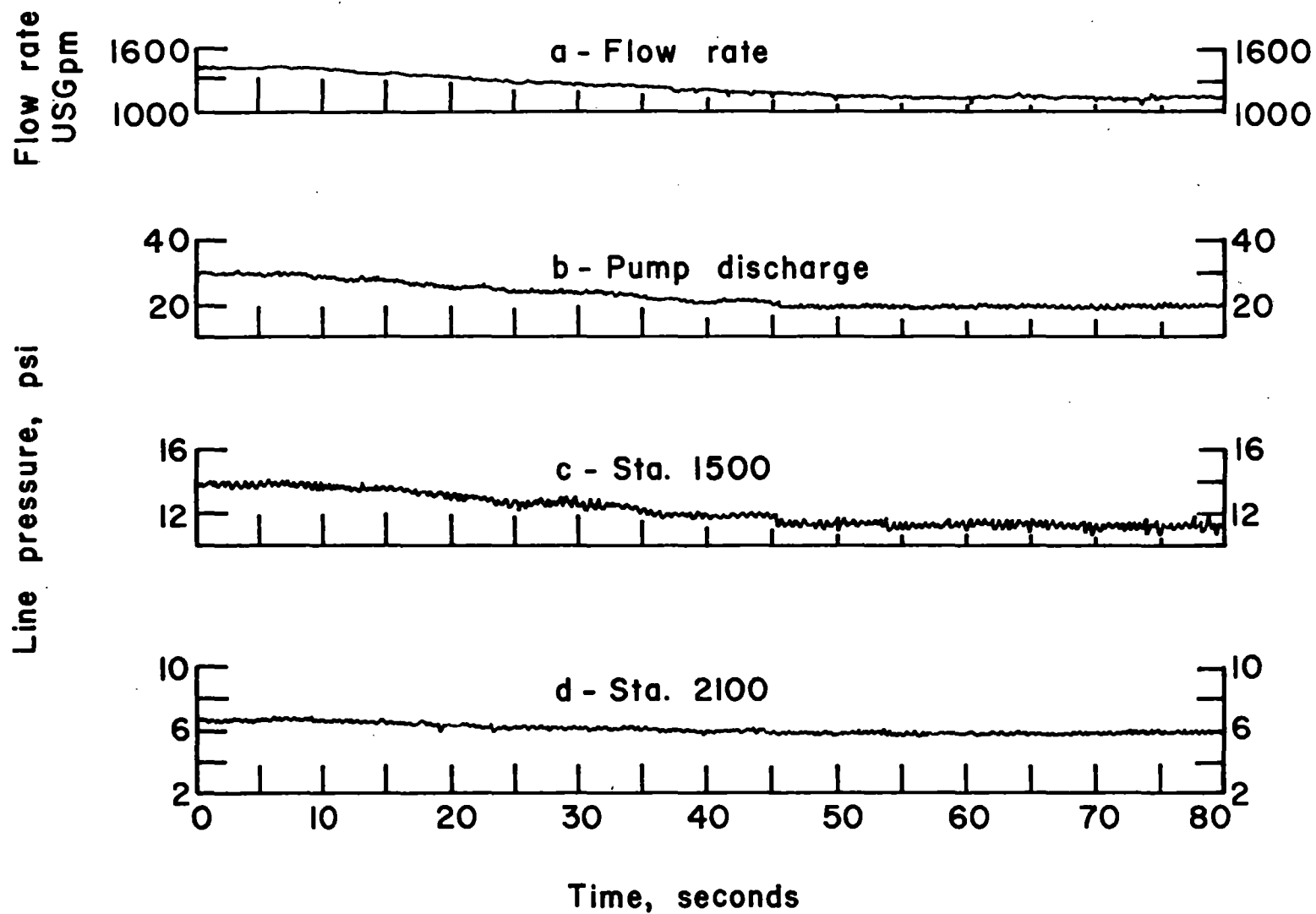
TABLE 7. Flow characteristics for non-steady conditions

Fig. No.	Run identification	Type of change	Pipe diameter in.	Initial conditions			Final conditions			Remarks
				Velocity fps	Concentration %	ψ	Velocity fps	Concentration %	ψ	
<u>Planned changes in flow</u>										
101	22-23	Flow increase	8.212	6.66	15.3	729	8.47	15.3	1498	Heterogeneous regime
102	21-22	Flow decrease	8.212	8.46	12.1	1803	6.66	15.3	729	Heterogeneous regime
103	34-35	Flow decrease	8.212	4.94	21.9	219	4.23	19.0	156	Saltation regime (critical velocity zone)
104	36-37	Flow decrease	8.212	3.53	17.6	96	2.31	16.3	29	Bed load regime
<u>Unplanned change (minor)</u>										
105	13	Steady	8.212	9.67	16.4	2105	No change			Heterogeneous regime
106	16	Steady	8.212	6.16	13.0	658	No change			Heterogeneous regime
<u>Unplanned change (major)</u>										
107	14-15 (1)	Steady	8.212	5.44	15.0	380	Short-time stoppage			Heterogeneous-saltation regime
108	14-15 (2)	Steady	8.212	4.54	8.0	362	Short-time stoppage			Heterogeneous-saltation regime
109	25	Steady	8.212	4.73	13.4	296	Short-time stoppage			Heterogeneous-saltation regime
110	58	Steady	8.212	4.79	7.8	457	Long-time stoppage			Heterogeneous-saltation regime
			12.375	2.10	7.8	33				Bed load regime



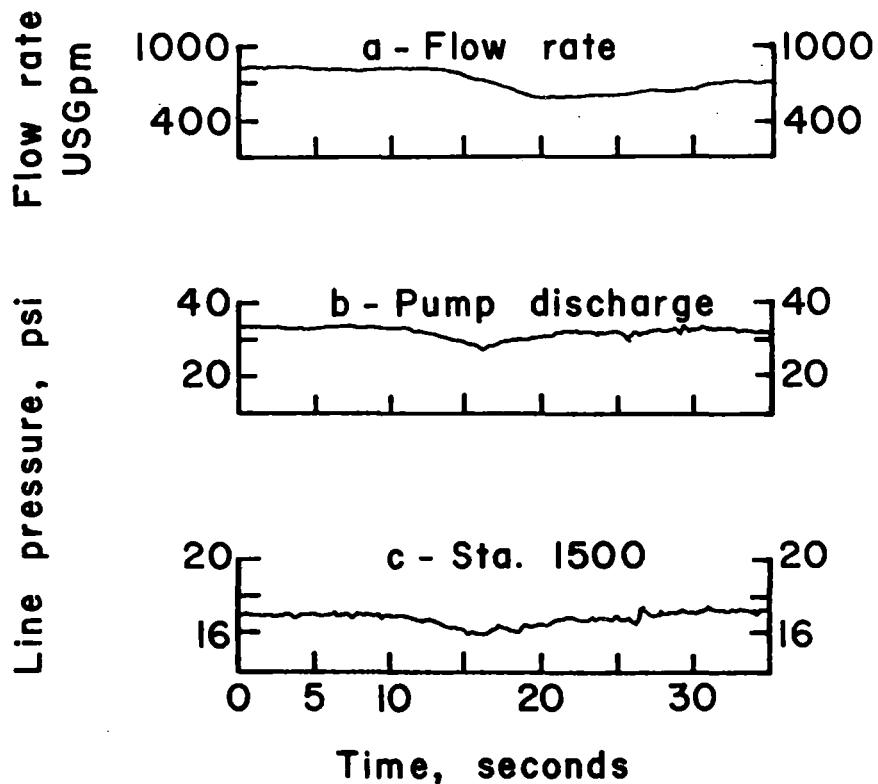
Run 22-23, $C = 15\%$, $\psi_i = 729$, $\psi_f = 1498$

FIG. 17. PLANNED INCREASE IN FLOW RATE.



Run 21-22, $C = 15\%$, $\psi_i = 1803$, $\psi_f = 729$

FIG. 18. PLANNED DECREASE IN FLOW RATE.



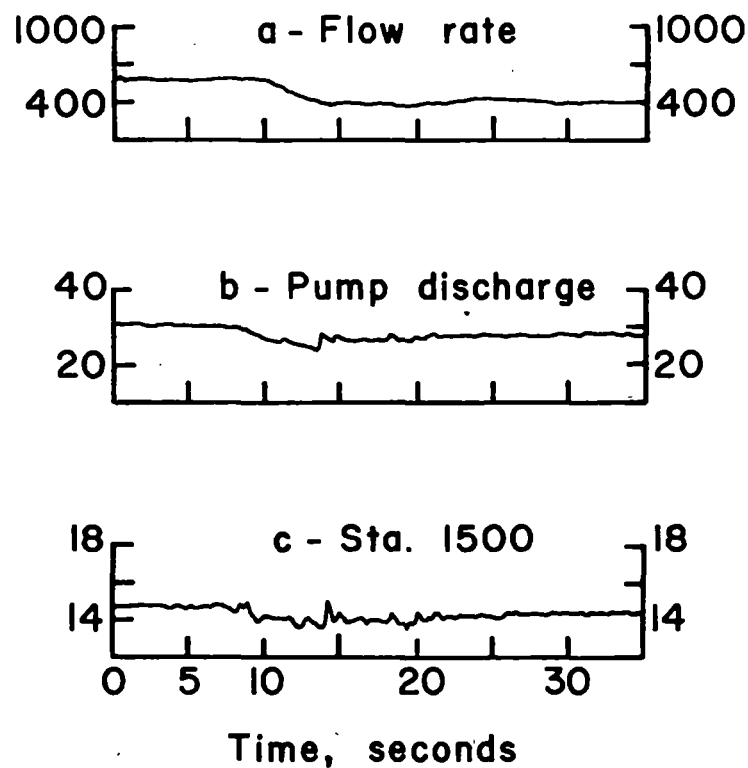
Run 34-35

C = 20 %

$\psi_i = 219$

$\psi_f = 156$

FIG. 19.



Run 36-37

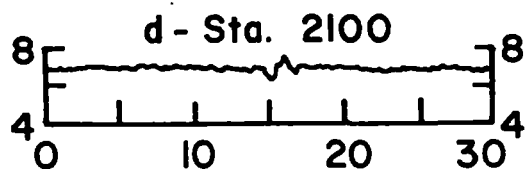
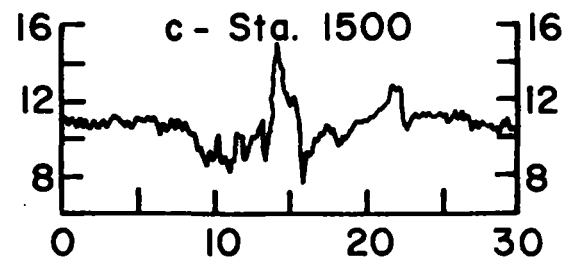
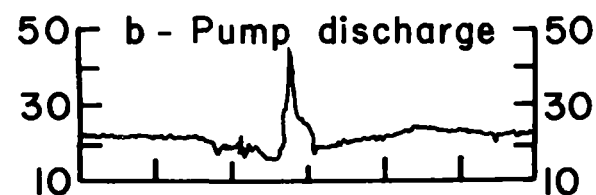
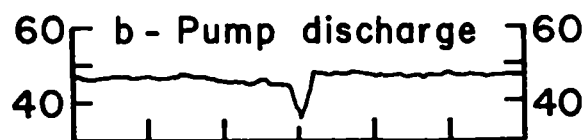
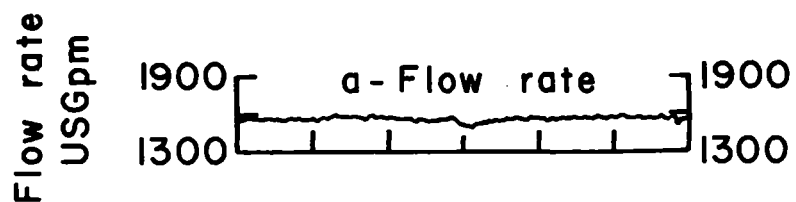
C = 20 %

$\psi_i = 96$

$\psi_f = 29$

FIG. 20.

PLANNED DECREASE IN FLOW RATE



Time, seconds

Run 13

C = 16%

ψ = 2100

FIG. 21.

Time, seconds

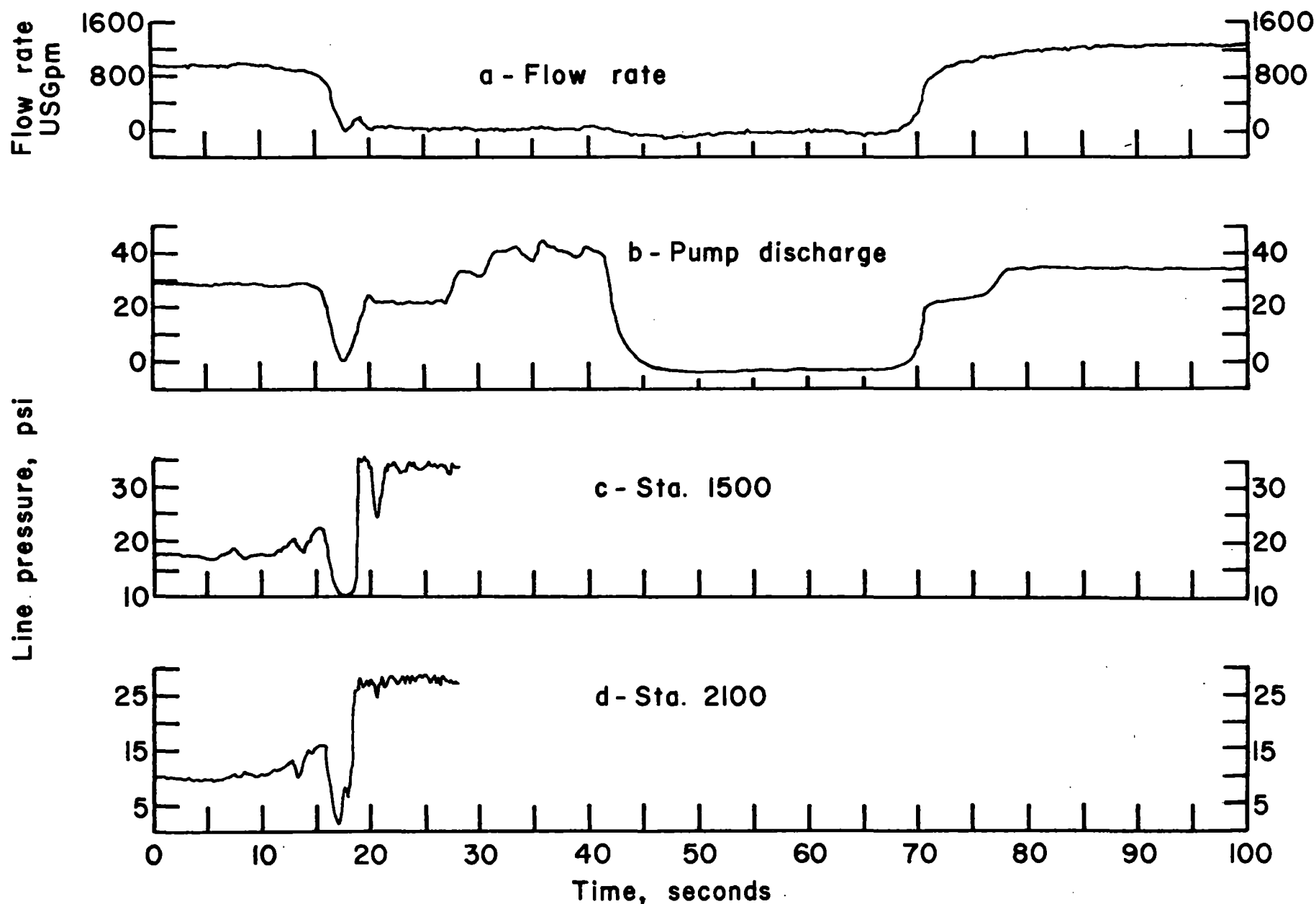
Run 16

C = 13%

ψ = 658

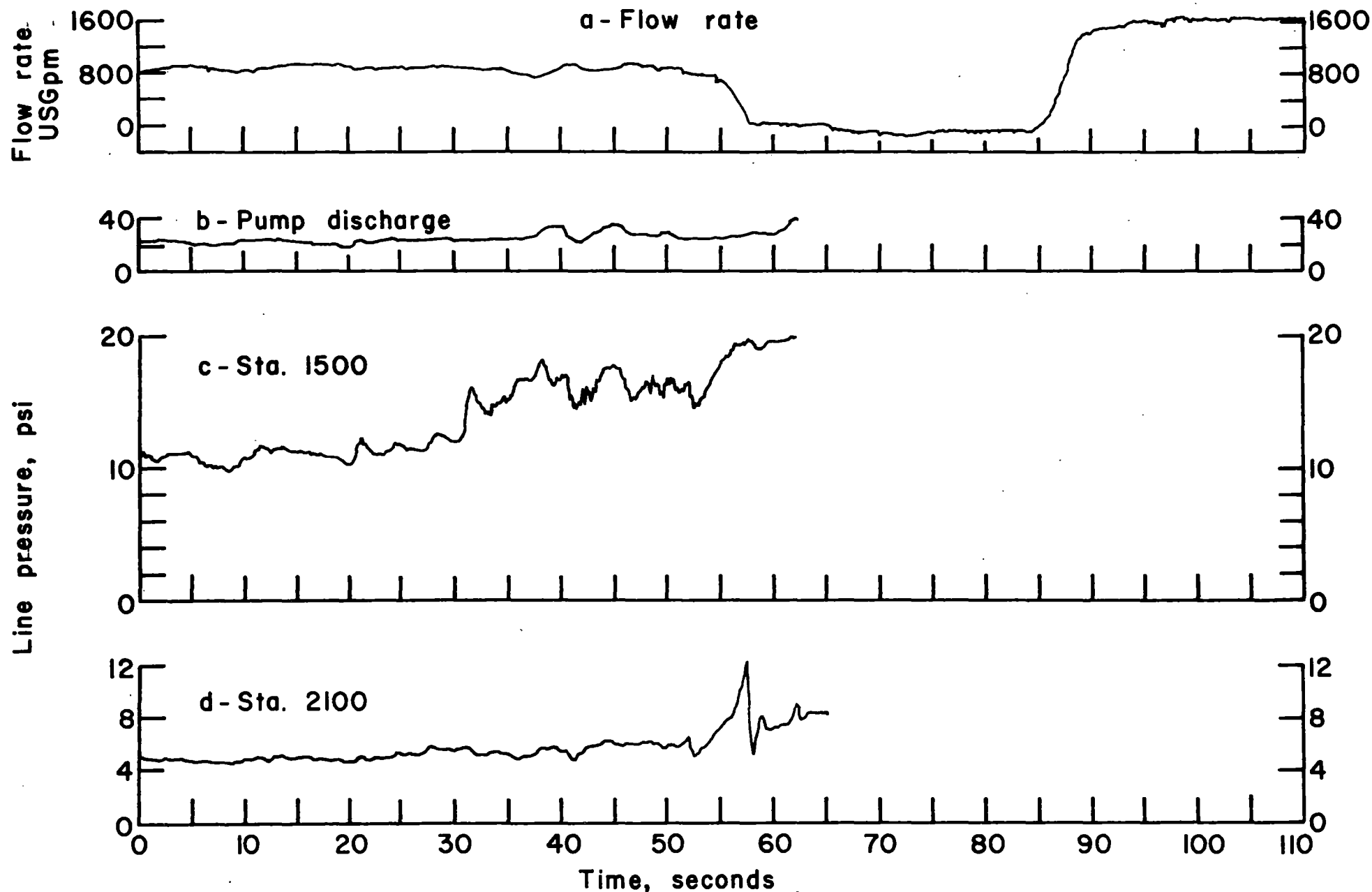
FIG. 22.

- MINOR UNPLANNED CHANGES



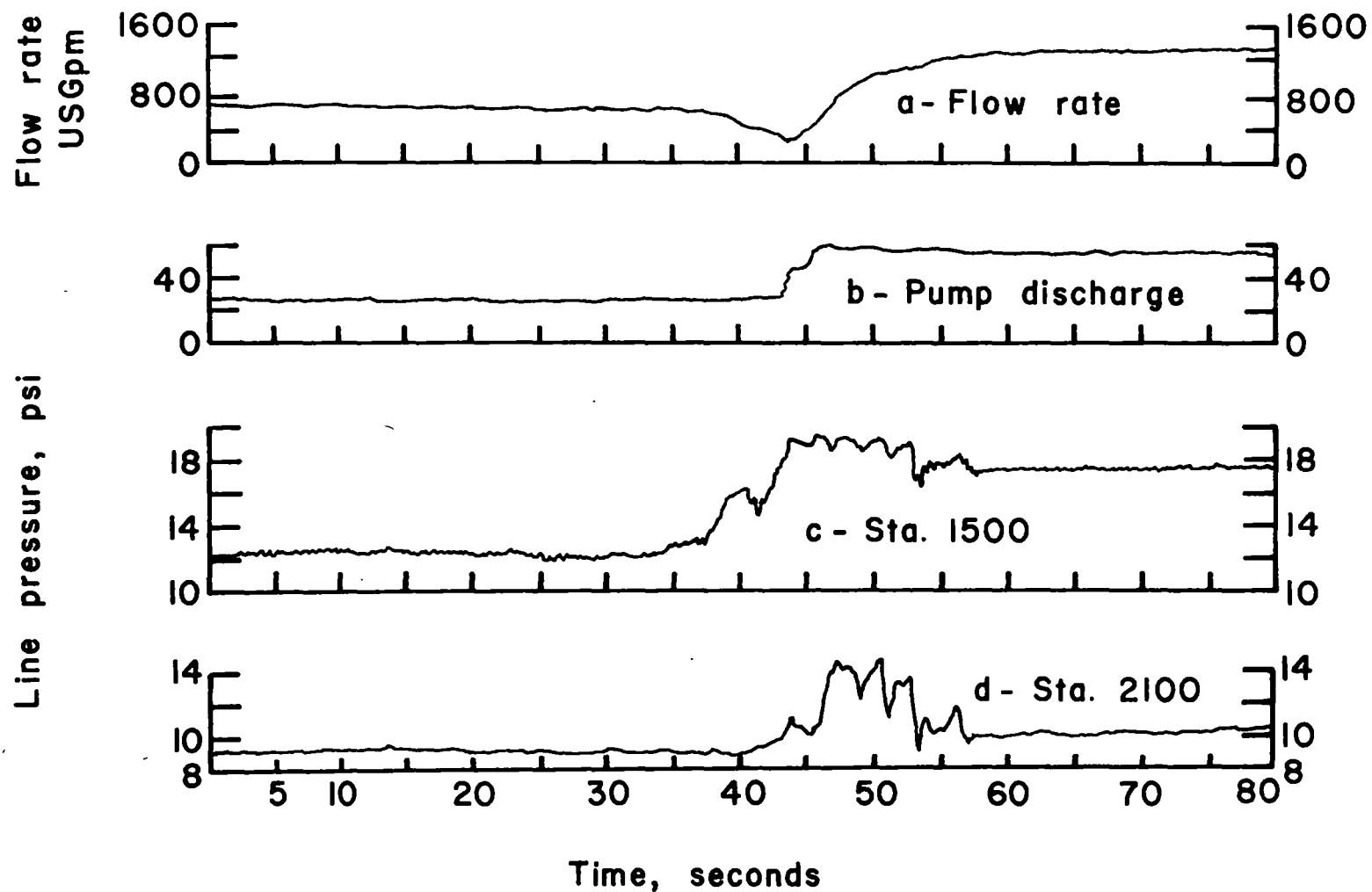
Run 14-15(1), $C=15\%$, $\psi=380$

FIG. 23. MAJOR UNPLANNED CHANGE IN FLOW RATE.



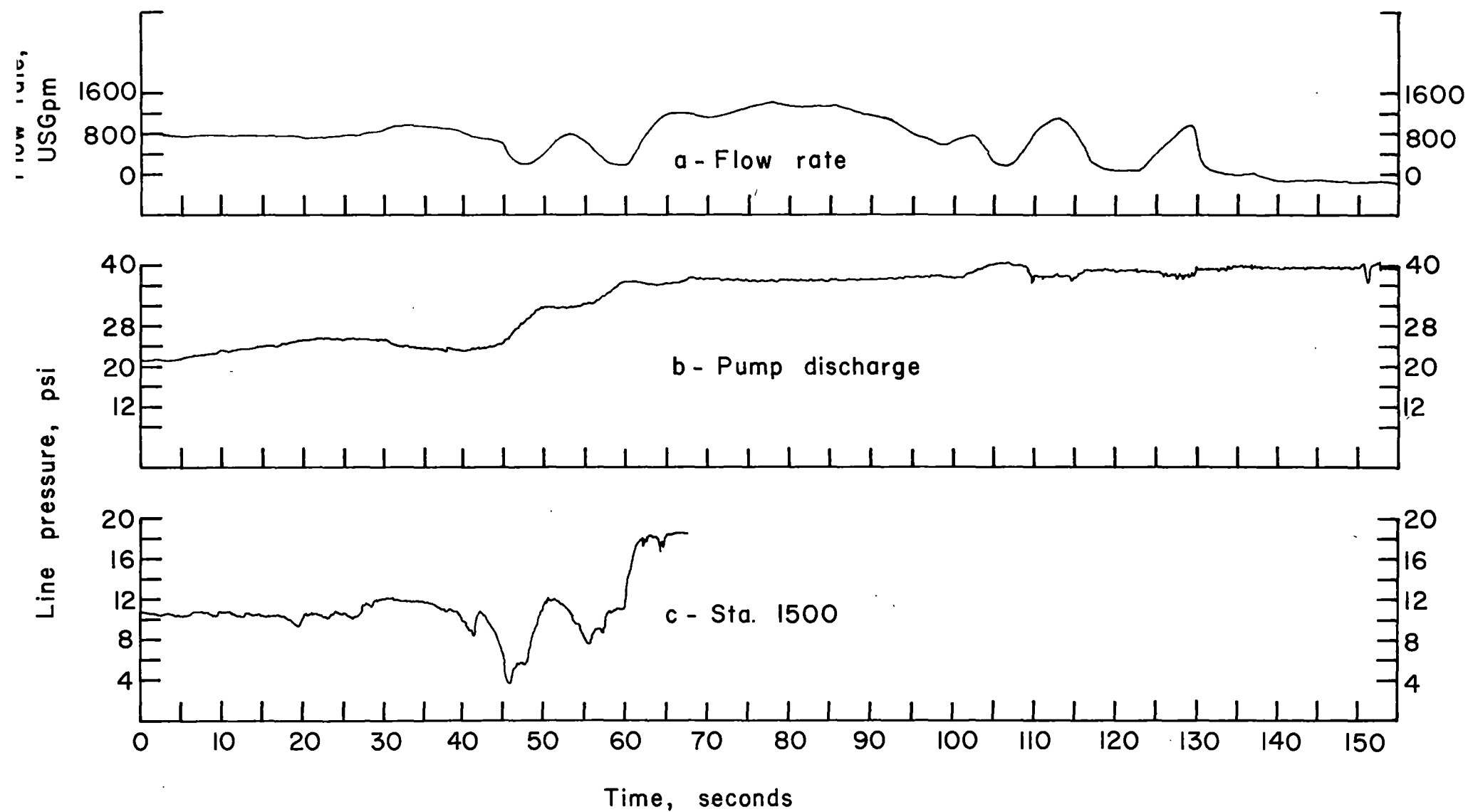
Run 14-15(2), C = 8%, $\psi = 362$

FIG. 24. MAJOR UNPLANNED CHANGE IN FLOW RATE.



Run 25, C=13%, $\psi = 296$

FIG. 25. MAJOR UNPLANNED CHANGE IN FLOW.



Run 58, $C = 8\%$, $\psi = 33$

FIG. 26. MAJOR UNPLANNED CHANGE IN FLOW; RESULTING BLOCKAGE FORCED SHUT DOWN OF PIPE.

The effect of a controlled increase in the velocity from 6.7 to 8.5 fps (2.04 to 2.59 m/s) with a 15-percent concentration of wood chip between runs 22 and 23 is shown in Fig. 17. The rotational speed of the pump is increased in two steps, one at $t = 8.5$ sec, the other at $t = 16.5$ sec. A close study of the strip chart, where a 1mm length on the time scale is 0.5 sec, shows the line pressure at the pump discharge flange increases linearly for approximately 2 sec; the line pressures at Sta 1500 and Sta 2100 appear to increase slightly beginning approximately 0.5 sec later (at $t = 9$ sec), and the flow increases in a non-linear manner over approximately a 5-sec interval starting approximately 1.5 sec after the rotational speed change is initiated (at $t = 10$ sec). These response time intervals for the changes observed in pressures and flow rate are in good agreement with the calculated travel time of the pressure wave generated by increasing the pump speed. The calculated response times are 0.39 sec, 0.55 sec and 1.25 sec, respectively, for Sta 1500, Sta 2100 and the increase of flow monitored just downstream from the discharge flange of the pump.

The second step (beginning at $t = 16.5$ sec) effects a fine adjustment to attain the velocity desired for Run 23.

The minor fluctuations in pressure at Sta 2100 between 16 and 22 sec were thought to be caused by an accumulation of wood chips passing the peizometer connection for the pressure transducer controlling the pen recording on the chart.

The gradual decrease of the velocity flow from 8.5 to 6.7 fps (2.59 to 2.04 m/s) with a 12- to 15-percent concentration of wood chips between runs 21 and 22 shown in Fig. 18 is effected by decreasing the pump speed

over the 37.5-sec interval from $t = 7.5$ to $t = 45$ sec. The flow rate continues to adjust to the new conditions for an additional 5 to 8 sec. The decrease in flow rate extends over a greater time interval than an increase to allow the flow to adjust without an excessive deposition of solids on the invert of the pipe. No unusual flow conditions were observed in this transition of flow rates.

The conditions depicted in both Figs. 17 and 18 are for flows well up into the heterogeneous regime with values of the dimensionless slurry parameter ψ of 729, 1498, and 1803 greatly exceeding the minimum of 200 for safe design velocities.

A decrease in the flow rate for conditions approaching the critical velocity as shown in Fig. 19 for a velocity reduction from 4.9 fps (1.52 m/s), $\psi = 219$, to 4.2 fps (1.28 m/s), $\psi = 156$, with approximately 20 percent wood chips between runs 34 and 35. The rotational velocity of the pump was decreased gradually over a 6.5-sec interval from $t = 10$ to $t = 16.5$ sec to what was thought to be a pre-determined value corresponding to the velocity of 2.3 fps (0.70 m/s). As the velocity was dropping below 2.3 fps (0.70 m/s) at $t = 16.5$ sec, the pump speed was increased to arrest the decrease in flow velocity. The velocity reached a minimum at $t = 20$ sec and was gradually increased to the desired value of 2.3 fps (0.70 m/s) at $t = 35$ sec by effecting a "hunting" process with the pump speed control. This "overshooting" caused the minor fluctuations in the line pressure at Sta 1500 shown between $t = 15$ and $t = 28$ sec which were dampened out by $t = 30$ sec.

A similar system response is shown in Fig. 20 for decreasing the velocity from 3.5 fps (1.07 m/s) $\psi = 96$, to 2.3 fps (0.70 m/s), $\psi = 29$, in bed load flow regime (values of ψ less than 100) between runs 36 and 37. The "overshooting" and subsequent "hunting" caused minor pressure fluctuations at Sta 1500 in the interval from $t = 12.5$ sec to $t = 25$ sec.

Minor unplanned changes in flow conditions are those occurring while a pipeline is operating in a programmed steady state mode and are self-stabilizing or may be stabilized to the prior flow conditions with minor adjustments of the controls. Examples of minor unplanned changes are illustrated in Figs. 21 and 22 showing what was interpreted as the effect of feeding the wood chips at a rate greater than the injection system could handle.

The minor disruption occurred in the steady flow of run 13, well up in the heterogeneous regime ($V = 9.7$ fps (2.96 m/s), $C = 16\%$, $\psi = 2105$), shown in Fig. 21 when a slug of wood chips with a concentration exceeding the normal workable limit of 25-30 percent "flooded" the intake to the pump (at $t = 13$ sec). This caused the pump speed to decrease rapidly, although only momentarily, causing the flow rate and line pressures throughout the system to decrease. As the heavy concentration cleared the pump and passed into the discharge line, the pump speed increased creating a higher pressure throughout the system noted from $t = 15$ to $t = 17$ sec. As the slug of heavy concentration was diffused axially along the flow, the velocity increased, and the pump head and line pressures returned to the original flow conditions.

When a similar event began developing in run 16 (at $t = 7.5$ sec in Fig. 22) following a 60-sec period of other minor unplanned changes in a

flow (not shown) with a velocity of 6.6 fps (2.01 m/s) and a concentration of 13 percent wood chips ($\psi = 658$), the pump speed was increased sharply by the operator until the flow rate exceeded that indicated at $t = 0$. The pump speed was reduced manually and the original flow conditions were re-established by a "hunting" process.

It was later determined that the "flooding" of the pump intake with wood chips on both these occasions were caused by a malfunction of the hydraulic motor driving the auger injecting the chips into the pump suction line. (The injection system will be described in greater detail in Section 4.5.) After these and subsequent problems in controlling the chip feed rate, the hydraulic motor was replaced by a constant speed A-C motor giving greater reliability to the system.

Major unplanned changes in flow conditions are those occurring during steady state or planned changes of flow with sufficient severity to cause a short-time or long-time stoppage of flow. A short-time stoppage is one in which the flow may be re-established using the normal pipeline flow control components. Starting the flow following a long-time stoppage requires utilizing apparatus and procedures not employed in the normal operation of the pipeline. Sudden extreme changes in the flow rates or line pressure at any point in the system may also be classified as major unplanned changes; this classification depends greatly on the subsequent flow conditions in the pipeline. Examples of events occurring in short-time stoppages encountered in the pilot line studies are shown in Figs. 23-24; events of a long-time stoppage are shown in Fig. 26.

The record of the flow conditions following a reduction in the velocity from 7.2 fps (2.19 m/s) in run 14 to 5.4 fps (1.65 m/s) for run 15 are given in Fig. 23. The flow was steady in the heterogeneous saltation regime ($\psi = 380$, $c = 15\%$) for approximately two minutes prior to the time $t = 0$. The increase in line pressure at Sta 1500 and Sta 2100 from $t = 10$ sec to $t = 15$ sec indicates a flow with a heavy concentration of chips with a tendency toward plugging was occurring downstream from Sta 2100 and causing a slight decrease in the flow rate. The records indicate a sudden loss of flow rate and line pressure at all observation points at $t = 15$ sec. This condition was similar to that in Figs. 21 and 22 caused by flooding the pump intake with wood chips followed by the loss of pump speed. At $t = 17.5$ sec the pump speed was increased sharply by the operator. The increase of pressure at all points in the line with no increase in flow rate indicated a blockage had formed downstream from Sta 2100. The discharge pressure was held at a constant level for approximately 7-8 sec, then increased in an irregular pattern shown in Fig. 23b from 27 to 42 sec in an attempt to dislodge the blockage. At $t = 27$ the peizometer lines transmitting the pressure from Sta 1500 and Sta 2100 were shut off from the transducers interfaced with the strip chart recording pens. The pump was shut off at $t = 42$ sec.

After allowing the system to remain depressurized for approximately 30 sec, the pump was restarted. The flow started immediately, increasing in proportion to the increase in the rotational speed of the pump, indicating the blockage had disintegrated.

The pipeline was cleared of wood chips following the blockage shown in Fig. 23 and a new series of tests were started with lower concentrations and flow velocities. A blockage shown in Fig. 24 similar to that in Fig. 23 developed during the steady state condition in the heterogeneous-saltation flow regime at a velocity of 4.5 fps (1.37 m/s), $\psi = 362$, $C = 8\%$. The records of the pressure observations indicate a blockage formed between Sta 1500 and Sta 2100, traveled downstream past Sta 2100 and probably caused a flow stoppage at the point where the pipeline rises approximately 10 ft on a 45-degree angle to empty into the rotating screened drum (at $t = 56$ sec). The pump speed was increased at $t = 61$ sec (the transducers connected to the pressure transducers were deactivated at this time to prevent internal damage from over-pressuring). After the pump was shut off for 20 sec and restarted, the blockage was again dislodged. The pen trace for the pump discharge pressure indicates a build-up of pressure was required to force the blockage out the end of the pipe. A comparison of Fig. 24 with Fig. 23 shows that the transducer signals to the pens tracing the pressures at Sta 1500 and Sta 2100 were amplified and the signal for the pressure at the discharge flange was decreased during this period of establishing a new test series.

The response by the operator to indications of a blockage forming resulted in preventing a flow stoppage at the end of run 25 as indicated in Fig. 25. A steady state velocity of 4.7 fps carrying a 13-percent concentration of wood chips ($\psi = 296$) prevailed until the flow rate began to decrease due to a blockage forming downstream from Sta 1500 at $t = 30$. When the increased pressure at Sta 1500 and the decreased velocity indicated

flow conditions continued to deteriorate for a period of 7 to 8 seconds (from $t = 36$ to $t = 43$), the operator increased the pump speed to build up sufficient pressure to increase the flow rate, disintegrate the potential blockage, and prevent a flow stoppage.

The conditions encountered in Figs. 23-25 occurred while the injection auger was powered by the hydraulic motor mentioned previously in the discussion of Figs. 21 and 22. The analysis of the unplanned changes occurring in Figs. 23-25 could not conclusively relate the cause of these instabilities to the hydraulic motor although it was replaced immediately after completing run 25. No further operational problems were encountered for the remainder of the tests conducted with the 8.212-in.-dia (208-mm-dia) pipe installed throughout the pilot line.

The most severe unplanned change in flow conditions occurred during the latter part of the experimental program when the 800-ft (244 m) section of 12.375-in.-dia (314-mm-dia) pipe was installed in the return flow line. The record of flow conditions preceding a long-time stoppage are shown in Fig. 26. This stoppage terminated a set of tests conducted with flow velocities in the 8.212-in.-dia (208-mm-dia) pipe ranging from 9.7 fps (2.96 m/s) to 4.8 fps (1.46 m/s) and the corresponding velocities in the 12.375-in.-dia (314-mm-dia) test section from 4.2 fps (1.28 m/s) to 2.1 fps (0.64 m/s), respectively. No major unplanned flow changes were experienced prior to this one following run 58. Steady state flow conditions had existed in the test loop for 3 or 4 minutes with an 8-percent concentration of wood chips and velocities of 4.8 fps (1.46 m/s) and 2.1 fps (0.64 m/s) giving ψ values of 457 and 33 in the 8.212- and 12.375-in.-dia (208- and 314-mm-dia)

pipe sections, respectively. The operator, in preparation for reducing the flow for the next run, noted that the flow rate was beginning to fall off slightly in the interval $t = 0$ to $t = 7$ sec and began to increase the pump speed gradually to stabilize the flow at the discharge rate of the previous run. A time $t = 20$ sec, the flow rate and pump discharge pressure appeared to be stable even though the line pressure at Sta 1500 (at the upstream end of the 12.375-in.-dia (314-mm-dia) test section) continued to fluctuate. At $t = 27$ sec the flow rate showed a slight increase and the pressure at the pump discharge decreased as that at Sta 1500 increased, indicating the blockage forming in the 8.212-in.-dia (208-mm-dia) line was diffused offering less resistance to flow in this section of pipe. The flow rate and line pressure at Sta 1500 started to drop off again at $t = 35$ sec and continued to decline until the pump speed was increased at $t = 45$ sec; the flow rate and line pressure at Sta 1500 appeared to be recovered again at $t = 50$ sec. A subsequent deterioration and another recovery of flow conditions between $t = 50$ sec and $t = 62$ sec appeared to have generated enough pressure and increased the flow rate sufficiently to clear the blockage through the system. The transducer giving the line pressure at Sta 1500 was shut off when the 3 or 4 relatively severe pressure surges appeared on the strip chart at $t = 62$ sec. At $t = 85$ sec the flow rate again began to decline even though the pump was operating close to its maximum speed and generating the maximum head. The flow rate continued to decline until the stoppage was complete at $t = 140$ sec.

An analysis of the limited data available from the strip charts (with the pen tracing the pressure trace at Sta 2100 inoperative throughout the

entire sequence and the transducer for the pressure at Sta 1500 cut off halfway through the unstable flow period) indicates the following sequence of events may have occurred: (1) a blockage developed in the 8.212-in.-dia line and was diffused sufficiently to restore flow conditions momentarily in the first phase ending at $t = 35$ sec, (2) two other blockages developed in this same section in the time interval between $t = 35$ sec and $t = 62$ sec, during this time the two surges of flow rates formed dunes of wood chips in the 12.375-in.-dia (314-mm-dia) line, and (3) these dunes were transported along the 12.375-in.-dia (314-mm-dia) line in the bed load flow regime to the nominal 12-in.-by-8-in. (300- by 200-mm) reducer where intermittent blockages were continuously formed and partially diffused until the re-entrance to the 8.212-in.-dia (208-mm-dia) line was completely plugged.

This blockage was anticipated as the dimensionless slurry parameter prior to the instability clearly indicated the flow to be in the bed load regime. The expansion from a pipe of one diameter to a larger one is only permissible in slurry flows when additional flow is introduced from an external source to create a higher velocity to accompany the increased pipe size (the confluence of two slurry streams). This experience also stresses that it is poor design procedure to place a reducer downstream from a section of pipe in which bed load flow may occur.

Summary. The design criteria and operational guidelines developed for wood-chip pipelines from the analysis of planned and unplanned changes in flow occurring in these pilot line investigations are summarized as follows:

1. A supervisory system for monitoring the flow conditions in a wood-chip pipeline should include the capabilities for

continuously recording the volumetric flow rate and line pressures at selected points along the pipeline.

2. The supervisory system should be automated to respond to unplanned changes in flow conditions on a suitable delayed-time basis. A velocity reduction of 10 to 15 percent which continues to decrease over a period of 6 to 10 sec are indicated as the allowable limits of unplanned flow changes and length of time delay interval based on the results of this study.
3. Increases in pipe diameters in wood-chip pipelines are permitted only when an additional volumetric flow rate capable of maintaining a minimum safe design velocity enters the system.
4. A safe working design velocity is obtained by using a value of 200 for the dimensionless slurry flow parameter ψ as given in Eq. (26).
5. Flow reductions with wood chips in the system should occur gradually at rate of change between 0.05 fps/sec (0.015 m/s^2) and 0.10 fps/sec (0.030 m/s^2) based on the findings of these tests.

4.5 Wood Chip Injection System

The reliability of a pipeline system for transporting large volumes of wood chips continuously depends on an injection system capable of feeding the wood chips into the pipeline continuously at large volumetric input rates. The previous studies on the hydraulics of wood-chip pipelines have not specifically addressed this topic as a system design problem.

The studies conducted at Queen's University and the Pulp and Paper Research of Canada used large, open cylindrical tanks in which the wood

chips and water were mixed by agitation with a large mechanical stirrer. This process resulted in a non-uniform feed rate with the concentration of chips entering the pipeline relying on the random pattern of chips gravitating into the "live" zone of influence of flow into the pump intake.

The design of an injection system is based on either one of two methods depending on whether the wood chips are injected into the system on (1) the suction, or (2) the discharge side of the pump. In the first, the proper proportions of wood chips and water are mixed in an open tank and drawn into the suction line of a pump station employing one or more centrifugal pumps in series. The second method requires an auxiliary mechanical system called a lock-hopper for injecting the chips into the line at a pressure equal to that on the discharge side of the pump station. Multi-stage centrifugal pumps or reciprocating pumps may be used as the mainline prime movers as they will be handling only clear water in the latter method. The limited experience with both types and an analytical study of the latter are reviewed briefly in the following paragraph.

Hendrix (1968) analyzed a lock-hopper system developed by Reichl and Jones (U.S. Patent No. 2,672,372) for coal slurry systems and found this method unsuitable because of the low volumetric feed rate, the incompatibility of the mechanical components required with the size and character of wood chips, and the complexity of the system required to keep the water hammer effects within allowable limits.

Shell Pipeline Research did not employ a continuous wood-chip feed system in the tests conducted in a 4000-ft (1220-m) test loop of 8-in.-dia (200-mm-dia) pipe; the woodchips were mechanically added, the pipe closed and the test line operated as a closed system.

A comparison of the pumping equipment, the initial and operating costs, the reliability factors, and the relative complexity of the lock-hopper and open mix-tank injection systems indicated the development of the latter type to have a greater economic feasibility and the higher probability of success. Based on the experience of the Pulp and Paper Research Institute at Marathon, Ontario, in 1964, a uniform feed rate of chips into the pump intake could not be produced with any degree of reliability using an open mix tank and an open propellor-type stirrer for the following reasons: (1) The small difference between the specific gravity of the wood chips and that of water facilitated the suspension of the chips by a minimum of agitation and, consequently, did not provide a uniform supply of chips entering the zone of influence of the pump intake. (2) The relatively small hemisphere forming the zone of influence of the pump intake line connected flush to the flat base of a cylindrical tank did not generate sufficient velocities over a large enough region in the mix tank to counteract the currents caused by the agitation in the mixing process. (3) The fresh unsaturated buoyant wood chips rising to the surface created a concentration inversion with more chips near the surface than at the bottom of the tank.

These problems were noted and solved during the studies conducted on a 4-in.-dia (100-mm-dia) pipeline by Gow (1971) by feeding the chips into a conical hopper with the apex at the bottom terminating in a 10-in.-dia (250-mm-dia) cylindrical tube housing a 9-in.-dia (225-mm-dia) grain auger shown in Fig. 27. The lower end of the auger housing was located immediately above a funnel section connecting the make-up water storage tank to

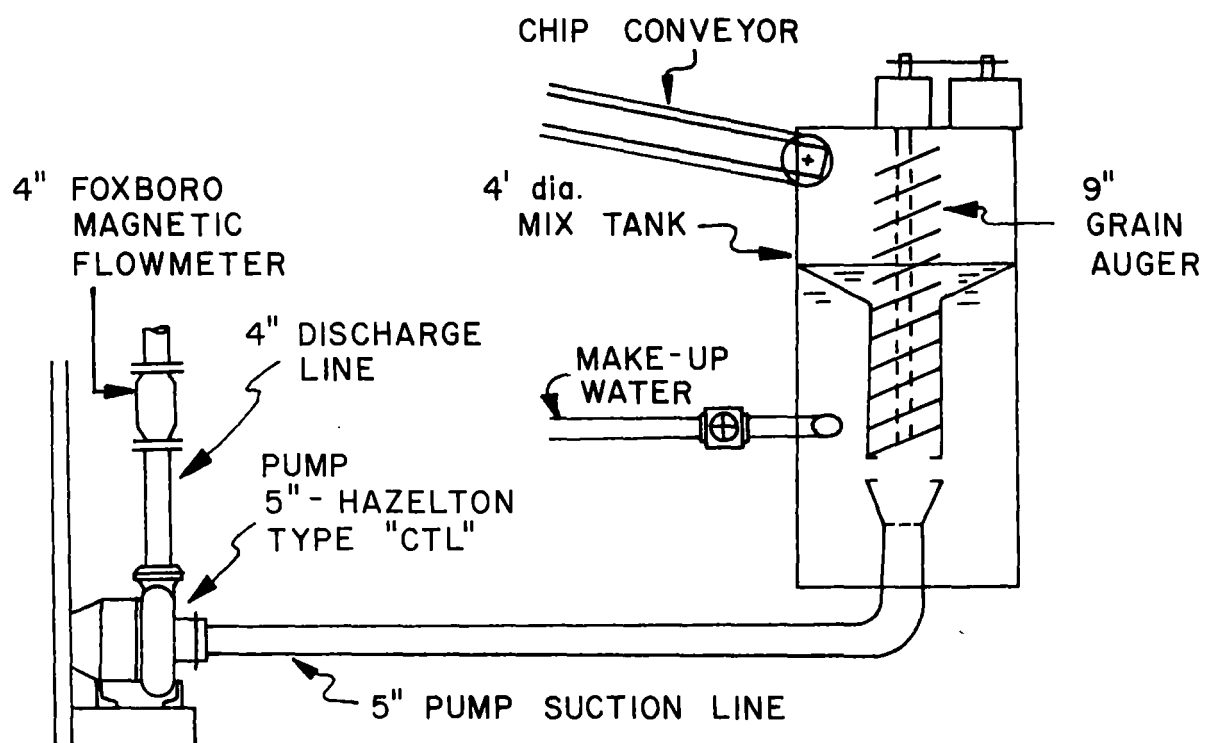


FIG. 27. CHIP INJECTION SYSTEM.
(4-in. laboratory test line)

the pump intake line located 12 to 18 inches (0.30 to 0.45 m) below the free surface of the storage tank. This arrangement alleviated all three difficulties with the open mix tank by feeding the wood chips at a uniform rate directly into the zone of increased velocity at the pump intake section. Problems initially encountered with air entrainment in the mixture entering the pump due to the vortex in the intake line caused by the pump and the auger rotating in the same direction were minimized by jetting the make-up water into the mix tank tangentially in the opposite direction neutralizing the vortex action. Visual observation of the uniformity of the concentration of wood chips flowing in the clear plastic pump suction line indicated this injection system to be superior to any methods employed previously at Montana State University and by other investigators.

The injection system for these studies conducted on the 2345-ft (715-m) pilot line with 8.212- and 12.375-in.-dia (208- and 314-mm-dia) pipes was a modification of that used by Gow (Fig. 27), is shown in Fig. 28. The wood chips enter the 6-ft-dia (1.83-m-dia) feed hopper from a surge bin by gravity or conveyor belt, are transferred through a 16-in.-dia (400-mm) grain auger continuously to the main velocity stream of the make-up water entering the pump intake, and are mixed to a uniform consistency by a combination of the vortex action created by the rotation of the pump impeller and auger prior to entering the pump suction. The principal design considerations for this auger-driven system are (1) selecting an auger with the relationship among the diameter, pitch and spacing flights and rotational speed of the auger capable of injecting the maximum design feed rate of wood chips into the pump intake, and (2) restricting the space between

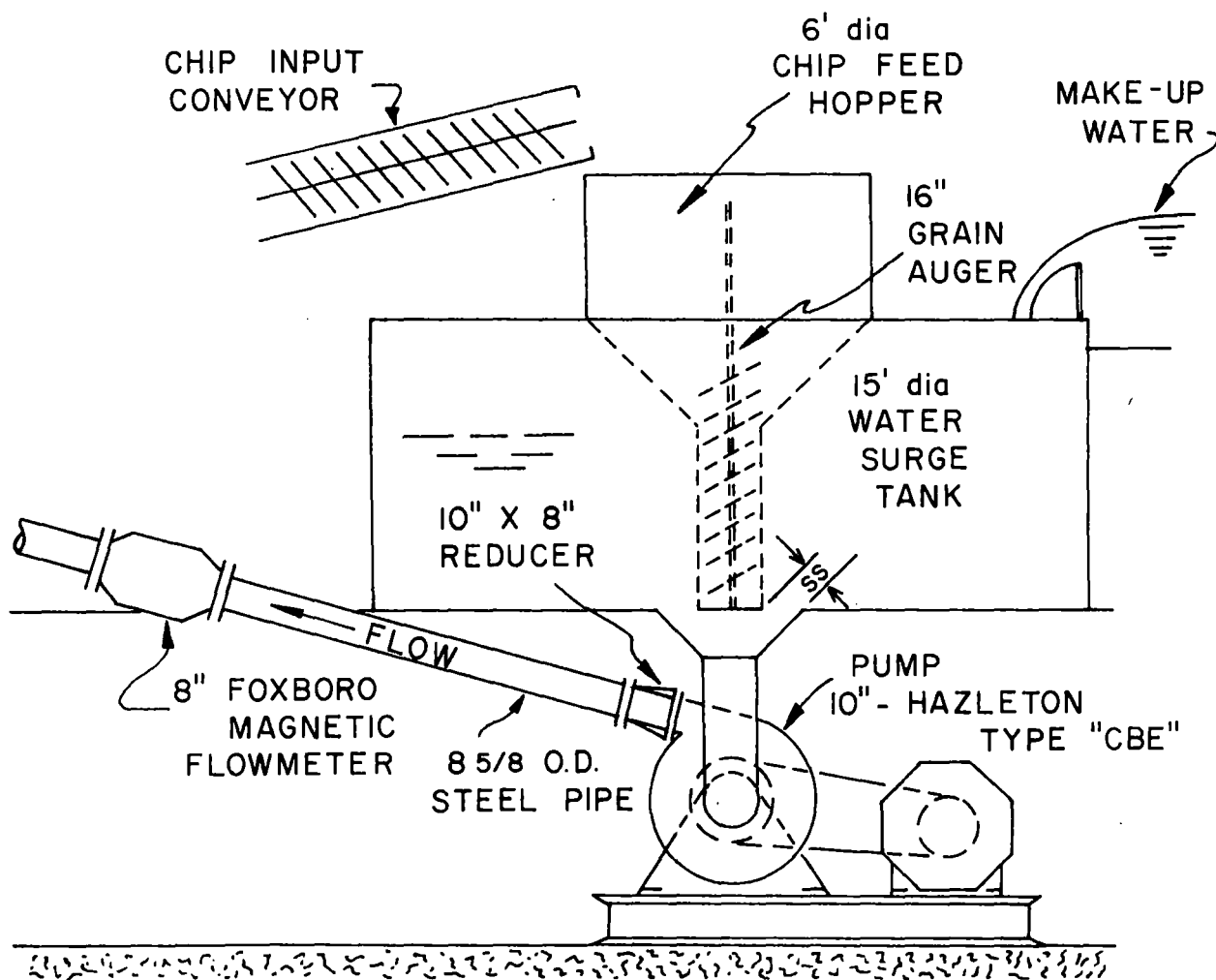


FIG. 28. CHIP INJECTION SYSTEM (Pilot line studies)

the auger housing and the pump intake cone (distance ss in Fig. 28), an inflow velocity great enough to counteract the velocity of rise for unsaturated wood chips. (For oven-dry lodgepole pine chips used in these studies, the maximum rise velocity was found to be approximately 0.35 fps, 0.11 m/s).

The water storage tank for the pilot line installation was designed to hold a volume equal to the volume of the pipeline. This criteria was selected for this particular installation only because the line was filled initially and after subsequent drainings from this reservoir. The design of the make-up water storage tanks for prototype installations are governed by local conditions for each pipeline but should include consideration of (1) the minimum depth of water above the eye of the pump impeller required to prevent a vortex from introducing large volumes of air into the pump casing, and (2) the maximum volume of make-up water required to supply fluctuations in the flow rate in the pipeline and to maintain the flow if the make-up water supply is disrupted.

Initially, the auger in the injection system was powered by a variable speed hydraulic motor driven by a gear pump. The variation in auger speed caused by variations in the torque loading during the initial start-up and during periods of heavy chip concentrations being recycled through the test loop created the major and minor unplanned changes in flow conditions discussed in Sec. 4.4. After the hydraulic motor was replaced by a constant speed drive motor, the injection system provided a continuous feed rate of uniform concentration for subsequent test runs.

Two or more injection augers of this type may be installed in parallel units to supply a high capacity pipeline system if a preliminary feasibility study indicates a single-unit system is not as economical or as reliable from an operational standpoint as a multiple-unit installation.

The injection system with an open mix tank and enclosed auger permits the design of a pump station utilizing a bank of fixed-speed single-stage centrifugal pumps installed in series with one or more variable speed units to provide the additional head required to allow for unplanned changes in the flow conditions.

5. CORROSION STUDIES^{2/}

5.1 Scope of Problem

The internal corrosion of pipe walls is a major factor in the study of the hydraulic transportation of woodchip-carrier water mixtures in pipelines. The corrosion results from acids leached from the wood chips by the carrier water; Asano, Towlerton, and Sanks (1974) have shown that these acids include acetic from the acetyl groups, uronic and organic from carbohydrates and vanillic from lignins. All are responsible for reducing the pH of the carrier water to a range of 4.7 to 5.5. Corrosion is also enhanced by a high dissolved oxygen content in the carrier water.

Knowledge of the rate of corrosion of these interior pipe walls caused by the carrier water is important to a designer. This rate can be combined with the other design parameters to allow a truly economic optimization of design.

The investigation of various methods which provide tests yielding a rapid determination of a rate of corrosion was undertaken. The result was the development of a method using a device called a corrosometer. The development and application of a corrosometer utilizing the mixed potential theory for obtaining polarization curves to establish the corrosion rates of the interior walls in a pipeline transporting a woodchip-carrier water mixture is given in this report.

5.1.1 Purpose. The purpose of this part of the pilot line study was to determine a method for computing an instantaneous rate of corrosion of the

²Corrosion studies were conducted and reported by James E. Borg; final editing of this portion of the report was done by Dr. William A. Hunt.

interior wall of a pipeline transporting a mixture of wood chips and water. The criteria for the method selected were: (1) applicable to bench-scale tests in the laboratory using simulated mixtures of wood chips and carrier water, (2) applicable to pilot-line tests, (3) easy to operate, (4) inexpensive, and (5) capable of giving the rate of corrosion nearly instantaneously.

5.1.2 Specific objectives. The specific objectives were (1) to evaluate the effects of pH, velocity of woodchip-carrier water and changes in dissolved oxygen on the rate of corrosion of the pipe walls, (2) to formulate rates of corrosion for bench-scale and pilot-line tests, (3) to compare the results of the bench-scale and pilot-line tests, and (4) to make a preliminary evaluation of the magnitude of corrosion losses possible in the hydraulic transport of wood chips in steel pipelines.

5.2 Review of Methods

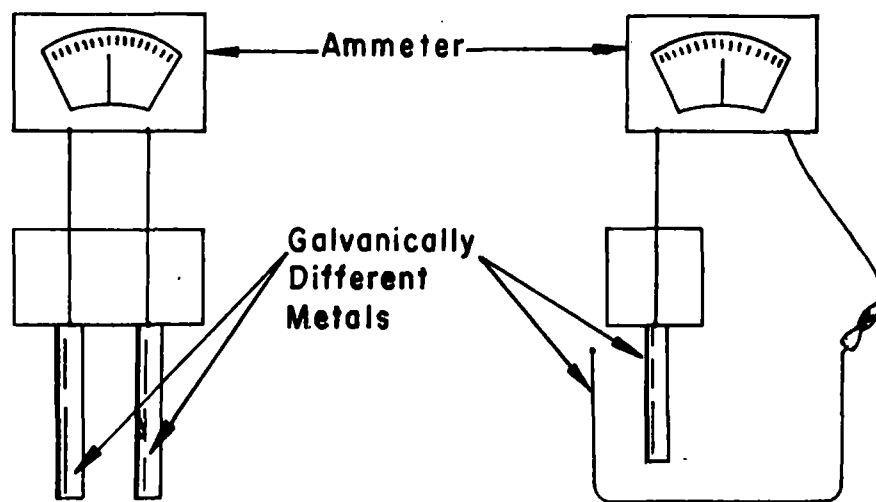
The following section describes various methods used to determine corrosion rates of the interior walls of pipelines transporting corrosive liquids. The discussion includes destructive methods such as the spool and coupon tests, and non-destructive methods such as the galvanic, electrical resistance, ultrasonic and polarization techniques.

5.2.1 Spool test. The spool test requires that a removable section of pipe be taken out of the line after a period of service and weighed to determine its weight loss due to internal wall corrosion. The corrosion rate is calculated by dividing the weight loss of the spool by its time in service. The method is simple and accurate but cumbersome and

time-consuming because the spool must remain in service a considerable length of time before the rate of corrosion can be determined. The method fails to provide any indication of the variation of the rate of corrosion with time.

5.2.2 Coupon test. The coupon test is similar to the spool test in that it too is a measure of weight loss per unit time. "Monitoring Corrosion" (Grant Oil Tool Co.) describes the coupon as a small plate of the sample material 4 3/4 inches (12.0 cm) long, 1/2 (1.0 cm) inch wide, and 1/8 inch (0.3 cm) thick inserted in the pipe perpendicular to the wall with the edge presented to the flow to minimize impingement. One disadvantage of the coupon is an unequal rate of corrosion occurs at different areas of coupon causing a non-uniform dissolution of metal. Consequently, a false overall corrosion rate is obtained when the total weight loss is divided by the time of exposure. A second disadvantage is the possible hindrance to flows of suspensions when the coupon is inserted into the pipeline. The coupon fails to measure the variation of the corrosion rate with time.

5.2.3 Galvanic method. The galvanic method provides a qualitative measure of a liquid's corrosivity using the apparatus shown in Fig. 29. NACE (Publication 3D170) describes the apparatus as an ammeter connected to two electrodes of dissimilar metals which are inserted into the solution to be studied. Because corrosion is an electrochemical process, the higher the conductance of the solution the greater the corrosion rate. Serious disadvantages of the galvanic method are caused by the electrodes which: (1) are inserted into the pipe, causing impingement and possible obstruction of



(a) Two Electrode Assembly (b) Single Electrode; Vessel is Second Electrode

FIG. 29.

TWO METHODS OF USING THE GALVANIC PRINCIPLE FOR CORROSION MEASUREMENTS.

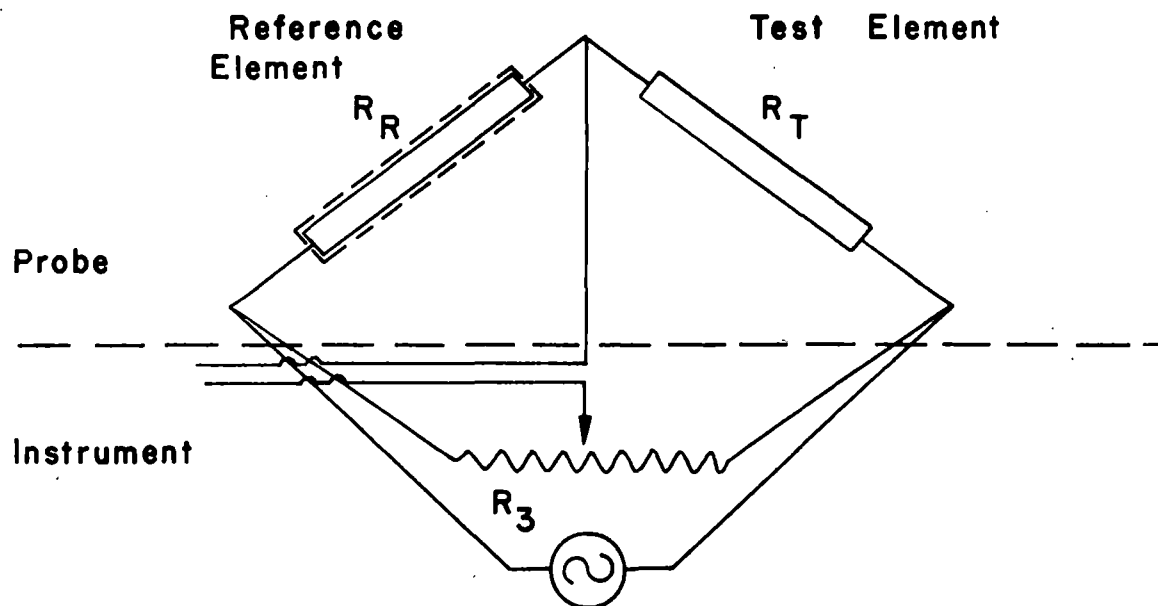


FIG. 30.

A SCHEMATIC OF THE CIRCUITRY UTILIZED IN THE ELECTRICAL RESISTANCE METHOD FOR CORROSION MEASUREMENT.

the flow of liquid-solid mixtures and (2) become easily fouled by the test electrolyte. Also, this method is only a qualitative measurement of corrosion.

5.2.4 Electrical resistance. The method shown in Fig. 30 for determining corrosion rates of metals in their liquid environments utilizes the change of resistance to a metallic specimen as its cross-sectional area decreases from a loss of metal. Weight losses are correlated directly with the change in resistance of the test specimen. The corrosion rate is determined by dividing the weight loss by the time between measurements. Advantages of this technique are (1) the investigator does not come into contact with the corrosive environment and (2) changes in the corrosion rate with time may be observed. Serious disadvantages include (1) the apparatus is easily short-circuited, (2) conductive corrosive liquids alter the resistance of the test element, and (3) insertion into the pipe may obstruct the flow of suspensions.

5.2.5 Ultrasonic devices. Devices to determine the thickness of pipe walls by ultrasonic methods are available commercially from firms such as the Krautkramer Company. These instruments provide valuable information about the pitting tendencies of the walls' specific pipe locations, but cannot be utilized effectively in general corrosion studies because of the large number of locations required and the amount of data required to observe the corrosion at each point. This method, like the spool and coupon methods, requires that the specimen actually be in service for a length of time before a corrosion rate can be determined.

5.2.6 Polarization resistance method. An electrochemical testing technique (hereafter referred to as the polarization method) was chosen to be investigated more fully in this study for three reasons: (1) the method provides an instantaneous corrosion rate, (2) the device used in the polarization method can be altered for use in both bench-scale and pilot-line tests, and (3) the method is simple and provides the amount of data needed to determine a rate of corrosion with only 15 minutes of observation. The following section presents polarization theory in greater detail.

5.3 Theory of Polarization Method

Once an engineer has determined corrosion will occur, his second thought concerns the kinetics, or rate of corrosion. Fontana and Greene (1967) show thermodynamics may be used in determining whether or not corrosion will occur. Because the corroding system is not in equilibrium, methods for determining rates of corrosion have not been formulated from thermodynamic principles. Methods employing electrode kinetics to determine the rates of corrosion requiring short test periods have been developed and are reported by NACE (n.d.), Fontana and Greene (1967), Eaton and Annand (n.d.), Morris and Scarberry (1972), Reinoehl et al. (1970), and Makrides (1962).

5.3.1 Definitions. Before the fundamental theory of electrode kinetics and, subsequently, the polarization technique are presented in detail, a number of basic terms must be precisely defined for use in the context of corrosion reaction rates:

Anode: an electrode at which net oxidation occurs

Cathode: an electrode at which net reduction occurs

Equilibrium potential: electromotive force series potential

Overvoltage: the potential of an electrode displaced from its equilibrium potential

Oxidation: A reaction in which an element undergoes a net decrease in electrons

Polarization: the displacement of an electrode potential from its equilibrium resulting from a net current

Reduction: a reaction in which an element undergoes a net increase of electrons

5.3.2 Exchange current density. The principle of the exchange current density is illustrated by what occurs on the reversible hydrogen electrode established on platinum shown in Fig. 31. The hydrogen undergoes oxidation when it loses its electrons as it ionizes and goes into solution and reduction when it acquires electrons from the surface of the platinum to form hydrogen gas. At equilibrium the reaction rate of oxidation, r_1 , must equal the reaction rate of reduction, r_2 . This is measured as a finite rate of hydrogen interchange in moles of hydrogen reacting per unit surface area per unit time. Because electrons are being transferred in this reaction, this rate may also be stated in terms of electrical charge transferred per unit electrode surface area per unit time, or current per unit electrode surface area. This current per unit area will be defined as the current density and will have the units of amps/cm^2 .

Using Faraday's Law:

$$r_{\text{oxidation}} = r_{\text{reduction}} = i_o/nF \quad (30)$$

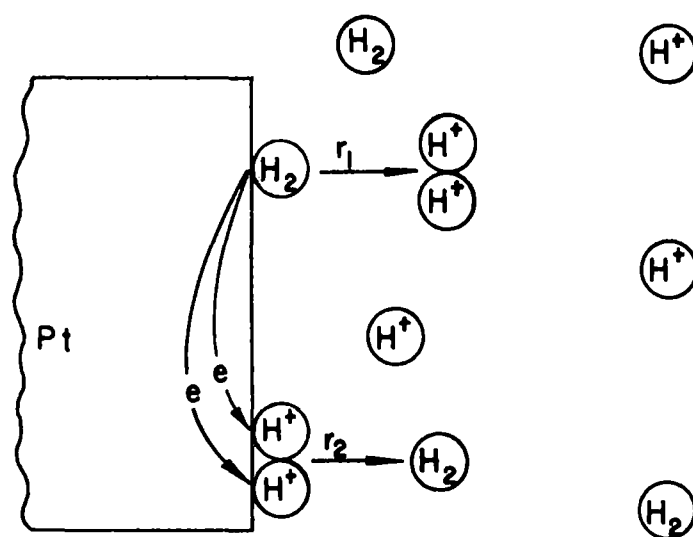


FIG. 31.
HYDROGEN ELECTRODE ON PLATINUM.

where $r_{\text{oxidation}}$ and $r_{\text{reduction}}$ are the rates of oxidation and reduction, i_0 is the exchange current density, n is the number of electrons transferred and F is Faraday's constant.

The exchange current density is a function of the composition and emf potential of the reacting electrode, the temperature of the solution and the ratio of the amount of substance in solution in oxidation to the amount of substance in reduction in the solution. Because of the large number of parameters influencing the exchange current density of an electrode in a solution, the exchange current density must be determined experimentally.

5.3.3 Polarization types. The limiting process governing the rate of polarization of a metal in an electrolyte is used to identify the type of polarization occurring.

Activation polarization refers to polarization of a metal in an electrolyte whose current density is controlled by the slowest step in a reaction sequence. In the illustration of the hydrogen electrode on platinum the slowest reaction step might be the transfer of the electrons from the platinum surface to the hydrogen ion, or the joining of the hydrogen atoms to form a hydrogen molecule. Activation polarization can be defined in terms of current density and overvoltage by the following relationship:

$$\eta_a = \pm \beta \log(i/i_0) \quad (31)$$

where η_a is the activation overvoltage, i is the current density, i_0 is again the exchange-current density and β is the Tafel constant, which is defined in the following paragraph.

The overvoltage is shown as a linear function of the current density on the semi-logarithmic graph in Fig. 32. The β slope, or Tafel constant,

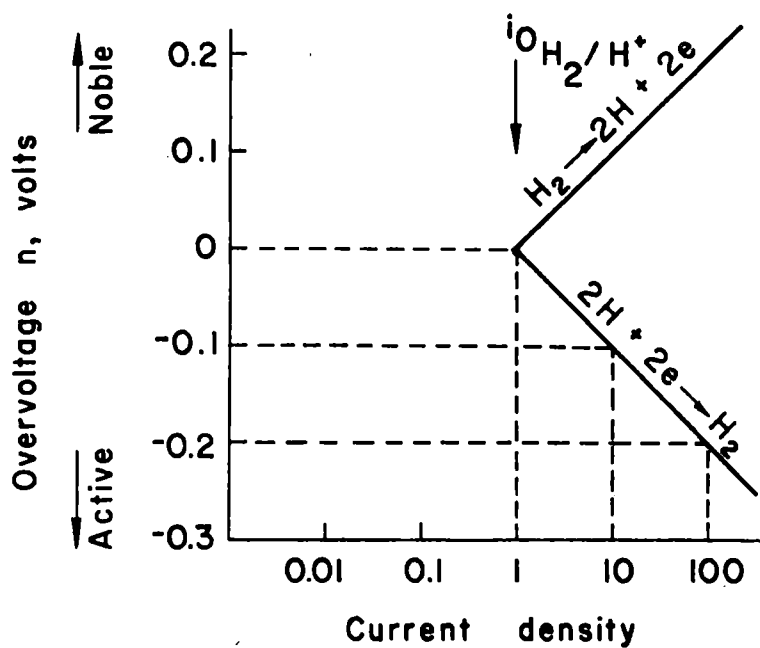


FIG. 32.
ACTIVATION-POLARIZATION CURVE OF A HYDROGEN ELECTRODE.

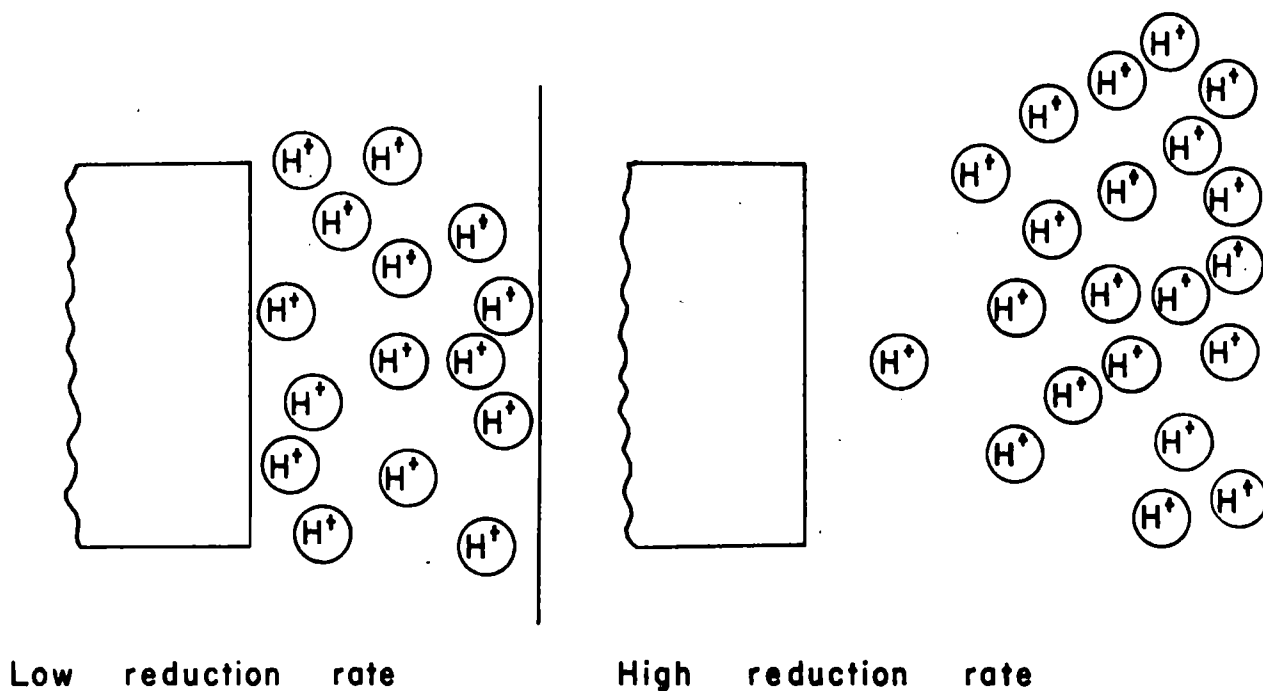


FIG. 33.
CONCENTRATION GRADIENTS DURING HYDROGEN EVOLUTION - SCHEMATIC

is the slope of the relationship in volts of overvoltage per order of magnitude of current density. A positive β slope indicates the hydrogen is undergoing oxidation and the overvoltage is proceeding in a direction more positive or noble than its emf potential. A negative β slope indicates the hydrogen is undergoing reduction resulting in an overvoltage more negative, or active, than its emf potential.

Concentration polarization refers to polarization of a metal in an electrolyte whose current density is controlled by the number of reactants adjacent to the electrode. This condition is illustrated in Fig. 33. At low reduction rates the distribution of hydrogen ions in solution is uniform. Reduction rates increase until limited by the diffusion rate of hydrogen ions through the electrolyte layer adjacent to the electrode surface. Concentration polarization occurs when the overvoltage-current density relationship is controlled by the number of ions in the electrolyte layer adjacent to the electrode. Current is, in this case, controlled by the movement of the charged hydrogen ions in the electrolyte which receives the electrons on the surface of the metal electrode. At higher reduction rates, the number of hydrogen ions adjacent the metal electrode is depleted. The current then becomes a function of how quickly the hydrogen ions can diffuse into the adjacent layer from the surrounding electrolyte.

This limiting diffusion current density, i_L , is defined by the following relationship:

$$i_L = \frac{DnFC_B}{X} \quad (32)$$

where D is the diffusion coefficient of the reacting ions, C_B is the concentration of the reacting ions in the bulk solution, X is the thickness of

the diffusion layer of the electrolyte adjacent to the electrode (a function of the shape of the electrode, geometry of the system and agitation of the electrolyte), n and F were defined previously. Fontana and Greene (1967) state η_c , the concentration overvoltage, is then:

$$\eta_c = \frac{2.3RT}{nF} \log(1 - i/i_o) \quad (33)$$

where i is the current density, R is the gas constant and T is the absolute temperature.

Concentration polarization does not become apparent until the net reduction current density approaches the limiting condition where the reduction current density is independent of the concentration overvoltage as shown in Fig. 34. The physical meaning of this phenomenon is that regardless of the amount of voltage placed on the electrode, the electron transfer proceeds only as rapidly as the rate that the hydrogen ions diffuse through the adjacent electrolyte layer to combine with these electrons in the production of hydrogen gas.

At any electrode, activation and concentration polarizations occur simultaneously. Activation controls at low reaction rates and low current densities, and concentration polarization controls at high reaction rates and high current densities. The total polarization of an electrode is the sum of these polarizations or:

$$\eta_T = \eta_c + \eta_a \quad (34)$$

Consider the oxidation process at a zinc electrode in a zinc ion solution shown in Fig. 35. As previously defined, oxidation occurs when an element undergoes a decrease of electrons. In the case of the zinc electrode, the zinc passes into solution and the electrons flow within the

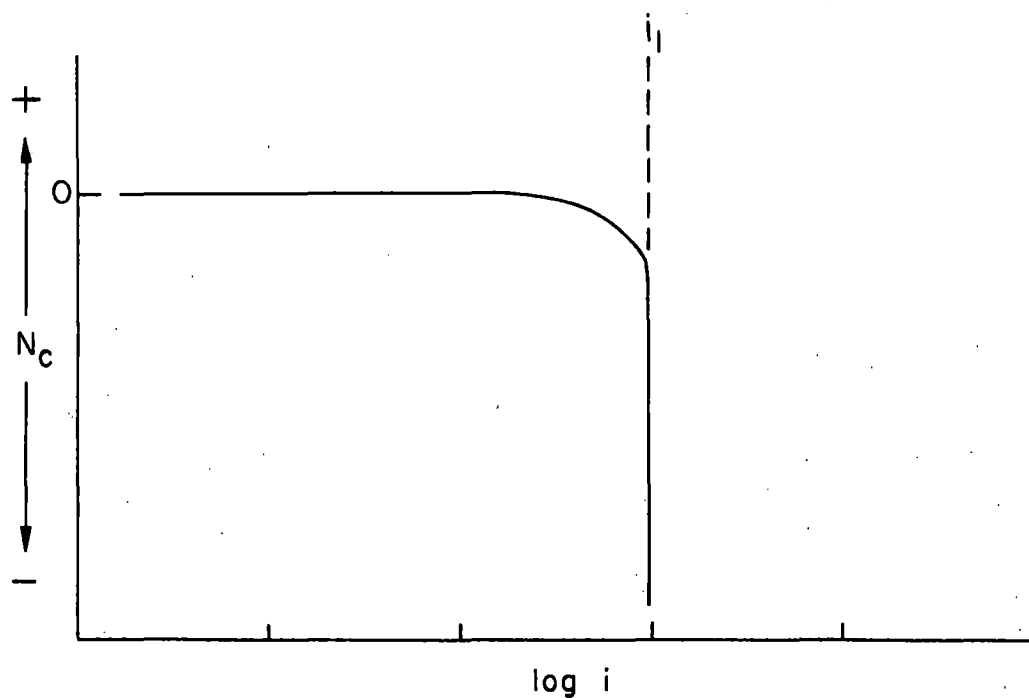


FIG. 34.
CONCENTRATION POLARIZATION CURVE (REDUCTION PROCESS)

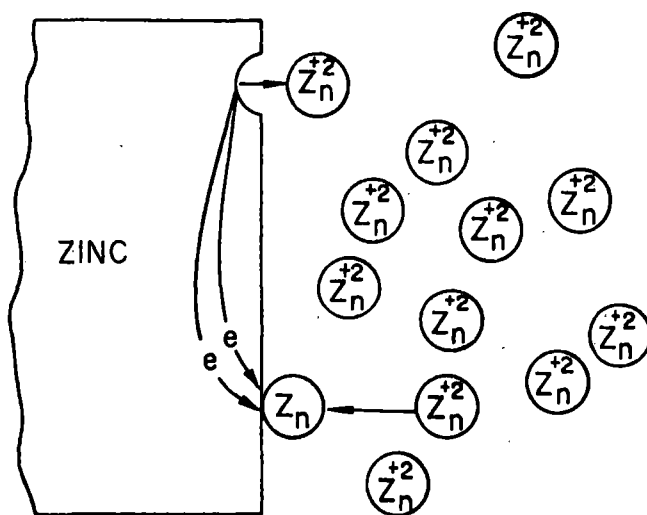


FIG. 35.
REVERSIBLE ZINC ELECTRODE

electrode to a point where they combine with a zinc ion to form a reduction reaction. Because the rate of zinc ions going into solution in the upper portion of the electrode is independent of the concentration of zinc ions adjacent the zinc electrode, concentration polarization cannot occur. This situation of zinc ions going into solution is called anodic dissolution. The equation of the total polarization of this situation is:

$$\eta_T = \beta \log i/i_o \quad (35)$$

The number of zinc ions in the electrolyte diffusion layer adjacent to the lower portion of the electrode of Fig. 35 is a governing factor in the reduction rate of the system. Here concentration polarization occurs and is included in the equation of total polarization which becomes:

$$\eta_T = -\beta \log i/i_o + \frac{2.3RT}{nF} \log (1 - i/i_o) \quad (36)$$

with a negative activation polarization term resulting from the reduction process which occurs. This reduction process is also termed cathodic polarization.

The importance of Eqs. (35) and (36) cannot be overemphasized, for they are the basic equations for all electrochemical reactions. Eq. (35) applies to every anodic dissolution reaction, with the exception of active-passive metals which will be discussed later, while Eq. (36) defines every reduction reaction. By using i_o , β and i_L , the kinetics of all corrosion reactions can be precisely described.

5.3.4 Mixed-potential theory. The mixed potential theory of electrode kinetics as described by Fontana and Greene (1967) contains two hypotheses:

- (1) any electrochemical reaction can be divided into two or more partial

oxidation and reduction reactions and (2) no net accumulation of electrical charge can occur during an electrochemical reaction. An example of the second hypothesis occurs when a metal electrode is immersed in an electrolyte, the electrode cannot spontaneously accumulate electrical charge. These hypotheses form the basis for the assumption that when an electrically-isolated metal sample corrodes, the total rate of oxidation must equal the total rate of reduction. These mixed-potential hypotheses combine with the kinetics equations previously presented to form the basis of modern electrode-kinetics theory. Utilization of the mixed-potential theory can be best demonstrated by considering mixed electrodes.

A mixed electrode is an electrode where two or more oxidation-reduction systems occur simultaneously as illustrated by the zinc electrode in the zinc ion solution in Fig. 36. The zinc electrode now becomes a mixed electrode by the additional presence of hydrogen ions. Zinc and hydrogen oxidize to their respective ions in solution while zinc and hydrogen ions reduce to zinc metal and hydrogen gas.

The polarization curves of zinc and hydrogen oxidation and reduction are shown in Fig. 37. The only point on the curves where the oxidation rate is equal to the reduction rate is the intersection of the zinc oxidation curve with the hydrogen reduction curve. This intersection defines both the corrosion potential in reference to the hydrogen emf potential theoretically, or practically, to some arbitrarily chosen reference electrode, E_{corr} , and the corrosion current density, i_{corr} .

An example of this is a zinc pipe containing an acid. The rate of zinc dissolution, in this case corrosion, must equal the rate of hydrogen

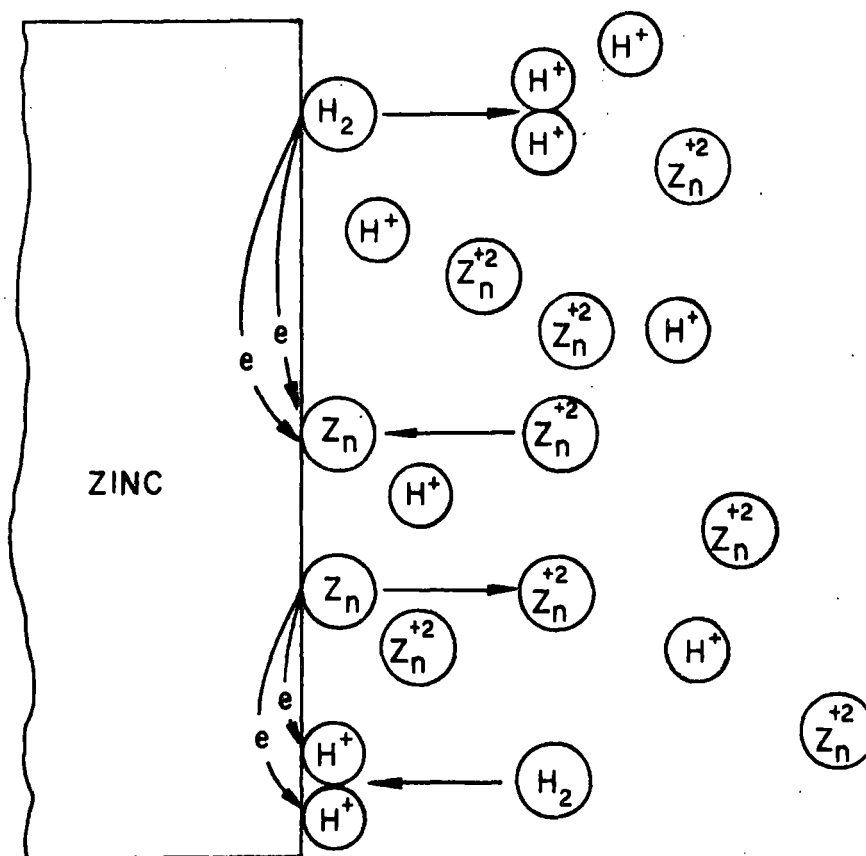


FIG. 36.
A ZINC MIXED ELECTRODE

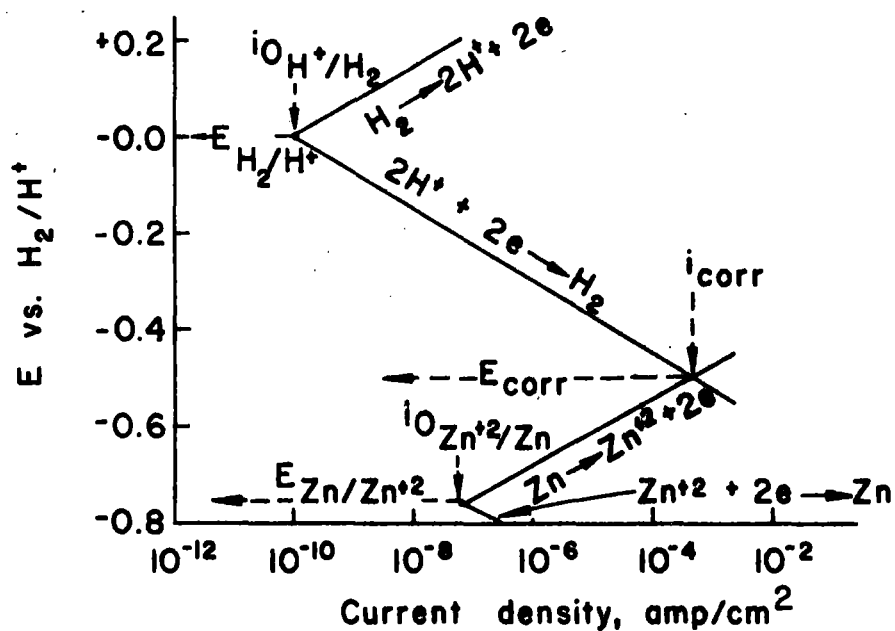


FIG. 37.
ELECTRODE KINETIC BEHAVIOR OF PURE ZINC IN
ACID SOLUTION - SCHEMATIC.

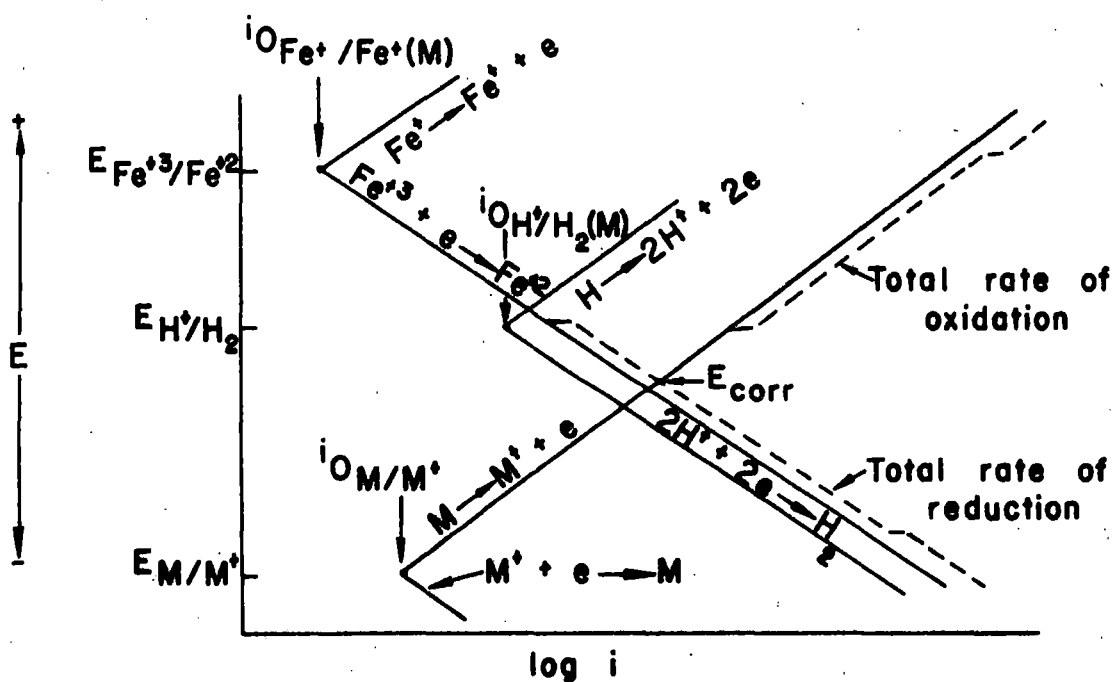


FIG. 38.
BEHAVIOR OF METAL M IN ACID SOLUTION CON-
TAINING FERRIC SALTS SHOWING DETERMINATION
OF E_{corr} .

gas formation. These rates are in terms of the corrosion current density, i_{corr} . This can be taken further in the consideration of a pipe of metal M carrying an acid solution containing ferric salts. The polarization curves for the three reversible reactions are shown in Fig. 38. Once again the corrosion current density and potential occur at the point where the total reduction equals the total oxidation. In this case this occurs at the intersection of the algebraic addition of the current-densities of the iron and hydrogen reduction curves for a given overvoltage and the metal in oxidation curve.

The conversion of these corrosion current densities into actual corrosion rates of milli-inches per year will be discussed later.

5.4 Effects of Changes of System Parameters

All of the previous development of theory has been for quiescent systems. The following section gives an insight into the effects of increasing the velocity, oxidizer concentration, temperature and pH of the electrolyte on the corrosion rate calculated from the polarization curves.

5.4.1 Velocity. A change in the velocity of the electrolyte affects the amount of control the concentration polarization exerts on reduction or cathodic polarization curves. An increase in velocity provides a fresh supply of ions in the electrolyte adjacent to the electrode. The additional availability of ions causes an increase in the limiting current density and an increase in the corrosion current density, i_{corr} , as is shown in Fig. 39.

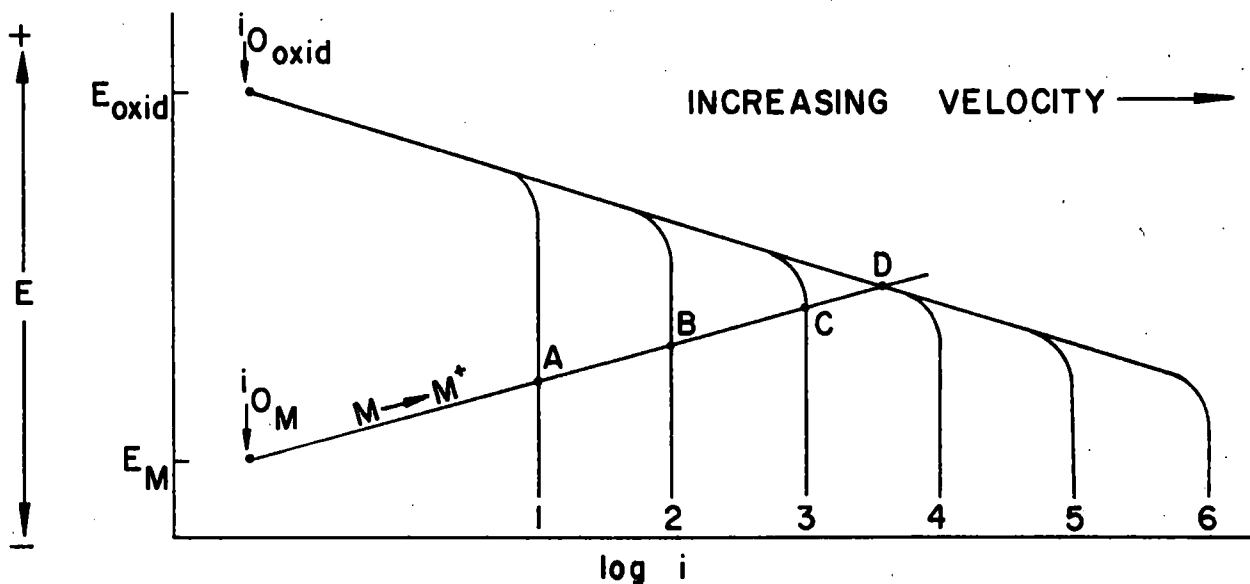


FIG. 39.
EFFECT OF VELOCITY ON THE ELECTROCHEMICAL BEHAVIOR
OF A NORMAL METAL CORRODING WITH A DIFFUSION-
CONTROLLED CATHODIC PROCESS.

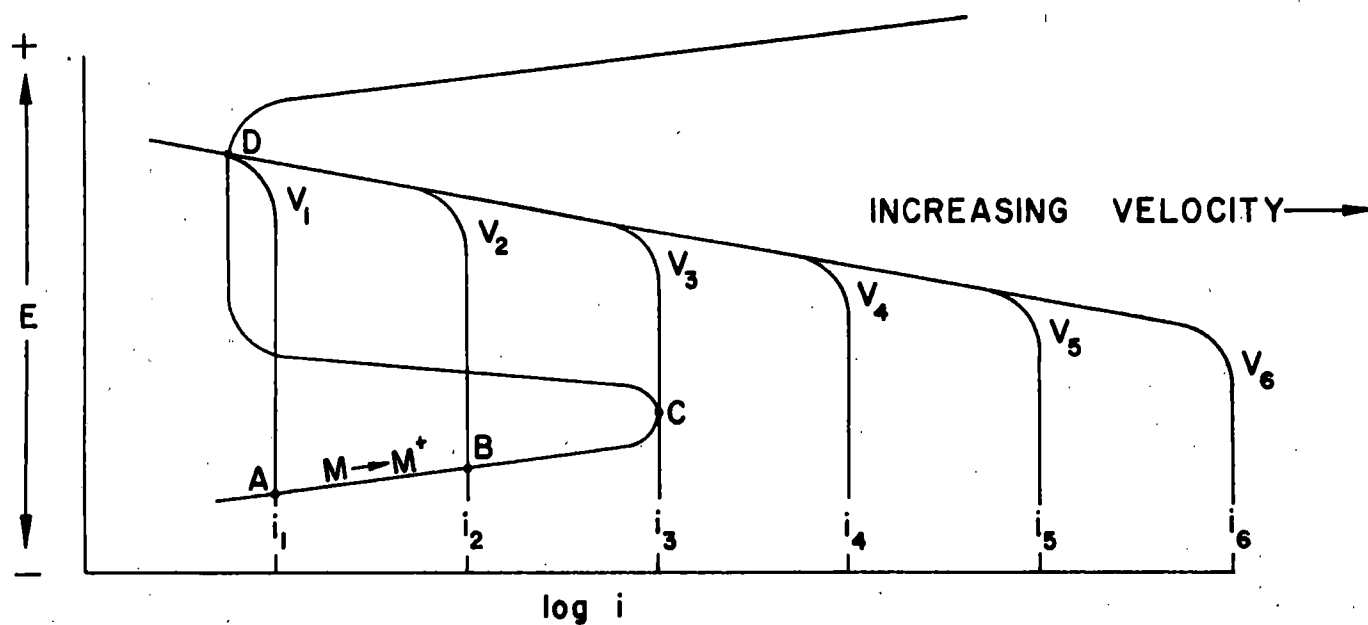


FIG. 40
EFFECT OF VELOCITY ON THE ELECTROCHEMICAL BEHAVIOR
OF AN ACTIVE-PASSIVE METAL UNDER DIFFUSION CONTROL

The effects of an increase in the velocity of an electrolyte on the corrosion rate of an active-passive metal is shown in Fig. 40. Active-passive electrochemical behavior occurs when the oxidation of a metal is hindered by a deposit of corrosion product on the surface of the electrode. This deposit results in the "loop" which reduces the corrosion current to a constant value. An overvoltage does exist which is great enough to cause current densities to again increase with increasing overvoltage. How the curve leaves the passive region again is also shown in Fig. 40 and is called the trans-passive region. Ferric hydroxide is an example of iron displaying the passive characteristic of active-passive electrochemical behavior. In the cases of velocities 4 and 5 in Fig. 40, the intersections of the reduction polarization curves with the oxidation polarization curve gives smaller value for the corrosion current densities and corrosion rates than occur with the intersections given with slower velocities 1, 2 and 3. In general, two rules are evident concerning velocity effects:

1. Electrolyte velocities affect the corrosion rates of systems dominated by concentration polarization. Velocities have no effect on systems dominated by activation polarization because the corrosion rate is controlled by the slowest step of the reaction sequence, which is independent of the number of ions in solution adjacent to the electrode.
2. The corrosion rate of a metal in a diffusion-controlled system becomes independent of electrolyte velocity at very high velocities. This is shown in Fig. 40 for velocities greater than that indicated by velocity 3.

5.4.2 Oxidizing agent. The concentration of an oxidizing agent also alters the corrosion rate. For example, an increase in dissolved oxygen in a system increases the corrosion current density and consequently the corrosion rate for a metal dominated by activation polarization. This

condition is shown in Fig. 41. The total reduction curve is the algebraic addition of the current densities for given overvoltages of the hydrogen and oxidizing agent reduction curves. As the concentration of oxidizing agent is increased, the additional curve must be added to the existing curve. This results in a curve which is shifting with increasing oxidation concentration to the right, or larger current density, direction on Fig. 41.

The loop and its corresponding passive corrosion current density in the case of a metal displaying an active-passive system presents a different situation.

Generally, the corrosion current density increases in the active-passive metal system until point C shown in Fig. 42 is reached. The current density where the "nose" of the oxidation polarization curve occurs is termed the critical current density. As the reduction polarization curve proceeds past this "nose" in the noble direction into the passive region, the corrosion current density becomes smaller, the intersection shown by points F, G, and H. When the reduction curves goes far enough to the right to intersect the oxidation curve in the transpassive region, the corrosion current density, and consequently the corrosion rate, will again increase with an increasing oxidizing agent concentration.

5.4.3 Temperature. The effect of an increase in temperature on the oxidation polarization curve is shown in Fig. 43. In general, any increase in temperature, in an active-passive metal system increases the current densities for given potentials and specifically raises the critical current density significantly.

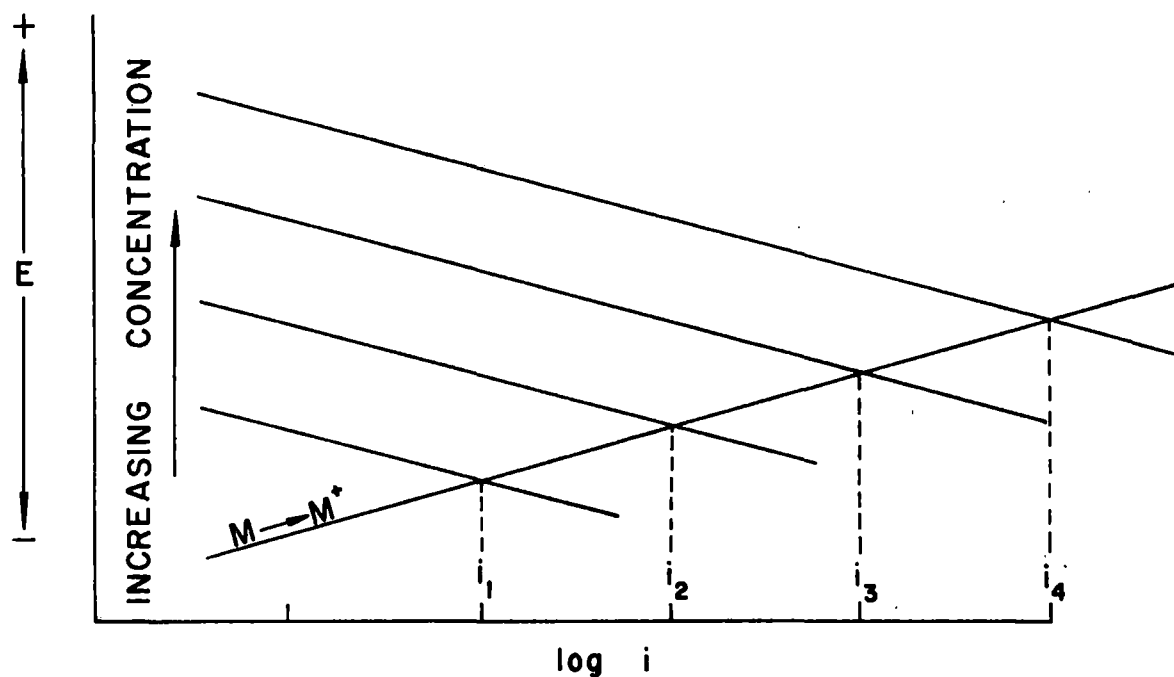


FIG. 41.
EFFECT OF OXIDIZING AGENT CONCENTRATION ON
CURRENT DENSITY.

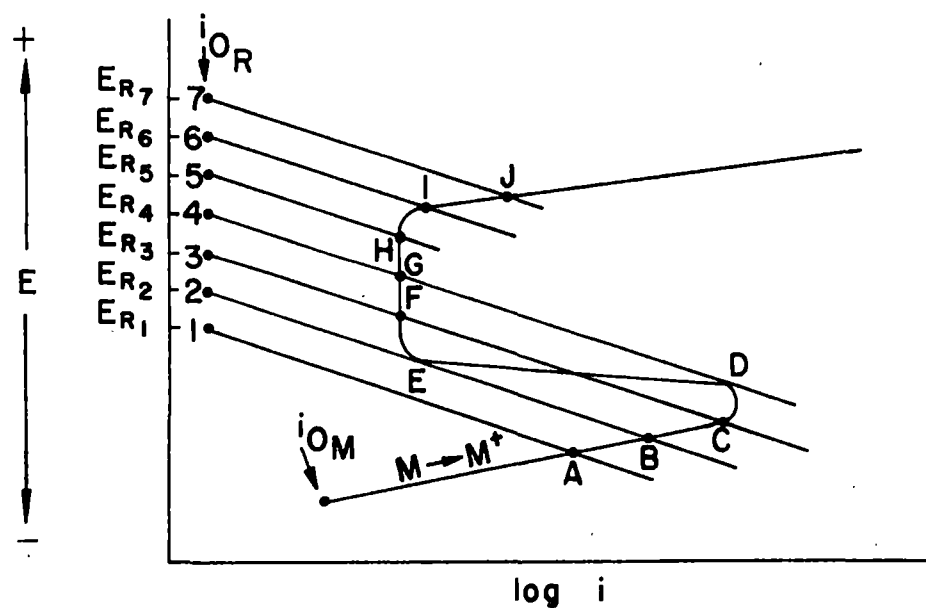


FIG. 42.
EFFECT OF OXIDIZER CONCENTRATION ON THE
ELECTROCHEMICAL BEHAVIOR OF AN ACTIVE-
PASSIVE METAL.

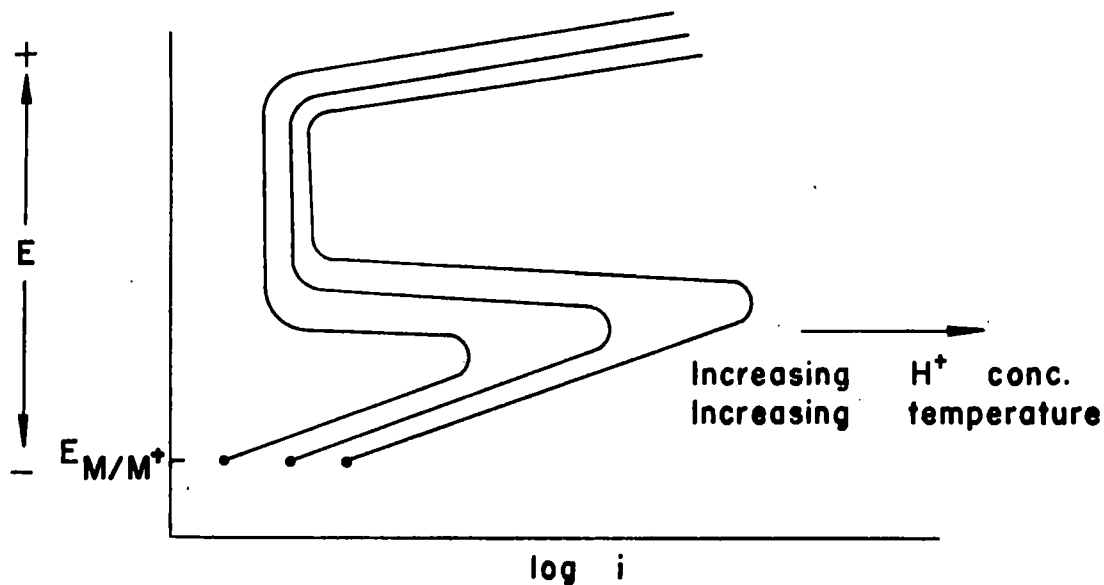


FIG. 43.
EFFECT OF TEMPERATURE AND ACID CONCENTRATION
ON ANODIC DISSOLUTION BEHAVIOR OF AN ACTIVE-
PASSIVE METAL.

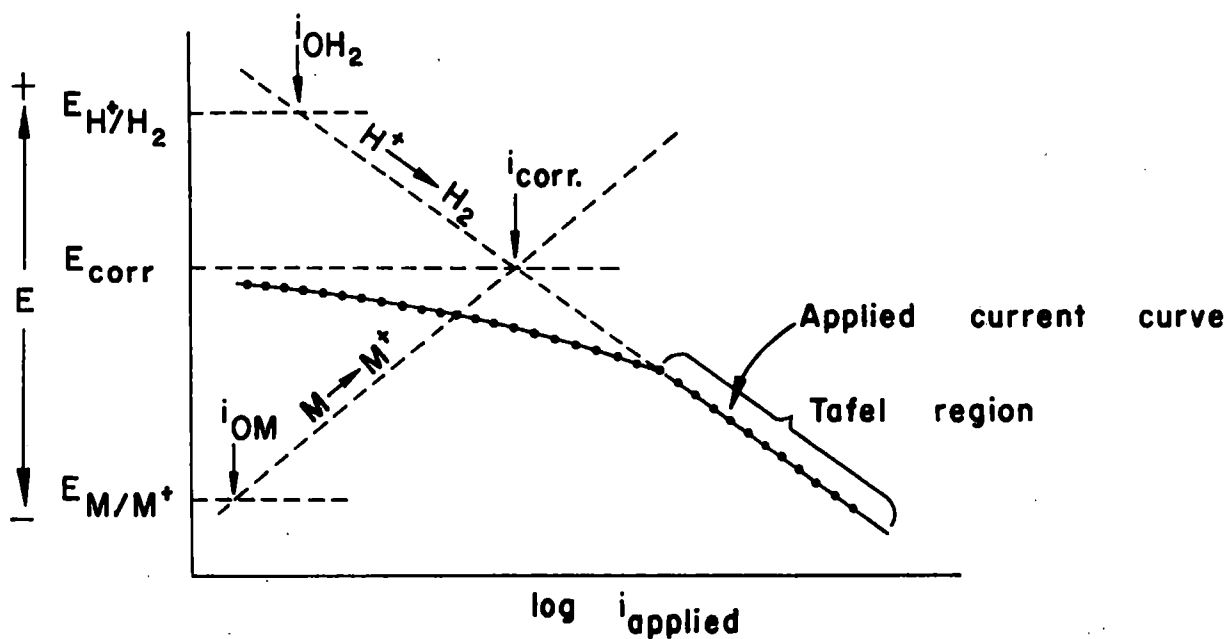


FIG. 44.
APPLIED CURRENT CATHODIC POLARIZATION CURVE OF
A CORRODING METAL SHOWING TAFEL EXTRAPOLATION.

5.4.4 pH. An increase in the hydrogen ion concentration (decrease in pH) affects the system in much the same manner. Further information on the effects of temperature and hydrogen ion concentration increases may be found in a study by Eaton and Annand (n.d.).

5.5 Application of Polarization Method

The method Traud and Wagner (cited by Fontana and Greene, 1967) developed for determining corrosion rates utilizing the mixed potential theory and its application to calculating the amount of metal loss occurring by corrosion is outlined in the following paragraphs.

5.5.1 Tafel extrapolation. Data for cathodic (reduction) polarization curves are obtained by increasing the current through a working electrode immersed in an electrolyte and observing the change in the potential between the working and reference electrodes. The polarization curve determined by graphing the change in the potential of the test electrode as a function of current density is shown in Fig. 44. The linear region of the higher current densities is called the Tafel region and the slope of the section of the curve is the Tafel constant, β , discussed previously in the section on activation polarization. The slope is negative because this is a reduction process. At current densities whose corresponding overvoltages are within 50 mv of E_{corr} , local anode-cathode effects on the metal surface cause the curve to deviate from the Tafel slope and become tangent to the E_{corr} line at very small current densities. When the tangent in the region is extrapolated in the direction of the noble potential, it intersects the line of constant corrosion potential and the anodic dissolution (oxidation)

polarization curve at a point corresponding to the corrosion current density, i_{corr} , on the abscissa scale. E_{corr} is the open circuit potential between the working and reference electrodes.

5.5.2 Weight loss calculation. Morris and Scarberry (1972) converted the corrosion current density into a corrosion rate of milli-inches of surface lost per year. Faraday's Law, Eq. (30), is combined with the relationship between weight loss per unit time and surface area to compute the corrosion rate. A number of equations have been developed to simplify the calculation of the corrosion rate.

The theoretical electrochemical equivalent for a particular metal sample assumes each major element in an alloy has a valence equal to the number of electrons in the outermost principle shell of the elemental atom. The electrochemical equivalent is found using the following equation:

$$K = W_{\text{aw}} / (96500 B_v) \quad (37)$$

where K is the electrochemical equivalent in grams/coulomb, W_{aw} is the gram atomic weight and B_v is the valence of the atom. Table 1 lists the electrochemical equivalents for a number of major elements.

Table 8. Electrochemical equivalents for various elements

Element	Gram Atomic Weight	Valence ⁽¹⁾	Electrochemical equivalent, gm/coul x 10 ⁻⁴
Nickel	58.71	2	3.044
Chromium	52.01	1	5.389
Iron	55.85	2	2.893
Molybdenum	95.95	1	9.943
Copper	63.54	1	6.584

(1) Number of electrons in outermost shell

The total electrochemical equivalent for an alloy is the weighted sum of the various elements in that alloy. An alloy containing 30 percent and 70 percent iron would have an electrochemical equivalent, K_T , of:

$$K_T = .30 K_{Cu} + .70 K_{Fe} \quad (38)$$

The theoretical loss of metal in grams for a test electrode of surface area A in cm^2 subjected to a corrosion current density I in amp/cm^2 for the time t in sec calculated using the equation:

$$M = KITA \quad (39)$$

where K is the electrochemical equivalent for the alloy in grams/coulomb, and M is the mass of the metal lost in grams.

This metal loss in grams, transformed into milli-inches of surface thickness lost per year (hereafter designated as mpy), is calculated as follows:

$$M = KITA = \rho Z_1 \quad (40)$$

where ρ is the density of the electrode in gm/cm^3 , Z_1 is thickness of uniform layer of metal loss in cm. The thickness in milli-inches, Z , is $.00254Z_1$, giving the equation

$$Z = KIT/ (.00254\rho) \quad (41)$$

Application of the theory of polarization to determine the corrosion rate of the interior wall of a pipe carrying a mixture of wood chips and carrier water is presented in the following sections.

5.6 Development of Mixed Potential Corrosometer

The Tafel extrapolation of the cathodic polarization curve given by Morris and Scarberry (1972) presented a method for determining the corrosion

rates and quantity of metal loss in a short test period. The application of this technique for use in field tests of estimating the corrosion rates for interior walls of pipes in which fluids flow was investigated in this study. Because previous studies utilizing the polarization curves for corrosion rates had not been conducted with pipelines flowing under pressure, it was necessary to modify the configuration of the instrumentation system used by previous investigators for pipeline installations in the field.

The design and development of a device for monitoring the corrosion rate of interior pipe walls was divided into three phases: (1) the design, development and fabrication of the basic instrumentation system, (2) the performance of a series of bench tests to develop techniques of collecting data, to evaluate the operation and accuracy of the apparatus and to examine the corrosion rate for the pipe material exposed to carrier water for a mixture of wood chips and water, and (3) the performance of a series of tests on a test pipeline using prototype-scale pipes to determine the range of corrosion rates for the interior walls of a pipeline transporting mixtures of wood chips and water.

The instrumentation system developed will be referred to as the corrosometer.

5.6.1 Principles of corrosometer design. The preceding discussion shows that a device for determining corrosion rates utilizing cathodic (and/or anodic) polarization curves is based on the following principle:

When the potential of a working (corroding) electrode immersed in an electrolyte is shifted to a potential different from that of an electrode arbitrarily installed (called an auxiliary

electrode) to complete a circuit, a net current flows through the circuit. (The potential difference is supplied by an external source connecting the working and auxiliary electrodes.)

The cathodic polarization curve is the graph of the potential of the working electrode as a function of the logarithm (base 10) of the applied current obtained by direct measurement from the circuit similar to that presented by Fontana and Greene (1967) shown in Fig. 45.

The current is passed between the working electrode and auxiliary electrode using the variable D.C. power source; the current is measured in micro- or milli-amperes; the potential of the working electrode is measured in millivolts against the reference electrode shown in Fig. 45. A calibrated electrode of known potential with respect to the zero emf potential of hydrogen is used as a "reference" electrode because the potential of the working electrode with respect to hydrogen cannot be measured directly.

The reference finally used in this study was a calomel electrode with a potential of 0.2445 volts.

5.6.2 Bench-scale tests. Two series of bench-scale laboratory tests were conducted using electrodes fabricated from specimens of the pipe wall of the 2345-ft (715-m) pilot line to be used in the flow tests. These tests were run for the following reasons: (1) to develop a technique for obtaining data for polarization curves to be used to determine corrosion rates, (2) to verify the operation and accuracy of the apparatus by comparing the data observed for the electrodes of the pipe wall material with those observed by other investigators using electrodes of similar materials in a standard electrolyte, and (3) to determine an approximate corrosion rate of

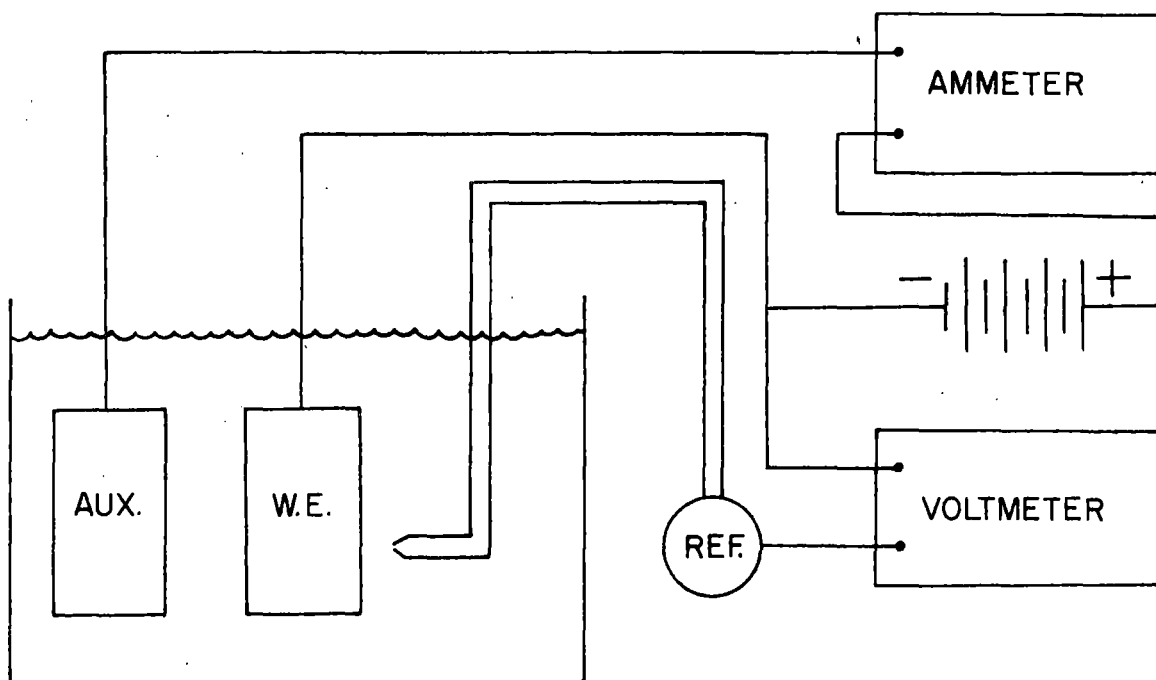


FIG. 45.
CORROSION CIRCUI T DIAGRAM FOR CATHODIC
POLARIZATION STUDIES

the pipe walls using the carrier water of a mixture of wood chips and water agitated in a closed container in the laboratory.

Apparatus. The circuit for the laboratory model corrosometer was assembled as shown in Fig. 45 using the following components.

All alloy test electrodes were prepared from a section of pipe wall to be used in the pilot-line study of the hydraulic transportation of wood chips. The dimensions of the working electrode were 0.50 by 0.70 in. (1.27 by 1.78 cm) with a thickness equal to that of the pipe wall, 0.188 in. (0.48 cm). These dimensions were the same as used in the study by Morris and Scarberry. Two auxiliary electrodes were prepared from the pipe wall; one, the same dimensions as the working electrode; the other, 1 inch (2.54 cm) square. The composition of the steel alloy of the electrodes (and pipe wall) are given in Table 9 along with data on samples used by Morris and Scarberry (1972) and Reinoehl et al. (1970).

Table 9. Analysis of test electrode materials

Study	Material/Composition, %								
	Fe	Ni	Cr	Mn	C	Si	Cu	S	other
Morris & Scarberry ()	46.400	31.330	20.600	0.860	0.050	0.310	0.420	0.007	0.023
Reinoehl, et al. ()	99.995	--	--	--	0.003	--	--	--	0.002
MSU Pipe- line Corro- someter	99.100	--	--	0.650	0.200	0.010	--	0.019	0.021

The two sizes of auxiliary electrodes were used to determine the effect of the surface area of the auxiliary electrode on the data generated by the corrosometer. All electrode surfaces other than the test surfaces were isolated from the electrolyte by a layer of epoxy.

A silver reference electrode was used during the initial tests run to establish the data collection procedure. After experiencing apparent instabilities test points and non-repeatability of data, a calomel electrode (Thomas, large-area junction, industrial Ag-AGCl, Model No. 4105-L) was employed. The spacing between the reference and working electrodes should be no greater than two diameters of the reference electrode tip to minimize any electrolytic effect on the potential readings according to the study by Makrides (1962). This spacing was chosen at 0.25 inch (6.3 mm). The spacing between the auxiliary and working electrodes was arbitrarily chosen at 2 inches (50.8 mm).

The electrodes and test electrolyte were placed in a 1000-ml beaker for conducting the bench tests.

A 1-amp, variable D.C. power source was used during the initial tests; this, too, was later replaced by a 5-amp power source. The potential of the working electrode with respect to the reference electrode and the current in the circuit were measured with a digital volt-ohmmeter and a D.C. vacuum tube ammeter.

Test procedure. The tests were conducted using a procedure similar to that used by Morris and Scarberry.

The exposed surfaces of the auxiliary and working electrodes were prepared for each test by sanding with 120 grit paper, degreasing with 1,

1, 1 trichlorethane, rinsing with distilled water and air drying. Electrodes were immersed in the test solution within 5 minutes after preparation to minimize any contamination which may result from their exposure to an impure atmosphere.

The open circuit potential was noted as soon as the electrodes were immersed in the electrolyte; the system was allowed to stabilize for 5 minutes after the power supply was energized with no current flowing.

A data scan was made while the current was varied over a range of 1000 milliamperes. A "scan" as used in this study refers to the set of current readings and corresponding emf potentials between the working and reference electrodes obtained as the current was varied incrementally in one direction. Each test consisted of two scans, one while the current was increased from zero to the maximum value and one while the current was decreased from the maximum to zero. This is different from the procedure of Fontana and Greene in which the potential difference between the working and reference electrodes was varied while the corresponding current was recorded. The average scan rate was 300 ma/min which is 45 volts/hr for the apparatus and is comparable to the 50 volts/hr used by Morris and Scarberry. Reinoehl et al. used 18 volts/hr. Data were recorded at 100 ma intervals during both scans.

At the completion of each test, the working electrode remained immersed for five minutes to allow its potential to stabilize to the corrosion potential, E_{corr} .

The data for each run were plotted on corrosion behavior diagrams (CBD) as each run (or series of similar runs) was completed. The potential

of the working electrode with respect to the reference electrode was graphed as a function of the current density (obtained by dividing the current by the exposed surface area of the working electrode) on semi-logarithmic graph paper with the current densities along the abscissa scale and the potentials along the linear ordinate scale.

Calibration tests. The electrolyte was prepared by dilution of the reagent H_2SO_4 with distilled water to form a 10 percent solution by volume. A fresh quantity was prepared daily to minimize weakening or contamination and add consistency to results. The electrolyte was allowed to cool to room temperature 23°C before starting a test. A 10 percent solution of (sulfuric) acid was used in the Morris and Scarberry study; one percent in the study by Reinoehl, Beck and Fontana.

Initially, a series of 39 tests was run to (1) develop the procedure, (2) establish the validity of the results, (3) determine the effect of the surface area of the auxiliary electrode, and (4) determine the number of tests possible using the same electrolyte. Each working electrode was tested for four conditions and the number of replications is shown in Table 10 which summarizes the averages of the data for each test condition.

The data obtained from the individual observations were used to construct the anodic polarization curves shown in Figs. 46-49 for comparison with those shown by Morris and Scarberry and Reinoehl et al. (All data are on file in the Department of Civil Engineering, Montana State University.) The primary passive potential and critical current density were noted as the point where the current decreases rapidly for a small increase in overvoltage in the anodic polarization.

Table 10. Anodic polarization characteristics for bench tests of pipeline corrosometer in 10 percent H_2SO_4

Test conditions	Working electrode size (cm ²)	Number of tests	Ave. scan rate (volts/hr)	Ave. Primary passive potential (volts)	Ave. Critical current density (ma/cm ²)	Ave. Open-circuit potential (volts)	Temp. °C
1S	2.26	4	43.3	-.023	319.	-0.486	23
1L	6.48	5	47.3	-0.22	310.	-0.487	23
2S	2.26	4	43.7	+.003	321.	-0.486	23
2L	6.48	6	50.9	-.013	317.	-0.484	23
3S	2.26	4	45.7	+.018	310.	-0.487	23
3L	6.48	6	48.3	-.017	310.	-0.485	23
4S	2.26	4	40.9	-.018	332.	-0.485	23
4L	6.48	6	49.1	-.020	303.	-0.482	23

Test conditions: 1) fresh electrolyte, clean electrodes; 2) once used electrolyte, clean anode; 3) twice used electrolyte, clean anode; 4) thrice used electrolyte, clean anode.

Table 11. Anodic polarization curve parameters of an active-passive metal in sulfuric acid solutions

	Temperature °C	Solution H_2SO_4 by volume %	Test scan rate (volts/hr)	Open circuit, corrosion potential, E_c (volts)	Primary passive potential, V (volts)	Critical current density, I_c (ma/cm ²)
Morris and Scarberry (1972)	25	10	50	-.280	-.160	0.58
	80	10	50	-.280	-.200	3.10
Reinoehl, Beck and Fontana (1970)	25	1	18	-.500	0.000	350.000

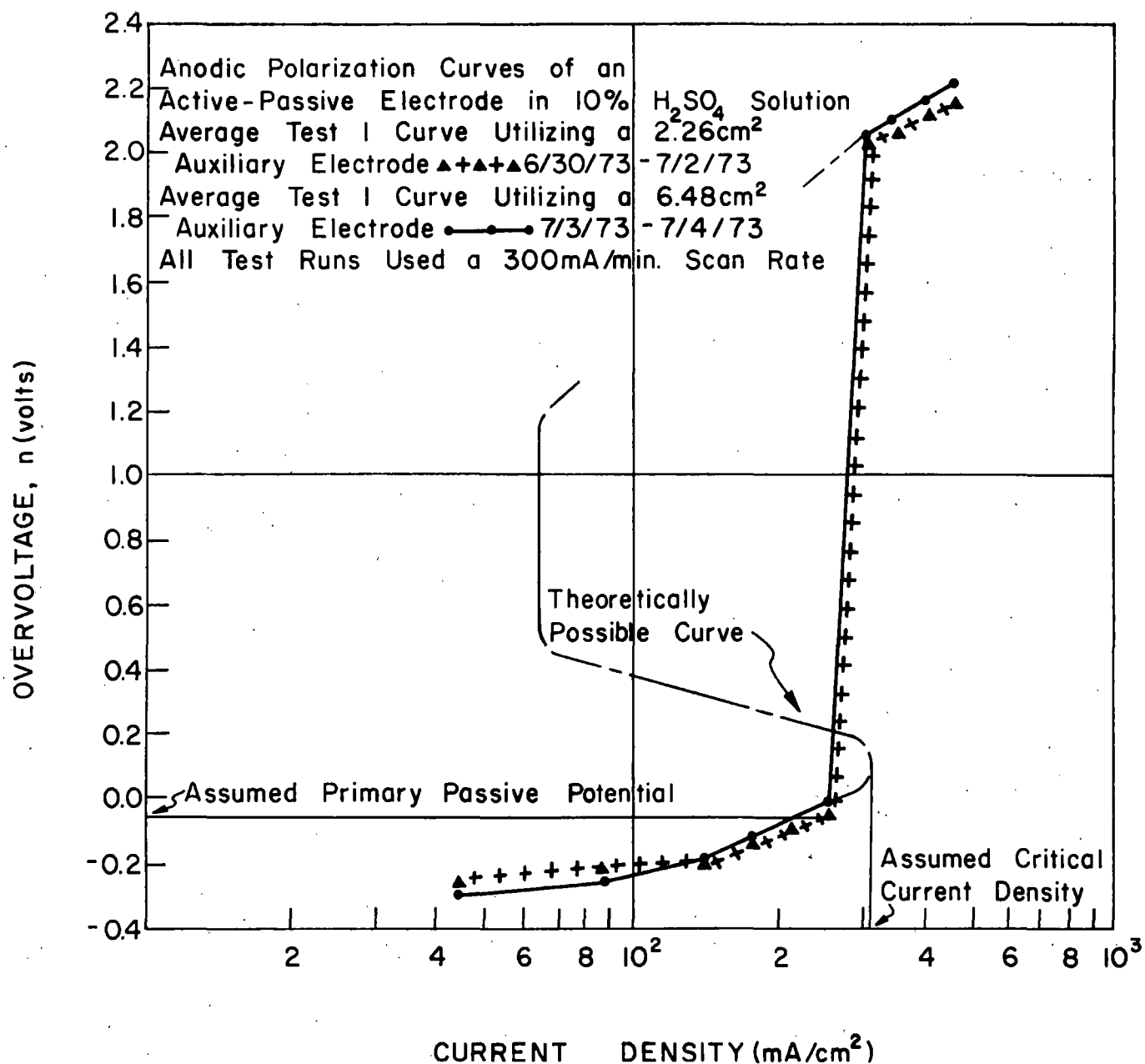


FIG. 46. ANODIC POLARIZATION OF ACTIVE-PASSIVE ELECTRODE.

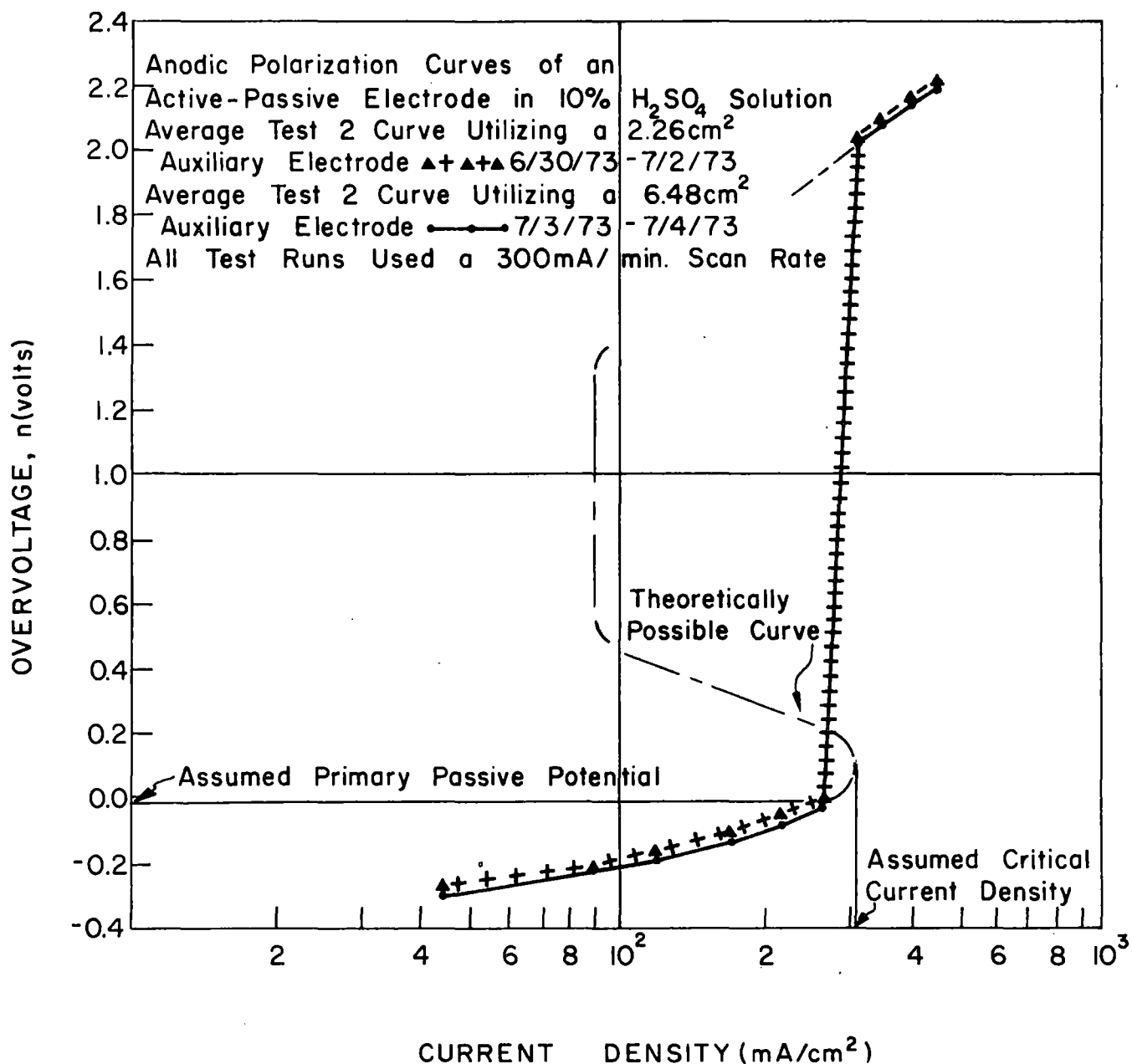


FIG. 47. ANODIC POLARIZATION OF ACTIVE-PASSIVE ELECTRODE.

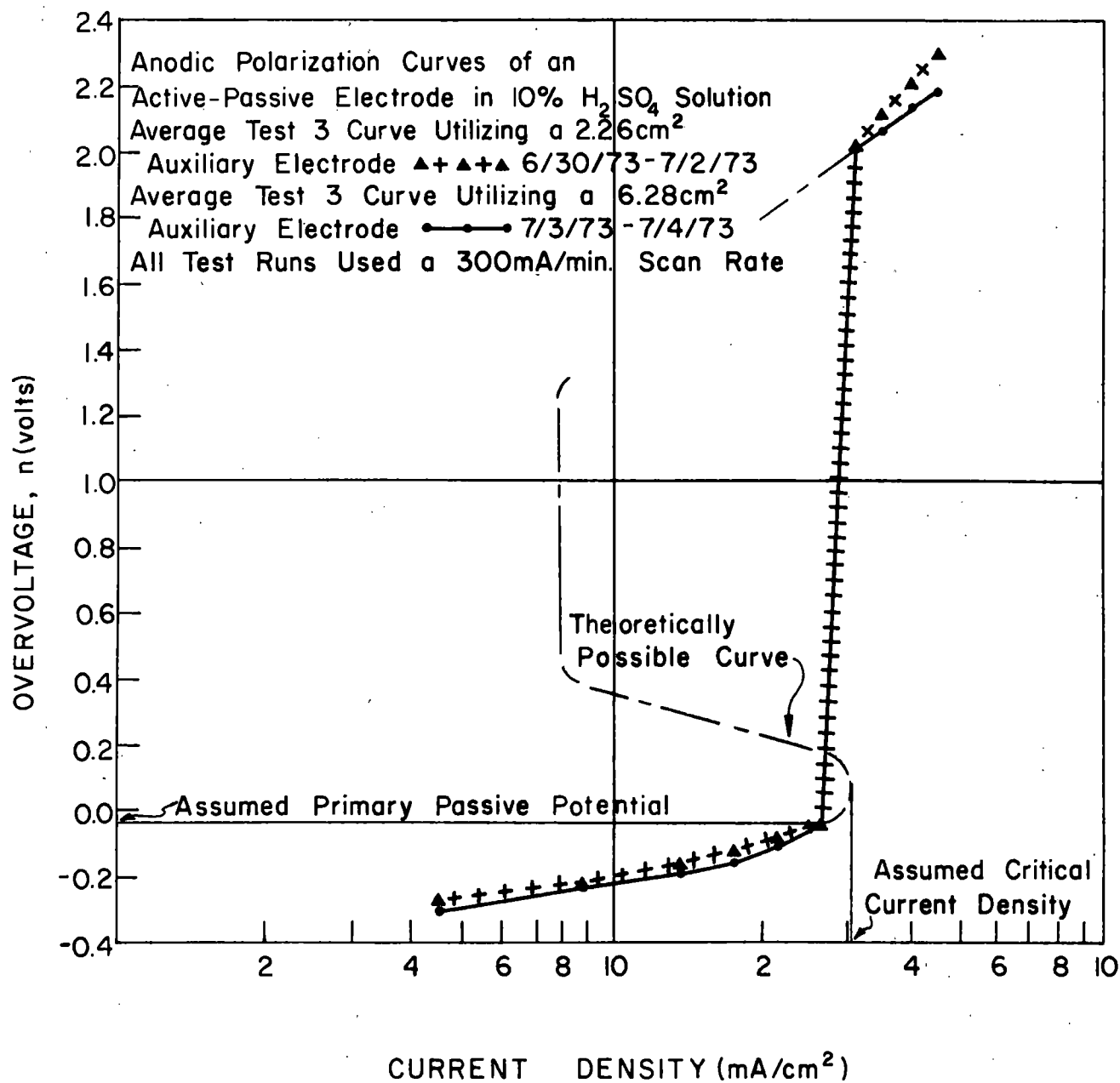


FIG. 48. ANODIC POLARIZATION OF ACTIVE-PASSIVE ELECTRODE.

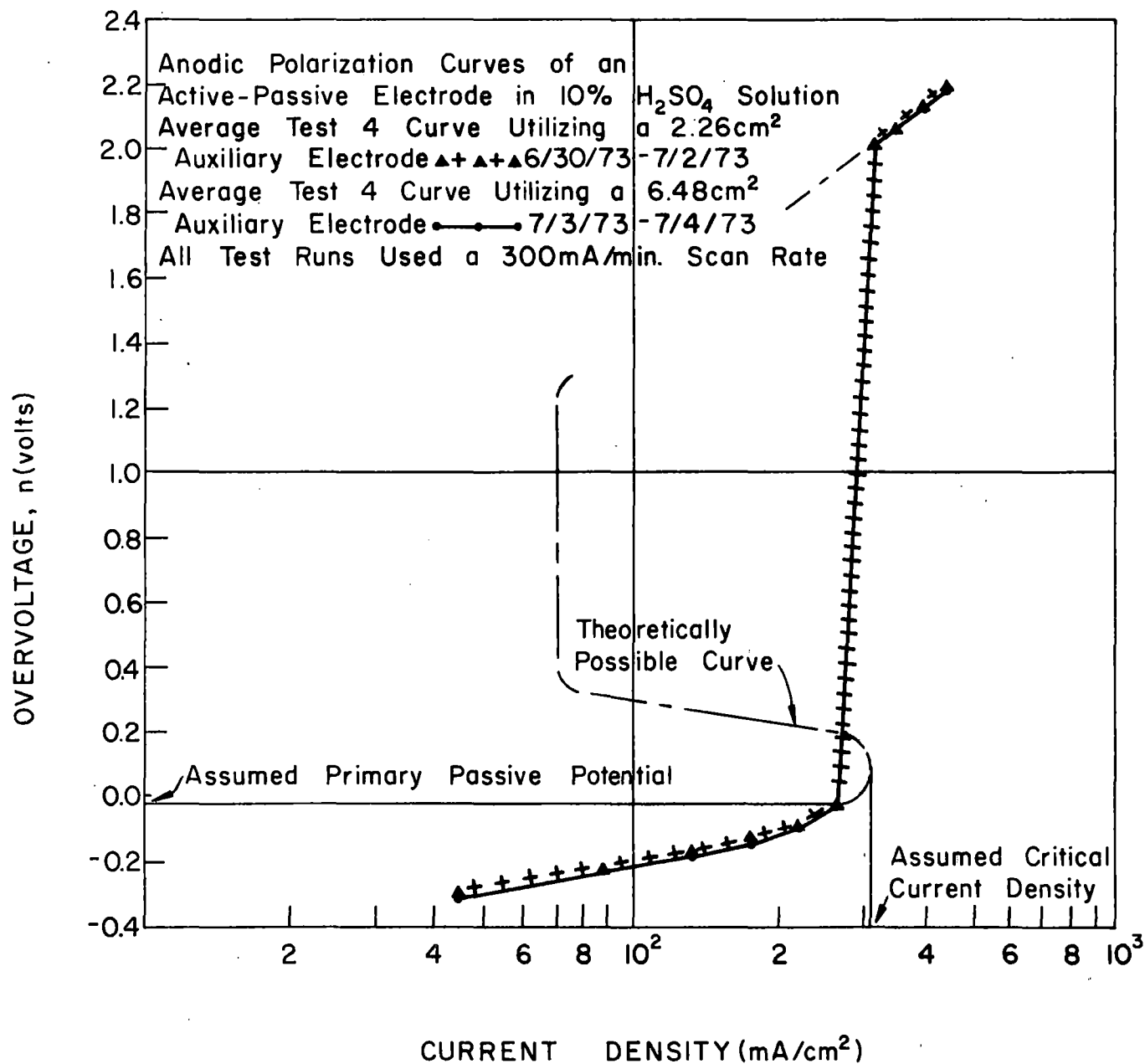


FIG. 49. ANODIC POLARIZATION OF ACTIVE-PASSIVE ELECTRODE.

Results from the studies by Morris and Scarberry and Reinoehl, Beck and Fontana are listed in Table 11 giving the CBD parameters of temperature and scan rate and corrosion parameters of critical current densities, primary passive potentials and the open circuit corrosion potentials.

A comparison of the data of Tables 10 and 11 shows the open circuit and primary passive potentials of all three studies display similar characteristics.

The open circuit and primary passive potentials of the three studies were approximately equal. The critical current densities of the study by Morris and Scarberry were 0.58 and 3.10 ma/cm² for 25°C and 80°C, respectively, while the critical current density in the Reinoehl and the MSU corrosometer studies were 350 and 300-320 ma/cm², respectively. Because the composition of the materials used is the major difference between the Morris study and the Reinoehl and the MSU corrosometer studies, it is assumed that this causes the difference between the critical current density of the Morris study and that of the others.

The curves of Figs. 46-49 show that the effect of the surface area of the auxiliary electrode is not a significant factor in the polarization characteristics.

The close correlation of results in the corrosometer and Reinoehl study justified the application of the corrosometer in the study of the corrosion rate of laboratory simulated woodchip-carrier water mixtures.

5.6.3 Carrier water tests. A second series of laboratory tests was then conducted to determine if the corrosometer principle could be used in an electrolyte with a much greater resistivity and higher pH than a 10 percent

sulfuric acid solution, to determine the effect of the location of the electrode connection to a pipe ring band used as the auxiliary electrode, and to calculate a corrosion rate from the bench-scale tests.

Apparatus modification. The corrosometer circuit was altered by reversing the polarity on the leads from the power source for determining the cathodic polarization curves of the specimen of pipe material in a woodchip-carrier water mixture simulated in the laboratory. Other changes in the apparatus from that used in the 10 percent sulfuric acid tests were the substitution of section of uncleaned pipewall for the cleaned auxiliary electrode as shown in Fig. 50 and the use of a plastic tray in place of the 1000-ml beaker to accommodate the pipewall auxiliary electrode. The working electrode and its preparation for test runs were the same as in the calibration tests.

Electrolyte preparation. A study by Asano, Towlerton and Sanks (1974) has shown that most acids are leached from the wood chips by the carrier water within 5 hours of contact; this period was used for the mixing time in this study. Both mechanical and pneumatic methods were used for agitating the wood chips in the carrier water. The mixtures used contained 10 percent by volume of lodgepole pine wood chips.

Mechanical mixing apparatus consisted of a 42-inch (107-cm) length of 8-in.-I.D. (200mm-I.D.) PVC pipe capped with plexiglass disks at both ends. The PVC vessel was mounted with its longitudinal axis at right angles to another horizontal shaft which was rocked in an oscillatory motion through a 90-degree arc by a variable speed motor equipped with a speed reducer.

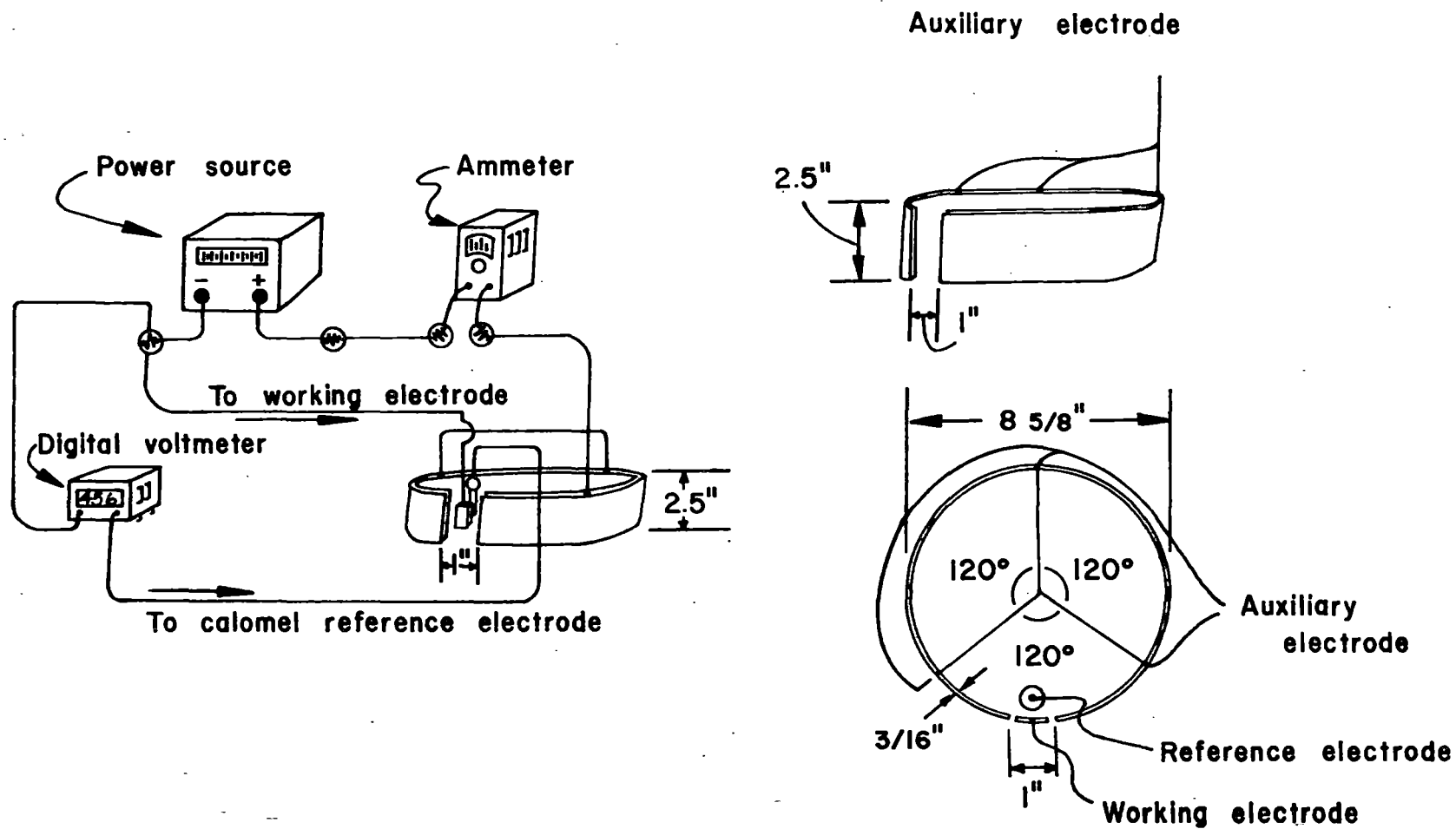


FIG. 50. PIPE-RING CORROSOMETER TEST APPARATUS.

The pneumatic mixing consisted of injecting compressed air into the mixture near the bottom of a 20-liter laboratory bottle holding the carrier water and wood chips. Tap water was used as the carrier water to duplicate approximately the conditions obtained in the pilot line and in prototype installations.

The two mixing techniques were used to observe the effect of the BOD load of the wood chips on the dissolved oxygen in the carrier water during the mixing process. The mechanical mixing method is closed to the atmosphere, which may cause a decreased dissolved oxygen level as compared to the pneumatic mixing. This was thought to be significant because the dissolved oxygen content of the water of the pilot line was near the saturation level. It was desirable to duplicate these conditions as closely as possible.

Because of the decrease in conductivity of the mixture compared with that of the sulfuric acid solution, a 20 ma upper limit on the scans was substituted for the 1-amp limit in the tests conducted with a 10 percent sulfuric acid solution. The scan time was increased from 4 to 6 minutes to permit taking more data to produce a better polarization curve in the Tafel region and, subsequently, a better determination of the corrosion current, I_{corr} .

Test results. A total of 22 tests were run using the pipe-ring immersed in the electrolyte obtained from tap water agitated with a charge of lodgepole pine wood chips. The test conditions are summarized in Table 12.

Each new quantity of electrolyte was used three times as indicated in Table 12. Dissolved oxygen determinations made before and after the tests

Table 12. Conditions for cathodic polarization tests of pipe-ring
corrosometer using woodchip-carrier water

Test series no.	Agitation of chips		Carrier water characteristics				Series temp. (°C)	Test scan rate (ma/min)		
	Type	Time (hr)	pH	Pre-test	post-test	Dissolved oxygen Pre-test post-test		a	b	c
1	Pn	5		6.77	--	7.4	--	19	1.87	1.87 1.73
2	Pn	5		7.05	6.92	7.8	6.9	18	2.000	2.15 2.00
3	Pn	5		6.80	6.82	7.5	6.5	20	2.000	2.00 --
4	Me	5		7.10	7.07	7.5	7.1	15	2.310	2.31 --
5	Me	5		6.28	6.56	6.3	6.1	20	2.35	2.35 2.22
6	Me	5		6.14	6.38	--	--	20	2.35	2.23 2.23
7	Me	24		6.29	6.46	4.4	--	20	2.36	2.36 2.28
8	Pn	8		7.96	7.84	7.1	5.8	20	1.78	1.94 2.22

Conditions for tests within each 3-test series: Anode (working electrode) cleaned prior to each test; a) fresh electrolyte, b) once-used electrolyte, c) thrice-used electrolyte. Series 1-7 were conducted using the Sorenson 5-amp power source; series 8 was run with a Hewlett-Packard Model 6294A d-c power source

Table 13. Corrosion rates for wood-chip pipeline determined
from bench tests

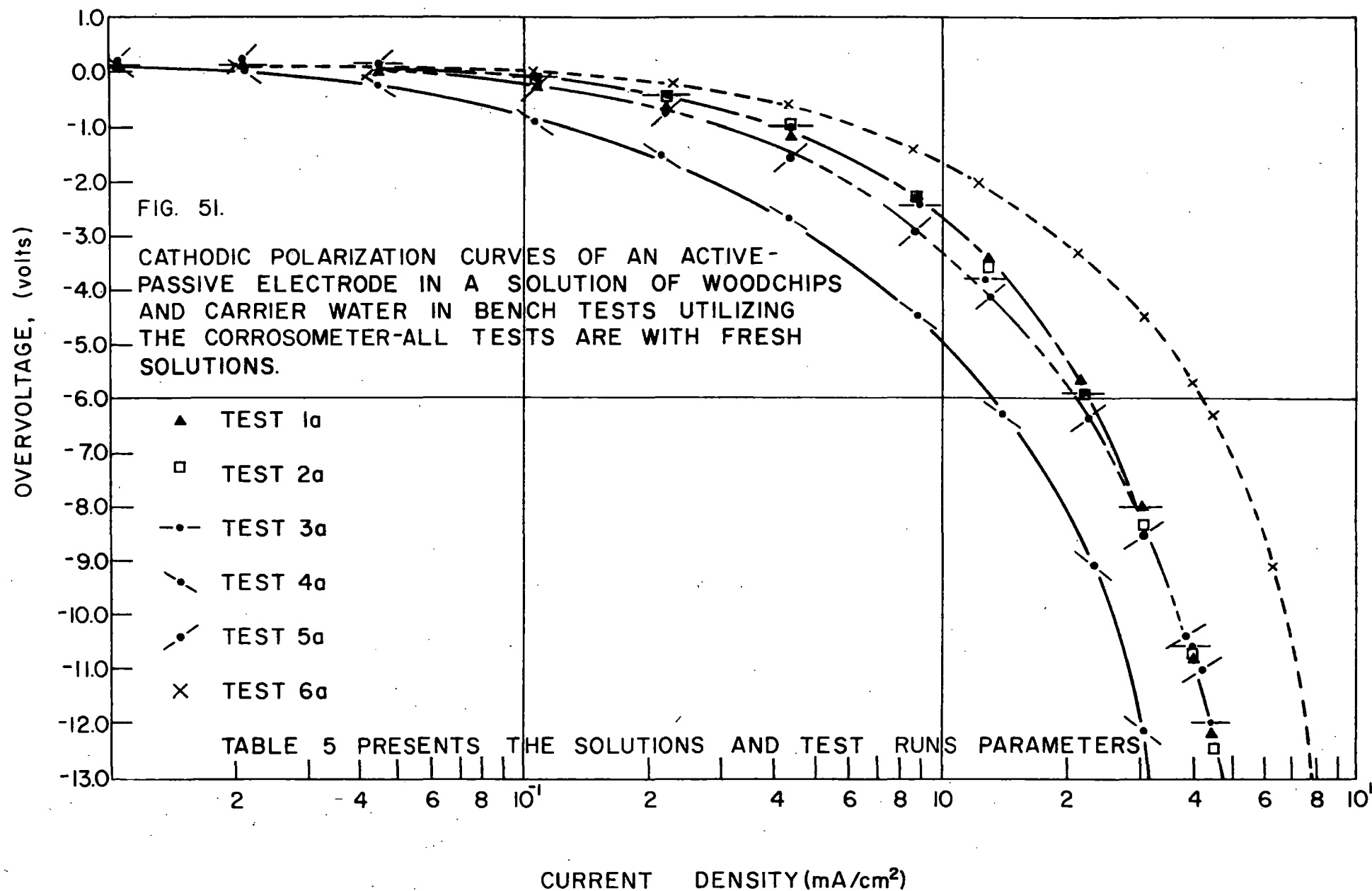
Test	Minimum corrosion rate			Maximum corrosion rate		
	$\beta, \frac{\text{volts}}{i_{\text{order}}}$	$i_c, \frac{\mu\text{A}}{\text{cm}^2}$	Rate, mpy	$\beta, \frac{\text{volts}}{i_{\text{order}}}$	$i_c, \frac{\mu\text{A}}{\text{cm}^2}$	Rate, mpy
4a	0.1	0.32	0.14	1.28	45	20.20
5a	0.1	0.05	0.02	2.56	143	64.40
6a	0.1	0.32	0.14	2.14	136	61.20
7a	0.1	0.09	0.04	2.92	128	57.70
8a	0.1	0.76	0.34	3.24	182	82.00

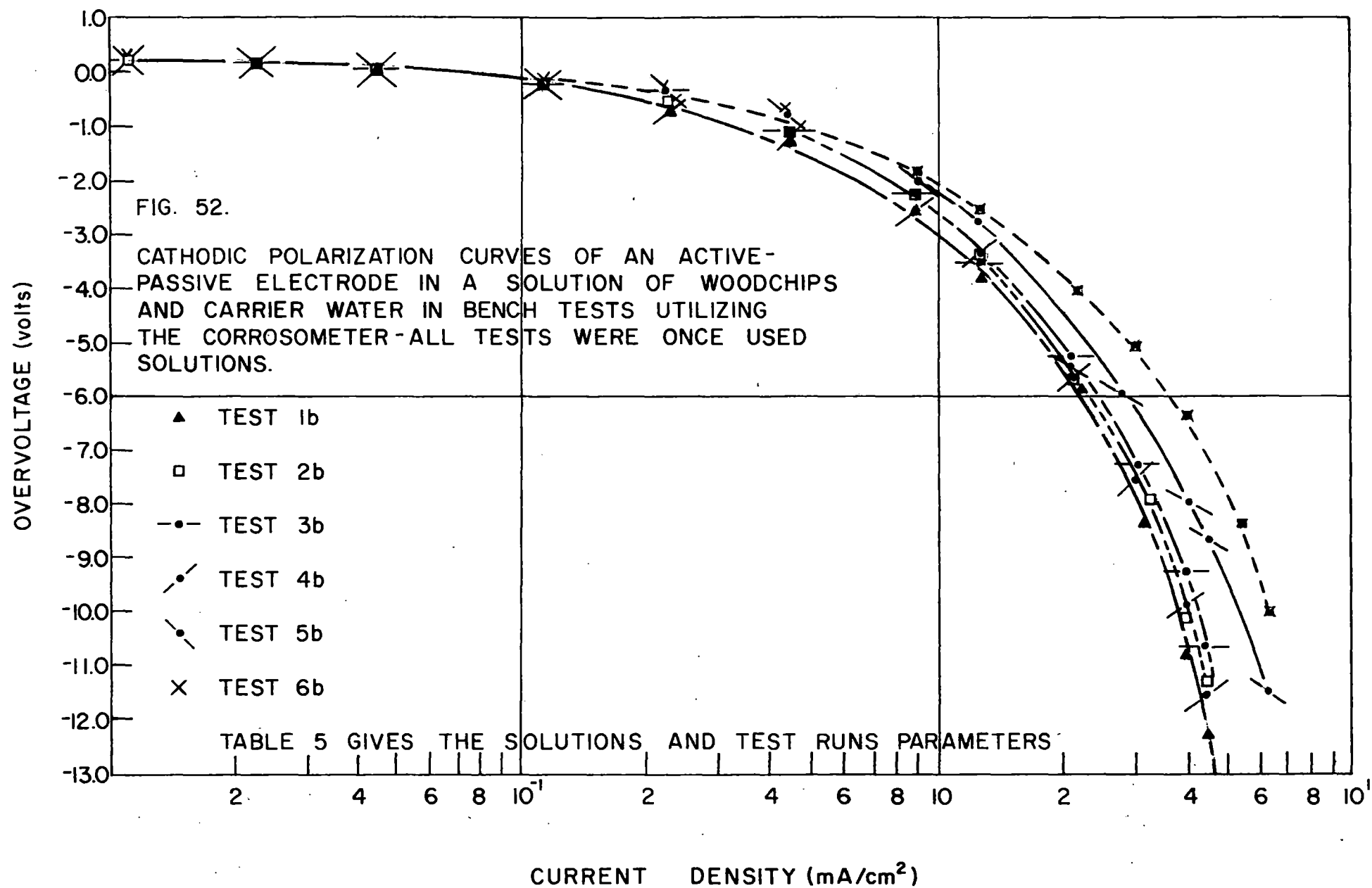
show dissolved oxygen decreases by an amount ranging up to 2.0 ppm in experimental series of three-test runs. The pH was observed to increase for some 3-test series and decrease for others. The temperature of the electrolyte did not vary in a 3-test series. The cathodic polarization curves for the 3-test series are shown in Figs. 51-53. (Data for the individual observations are on file in the Department of Civil Engineering of Montana State University.)

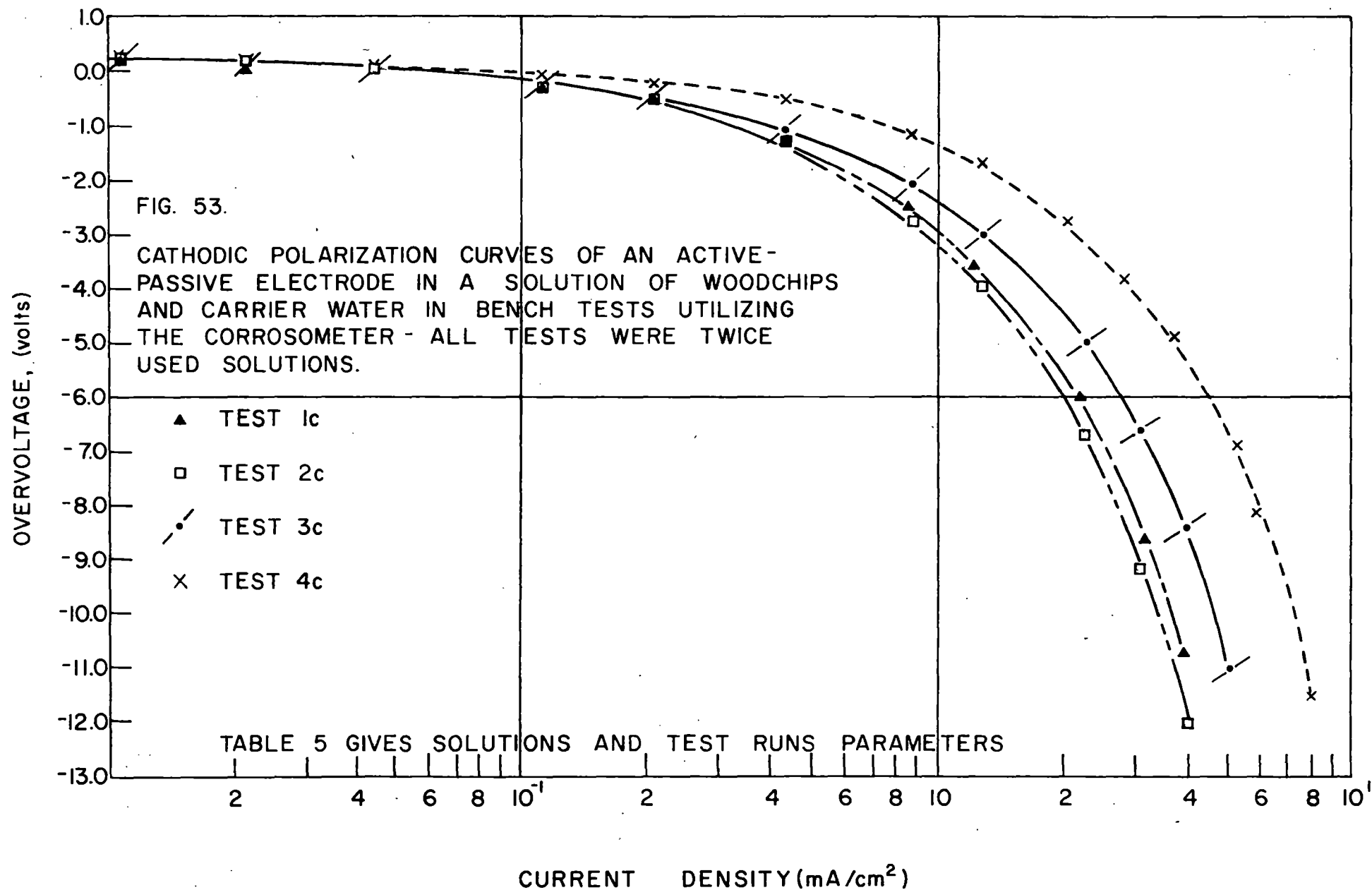
Observation of the polarization curves shows the concentration polarization effect dominating the curve and the Tafel region nonexistent. Fontana and Greene (1967) state that in general, the value of the Tafel slope, β , is usually 0.1 volt for every order of magnitude of current density. This slope is drawn tangent to the polarization curve and the intersection of this tangent with the corrosion potential line gives the minimum corrosion current density needed to compute the corrosion rate. This corrosion rate will be the minimum in the forthcoming corrosion rate range.

The maximum corrosion rate is determined using the assumption that the Tafel slope will be tangent to the point where the concentration polarization effect takes place. Fig. 54 shows the Tafel slope extended with voltage increases. The intersection of that tangent with the corrosion potential determines the corrosion current density which is used to calculate the maximum corrosion rate.

The polarization curves indicating the maximum and minimum corrosion current densities for the tests conducted with the mechanical mixing and fresh electrolyte are shown in Figs. 55-58. Table 13 shows the range of







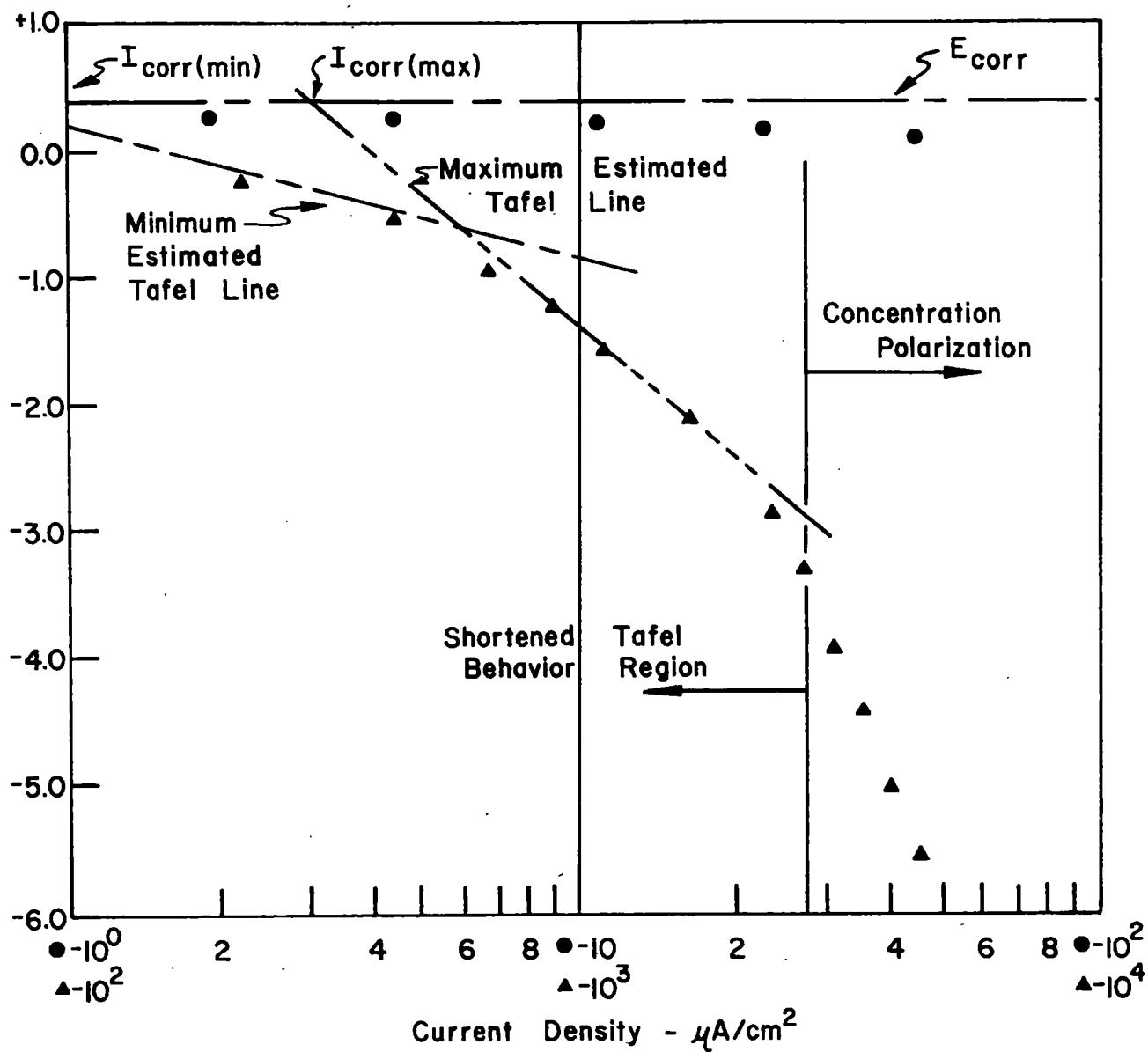
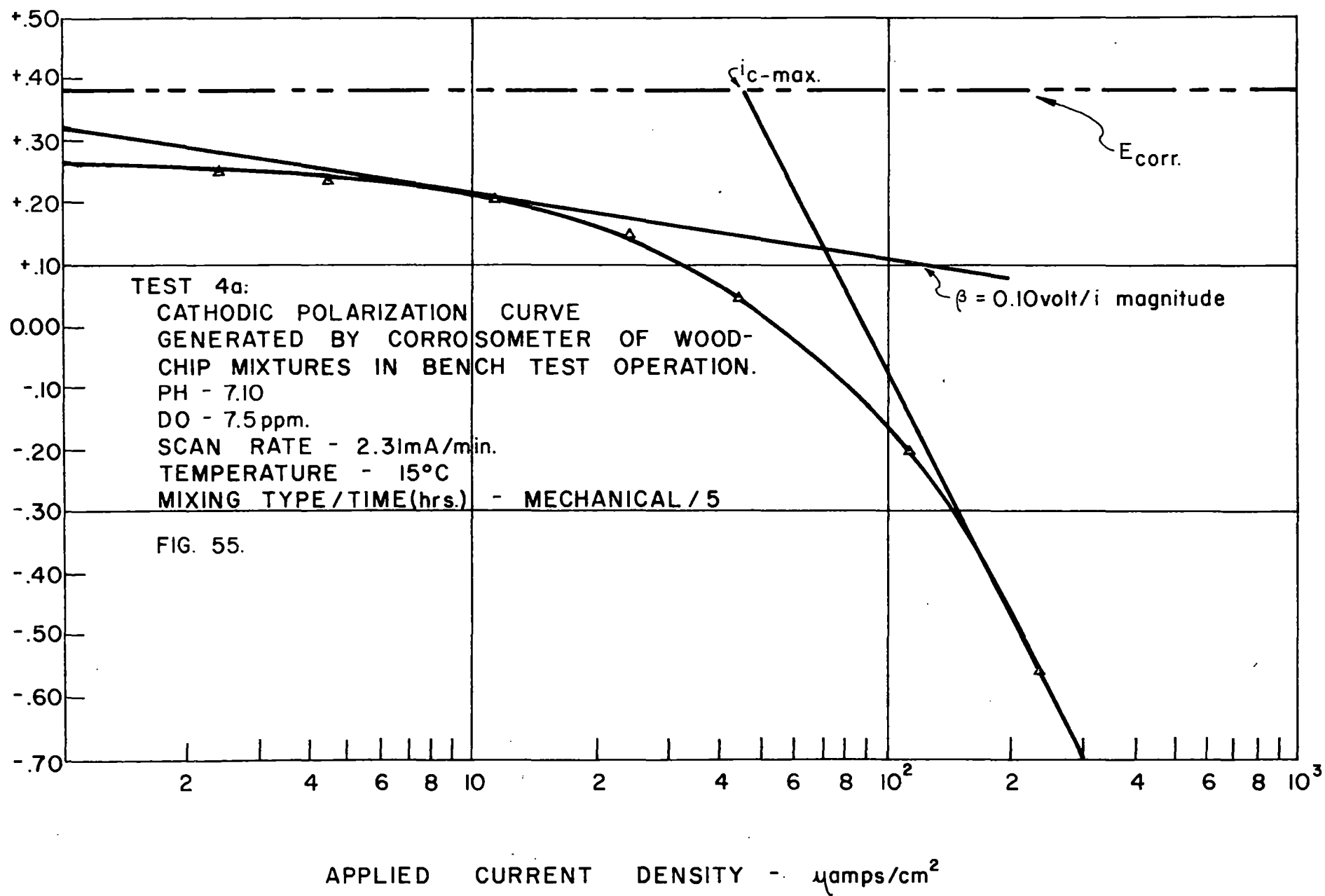
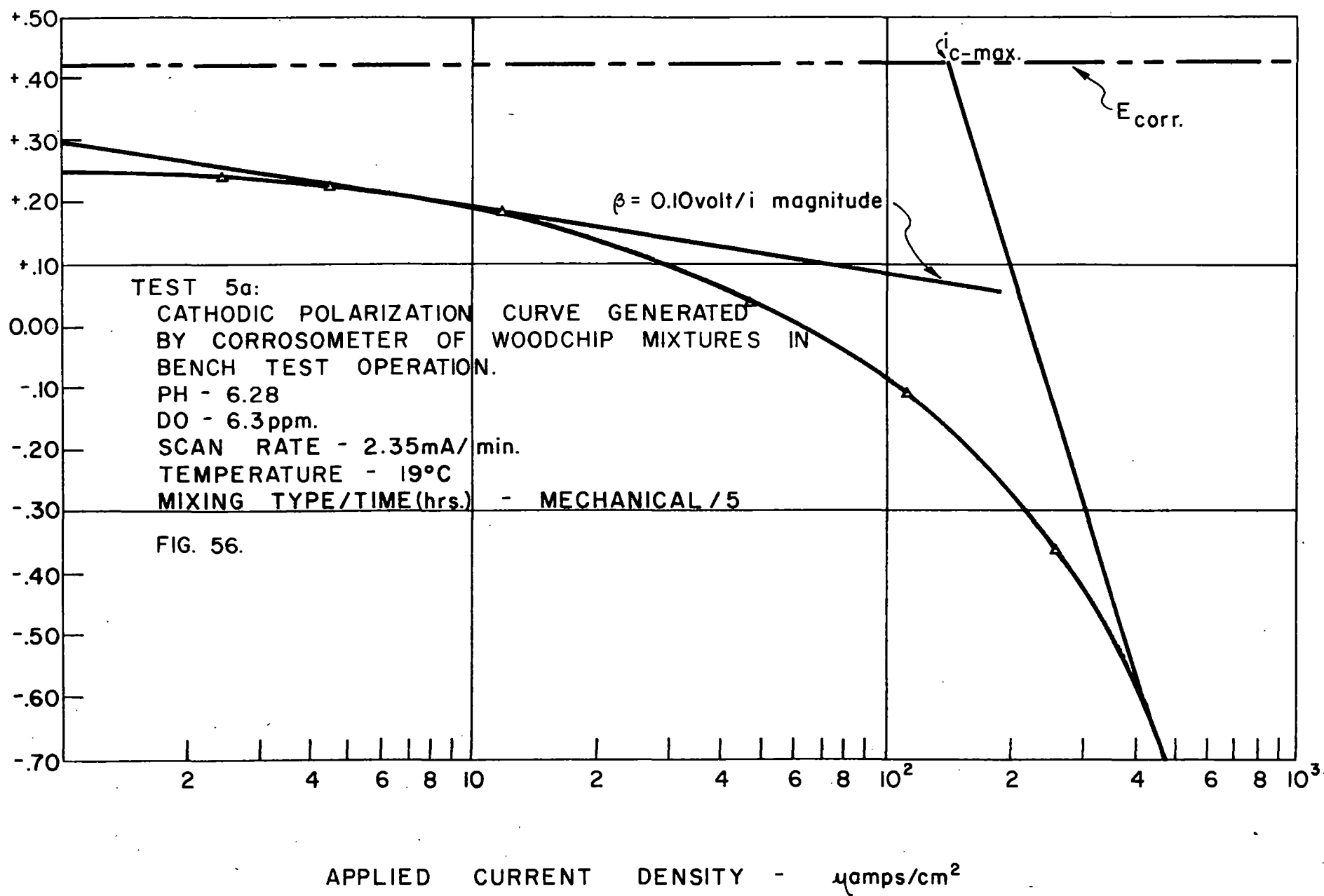
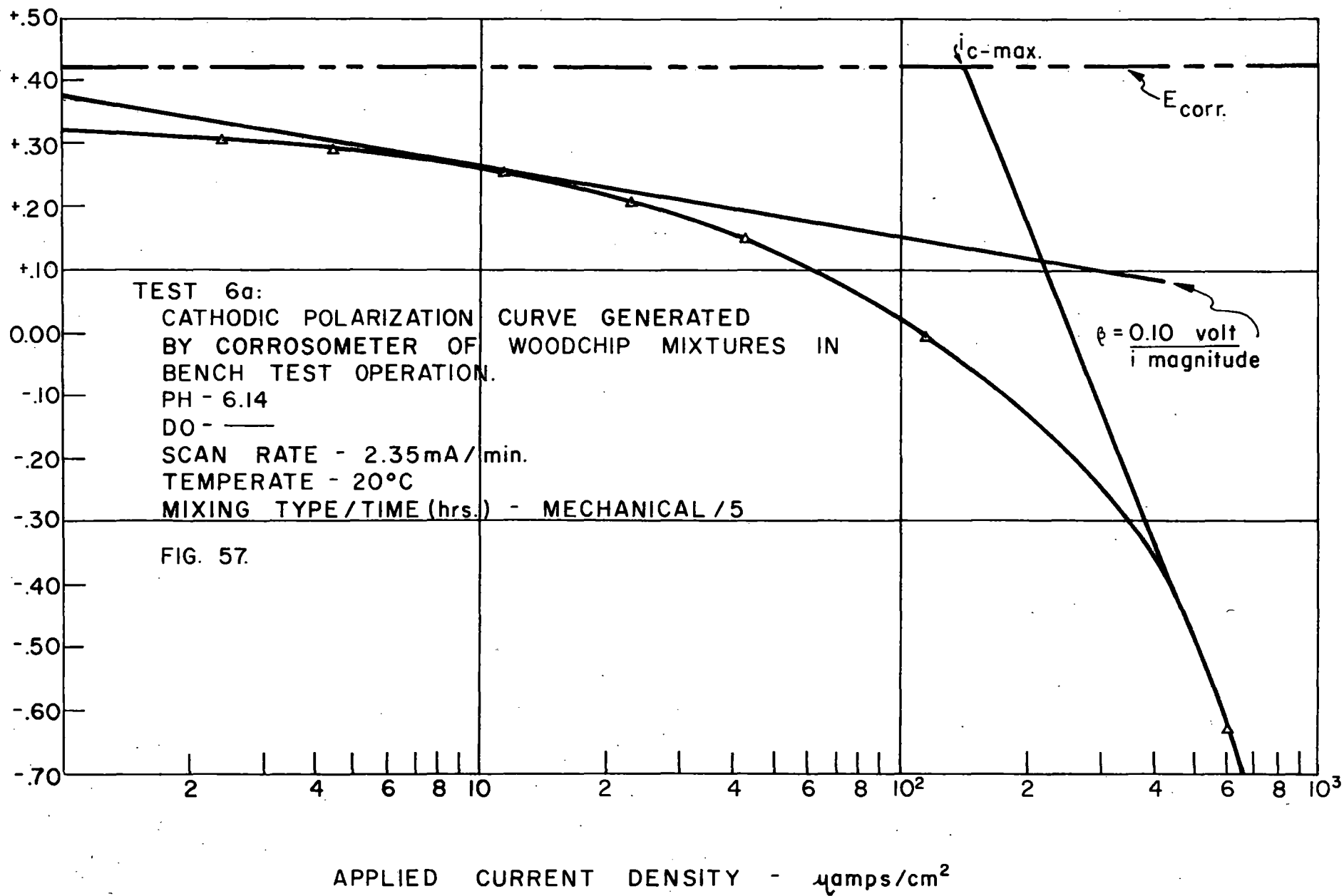
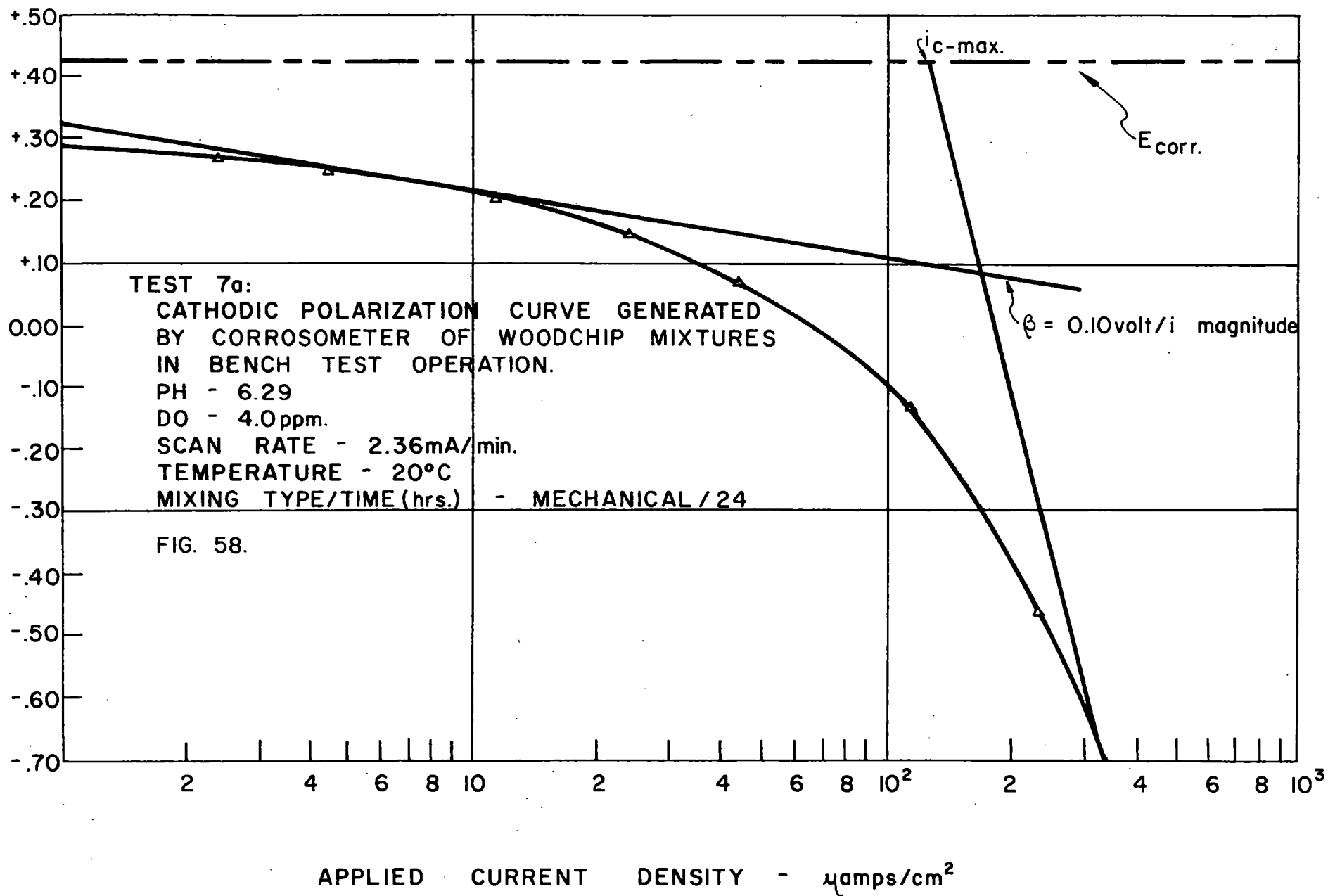


FIG. 54. EFFECT OF CONCENTRATION POLARIZATION ON TAFEL REGION & MAX. & MIN. CORROSION CURRENT DENSITIES FOR BENCH SCALE TESTS OF WOOD-CHIP MIXTURES.









corrosion rates for each test calculated from Eq. (41) using 2.89×10^{-4} gm/coul, 31.536×10^6 and 7.87 gm/cm^2 as K, I and ρ , respectively.

Inconsistency in the test tap water content used for the woodchip-carrier water mixture caused disagreement in the values of the potential differences observed throughout the test series. The reduction of the dissolved oxygen by the BOD of the carrier liquid in the mixture proved to be negligible with a 5-hour mixing period.

The laboratory tests of the pipe-ring corrosometer using the carrier water from a mixture of wood chips and water indicated the method is valid to determine a range of rates for estimating the corrosion effects on pipe walls with the same accuracy as other short time tests. The method was then developed for use on a pipeline flowing under pressure.

5.7 Pilot-Line Corrosion Tests

The purposes of the pilot-line study were (1) to observe the effects of velocity of mixture and pressure on the operation of the corrosometer and, (2) to determine corrosion rates of the wall of the pilot pipeline transporting a mixture of wood chips and water.

5.7.1 Apparatus modification.

Modifications to the corrosometer and the operating procedure were required for conducting the pilot-line tests.

The mixture of carrier water and wood chip is flowing under pressure in these tests. As the movement of wood chips causes abrasion on the tip of a standard reference electrode immersed in the flow and a line pressure greater than the internal pressure in the reference cell causes the carrier liquid to flow into the electrode and contaminate the tip, an industrial

calomel reference electrode was used for this series of tests. It was fitted with an abrasion-resistant tip and a pressurized potassium chloride (KCl) reservoir designed to withstand pressures up to 50 psi. An internal overpressure of 1.5 psi in excess of the pipeline pressure was required to maintain a positive KCl flow from the electrode.

A differential pressure control system, Figs. 59 and 60, consisting of a compressed air tank, manometer, air regulator and five valves for purging air and water from the system was utilized to maintain the 1.5 psi overpressure in the reservoir of the reference electrode.

The auxiliary electrode was a 12-in. (30-cm) length of the 2345-ft (715-m) pilot line having an 8.625-in. (219-mm) outside diameter and an 0.188-in. (4.77-mm) wall thickness. This section was insulated from the adjacent sections of the pipeline by specially-constructed, electrically-insulated fiberboard flanges. Electrical jacks were soldered to external pipe walls to complete the wiring circuit.

A special fiberboard plug shown in Figs. 61 and 62 was utilized to insert the industrial calomel reference and working electrodes into the line through a 1 1/4-in. (32-mm) gate valve during the test runs. This gate valve was closed when the corrosometer was not in use; its threaded connection secured the threaded plug during tests.

The working electrode configuration was altered from its 0.50- by 0.70-in. (1.27- by 1.78-cm) rectangular dimensions to a washer shape with an ID of 0.352 in. (8.94mm) and an OD of 0.814 in. (20.67mm). This design enabled the working electrode to be concentric with the reference electrode tip. The reference and working electrode assembly are shown in Figs. 61

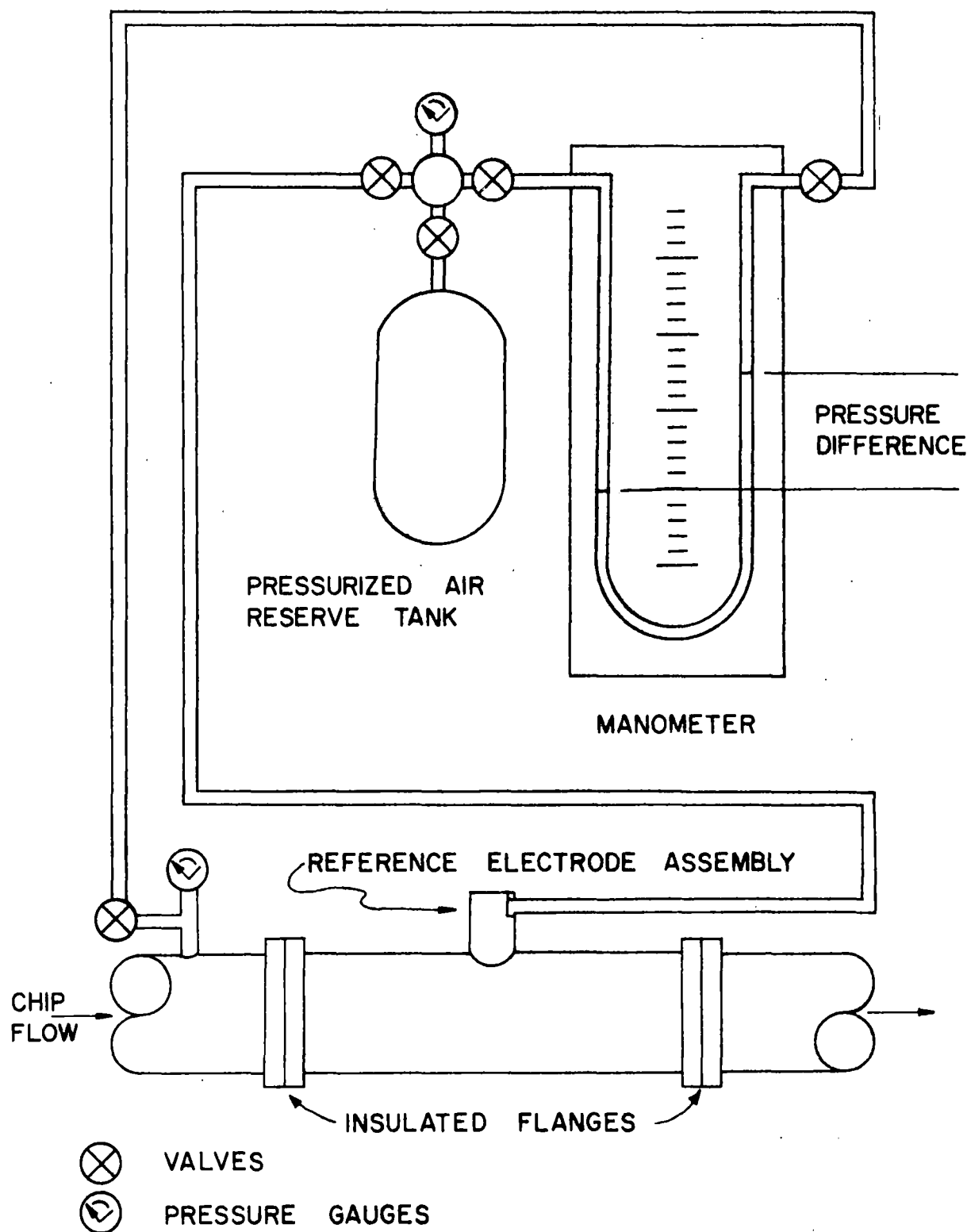


FIG. 59. DIFFERENTIAL PRESSURE CONTROL SYSTEM.

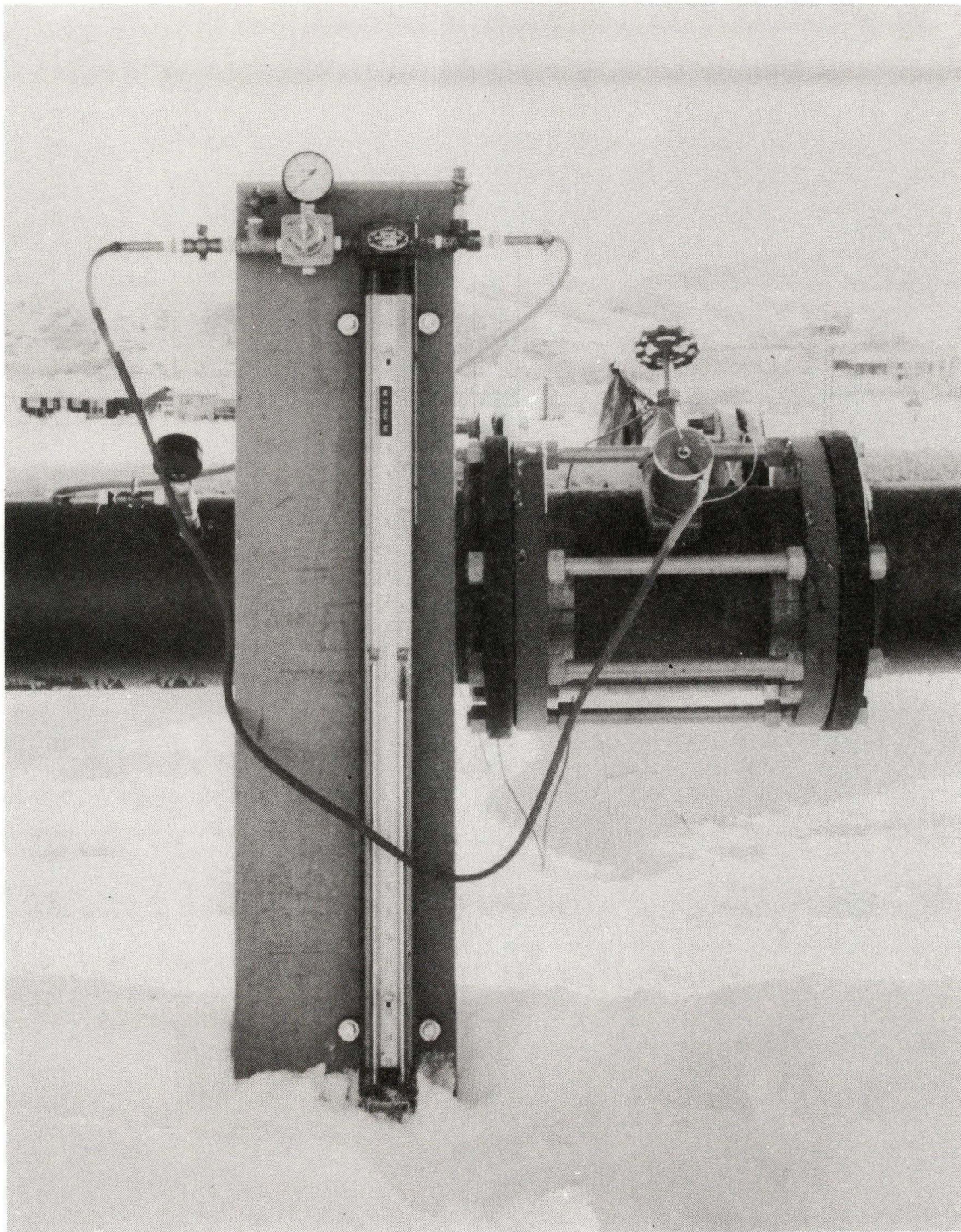


Fig. 60. Differential pressure control system

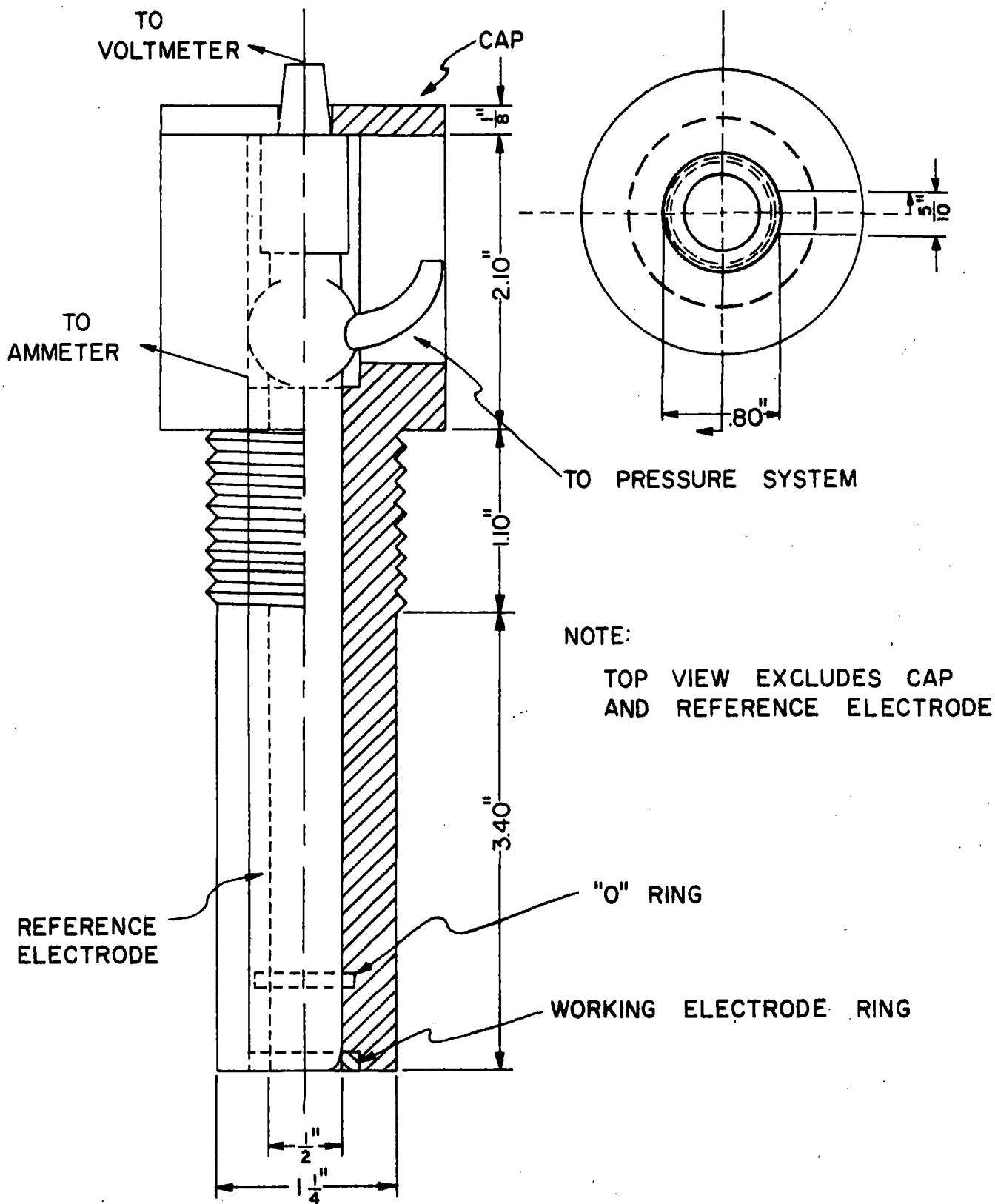


FIG. 61. PIPELINE CORROSOMETER ELECTRODE ASSEMBLY.

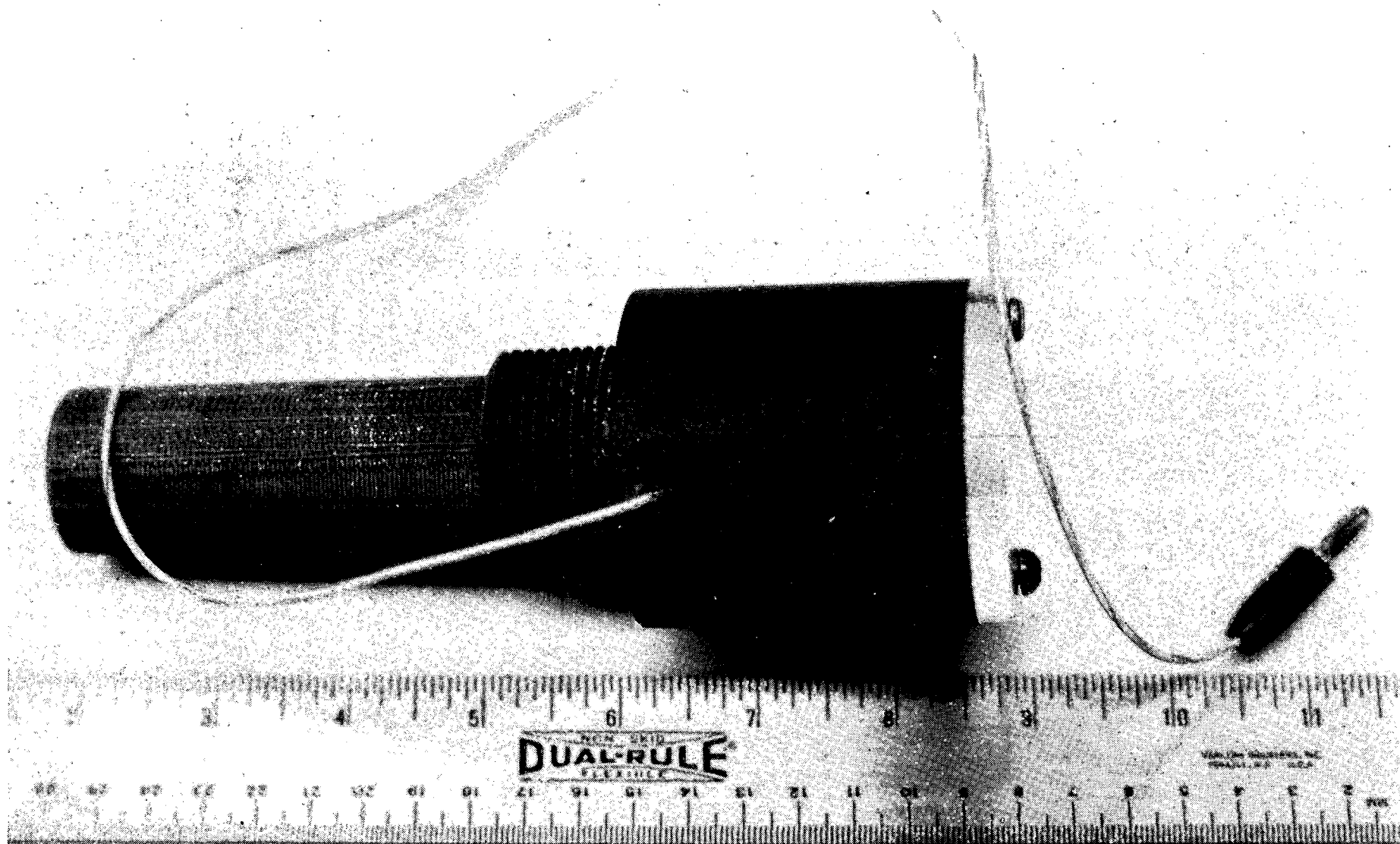


Fig. 62. Pipeline Corrosometer electrode assembly

and 62 as an integral part of the fiberboard plug assembly. The assembly was machined and carefully inserted into the line so the working electrode was positioned flush with the internal wall of the pipe. The corrosometer was installed in the pipeline at a point approximately 2300 ft (701-m) from the injection system and approximately 50 ft (15-m) from where the pipeline discharged into the atmosphere.

The pilot line was operated as an open loop system. The mixture of wood chips and water was discharged into a rotating screened drum where the chips were separated from the carrier water. The chips tumbled into a feed hopper and the water was metered with a surge tank holding make-up water. The chips and water were remixed and recycled through the test loop.

5.7.2 Test procedure. The procedures used in the pilot line tests for preparation of the working electrode, generation of data and control of scan times were similar to those developed in conducting the calibration tests with 10 percent sulfuric acid solution and the bench tests using the simulated carrier water.

The test operating procedure, modified because of the added complexity of the corrosometer with its auxiliary systems, was conducted in the following sequence:

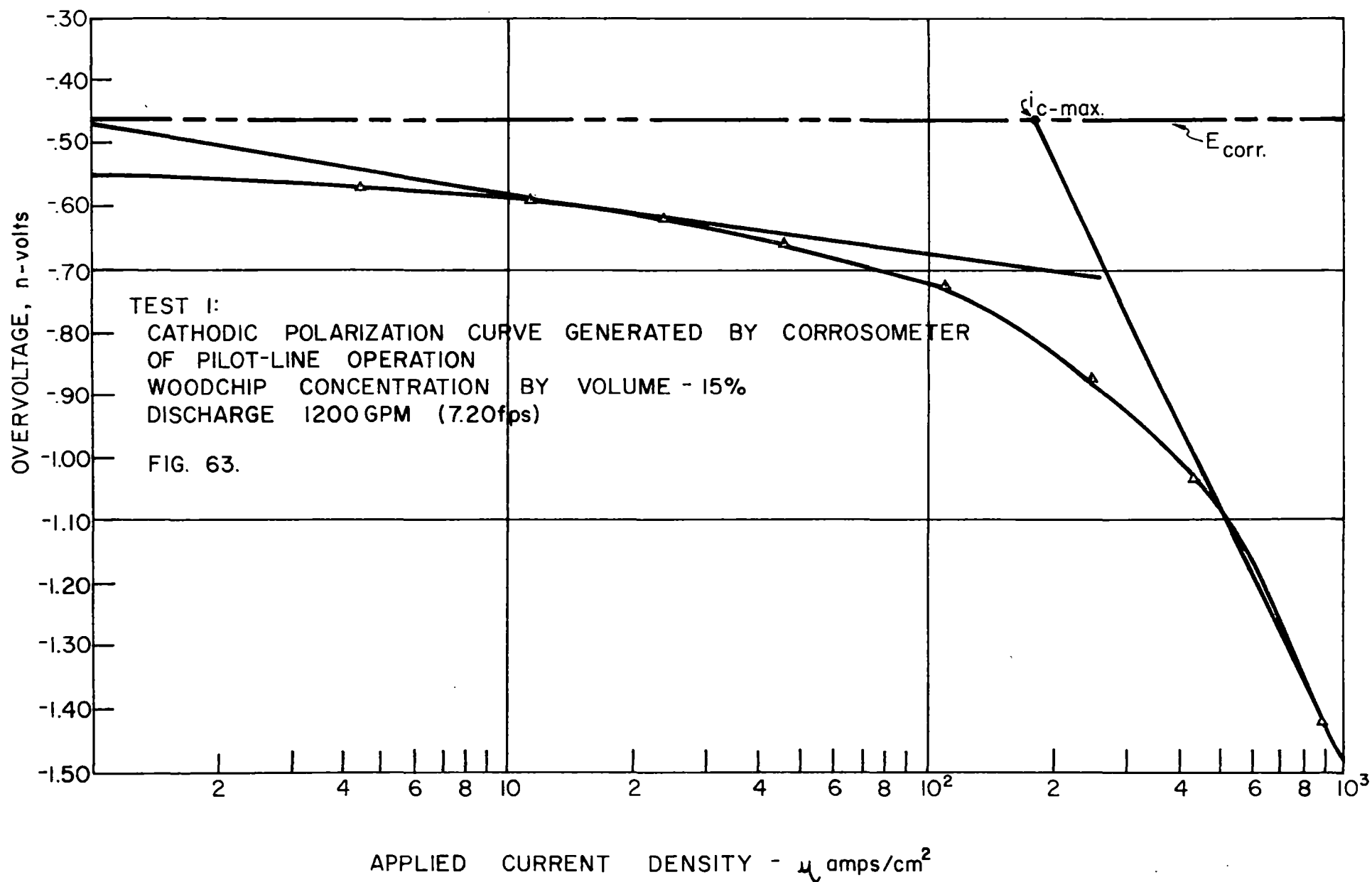
1. connect the pressure differential system to the pipeline,
2. remove air from the leg of the manometer connected to the pipe immediately upstream from the gate valve,
3. with the valve in the manometer line connected to reservoir closed, adjust air pressure to 1.5 psi over that in the manometer line connected to the pipe,
4. prepare working electrode,

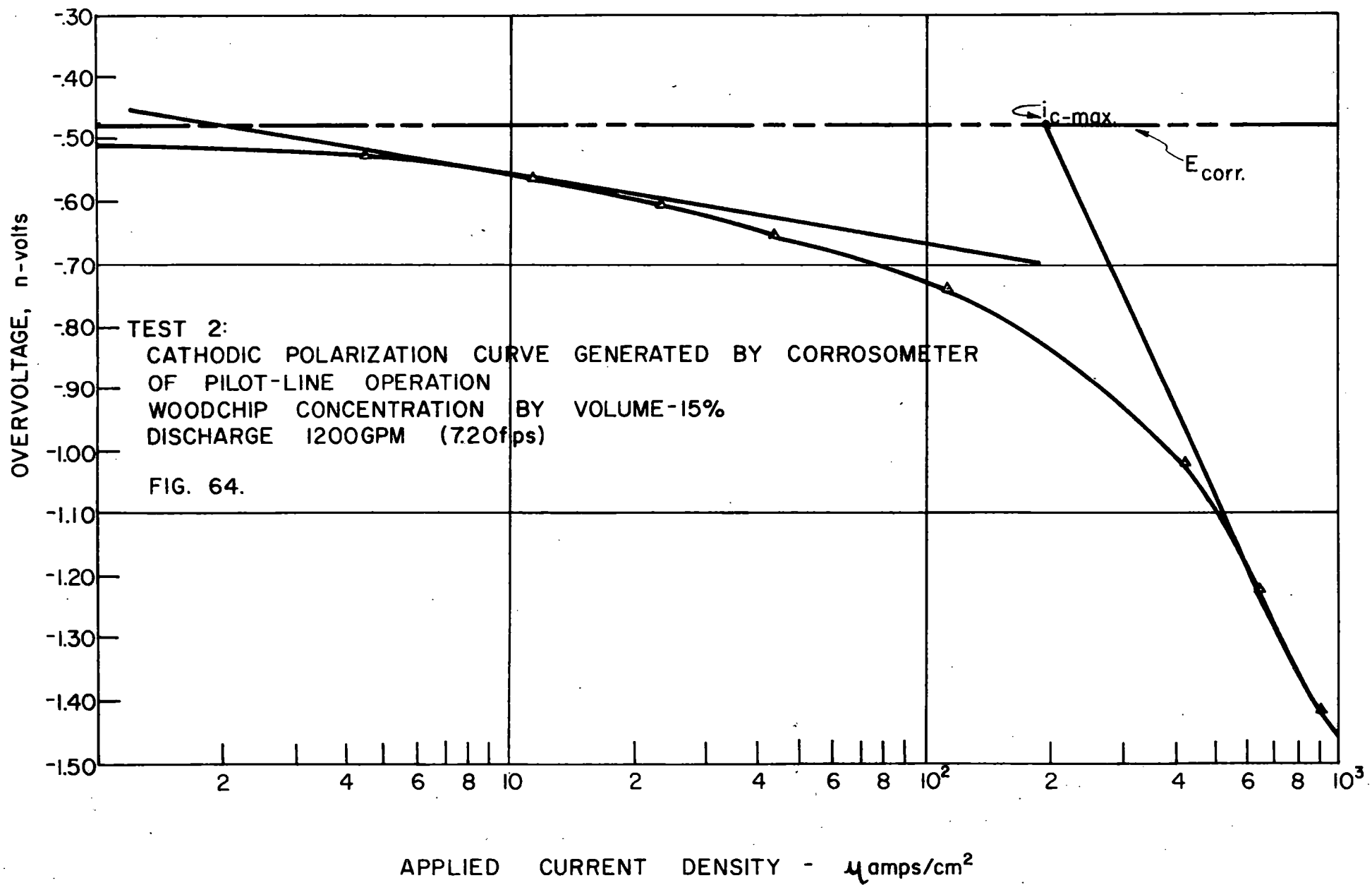
5. insert reference electrode into fiberboard plug,
6. connect reservoir to the manometer line,
7. open valve in manometer line connected to reservoir,
8. insert plug into gate valve,
9. open gate valve and insert plug into line,
10. secure plug and make any necessary wiring connections, and
11. start data acquisition run.

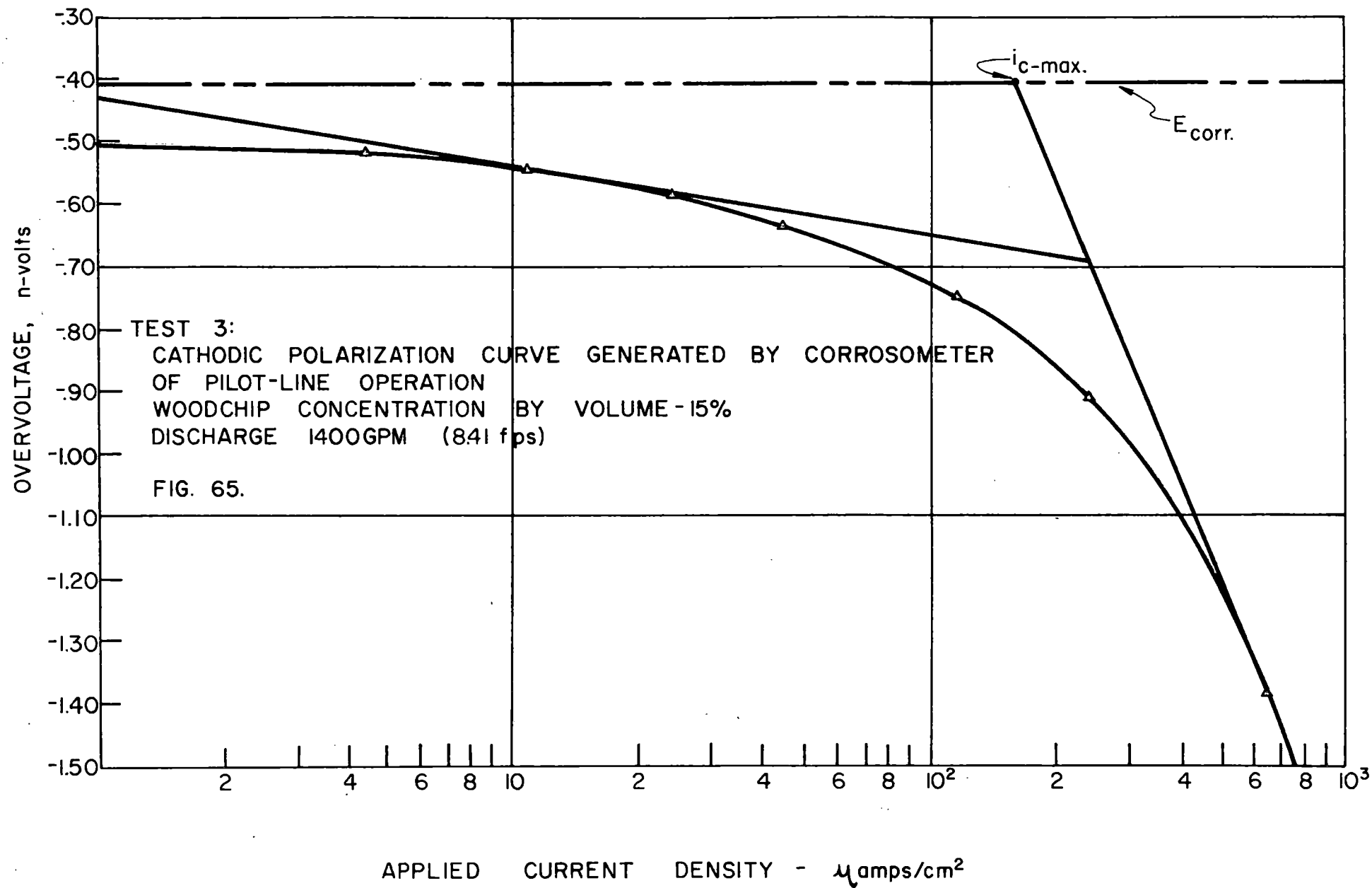
5.7.3. Test results. A total of 13 tests of the pilot line corrosometer was run to determine the range of corrosion rates for the internal pipe walls. The polarization curves graphed from the observed data (on file in the Department of Civil Engineering, Montana State University) to determine the maximum and minimum corrosion currents are shown in Figs. 63-75. The polarization curves observed with the corrosometer in the pilot-line tests were dominated by the concentration polarization effect. Although precise corrosion rates could not be determined because of the absence of the Tafel region, ranges of corrosion rates were calculated from the method described in the bench-scale tests conducted with the simulated carrier water as the electrolyte. The corrosion currents and calculated corrosion rates are summarized in Table 14.

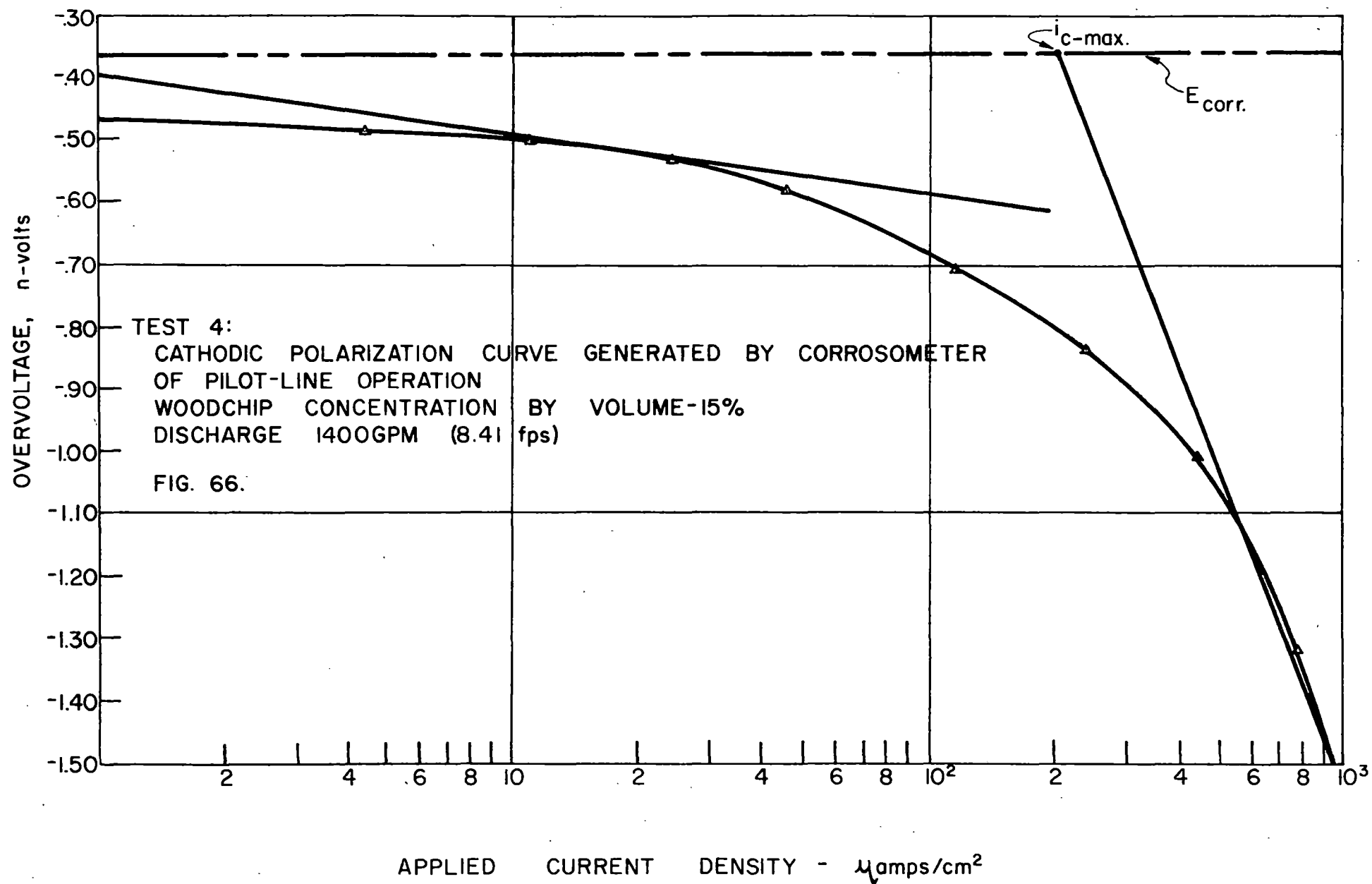
5.8 Evaluation of Corrosometer Studies

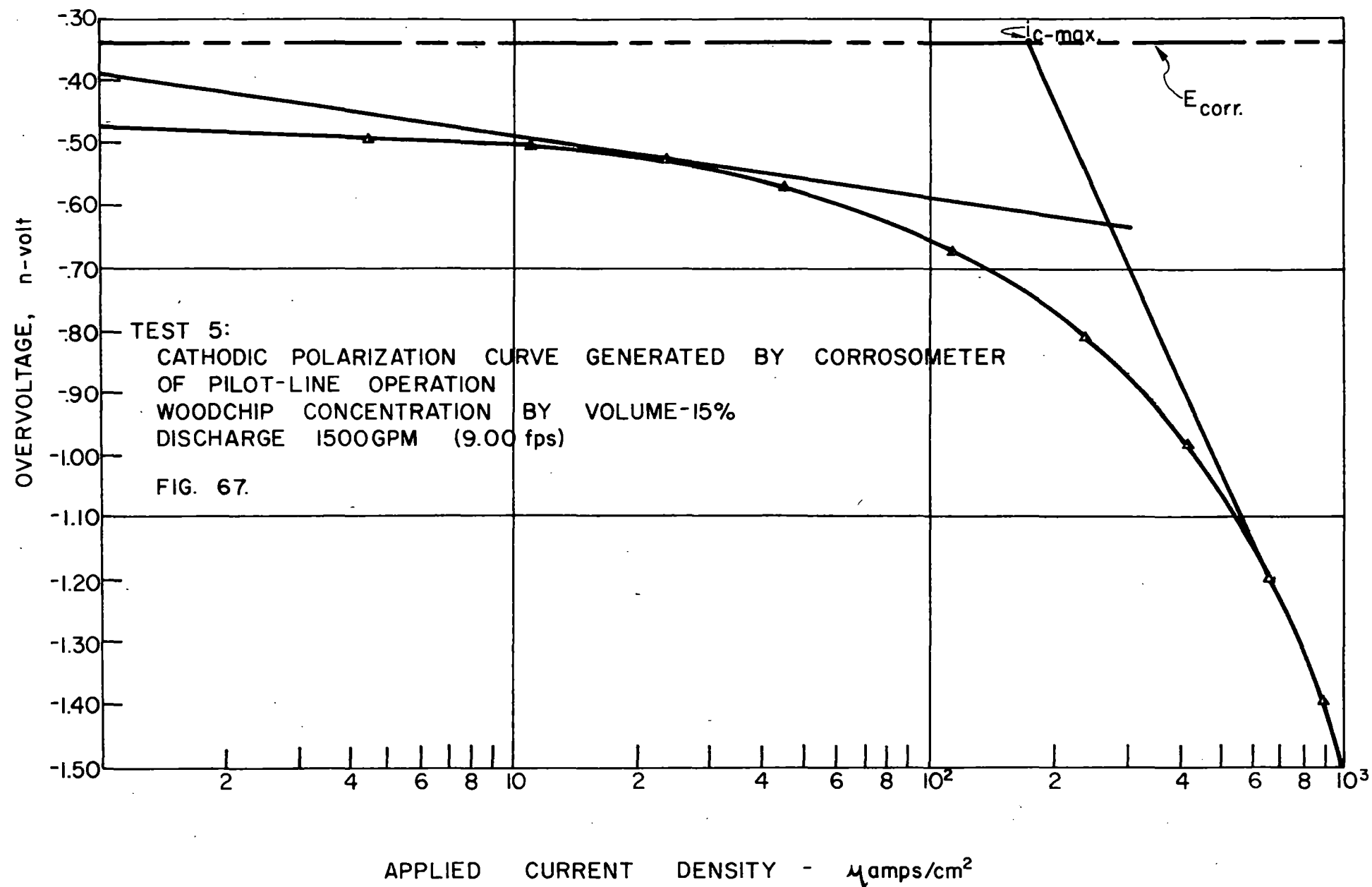
The results of the corrosion of the internal walls of a wood-chip pipeline using a corrosometer developed for use with the polarization resistance methods are evaluated in three parts: (1) specific pilot line corrosion rates, (2) utility of polarization resistance techniques for

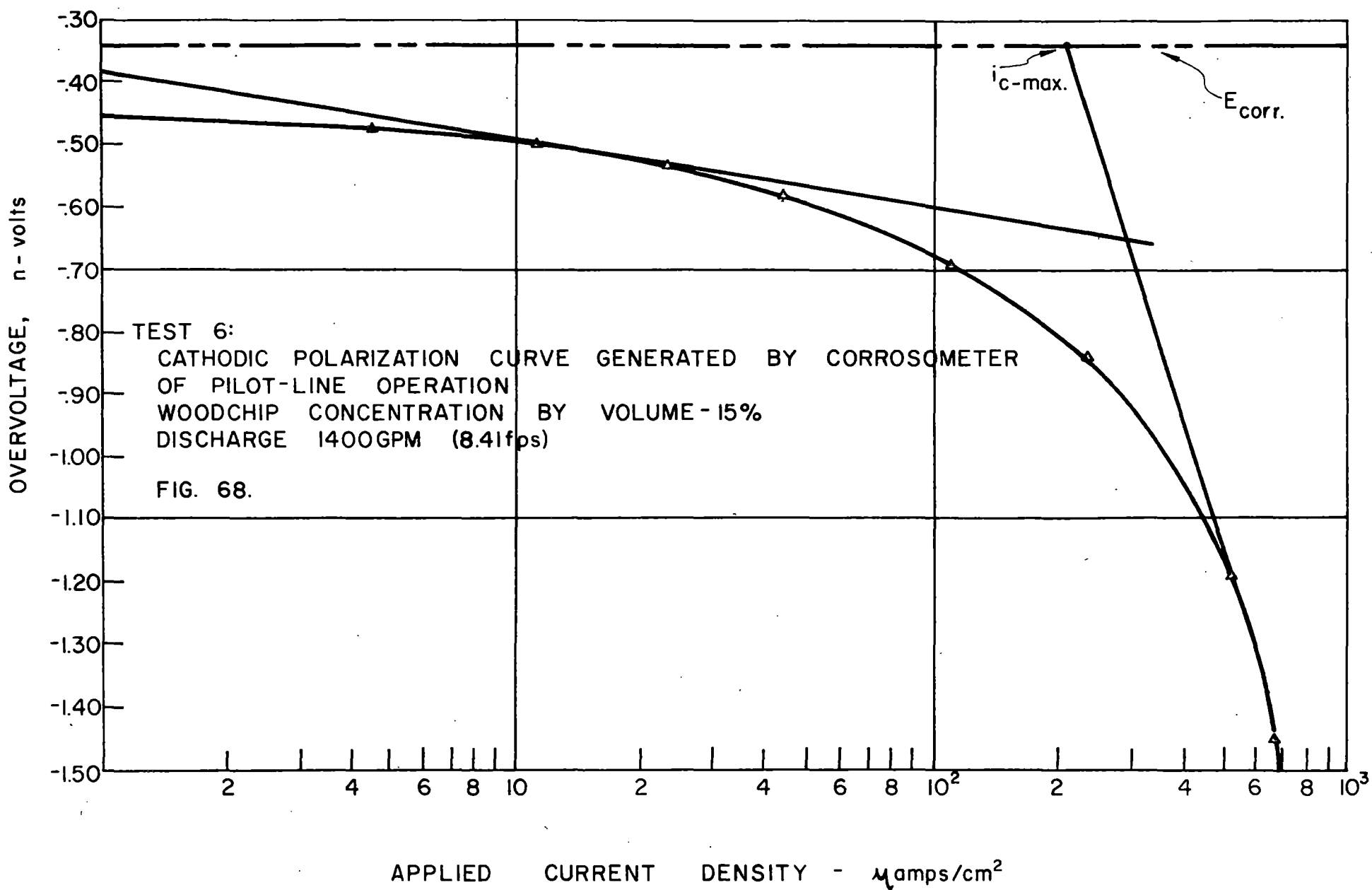


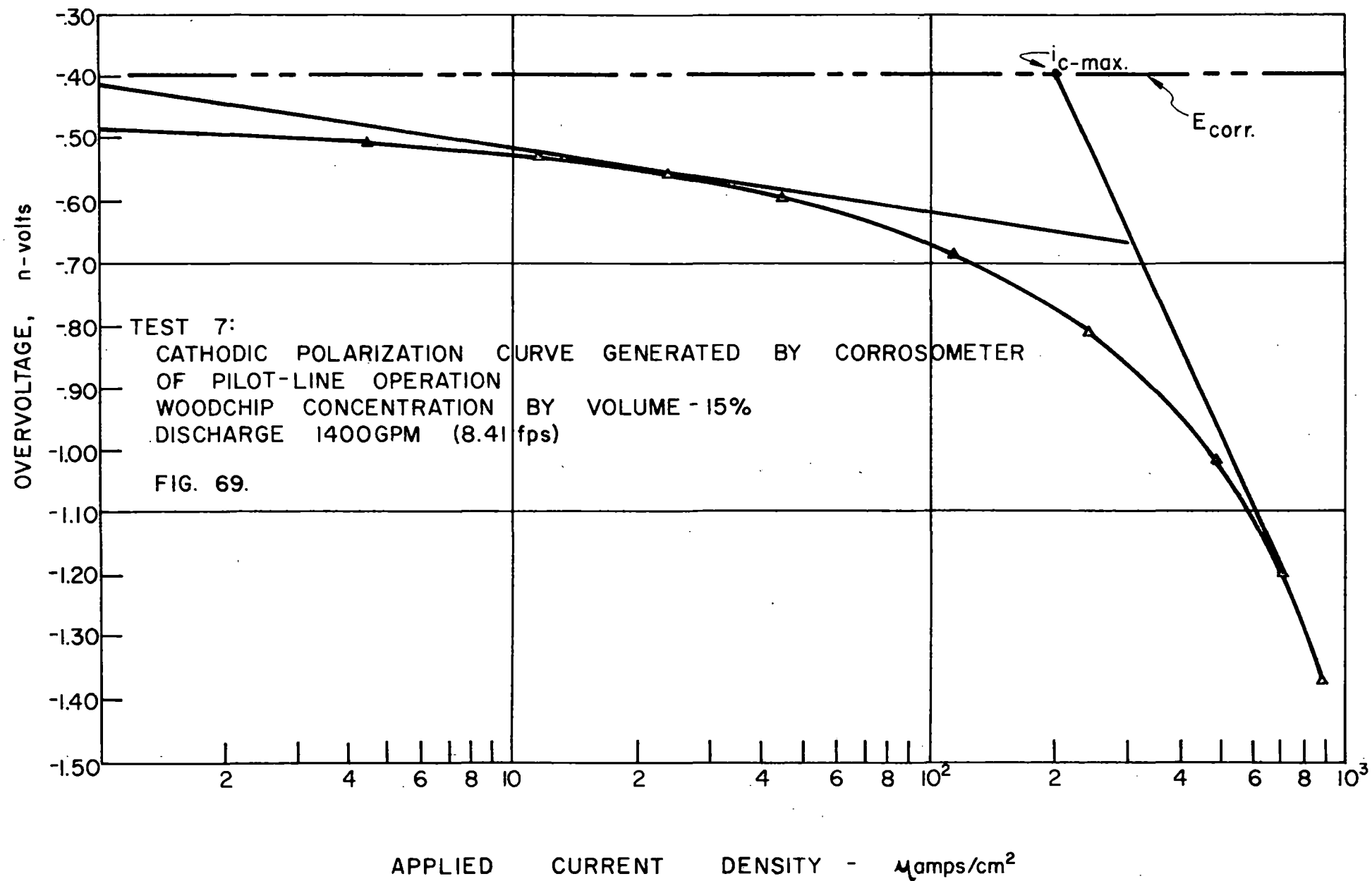


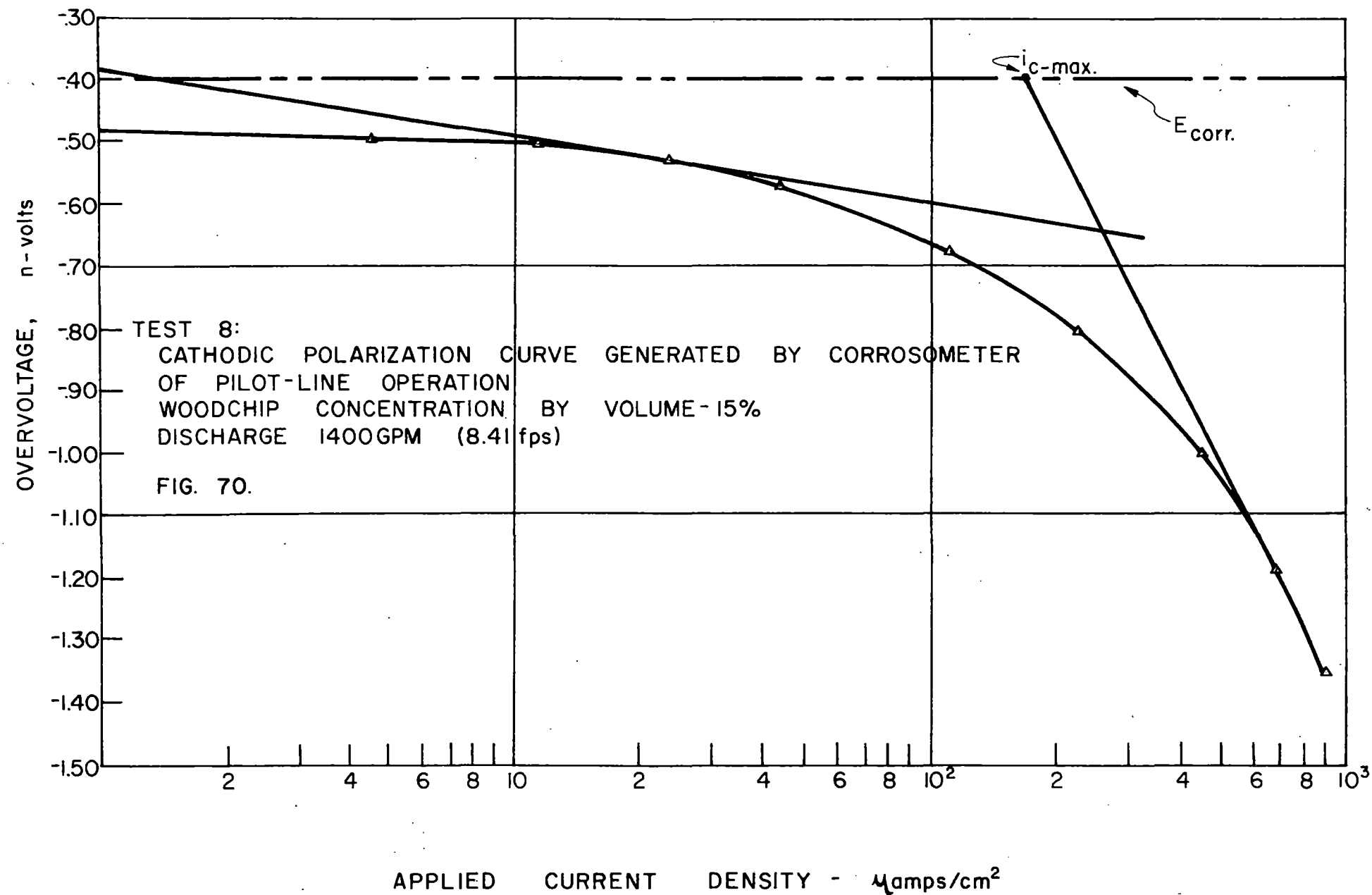


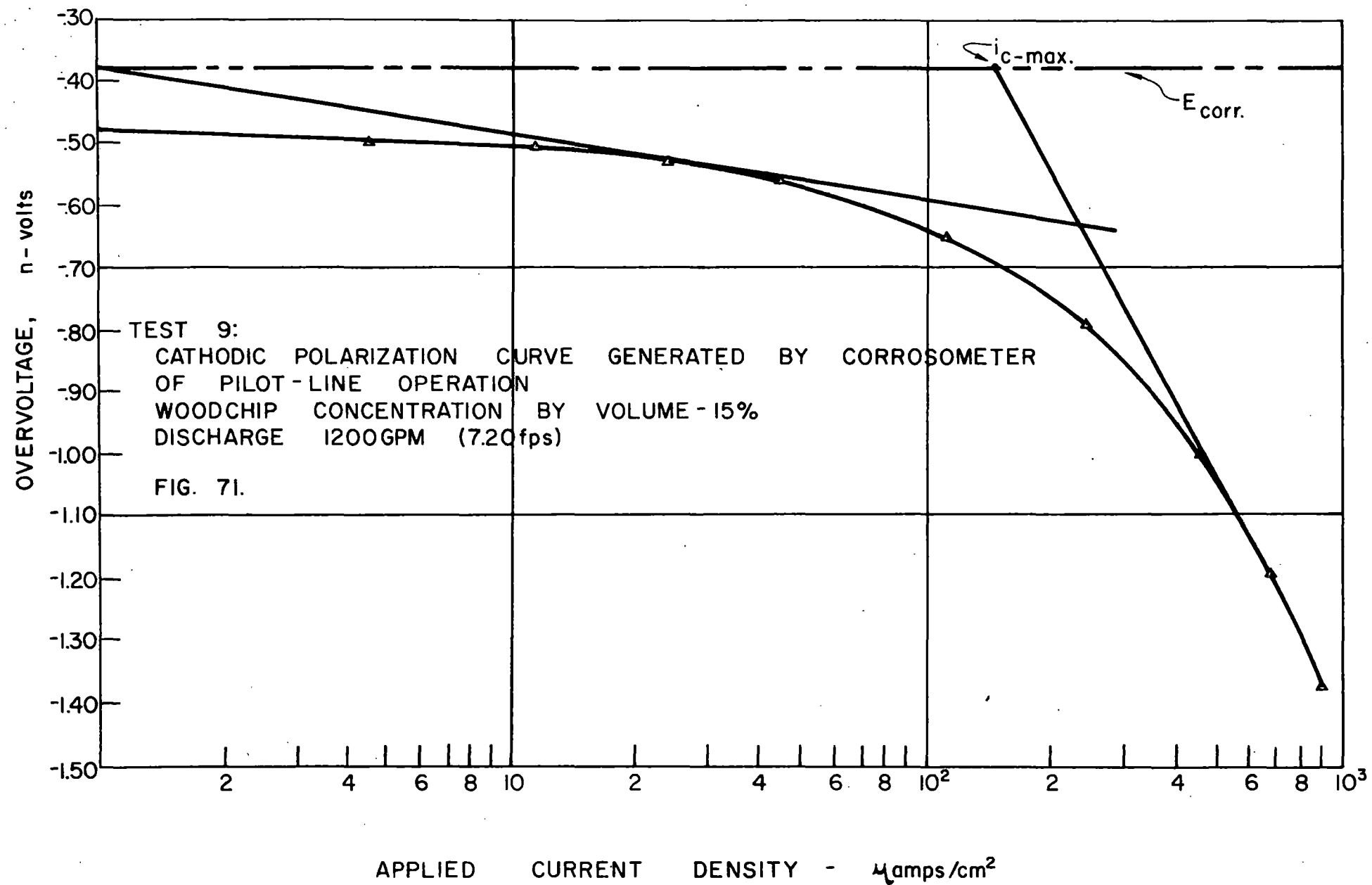


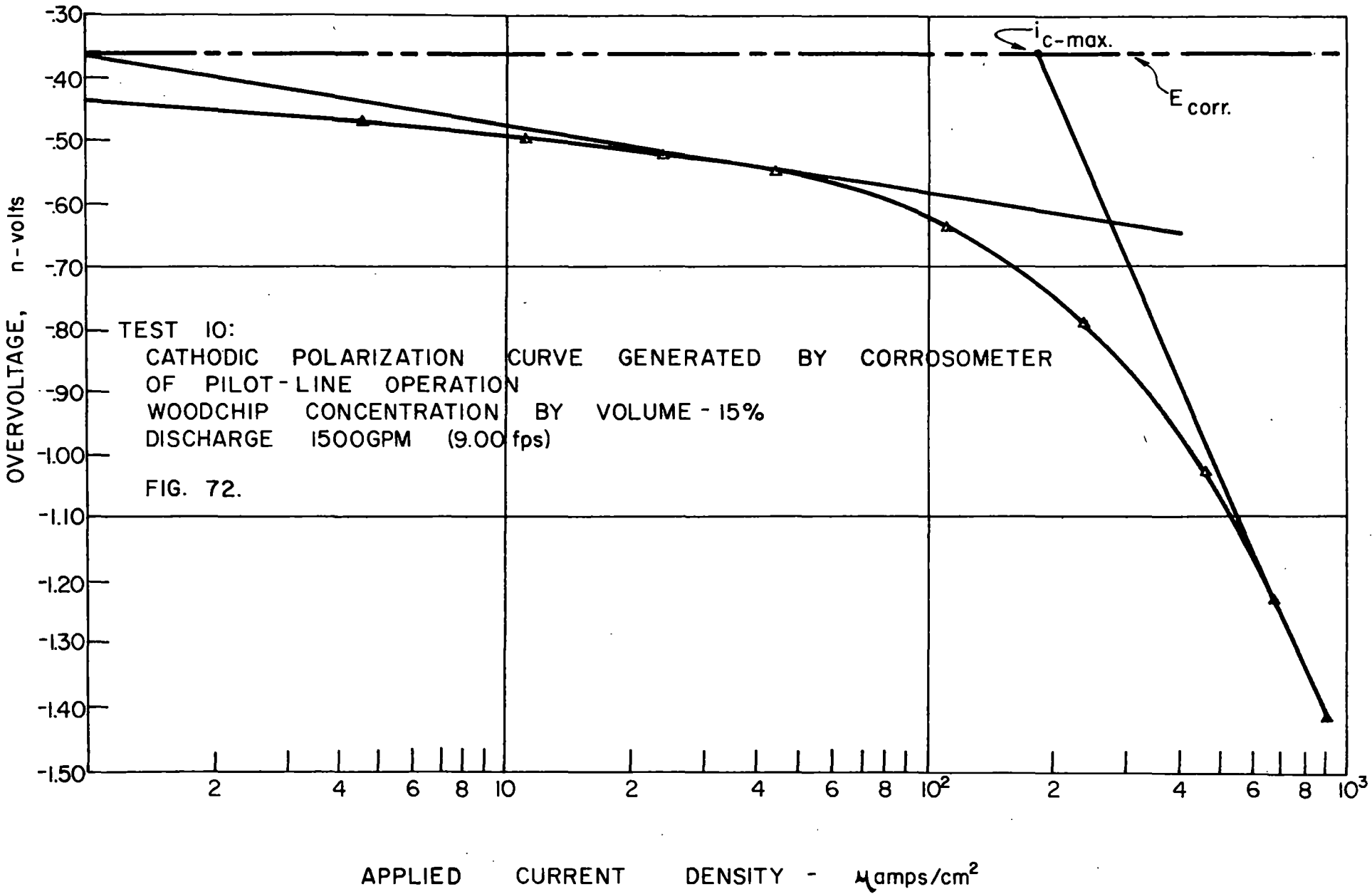


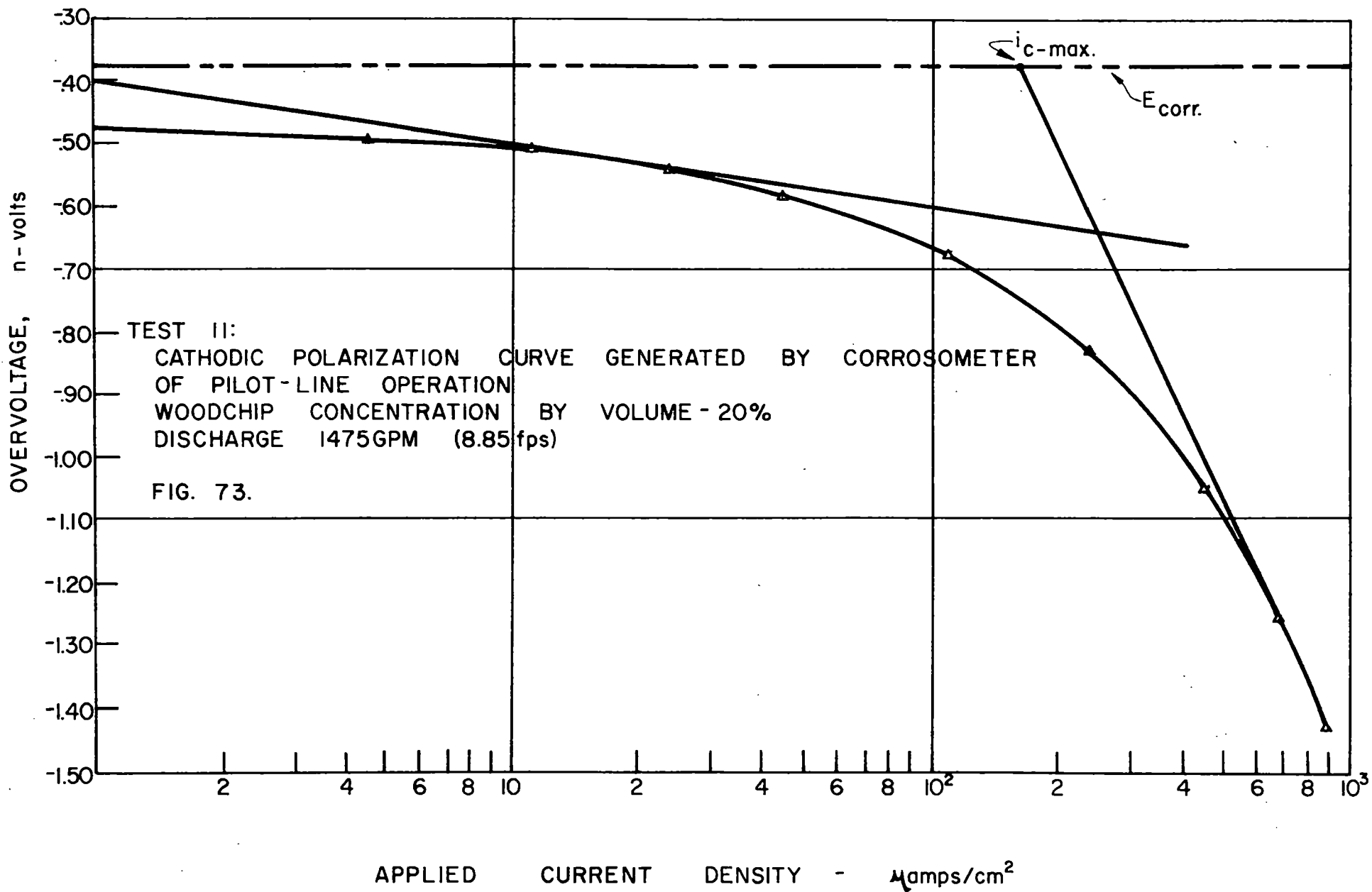


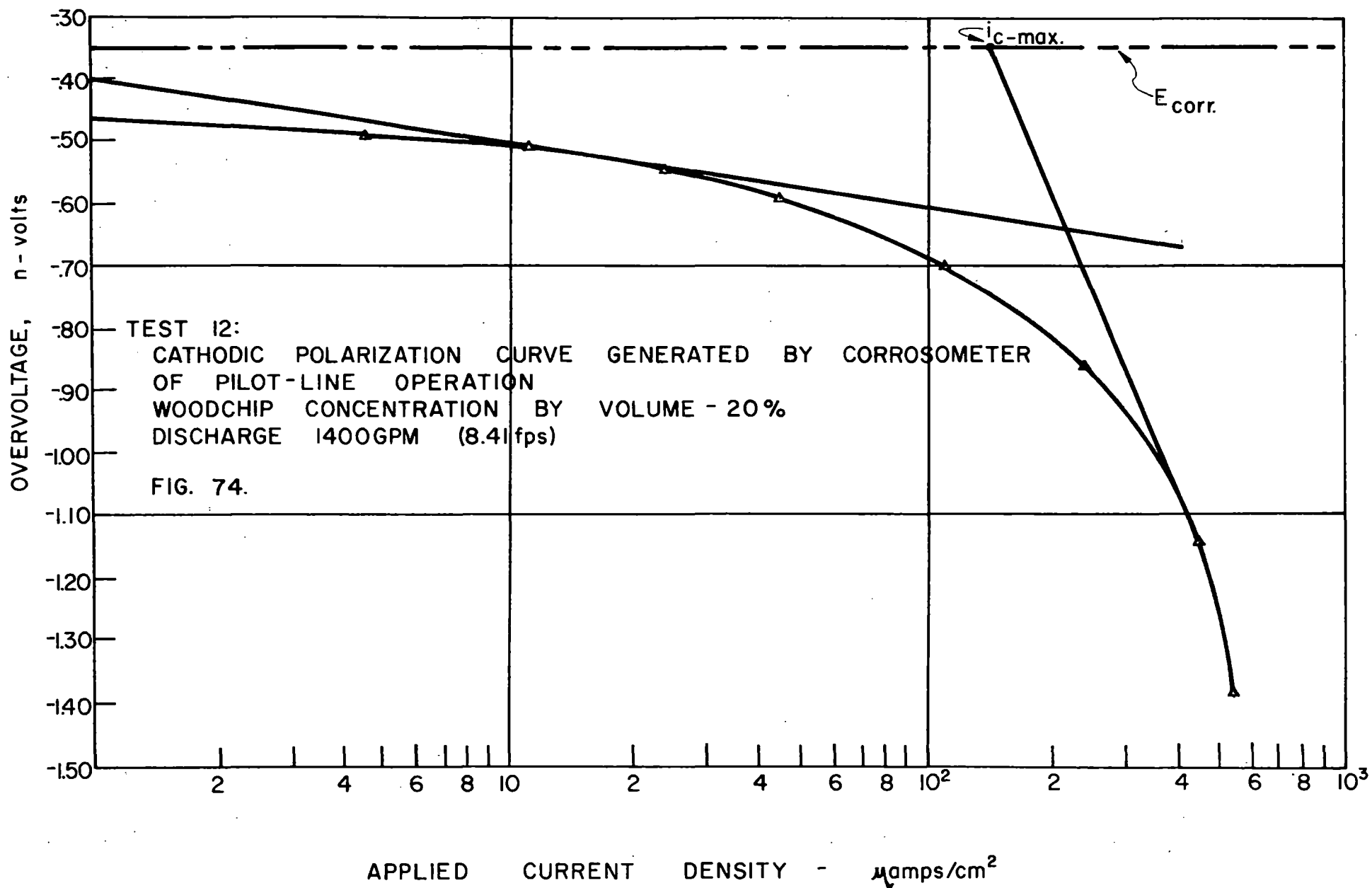












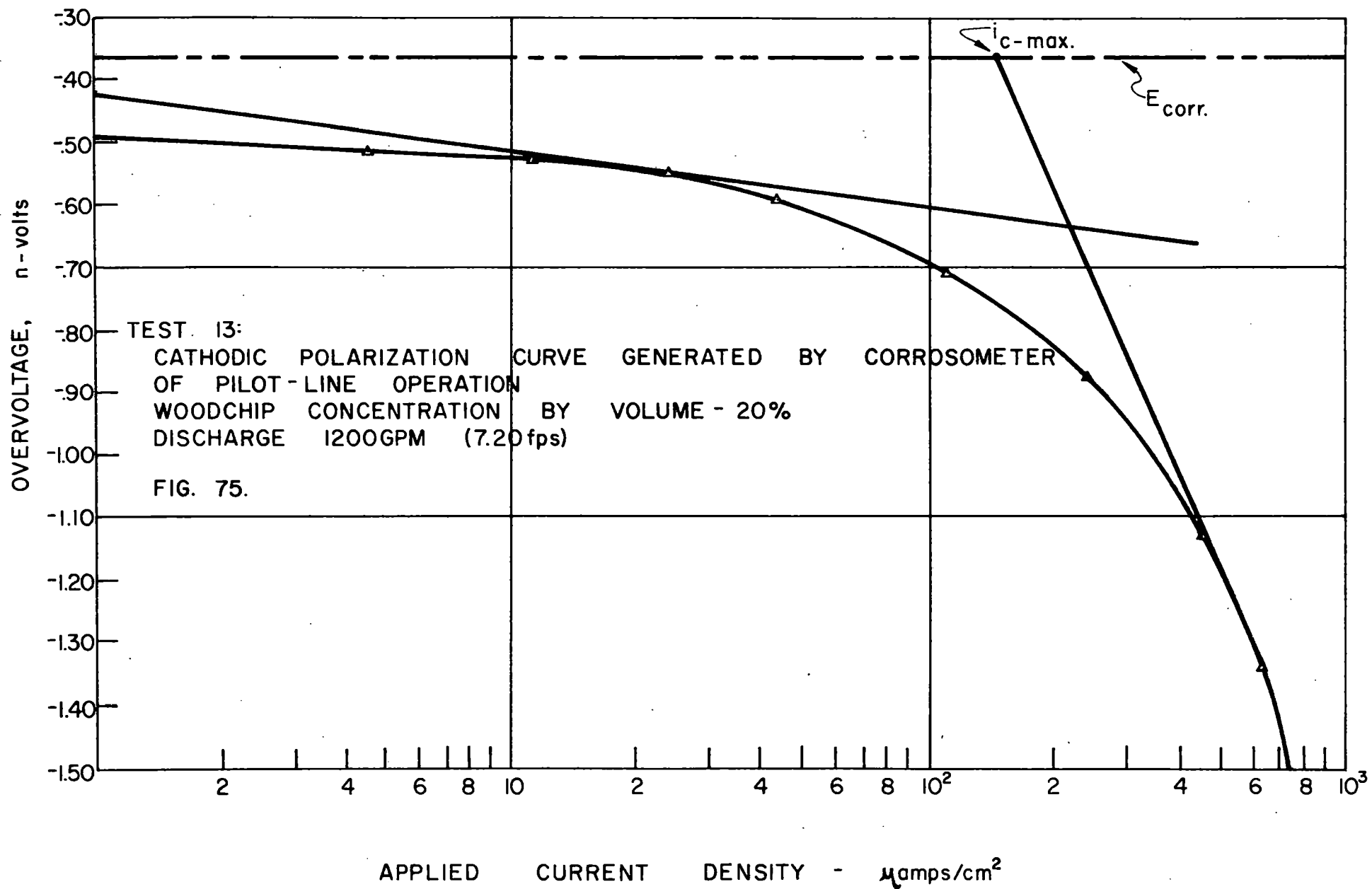


Table 14. Pilot Line Corrosion Parameters and Rates

Test	Average velocity, ft/sec	Wood chip concentration percent	Carrier water temp., °C	Minimum current density, $\mu\text{A}/\text{cm}^2$	Minimum corrosion rate, mpy*	Maximum current density, $\mu\text{A}/\text{cm}^2$	Maximum corrosion rate, mpy*
1	7.20	15	7.5	0.92	41.4	180	81.0
2	7.20	15	7.5	1.38	62.2	185	83.3
3	8.41	15	7.5	0.50	22.5	159	71.6
4	8.41	15	7.5	0.58	26.1	212	95.5
5	9.00	15	7.5	0.31	13.6	158	71.2
6	8.41	15	9.0	0.40	18.0	213	96.0
7	8.41	15	9.0	0.70	31.5	186	83.8
8	8.41	15	9.0	1.22	55.0	170	76.6
9	7.20	15	10.0	1.10	49.5	140	63.0
10	9.00	15	10.0	1.00	45.0	196	85.6
11	8.85	20	11.0	0.62	27.9	170	76.6
12	8.41	20	10.5	0.38	17.1	140	63.0
13	7.20	20	10.5	0.27	12.2	163	73.5

pipeline applications, and (3) recommendations for further studies to verify the method and extend the results.

5.8.1 Wood-chip pipeline results. The results of the pilot line corrosion studies conducted with flowing mixtures of wood chips and water given in Table 14 indicate the following:

1. the overall range of the maximum corrosion rates predicted from the corrosometer apparatus developed are great enough to influence the wall thickness design of a steel pipeline transporting a mixture of lodgepole pine wood chips and water,
2. the variations in the maximum predicted corrosion rates are not correlated with the flow velocity or the concentration of wood chips in the mixture because of the limited range of these latter two variables, and
3. the polarization resistance method can be applied for determining corrosion rates of interior walls of pipelines in which liquids are flowing under pressure when the apparatus for conducting corrosion tests under static conditions in the laboratory is modified for the dynamic conditions of pipeline flow.

5.8.2 General conclusions. In addition to the specific results for the corrosion tests conducted in the pilot line listed in the preceding section, the study of the polarization resistance method as a tool for determining corrosion rates on the interior walls of pipelines indicates the following general conclusions:

1. The concentration polarization effect is reduced when the velocity of the electrolyte sweeps it past the working and auxiliary electrodes. This is indicated when the cathodic polarization curves of the bench tests using the simulated carrier water (Figs. 55-58) are compared with the same curves of the pilot line tests (Figs. 63-75). This comparison shows the "knee" of the polarization curves for the pilot line tests to be translated approximately a half an order of magnitude in the direction of increased current densities. This shift causes the corrosion rates indicated for the pipeline tests to be greater than those in the bench tests; these results are seen by comparing the predicted corrosion rates of Table 14 with those in Table 13.

2. The corrosometer developed in this study indicates (a) corrosion of the interior walls of a pipeline transporting a mixture of wood chips and water does occur and (b) the corrosion rate indicated is in the range from 13 to 96 mils per year. Although control tests using the coupon immersion, or other long term, tests were not run as a control due to the intermittent operation of the pilot line, the tests conducted with the pilot line show corrosion rates of the same order magnitude as tests reported by Mullen and Ritter (1966) conducted on the effluent of a water treatment plant discharging into municipal distribution system using the coupon immersion method with AISI C-1010 mild steel specimens. The corrosion rates ranged from 8 to 18 mils per year. This comparison of the results of the tests reported by Mullen and Ritter with those of this study indicates the corrosometer developed to be of sound basic design.

The maximum corrosion rates indicated for the pilot line tests may be considered as conservative for design purposes for the following reasons:

- a) the pilot line was operated intermittently allowing air to enter the pipe in the interim between test runs; air trapped in the interstices of the pipe wall roughness would tend to accelerate the corrosion process, and
- b) the imperfect method for determining the maximum corrosion current in the absence of a well-established Tafel region caused the investigators to be overly conservative in the location of the tangent to the polarization curve.

5.8.3 Recommendations. Based on a review of the methods and results of this preliminary investigation of utilizing the polarization resistance method for determining the corrosion rates for the interior walls of pipelines while fluid is flowing, the following recommendations for further study are given:

1. A comprehensive review should be conducted on the factors influencing the slope of the reduction curve in the Tafel region in order to develop a suitable method for calculating the β -slope in the pseudo-Tafel region of cathodic polarization curves controlled by concentration polarization effects.

2. The design of the corrosometer developed in this investigation and the procedure for its use should be modified to allow for performing corrosion tests in pipelines operating at higher pressures.
3. A series of 30-, 60-, or 90-day continuous controlled tests should be conducted to compare the results obtained by the corrosometer developed in this study with those obtained by the coupon and/or spool test methods.
4. The corrosometer of this study should be used in obtaining a set of complete corrosion behavior diagrams (CBD) for pipelines in which liquids are flowing. The CBD so determined can then be compared with (a) those of other investigators and (b) those conducted in a pipeline environment with the liquid at rest. Information from these comparisons would add to the basic understanding of the corrosion process.

6. APPLICATION OF FRICTION LOSS CORRELATIONS

The procedure for selecting the pipe diameter, flow velocity, and concentration of wood chips to transport a given throughput with minimum power requirements is presented to illustrate the application of the friction loss correlation, Eq. (27) of Chapter 4.

Although the analysis requires an iterative solution more conveniently performed on a computer or programmable calculator, the individual steps are outlined so the reader may determine those steps where his data may differ from that of the example.

Illustrative example: Determine the pipe diameter and flow conditions (velocity, wood-chip concentration) giving the minimum power requirements and safe flow regime transporting an annual volume of 700,000 tons (U.S. measure), (634,780 metric tons), dry weight basis, through a pipeline using water as the carrier. Assume a 90 percent utilization factor and a 360 day per year maximum utilization.

1. The daily throughput, dry weight basis, is calculated:

$$\begin{aligned}\dot{W} &= 700,000 / (0.9 \times 360) = 2160 \text{ tons/day (U.S.)} \\ &= 1959 \text{ metric tons/day}\end{aligned}$$

2. The volumetric throughput of chips, Q_c , (ft^3/sec , m^3/sec) is calculated from the following equations:

$$Q_c (\text{ft}^3/\text{sec}) = \frac{\dot{W}(\text{tons/day}) \times (2000 \text{ lbf/ton})}{86,400(\text{sec/day}) \times (62.4 S_{\text{odc}}) (\text{lbf/ft}^3)}$$

$$Q_c = 3.7096 \times 10^{-4} \dot{W} / S_{\text{odc}} (\text{ft}^3/\text{sec}) \quad (42-a)$$

$$Q_{cm} (m^3/sec) = \frac{\dot{W}_m (\text{metric tons/day}) \times 9.81 (\text{kN/metric ton})}{86,400 (\text{sec/day}) \times 9.81 S_{odc} (kN/m^3)}$$

$$Q_{cm} = 1.1574 \times 10^{-5} \dot{W}_m / S_{odc} (m^3/sec) \quad (42-b)$$

In Eqs. (42-a) and (42-b), S_{odc} = specific gravity of wood chips, dry weight basis.

3. The range of probable pipe diameters is narrowed to three of four by expressing the diameter, D , as a function of flow velocity, V_m ; concentration, C ; dry-weight specific gravity of wood chips, S_{odc} ; and the daily throughput rate, \dot{W} . Using Eq. (11) defining the relation between the concentration, C , the volumetric flow rate of wood chips, Q_c , and the volumetric flow rate of the mixture, Q_m , and Eq. (42) giving Q_c as a function of \dot{W} and S_{odc} , the expressions for Q_m are developed as:

$$Q_m = Q_c / C = 3.7096 \times 10^{-4} \dot{W} / (C S_{odc}) (ft^3/sec) \quad (43-a)$$

and

$$Q_{m_n} = 1.1574 \times 10^{-5} \dot{W}_m / (C S_{odc}) (m^3/sec) \quad (43-b)$$

- b. Using $Q_m = \pi D^2 V_m / 4$ and Eqs. (43-a) and (43-b), the equations for the diameters become:

$$D(ft) = 0.02173 \sqrt{\dot{W} / (C S_{odc} V_m)} , \text{ and} \quad (44-a)$$

$$D(m) = 0.003839 \sqrt{\dot{W}_m / (C S_{odc} V_{mM})} \quad (44-b)$$

- c. Using a probable economic velocity range of 4 to 8 fps (1.5 to 3 m/sec), a probable range of concentrations of 18 to 30

percent and a specific gravity of 0.4 for wood chips (Lodgepole pine), the range of probable economic diameters may be determined:

$$D(\text{ft}) = 0.02173 \sqrt{\frac{2160}{0.4Cv_m}} = 1.597/\sqrt{Cv_m} \quad (45-a)$$

and

$$D_M(\text{m}) = 0.003839 \sqrt{\frac{1959}{0.4Cv_{mM}}} = 0.2687/\sqrt{Cv_{mM}} \quad (45-b)$$

d. Substituting the pairs of values of velocity and concentration giving the maximum and minimum probable diameters yields

$$\text{Max } D(\text{ft}) = 1.597/\sqrt{0.18(4)} = 1.882 \text{ ft (22 in.)}$$

$$\text{Min } D(\text{ft}) = 1.597/\sqrt{0.30(8)} = 1.031 \text{ ft (12 in.)}$$

$$\text{Max } D_m(\text{m}) = 0.2687/\sqrt{0.18(1.5)} = 0.517 \text{ m (500 mm)}$$

$$\text{Min } D_M(\text{m}) = 0.2687/\sqrt{0.30(3)} = 0.283 \text{ m (250 mm)}$$

The trial diameters selected for further analysis are 16, 18, and 20 inches (400, 450, and 500 mm).

4. Values of V_m for the different values of C are found for each diameter from Eqs. (45-a) and (45-b) rewritten as:

$$V_m(\text{ft/sec}) = 2.550/(CD^2) \quad (46-a)$$

$$V_{mM}(\text{m/sec}) = 0.07220/(CD_m^2) \quad (46-b)$$

The values of V_m for concentrations from 18 to 34 percent are shown in Tables 15-a and 15-b for the U.S. and metric units, respectively.

Table 15-a. Head loss and power for 700,000 tons/year throughput.

Concentration C	Velocity V _m (fps)	Friction factor f _m	Head loss h _L (ft/1000 ft)	Power P (hp/1000 ft)	Flow factor ψ
<u>D = 16 in.</u>					
.18	7.9	.020	14.5	18.1	609
.20	7.2	.023	13.9	15.8	415
.22	6.5	.026	12.8	13.2	277
.24	5.9	.032	12.9	12.1	189
.26	5.5	.037	13.0	11.3	141
.28	5.1	.045	13.6	11.0	104
.30	4.8	.054	14.5	11.0	80
.32	4.5	.064	15.3	10.9	62
<u>D = 18 in.</u>					
.16	7.1	.022	11.5	16.4	442
.18	6.3	.027	11.1	14.0	274
.20	5.7	.032	10.8	12.3	184
.22	5.2	.040	11.2	11.7	127
.24	4.7	.051	11.7	11.0	86
.26	4.4	.063	12.6	11.1	65
.28	4.0	.084	11.2	11.2	45
.30	3.8	.101	15.1	11.5	36
<u>D = 20 in.</u>					
.14	6.6	.024	9.7	15.9	365
.16	5.7	.030	9.1	12.8	208
.18	5.1	.039	9.5	12.0	133
.20	4.6	.050	9.9	11.3	88
.22	4.2	.066	10.9	11.4	61
.24	3.8	.090	12.1	11.4	41
.26	3.5	.119	13.6	11.8	30
.28	3.3	.149	15.1	12.3	23

Table 15-b. Head loss and power for 634,780 metric tons/year throughput.

Concentration C	Velocity V _m (fps)	Friction factor f _m	Head loss h _L (ft/1000 ft)	Power P (hp/1000 ft)	Flow factor ψ
<u>D = 400 mm</u>					
.16	2.82	.018	18.3	63.6	1071
.18	2.51	.020	16.1	49.8	687
.20	2.26	.022	14.3	39.8	451
.22	2.05	.025	13.3	33.6	310
.24	1.88	.029	13.0	30.1	219
.26	1.74	.134	13.1	28.1	160
.28	1.61	.042	13.8	27.4	117
.30	1.50	.050	14.3	26.4	88
<u>D = 450 mm</u>					
.16	2.23	.022	12.3	42.8	482
.18	1.98	.026	11.6	35.8	301
.20	1.78	.031	11.1	30.8	198
.22	1.62	.038	11.3	28.6	136
.24	1.49	.047	11.8	27.4	97
.26	1.37	.060	12.8	27.4	70
.28	1.27	.075	13.7	27.1	51
.30	1.19	.094	15.1	28.0	39
<u>D = 500 mm</u>					
.14	2.06	.023	9.9	39.4	399
.16	1.81	.028	9.3	32.4	234
.18	1.61	.036	9.4	29.1	143
.20	1.44	.047	9.9	27.5	97
.22	1.31	.062	10.9	27.5	66
.24	1.20	.081	11.9	27.5	47
.26	1.11	.106	13.3	28.4	34
.28	1.03	.137	14.8	29.4	25

b. The friction factor, f_m , for the mixture of wood chips and water for each diameter, velocity, and concentration are calculated from Eq. (27):

$$(f_m/f) - 1 = 197 \frac{D^{.970} g^{1.312} v_m^{.342}}{v_m^{2.964}} \frac{C}{1-C} \cdot .838 + .930 \ln(1-k) \quad (27)$$

(1) Using $k = d_c/D$ based on $d_c = 0.104$ ft (1.25 in., 3.18 cm),

$$v = 1.2 \times 10^{-5} \text{ ft}^2/\text{sec}, (1.11 \times 10^{-6} \text{ m}^2/\text{s}), g = 32.2 \text{ ft/sec}^2$$

(9.81 m/sec²), Eq. (27) becomes:

$$(f_m/f) - 1 = 197 \frac{a_i}{v_m^{2.960}} \frac{C}{1-C} x_i = \phi_i \quad (47)$$

where a_i and x_i have the following values for the pipe diameter i :

U.S. units			SI units		
i	a_i	x_i	i	a_i	x_i
16	2.609	0.762	400	.0756	.755
18	2.925	0.771	450	.0847	.764
20	3.241	0.777	500	.0839	.772

(2) The friction factor, f , for water flowing in 16- to 20-in.-dia (400- to 500-mm-dia) steel pipes is between 0.016 and 0.014 for velocities between 4 and 8 fps (1.22 and 2.44 m/sec). An average value of 0.015 was used for calculating the values of f_m shown in Tables 15-a and 15-b using Eq. (47).

c. The values of friction head loss gradient, ft/1000 ft, (m/km), are calculated using the Weisbach equation, Eq. (4):

$$h_L = f(L/D) V_m^2 / 2g \quad (4)$$

The head loss gradient is shown as a function of flow velocity in Fig. 76(a).

d. The values of power required to overcome the friction losses calculated from the equation

$$P = Q_m \gamma_m h_L = \pi D^2 \gamma_m h_L V_m / 4 \quad (48)$$

are tabulated in Tables 15-a and 15-b and shown in Fig. 76(b) in terms of horsepower per 1000 ft (hp/1000') (U.S. units) and kilowatts per kilometer (kw/km). The specific weight of the mixture, γ_m , is taken as that of water, 62.4 lbf/ft³ (9.81 kN/m³).

e. The values of the flow parameter ψ , given by Eq. (26) and determined from Eq. (47) as

$$\psi_i = (197/\Phi_i)^{1/.988} \quad (49)$$

are also given in Tables 15-a and 15-b.

5. The results given in Tables 15-a and 15-b and in Fig. 76 show the
 - (a) minimum head loss occurs between 5.6 and 6.0 fps (1.71 and 1.83 m/sec),
 - (b) the minimum power requirement is approximately 11.0-11.3 hp/mi (26.9-27.6 kw/km) and occurs at flow velocities of 4.5-5.0 ft/sec (1.37-1.52 m/sec),
 - (c) the minimum head loss corresponds with the safe design value of 200 for the flow factor ψ ;
 the minimum power occurs at velocities below the critical ψ .

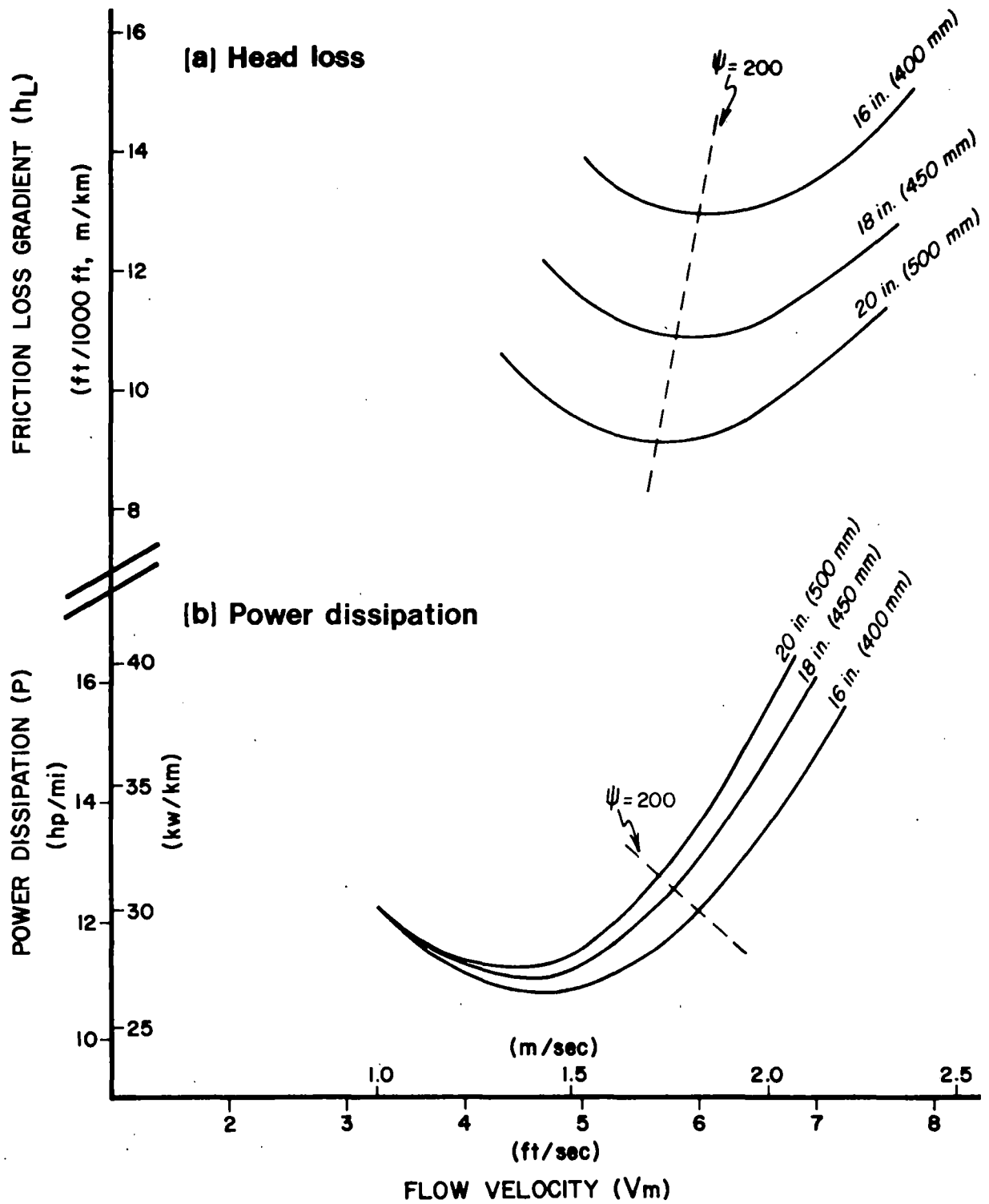


FIG. 76. HEAD LOSS AND POWER DISSIPATION FOR 700,000 TONS/YEAR

The design flow conditions based on $\psi = 200$ for the different pipe diameters capable of delivering 700,000 tons (634,780 metric tons) annually are listed in Table 16. Based on the alternatives shown in Table 16 and assuming cost of the pipe and carrier water handling are proportional to pipe diameter, the 16-in.-dia (400-mm-dia) is to be recommended.

Table 16. Design alternatives 700,000 tons/year throughput

Diameter D, in. (mm)	Concentration C%	Flow velocity V_m , fps (m/s)	Head loss h_L , ft/1000 ft (m/km)	Power P, hp/mi (kw/km)	Carrier water Q_w , cfs (m ³ /s)
16 (400)	23.9	6.00 (1.83)	12.9	12.2 (29.9)	6.37 (0.181)
18 (450)	19.5	5.82 (1.78)	10.8	12.5 (30.7)	8.28 (0.234)
20 (500)	16.2	5.65 (1.72)	9.1	12.8 (31.2)	10.32 (0.292)

ACKNOWLEDGMENTS

This study was sponsored by the USDA Forest Service as Agreement No. FS-INT No. 1, Grant 7 U.S.C. 450i PL 89-106 between the Endowment and Research Foundation of Montana State University and the Intermountain Forest and Range Experiment Station, USDA Forestry Sciences Laboratory, Bozeman, Montana.

The success of this project is due to the effort, interest, enthusiasm and cooperation of a number of people contributing to the "Wood-Chip Pipeline Group" at different stages of the studies. The authors acknowledge and appreciate the efforts of these group members.

James J. Billmeyer (now with HKM Engineering, Billings, Montana) served as Project Engineer through the design, construction, and data collecting phases.

The following men worked as Graduate Research Assistants in the construction, instrumentation check-out, data collecting and analysis phases of the project: David Jochim (now with CH₂M-Hill Engineers, Portland, Oregon), Craig L. Riley (now with Daily-Peccia & Associates, Helena, Montana), and Larry H. Gruel (now with Montana Power Company, Butte, Montana).

Michael Gee and Raymond Otte served as undergraduate assistants for the data analysis and latter stage data collecting functions.

The construction and maintenance was performed at different times by Stephen Colgrove, James Drummond, George Franko, James Hodges, Arnold Kallestad, Leslie Keebler, Timothy King, Leon Kjellgren, and Roger Thieme.

LITERATURE CITED

- Anonymous. 1974. The CAST Report. Agricultural Eng. v(no):21.
- Anonymous. 1965. Wood-chip pipelines may cut Canadian forest costs sharply. Pipe Line News, Feb. 1965, pp. 34-35.
- Anonymous. 1964. "Chiplines"--cheaper than we think. Pulp & Paper 38(26):27.
- Anonymous. 1963. The transportation of solids in steel pipelines. Golden, Colo.: Colo. School of Mines Res. Found.
- Anonymous. Monitoring corrosion. Internal report, Cosasco Division, Grant Oil Tool Co., Los Angeles.
- Alger, G.R., and D.B. Simons. 1968. Fall velocity of irregular shaped particles. Jour. of Hydraulics Div. (Proc. of ASCE) 94(HY3):721.
- Asano, T., A.L. Towler, and R.L. Sanks. 1974. Leaching of pollutants from a wood-chip slurry. Jour. of Environmental Engr. Div. (Proc. of ASCE) 100(EE4):855.
- Bain, A.G., and S.T. Bonnington. 1970. The Hydraulic Transport of Solids by Pipeline. Pergamon Press, Oxford, England, p. 9.
- Bond, R.K. 1957. Chem. Engr. 64(10):249.
- Charley, R.W. 1966. The effect of chip-shaped solids on energy losses in axisymmetric pipe expansions. (Unpublished M.S. thesis, Mont. State Univ., Bozeman).
- Dauber, C. 1957. Pipeline coal transportation. Coal Age 62(4):82.
- Dixon, W.J. 1967. BMD Biomedical Computer Programs, University of California Press, Los Angeles, pp. 233-257.
- Dodge, D.W., and A.B. Metzner. 1959. Turbulent flow of non-Newtonian systems. AIChE Jour. 5(2):189.
- Durand, R.E., and E. Condolios. 1952. The transport of coal and solid materials in pipes. (Proc. of colloquium on hydraulic transport of coal, Scientific Dept., National Coal Board of Great Britain.)
- Eaton, P.E., and R.R. Annand. . Modern developments in polarization techniques for corrosion rate measurement. Report by TRETOLITE DIVISION, Petrolite Corporation, St. Louis, MO.

- Elliott, D.R., and W.H. de Montmorency. 1963. The transportation of pulp-wood chips in pipelines. Pulp & Paper Res. Inst. Can. Tech. Rep. 334, 69 pp.
- Faddick, R.R. 1963. Head loss studies of transport of wood chips in pipelines. (Unpublished M.S. thesis, Queen's Univ., Kingston, Ontario.)
- _____. 1970. Hydraulic transportation of solids in pipelines. (Unpublished Ph.D. thesis, Montana State University, Bozeman.)
- Fontana, M.G., and N.D. Greene. 1967. Corrosion Engineering, McGraw-Hill, New York, p. 344.
- Fulkerson, E.F., and J.E. Rinne. 1959. Gilsonite solids pipeline. Jour. of Pipeline Div. (Proc. of ASCE) 85(PL1):35.
- Gilbert, R. 1960. Transport hydraulique et refoulement des mixtures en conduites. Annales des Ponts et Chaussées (May-June):507.
- Gow, J.L. 1971. Hydraulic transport of wood chips in pipelines. (Unpublished Ph.D. thesis, Montana State University, Bozeman.)
- _____, and W.A. Hunt. 1971. Hydraulic transport of wood chips in pipelines. (Unpublished report to Intermountain Forest & Range Exp. Sta., Bozeman, MT.)
- Henderson, J.H. 1962. The gilsonite slurry pipeline. (Paper presented at AIChE National Meet., Denver, Colo.)
- Hendrix, G.A., and W.A. Hunt. 1968. Analysis of hydraulic transients in an injection device for two-phase flow. (Unpublished report to Intermountain Forest & Range Exp. Sta., Bozeman, MT.)
- Hoffman, I.C. 1967. A method for optimizing a network of pipelines for transporting wood chips. (Unpublished M.S. thesis, Mont. State Univ., Bozeman.)
- Hughes, R.C., W.A. Hunt, and J.D. Tennant. 1972. Feasibility and design considerations of solids pipelines. (Paper No. 72-PET-59 presented at the Petroleum Mech. Engr. and Pressure Vessels & Piping Conf., New Orleans, La.)
- Hunt, W.A. 1962. Continuous flow transport of low-valued forest products by hydraulic pipeline. (Unpublished report to Intermountain Forest & Range Exp. Sta., Bozeman, MT).
- _____. 1963. Some engineering considerations of a wood-chip pipeline. Forest Prod. Jour. 13(19):365.

- _____. 1965. An economic analysis of transporting low-valued forest products continuously in hydraulic pipelines. (Unpublished report to Intermountain Forest & Range Exp. Sta., Bozeman, MT.)
- _____, and R.E. Schmidt. 1965. Transport of wood chips in hydraulic pipelines: 1) mathematical model for economic analysis, 2) application of economic model to Alaskan pulpwood sale. (Paper presented at Northwest Scientific Assoc. Meet., Portland, OR.)
- _____, and I.C. Hoffman. 1968. Optimization of pipelines transporting solids. Jour. of Pipeline Div. (Proc. of ASCE) 94(PL1):89.
- Johnson, D.A., and W.A. Hunt. 1968. The effect of chip-shaped solids on valve head loss characteristics. (Unpublished report to Intermountain Forest & Range Exp. Sta., Bozeman, MT.)
- Love, F.H. 1969. The Black Mesa story. Pipeline Engr. Int. 41(12):38.
- Makrides, A.C. 1962. Some electrochemical methods in research. Corrosion 18(9):338t.
- Metzner, A.B., and J.C. Reed. 1955. Flow of non-Newtonian fluids--- correlation of laminar, transition and turbulent flow regions. AIChE Jour. 1(4):431.
- Morris, P.E., and R.C. Scarberry. 1972. Predicting corrosion rates with the potentiostat. Corrosion 28(12):444.
- Mullen, E.D., and J.A. Ritter. 1966. Potable water corrosion control. Jour. of AWWA 58(8):473.
- NACE. n.d. Modern electrical methods for determining corrosion rates. NACE Publication 3D170, Houston, TX.
- Page, K., and W.A. Hunt. 1966. The effect of chip-shaped particles on pump performance characteristics. (Unpublished report to Intermountain Forest & Range Exp. Sta., Bozeman, MT.)
- Pao, R.H.F. 1968. Fluid Mechanics, John Wiley & Sons, Inc., New York, pp. 221-2.
- Reese, S.E. 1975. Nearly 100,000 miles of pipelines planned or underway worldwide. Pipeline & Gas Jour. (Energy operations & equipment forecast) July 15:6.
- Reichl, E.H., and R. Jones. n.d. Consolidated Coal slug pump. U.S. Patent No. 2,672,372.

- Reinoehl, J.E., F.E. Beck, and M.G. Fontana. 1970. Effect of polarization in potentiokinetic anodic polarization of iron in 1N H_2SO_4 . Corrosion 26(4):141.
- Rouse, H. 1946. Elementary Fluid Mechanics, John Wiley, New York, pp. 209.
- Schmidt, R.E. 1965. An investigation of the effects of pressure and time on the specific gravity, moisture content and volume of wood in a water slurry. (Unpublished M.S. thesis, Mont. State Univ., Bozeman.)
- _____. 1968. A method for determining the moisture content and specific gravity of wood chips in a pressurized water system. TAPPI 54(4):164.
- Shane, J.M., N.S. Hawthorne, and T. Asano. 1975. Reclamation of wood-chip carrier water. Jour. of Environmental Engr. Div. (Proc. of ASCE) 10(EE2):215.
- Soucy, A. 1968. Data supplied to R.R. Faddick for Ph.D. thesis by Laval Univ., Quebec City, Quebec.
- Spells, K.E. 1955. Correlations for Use in Transport of Aqueous Suspensions of Fine Solids Through Pipes. Trans. Inst. of Ch. Engr., London 33:79-84.
- Vennard, J.K. 1961. Elementary Fluid Mechanics. 4th ed., John Wiley, New York, p. 545.
- Wasp, E.J. 1969. State of the art in solids pipelining. Pipeline Engr. Int. 41(12):56.
- Worster, R.C. 1952. Hydraulic Transport of Solids. Proc. of Colloquium on Hydraulic Transport of Coal, National Coal Board Scientific Dept., London.